



# University of HUDDERSFIELD

## University of Huddersfield Repository

Shaw, Paul B.

Studies of the Alkaline Degradation of Cellulose and the Isolation of Isosaccharinic Acids

### Original Citation

Shaw, Paul B. (2013) Studies of the Alkaline Degradation of Cellulose and the Isolation of Isosaccharinic Acids. Doctoral thesis, University of Huddersfield.

This version is available at <http://eprints.hud.ac.uk/id/eprint/19266/>

The University Repository is a digital collection of the research output of the University, available on Open Access. Copyright and Moral Rights for the items on this site are retained by the individual author and/or other copyright owners. Users may access full items free of charge; copies of full text items generally can be reproduced, displayed or performed and given to third parties in any format or medium for personal research or study, educational or not-for-profit purposes without prior permission or charge, provided:

- The authors, title and full bibliographic details is credited in any copy;
- A hyperlink and/or URL is included for the original metadata page; and
- The content is not changed in any way.

For more information, including our policy and submission procedure, please contact the Repository Team at: [E.mailbox@hud.ac.uk](mailto:E.mailbox@hud.ac.uk).

<http://eprints.hud.ac.uk/>

# Studies of the Alkaline Degradation of Cellulose and the Isolation of Isosaccharinic Acids

Paul B. Shaw MSci (Hons)



*University of*  
**HUDDERSFIELD**

A thesis submitted to the University of Huddersfield in partial fulfilment of  
the requirements for the degree of Doctor of Philosophy

Department of Chemical and Biological Sciences  
The University of Huddersfield

March 2013

## ABSTRACT

Cellulosic materials are expected to form a significant proportion of the waste proposed for disposal in underground repositories being designed for the storage of radioactive waste. Under the alkaline conditions of these facilities, cellulose degrades by a so called 'peeling' reaction resulting in the production of a complex mixture of products (CDPs), the major components being  $\alpha$ - and  $\beta$ -isosaccharinic acid ( $\alpha$  and  $\beta$ -ISA). A significant amount of research has been performed on ISA as part of the safety assessment for the development of these underground repositories due to the ability of ISA to complex with, and increase the solubility of radioactive isotopes. Until now, the vast majority of this research has involved the readily-available  $\alpha$ -ISA, only a limited number of studies have involved  $\beta$ -ISA because no simple procedure is available for its isolation. Therefore, in this project, a method for the synthesis and isolation of  $\beta$ -ISA was developed.

Cellulose degradation experiments which were performed to maximise solution concentrations of  $\beta$ -ISA are described in chapter 3. Microcrystalline cellulose was degraded under anaerobic conditions at either RT, 50 °C or 90 °C and comparisons were made between the use of NaOH and Ca(OH)<sub>2</sub> as the base catalyst. As expected, the major products of all degradation reactions were  $\alpha$ - and  $\beta$ -ISA, in addition, small amounts of free metasaccharinic acid (MSA) was detected in the Ca(OH)<sub>2</sub> reactions. The largest solution concentrations of  $\beta$ -ISA were produced when cellulose was degraded at 90 °C using NaOH; after 24 hrs of reaction, solution concentrations of 12.7 g L<sup>-1</sup> were achieved, whereas, in the equivalent Ca(OH)<sub>2</sub> reaction, after 4 days a maximum concentration of only 5.1 g L<sup>-1</sup> was produced. For this reason, cellulose was degraded at 90 °C using NaOH to produce degradation solutions to be used in procedures to isolate  $\beta$ -ISA. An additional finding was that significant amounts of ISA were being removed from degradation solutions due to absorption on to unreacted cellulose fibres; in the NaOH reaction, absorption was occurring rapidly and the percentage of ISA in both the solution and solid phases were very similar. In the Ca(OH)<sub>2</sub> reaction, the absorption was a slow process and the percentage of ISA on the solid phase (61 %) was lower than the percentage of ISA in the solution phase (84 %) suggesting that solid Ca(OH)<sub>2</sub> was affecting both the rate at which absorption was occurring and the composition of the absorbed species; this was possibly due to solid Ca(OH)<sub>2</sub> physically obstructing the access of ISA to the cellulose fibres and also catalysing the oxidation of some of the ISA into smaller fragmentation products.

Methods which were developed to isolate  $\beta$ -ISA are described in chapter 4. Isolation of  $\beta$ -ISA was initially achieved by eluting crude cellulose degradation solutions directly through a column of anion exchange resin. Using an automated system, a large throughput of material was possible resulting in the accumulation of relatively large amounts of  $\beta$ -ISA; after repeating the column 17 times, 1 g of pure  $\beta$ -ISA was isolated. However, using this method, the crude solutions severely fouled the anion exchange resin, concluding that anion exchange was more suited to small scale isolations of  $\beta$ -ISA. A final isolation procedure was developed which involved the elution of mixtures of benzoylated CDPs through normal phase silica columns. It was determined that prior to elution, coloured impurities could be efficiently removed by passing the derivatised mixture through a wide bed of silica. Slow elution of the resulting clean syrup through a large silica column allowed up to 7 g of tribenzoylated  $\beta$ -ISA<sub>L</sub> to be isolated and following de-benzoylation procedures, 2.6 g of  $\beta$ -ISA was isolated from a single column. The large protecting groups also allowed single crystals of both  $\alpha$ - and  $\beta$ -tribenzoate to be produced and the resulting

X-ray structures confirmed the absolute configuration of tribenzoylated  $\beta$ -ISA<sub>L</sub> as being 2R, 4S. Additional NMR analysis of collected fractions allowed several other polyhydroxylated compounds to be identified, also present as their perbenzoylated esters, these being: 3,4-dihydroxybutanoic acid, 2,5-dihydroxypentanoic acid, 2,3-dideoxypentanoic acid and 2,4,5-trihydroxypentanoic acid.

The isolation of large amounts of  $\beta$ -ISA allowed several solution phase physical properties of  $\beta$ -ISA to be measured and these are reported in chapter 5, including the aqueous  $pK_a$  (3.61) which was determined using NMR methods. The rate constants for the inter-conversion between ISAH and ISA<sub>L</sub> were also studied for both  $\alpha$ - and  $\beta$ -ISA. In acidic environments, ISAH undergoes an acid catalysed lactonisation to generate isosaccharino-1,4-lactone (ISA<sub>L</sub>), conversely in basic environments, ISA<sub>L</sub> undergoes a base catalysed ring-opening to produce ISAH. Using pH-stat autotitration, the second-order rate constants for the lactone hydrolysis reaction were determined, to which values of  $25.3 \text{ M}^{-1} \text{ s}^{-1}$  for  $\beta$ -ISA<sub>L</sub> and  $97.0 \text{ M}^{-1} \text{ s}^{-1}$  for  $\alpha$ -ISA<sub>L</sub> were observed. The acid catalysed lactonisation of ISAH was studied using <sup>1</sup>H NMR spectroscopy; the second-order rate constant for the lactonisation of  $\beta$ -ISAH ( $3.10 \times 10^{-3} \text{ M}^{-1} \text{ s}^{-1}$ ) was larger than the second order rate constant for the lactonisation of  $\alpha$ -ISAH ( $7.04 \times 10^{-4} \text{ M}^{-1} \text{ s}^{-1}$ ).

## ACKNOWLEDGEMENTS

First and foremost I would like to thank my supervisors Professor Andrew Laws and Dr Paul Humphreys for giving me the opportunity to undertake this interesting research project. I would especially like to thank Prof. Laws for his continuous guidance and mentorship throughout this entire project.

I would also like to thank the many members of technical staff at the University of Huddersfield who have provided support for this project; special mention goes to Dr. Neil McLay, for running NMR and mass spectrometry experiments; Dr. Richard Hughes, for help with aspects of chromatography; Prof. Craig Rice for performing single-crystal X-ray diffraction experiments and providing and solving the crystallographic data and Dr. Marcus Chadha for training on the pH stat autotitrator.

I would also like to thank other members of the Laws' group especially Glenn Robinson for his assistance in isolating beta ISA; also other PhD students for helpful discussions, most notably Ahmed Elmekawy and Kevin Ellis.

Finally, I would like to thank my partner Racheal for being understanding and supportive throughout my studies. And my children Melissa and Harry; I'm sorry for missing so much cherished spare time with you due to these studies – this work is dedicated to you.

## List of Abbreviations

~	Approximately
1D	One dimensional (NMR spectroscopy)
2D	Two dimensional (NMR spectroscopy)
ACW	Artificial cement pore water
AGU	D-anhydroglucopyranose unit
$\alpha$ -ISA	2-C-(hydroxymethyl)-3-deoxy-D-erythro-pentonic acid (alpha isosaccharinic acid)
$\alpha$ -ISAH	Protonated alpha isosaccharinic acid (free acid)
$\alpha$ -ISAL	2-C-(hydroxymethyl)-3-deoxy-D-erythro-pentono-1,4-lactone (alpha isosaccharinic acid-1,4-lactone)
B <sub>AC2</sub>	Base-catalyzed, acyl-oxygen fission, bimolecular mechanism
$\beta$ -ISA	2-C-(hydroxymethyl)-3-deoxy-D-threo-pentonic acid (beta isosaccharinic acid)
$\beta$ -ISAH	Protonated beta isosaccharinic acid (free acid)
$\beta$ -ISAL	2-C-(hydroxymethyl)-3-deoxy-D-threo-pentono-1,4-lactone (beta isosaccharinic acid-1,4-lactone)
c	Circa (approximately)
Ca( $\alpha$ -ISA) <sub>2</sub>	Calcium 2-C-(hydroxymethyl)-3-deoxy-D-erythro-pentionate (Calcium (alpha)-isosaccharinate)
Ca( $\beta$ -ISA) <sub>2</sub>	Calcium 2-C-(hydroxymethyl)-3-deoxy-D-threo-pentionate (Calcium (beta)-isosaccharinate)
Ca(OH) <sub>2</sub>	Calcium hydroxide
CDCl <sub>3</sub>	Deuterated chloroform
CDPs	Cellulose degradation products
CI	Crystallinity index
CoRWM	Committee on Radioactive Waste Management
COSY	Correlated spectroscopy
CZE	Capillary zone electrophoresis
d	Doublet
dd	Doublet of doublets
DDP	2,3-dideoxypentonic acid
DMAP	4-Dimethylaminopyridine

D <sub>2</sub> O	Deuterium Oxide
DEPT	Distortionless enhancement by polarization transfer
DHB	3,4-dihydroxybutanoic acid
DHB <sub>L</sub>	3,4-dihydroxybutano-1,4-lactone
DHP	2,5-dihydroxypentanoic acid
DP	Degree of polymerisation
ESI	Electrospray ionization
G	relative centrifugal force
GBq/te	Gigabecquerels per tonne
GC-MS	Gas chromatography – mass spectrometry
h	Hours
HCl	Hydrochloric acid
HLW	High level (radioactive) waste
HMBC	Heteronuclear multiple bond correlation
HPAEC-PAD	High performance anion exchange chromatography–pulsed amperometric Detection
HPIEC	High performance ion exclusion chromatography
HRMS	High resolution mass spectrometry
HSQC	Heteronuclear single quantum coherence
Hz	Hertz
ILW	Intermediate level (radioactive) waste
J	Coupling constant
K <sub>eq</sub>	Equilibrium constant
<i>k'</i> <sub>hyd</sub>	Pseudo-first-order rate constant (for acid catalysed lactone hydrolysis of ISA <sub>L</sub> )
<i>k</i> <sub>hyd</sub>	Second-order rate constant (for lactone hydrolysis of ISA <sub>L</sub> )
<i>k'</i> <sub>lac</sub>	Pseudo-first-order rate constant (for lactonization of ISAH)
<i>k</i> <sub>lac</sub>	Second-order rate constant (for lactonization of ISAH)
<i>k</i> <sub>obs</sub>	Pseudo-first-order rate constant (for base hydrolysis of ISA <sub>L</sub> )
LLW	Low level (radioactive) waste
LLWR	Low Level Waste Repository
m	Multiplet
M	Molar (mol dm <sup>-3</sup> )
mg L <sup>-1</sup>	Milligrams per litre

MRWS	Managing radioactive waste safely
MSA	Metasaccharinic acid
NaOD	Deuterated sodium hydroxide
NaOH	Sodium hydroxide
NMR	Nuclear magnetic resonance
NDA	Nuclear Decommissioning Authority
NIREX	Nuclear Industry Radioactive Waste Management Executive
PAD	Pulsed Amperometric Detection
pD	A measurement of acidity in deuterated solutions (equivalent to pH + 0.4)
PGRC	Phased Geological Repository Concept
PCM	plutonium contaminated material
ppm	Parts per million
Rf	Retardation factor
rpm	Revolutions per minute
RT	Room temperature
SEC	Size exclusion chromatography
Soln.	Solution
t $\frac{1}{2}$	half-life
TC	Terminal complexes
THP	2,4,5-trihydroxypentanoic acid
TOC	Total Organic Carbon
tr	Retention time
v/v	volume per volume
X-ISA	2-C-(hydroxymethyl)-3-deoxytetronic acid (xyloisosaccharinic acid)
X-ISA <sub>L</sub>	2-C-(hydroxymethyl)-3-deoxytetra-1,4-lactone (xyloisosaccharinic acid-1,4-lactone)
XRD	X-ray diffraction

## TABLE OF CONTENTS

1	General Introduction.....	1
1.1	Cellulose .....	1
1.1.1	Molecular Structure .....	2
1.1.2	Biosynthesis.....	3
1.1.3	Supramolecular Structure .....	6
1.1.4	Cellulose polymorphs .....	10
1.1.4.1	Cellulose I .....	10
1.1.4.2	Cellulose II .....	13
1.1.4.3	Cellulose III and IV .....	15
1.1.5	Cellulose Utilisation .....	16
1.2	Radioactive waste .....	17
1.2.1	Management of Radioactive Waste.....	18
1.2.1.1	Current management of HLW .....	19
1.2.1.2	Current management of LLW .....	19
1.2.1.3	Current management of ILW .....	20
1.2.2	Long-term solution for the UK's radioactive waste disposal .....	20
1.2.3	Phased Geological Repository Concept (PGRC) .....	21
1.2.4	Post-Closure Repository Safety Concerns.....	22
1.3	Past Research .....	24
1.3.1	Cellulose Degradation .....	24
1.3.2	Solubility and Sorption Studies .....	28
1.3.3	Kinetic studies and their use in modelling .....	30
1.3.4	Stability of ISA.....	36
1.3.5	ISA Sorption.....	36
1.3.6	Previous work on ISA .....	37
1.3.7	Preparation of ISA .....	38

1.3.7.1	Preparation of $\alpha$ -ISA .....	38
1.3.7.2	Previous methods for the production of $\beta$ -ISA .....	38
1.4	Method of analysis used for monitoring ISA production and CDP formation: HPAEC–PAD .....	40
1.4.1	Separation mechanism .....	41
1.4.2	Mobile phase .....	42
1.4.3	Stationary phase .....	42
1.4.4	Pulsed Amperometric Detection (PAD) .....	43
1.4.5	Development of pulsed waveforms .....	43
1.5	Aims and objectives .....	45
2	Experimental Methods .....	47
2.1	General Reagents .....	47
2.2	General Analytical Procedures .....	47
2.2.1	HPAEC–PAD .....	47
2.2.2	NMR .....	48
2.2.3	GC–MS .....	48
2.2.4	High resolution mass spectrometry (HRMS) .....	48
2.2.5	Total Organic Carbon (TOC) .....	48
2.2.6	Measurement of pH .....	49
2.3	Degradation Experiments – Investigating methods to maximise the production of crude beta ISA .....	49
2.3.1	Degradation of cellulose in NaOH at RT, 50 °C or 90 °C .....	49
2.3.2	Degradation of cellulose in Ca(OH) <sub>2</sub> at RT, 50 °C, and 90 °C .....	49
2.3.3	Degradation of cellulose in either Ca(OH) <sub>2</sub> , NaOH or a mixture of Ca(OH) <sub>2</sub> and NaOH at 90 °C .....	49
2.3.4	Extraction of unreacted solid from cellulose degradation experiments .....	50
2.3.5	Monitoring cellulose degradation reactions using HPAEC-PAD .....	50
2.3.6	Analysis of cellulose degradation samples using HPIEC .....	50

2.3.7	Total Organic Carbon Analysis of cellulose degradation samples.....	51
2.4	Preparative Methods .....	51
2.4.1	Preparation of Calcium 2-C-(hydroxymethyl)-3-deoxy-D-erythro- pentonate $\text{Ca}(\alpha\text{-ISA})_2 - (\alpha\text{-ISA})$ .....	51
2.4.1.1	GC-MS: determination of fragmentation pattern for characterisation of $\text{Ca}(\text{ISA})_2$	52
2.4.1.2	NMR analysis of $\text{Ca}(\text{ISA})_2$ .....	53
2.4.1.3	High resolution mass spectrometry (HRMS) of $\text{Ca}(\text{ISA})_2$ .....	53
2.4.1.4	HPAEC-PAD: – determination of retention time ( $t_r$ ) and linear range .	53
2.4.2	Preparation of 2-C-(hydroxymethyl)-3-deoxy-D-erythro-pentono-1,4- lactone – ( $\alpha\text{-ISA}_L$ ) .....	53
2.4.2.1	NMR analysis of $\alpha\text{-ISA}_L$ .....	54
2.4.2.2	High resolution mass spectrometry (HRMS)of $\alpha\text{-ISA}_L$ .....	54
2.4.2.3	HPAEC-PAD analysis of $\alpha\text{-ISA}_L$ – determination of purity .....	54
2.4.3	Ethanol solubility tests on liquors produced from the preparation of $\text{Ca}(\alpha\text{-}$ $\text{ISA})_2$	54
2.4.4	Preparation of 3,4-dihydroxybutanoic acid (DHB) .....	55
2.4.4.1	GC-MS: determination of fragmentation pattern for characterisation of DHB	56
2.4.4.2	NMR analysis of DHB .....	56
2.4.4.3	HPAEC-PAD analysis of DHB – determination of purity and retention time ( $t_r$ )	57
2.4.5	Preparation of 2-C-(hydroxymethyl)-3-deoxytetronic acid (xyloisosaccharinic acid, X-ISA).....	57
2.4.5.1	GC-MS: determination of fragmentation pattern for characterisation of X-ISA	58
2.4.5.2	NMR analysis of X-ISA .....	58
2.4.5.3	HPAEC-PAD analysis of X-ISA – determination of purity and the retention time ( $t_r$ ) .....	58

2.5	Preparation of crude beta ISA ( $\beta$ -ISA)	59
2.5.1	Preparation of crude $\beta$ -ISA using existing methods	59
2.5.2	Preparation of crude $\beta$ -ISA with optimised conditions	59
2.5.3	Preparation of crude $\beta$ -ISA using microwave heating	60
2.5.4	Preparation of crude $\beta$ -ISA using microwave heating using either 0.5 M or 5.0 M NaOH	60
2.6	Isolation of 2-C-(hydroxymethyl)-3-deoxy-D-threo-pentanoic acid ( $\beta$ -ISA)	61
2.6.1	Soxhlet Extraction followed by short-path distillation	61
2.6.2	Isolation of $\beta$ -ISA using preparative anion exchange chromatography	61
2.6.3	Isolation of $\beta$ -ISA using automated preparative anion exchange chromatography	62
2.6.4	Isolation of $\beta$ -ISA using derivatisation followed by normal phase chromatography	64
2.6.4.1	Acetylation of crude $\beta$ -ISA	64
2.6.4.2	Normal phase chromatography	64
2.6.4.3	Removal of acetyl groups	65
2.6.4.4	Benzoylation of crude $\beta$ -ISA – final procedure	66
2.6.4.5	Purification of the 2,5,6-tri- <i>O</i> -benzoyl-isosaccharino-1,4-lactones	66
2.6.4.6	NMR analysis of 2,5,6-tri- <i>O</i> -benzoyl- $\beta$ -isosaccharino-1,4-lactone ( $\beta$ -ISA tribenzoate)	68
2.6.4.7	High resolution mass spectrometry (HRMS) of 2,5,6-tri- <i>O</i> -benzoyl- $\beta$ -isosaccharino-1,4-lactone ( $\beta$ -ISA tribenzoate)	68
2.6.4.8	NMR analysis of 2,5,6-tri- <i>O</i> -benzoyl- $\alpha$ -isosaccharino-1,4-lactone ( $\alpha$ -ISA tribenzoate)	68
2.6.4.9	High resolution mass spectrometry (HRMS) of 2,5,6-tri- <i>O</i> -benzoyl- $\alpha$ -isosaccharino-1,4-lactone ( $\alpha$ -ISA tribenzoate)	69
2.6.4.10	Removal of benzoyl groups	69
2.6.4.11	NMR analysis of sodium 2-C-(hydroxymethyl)-3-deoxy-D-threo-pentionate ( $\beta$ -ISA)	69

2.6.4.12	High resolution mass spectrometry (HRMS) of sodium 2-C-(hydroxymethyl)-3-deoxy-D-threo-pentionate ( $\beta$ -ISA) .....	70
2.6.4.13	Preparation of 2-C-(hydroxymethyl)-3-deoxy-D-threo-pentono-1,4-lactone – ( $\beta$ -ISA <sub>L</sub> ).....	70
2.6.4.14	NMR analysis of 2-C-(hydroxymethyl)-3-deoxy-D-threo-pentono-1,4-lactone – $\beta$ -ISA <sub>L</sub> .....	70
2.6.4.15	High resolution mass spectrometry (HRMS) of 2-C-(hydroxymethyl)-3-deoxy-D-threo-pentono-1,4-lactone – $\beta$ -ISA <sub>L</sub> .....	71
2.6.4.16	Preparation of Calcium 2-C-(hydroxymethyl)-3-deoxy-D-threo-pentionate Ca( $\beta$ -ISA) <sub>2</sub> – ( $\beta$ -ISA).....	71
2.6.4.17	NMR analysis of Calcium 2-C-(hydroxymethyl)-3-deoxy-D-threo-pentionate Ca( $\beta$ -ISA) <sub>2</sub> – ( $\beta$ -ISA).....	71
2.6.4.18	High resolution mass spectrometry (HRMS) of Calcium 2-C-(hydroxymethyl)-3-deoxy-D-threo-pentionate Ca( $\beta$ -ISA) <sub>2</sub> – ( $\beta$ -ISA).....	71
2.7	Investigating the physical properties of $\beta$ -ISA and $\alpha$ -ISA in aqueous solution ...	72
2.7.1.1	Determination of the aqueous $pK_a$ of $\beta$ -ISA using <sup>13</sup> C NMR spectroscopy .....	72
2.7.2	Determination of the rate of the base catalysed conversion of ISA <sub>L</sub> to ISAH	73
2.7.3	Determination of the rate of the acid catalysed conversion of ISAH to ISA <sub>L</sub>	73
3	Degradation of cellulose: attempts to maximise the solution concentration of $\beta$ -ISA solution .....	74
3.1	Introduction.....	74
3.2	Preparation of an analytical standard of $\alpha$ -ISA and characterisation of $\alpha$ -ISA using HPAEC-PAD, NMR, GC-MS and HRMS.....	75
3.2.1	Characterisation of $\alpha$ -ISA.....	75
3.2.1.1	Characterisation of $\alpha$ -ISA by NMR .....	75
3.2.1.2	Characterisation of $\alpha$ -ISA by GC-MS.....	76

3.2.1.3	Characterisation of $\alpha$ -ISA by HPAEC–PAD .....	77
3.2.2	Preparation and characterisation of $\alpha$ -ISA <sub>H</sub> and $\alpha$ -ISA <sub>L</sub> .....	77
3.2.2.1	HPAEC-PAD analysis of $\alpha$ -ISA <sub>H</sub> and $\alpha$ -ISA <sub>L</sub> .....	80
3.2.3	Analysis of crude $\alpha$ -ISA solution .....	82
3.2.4	Ethanol solubility experiments – Attempts to preferentially precipitate one of the saccharinic acids using fractional precipitation .....	85
3.3	Optimisation of reaction conditions for the production of $\beta$ -ISA using cellulose as a substrate .....	89
3.3.1	Type of cellulose .....	89
3.3.2	Cellulose loading .....	91
3.3.3	Reaction temperature .....	92
3.3.4	Anaerobic conditions .....	92
3.3.5	Concentration of alkaline solution.....	93
3.4	Degradation of cellulose using sodium hydroxide solution.....	96
3.4.1	Identification of degradation products.....	96
3.4.2	Monitoring the production of $\alpha$ -ISA and $\beta$ -ISA using HPAEC-PAD.....	105
3.4.3	Determination of solution concentrations of $\alpha$ - and $\beta$ -ISA .....	106
3.5	Degradation of cellulose in calcium hydroxide solution .....	112
3.5.1	Identification of degradation products.....	112
3.5.2	Monitoring the production of $\alpha$ -ISA and $\beta$ -ISA using HPAEC-PAD due to the Ca(OH) <sub>2</sub> catalysed hydrolysis of cellulose .....	118
3.5.3	Monitoring the production of total organic carbon from the Ca(OH) <sub>2</sub> reactions.....	122
3.6	Degradation of cellulose using either Ca(OH) <sub>2</sub> , NaOH or a mixture of Ca(OH) <sub>2</sub> and NaOH at 90 °C.....	124
3.6.1	Monitoring the production of $\alpha$ -ISA and $\beta$ -ISA using HPAEC-PAD and the determination of the TOC.....	124

3.6.2	Extraction of unreacted solid produced in the cellulose degradation reactions	128
3.6.2.1	HPAEC-PAD analysis of extracted samples.....	128
3.6.2.2	TOC analysis of extracted samples .....	133
3.7	Summary and conclusion of results: production of ISA from the NaOH and Ca(OH) <sub>2</sub> reactions.....	137
3.8	Large scale cellulose degradation reaction using optimized conditions.....	139
3.9	Ongoing and future work to further reduce reaction time and increase solution concentration of β-ISA using microwave heating .....	140
4	Isolation of β-ISA.....	142
4.1	Introduction.....	142
4.2	Isolation of β-ISA using preparative anion exchange chromatography .....	143
4.3	Isolation of β-ISA using automated preparative anion exchange chromatography	149
4.4	Attempts to isolate β-ISA from cellulose degradation solutions using Soxhlet extraction followed by short-path distillation.....	155
4.5	Isolation of β-ISA using derivatisation followed by normal phase chromatography.....	162
4.5.1	Acetylation of crude β-ISA solution.....	163
4.5.2	Purification of 2,5,6-tri- <i>O</i> -acetyl-β-isosaccharino-1,4-lactone using normal phase chromatography; identification of impurities.....	164
4.5.3	Benzoylation of crude β-ISA solution.....	173
4.5.4	Purification of 2,5,6-tri- <i>O</i> -benzoyl-β-isosaccharino-1,4-lactone using normal phase chromatography.....	176
4.5.4.1	First isolation attempt.....	176
4.5.4.2	Removal of coloured impurities.....	179
4.5.4.3	Second isolation attempt .....	180
4.5.4.3.1	Short-path distillation of fractions 220 – 234: confirmation of the identification of DHB <sub>L</sub> and THP <sub>L</sub> .....	186

4.5.4.4	Extraction of collected fractions with saturated sodium carbonate solution: removal of benzoic acid.....	188
4.5.4.5	Final isolation procedure.....	190
5	Physical properties of $\beta$ -ISA in aqueous solution.....	195
5.1	Determination of the aqueous $pK_a$ of $\beta$ -ISA using $^{13}\text{C}$ NMR spectroscopy.....	195
5.1.1	Introduction.....	195
5.1.2	Results: the determination of the aqueous $pK_a$ of $\beta$ -ISA.....	197
5.2	Studies of the inter-conversion between $\beta$ -ISAH and $\beta$ -ISA <sub>L</sub> .....	202
5.2.1	The base catalysed conversion of ISA <sub>L</sub> to ISAH.....	202
5.2.2	The acid catalysed conversion of ISAH to ISA <sub>L</sub> .....	212
6	General Summary and Conclusions.....	222
6.1	Degradation of cellulose: attempts to maximise the solution concentration of $\beta$ -ISA solution.....	222
6.1.1	Future work related to the production of $\beta$ -ISA.....	227
6.2	Isolation of $\beta$ -ISA.....	229
6.2.1	Future work related to the isolation of $\beta$ -ISA.....	232
6.3	Physical properties of $\beta$ -ISA in aqueous solution.....	233
6.3.1	Future work related to further studies involving $\beta$ -ISA.....	236
6.4	Publications related to this thesis.....	237
7	References.....	238
8	Publications.....	246

## List of Figures

Figure 1: Molecular structure of cellulose, adapted from the work of Klemm <i>et al.</i> <sup>5</sup> .....	2
Figure 2: 25 nm diameter rosette terminal cellulose synthesizing complex on the P-fracture face of elongating epicotyls cells of Azuki bean, after immunogold labelling; adapted from the work of Itoh and Kimura <sup>15</sup> .....	3
Figure 3: An illustration of the biosynthesis of cellulose, recreated from the review by Gomez <i>et al.</i> <sup>16</sup> .....	4
Figure 4: An illustration of the structure of cellulose adapted from the work of Gomez <i>et al.</i> <sup>16</sup> : cellulose chains aggregate to form microfibrils; microfibrils aggregate to form macrofibrils and macrofibrils combine to form cellulose fibres. ....	5
Figure 5: A freeze-etch of secondary wall microfibrils, reproduced from Brown and Montezinos <sup>18</sup> .....	6
Figure 6: Cellulose microfibril, adapted from the work of Inagaki <i>et al.</i> <sup>29</sup> .....	7
Figure 7: The Segal method $(I_{002} - I_{AM})/I_{002}$ after subtracting a cellulose free background signal, adapted from the work of Park <i>et al.</i> <sup>33</sup> . The ‘peak’ at $I_{AM}$ represents the amorphous region and the peak at $I_{002}$ represents the intensity of the combined crystalline and amorphous regions, therefore the height of the $I_{AM}$ peak must be subtracted from the peak at $I_{002}$ to determine the intensity of the crystalline peak.....	8
Figure 8: Curvature and helicity witnessed in cultured bacterial cellulose <sup>45</sup> (top) and an illustration of the kinks in the chains caused by the fibril tightening <sup>53</sup> .....	9
Figure 9: SEM image of cellulose fibres showing their ribbon like structure (original image). ....	10
Figure 10: Intra- and inter-chain hydrogen bonding in the parallel cellulose I chains.....	11
Figure 11: Parallel arrangement of the individual chains of cellulose I, with the reducing ends situated on the right of each chain (hydrogen bonding not shown). ....	14
Figure 12: Anti-parallel arrangement of the individual chains of cellulose II. The reducing end of each chain alternates in its direction between adjacent chains (hydrogen bonding not shown). ....	14
Figure 13: Inter and Intra-chain hydrogen bonding in cellulose I (left) and cellulose II (right), adapted from the review by Kontturi <i>et al.</i> <sup>10</sup> .....	15
Figure 14: The six known cellulose polymorphs and how they interconvert, adapted from the review by O’Sullivan <sup>32</sup> .....	16

Figure 15: Low Level Waste Repository (LLWR), Cumbria. England .....	19
Figure 16: An ILW storage facility <sup>92</sup> .....	20
Figure 17: An illustration of a generic deep geological repository designed for the United Kingdom's higher activity radioactive waste <sup>91</sup> .....	22
Figure 18: The peeling reaction.....	25
Figure 19: The stopping reaction.....	26
Figure 20: The open-chain and lactone forms of ISA .....	37
Figure 21: Quadrupole waveform utilised by the ED40 detector, modified from Dionex technical note 21 <sup>161</sup> .....	45
Figure 22: Synthesis and isolation of the sodium- $\beta$ -isosaccharinate.....	72
Figure 23: <sup>1</sup> H NMR spectrum of the calcium salt of $\alpha$ -ISA .....	75
Figure 24: GC-MS electron impact ionisation spectrum of $\alpha$ -ISA.....	76
Figure 25: <sup>1</sup> H NMR spectra of $\alpha$ -Ca(ISA) <sub>2</sub> (bottom) and $\alpha$ -ISAH (top).....	78
Figure 26: <sup>1</sup> H spectrum of $\alpha$ -ISA <sub>L</sub> .....	79
Figure 27: HPAEC-PAD chromatograms of the Ca( $\alpha$ -ISA) <sub>2</sub> , (left), the crystalline $\alpha$ -ISAH (centre) and a combined sample of Ca(ISA) <sub>2</sub> /ISA <sub>L</sub> (250 ppm) indicating a single peak, (right). .....	80
Figure 28: Calibration curve of $\alpha$ -ISA using HPAEC-PAD .....	81
Figure 29: HPAEC-PAD chromatogram of the crude $\alpha$ -ISA solution before the removal of any Ca( $\alpha$ -ISA) <sub>2</sub> . .....	82
Figure 30: <sup>13</sup> C NMR spectrum of the crude alpha ISA sample .....	84
Figure 31: HPAEC-PAD chromatogram of the filtrate following the precipitation of $\alpha$ -ISA, showing that large quantities of $\alpha$ -ISA are still present in the solution.....	85
Figure 32: The proposed yellow anion produced in cellulose degradation reactions. ....	86
Figure 33: Graph showing ISA and MSA peak areas as a function of ethanol concentration in the remaining crude $\alpha$ -ISA solution .....	87
Figure 34: Graph to show the ratio of MSA to ISA against % ethanol solution.....	88
Figure 35: The formation of the cellulose enolate anion.....	94
Figure 36: HPAEC-PAD chromatograms of (a) RT, (b) 50 °C and (c) 90 °C sodium hydroxide reactions.....	96
Figure 37: HPAEC-PAD chromatogram of crude $\beta$ -ISA solution (left) and the same solution after being eluted through a preparative anion exchange column resulting in the partial isolation of $\beta$ -ISA (right). .....	97

Figure 38: HPAEC chromatogram from Glaus <i>et al.</i> of the degradation of cellulosic materials with unknown peak No.4 .....	97
Figure 39: <sup>1</sup> H NMR spectrum of partially separated β-ISA (labelled peaks) and also the presence of additional peaks (yellow circles).....	98
Figure 40: COSY NMR spectrum allowing for the identification of 3,4-dihydroxybutano-1,4-lactone .....	98
Figure 41: Diagram showing the action of NaOH on 4-deoxy-2,3-hexodiulose, adapted from the results of Machell and Richards <sup>130</sup> .....	99
Figure 42: Comparison between the <sup>1</sup> H NMR spectrum of the synthesised 3,4-dihydroxybutanoic acid and the additional peaks in the cellulose degradation sample. ...	100
Figure 43: Cellulose degradation sample before (left) and after being spiked with 3,4-dihydroxybutanoic acid. ....	101
Figure 44: HPAEC-PAD chromatograms comparing the production of DHB under anaerobic (left) and aerobic conditions (right) when cellulose is degraded using NaOH (2 M) at 90 °C for 72 h. ....	102
Figure 45: HPAEC chromatograms comparing the production of 3,4-dihydroxybutanoic acid under anaerobic (left) and aerobic conditions (right) when cellulose is degraded using Ca(OH) <sub>2</sub> (saturated soln.) at 90 °C for 16 h.....	104
Figure 46: Structure of X-ISA .....	104
Figure 47: HPAEC chromatogram of a cellulose degradation sample (left) and after being spiked with xyloisosaccharinic acid (XISA). ....	105
Figure 48: HPAEC-PAD chromatogram of alpha and beta ISA (both 50 ppm). ....	106
Figure 49: Time course for the production of β-ISA (ppm) for the sodium hydroxide catalysed degradation of cellulose at RT, 50 °C and 90 °C (lines are a guide for the eye only).....	108
Figure 50: Time course for the production of α-ISA (ppm) for the sodium hydroxide catalysed degradation of cellulose at 50 °C and 90 °C (lines are a guide for the eye only). ....	108
Figure 51: Time course for the production of α-ISA and β-ISA (ppm) for the sodium hydroxide catalysed degradation of cellulose at either 90 °C (top) or 50 °C (bottom) (lines are a guide for the eye only). ....	110
Figure 52: HPIEC chromatogram of the solution produced from the degradation of cellulose at 90 °C using NaOH (2 M) solution.....	111

Figure 53: Example of a HPAEC-PAD chromatogram produced from the degradation of cellulose using saturated calcium hydroxide solution. ....	113
Figure 54: The base catalysed formation of MSA from the 3-deoxy-D-glucosone intermediate, R = the cellulose chain .....	114
Figure 55: Possible methods for the release of MSA into solution: via alkaline hydrolysis at the non-reducing end of the cellulose chain (top, left), resulting in the release of a glucose monomer which can react with base to produce MSA, or hydrolysis at the glycosidic linkage of an alkali stable end-group (top, right), directly releasing MSA into solution. ....	115
Figure 56: Mechanism to account for the production of free MSA during the peeling reaction <sup>193</sup> .....	116
Figure 57: Time course for the production of MSA (ppm) for the calcium hydroxide catalysed degradation of cellulose at RT, 50 °C and 90 °C (lines are a guide for the eye only).....	118
Figure 58: Time course for the production of β-ISA (ppm) for the calcium hydroxide catalysed degradation of cellulose at RT, 50 °C and 90 °C (lines are a guide for the eye only).....	119
Figure 59: Time course for the production of α-ISA (ppm) for the calcium hydroxide catalysed degradation of cellulose at RT, 50 °C and 90 °C (lines are a guide for the eye only).....	119
Figure 60: Time course for the production of TOC (mg L <sup>-1</sup> ) produced from the calcium hydroxide catalysed degradation of cellulose at RT, 50 °C and 90 °C. ....	123
Figure 61: Time course for the production of β-ISA (ppm) generated from the degradation of cellulose at 90 °C using either saturated Ca(OH) <sub>2</sub> soln., NaOH (2 M) or using both saturated Ca(OH) <sub>2</sub> soln. and NaOH (2 M). ....	125
Figure 62: Time course for the production of α-ISA (ppm) generated from the degradation of cellulose at 90 °C using either saturated Ca(OH) <sub>2</sub> soln., NaOH (2 M) or using both saturated Ca(OH) <sub>2</sub> soln. and NaOH (2 M). ....	126
Figure 63: Time course for the production of TOC (mg L <sup>-1</sup> ) produced from the degradation of cellulose at 90 °C using either NaOH (2 M) or using both saturated Ca(OH) <sub>2</sub> soln. and NaOH (2 M). ....	127
Figure 64: HPAEC-PAD generated time course for the concentration of ISA which was extracted from unreacted solid material present in samples produced from the Ca(OH) <sub>2</sub> catalysed degradation of cellulose at 90 °C.....	129

Figure 65: HPAEC-PAD generated time course for the concentration of ISA which was extracted from unreacted solid material present in samples produced from the NaOH catalysed degradation of cellulose at 90 °C.....	130
Figure 66: HPAEC-PAD generated time course for the concentration of ISA which was extracted from unreacted solid material present in samples produced from the mixed Ca(OH) <sub>2</sub> /NaOH catalysed degradation of cellulose at 90 °C.....	130
Figure 67: HPAEC-PAD generated time courses for the concentration of β-ISA (top) and α-ISA (bottom) which was extracted from unreacted solid material present in samples produced from the Ca(OH) <sub>2</sub> , NaOH or mixed Ca(OH) <sub>2</sub> /NaOH catalysed degradation of cellulose at 90 °C (lines are a guide for the eye only).....	131
Figure 68: Time course for the production of TOC (mg L <sup>-1</sup> ) from the extraction of unreacted solid material which was produced from the degradation of cellulose at 90 °C using either saturated Ca(OH) <sub>2</sub> soln., NaOH (2 M) or using both saturated Ca(OH) <sub>2</sub> soln. and NaOH (2 M) (lines are a guide for the eye only).....	133
Figure 69: Time course for the production of TOC (mg L <sup>-1</sup> ) from the degradation of cellulose at 90 °C using either saturated Ca(OH) <sub>2</sub> soln., NaOH (2 M) or using both NaOH and saturated Ca(OH) <sub>2</sub> soln. with the extraction results also added.....	138
Figure 70: Time course for the production of β-ISA, as indicated by the ratio of β-ISA peak area to ribonic acid (IS) peak area for the sodium hydroxide catalysed degradation of cellulose using conventional heating at 90 °C (diamonds) and microwave heating at reflux (squares). .....	141
Figure 71: The tribenzoate lactone which was isolated by Feast <i>et al.</i> (left) and the open-chain tetrabenzoate which was isolated by Whistler and BeMiller (right).....	142
Figure 72: <sup>1</sup> H NMR spectrum of lyophilised fractions which were collected from the preparative anion exchange chromatography of crude β-ISA solution. ....	146
Figure 73: <sup>1</sup> H NMR spectra showing the base catalysed transformation of β-ISA <sub>L</sub> (bottom spectrum) to the open-chain form of β-ISA (top spectrum) due to the addition of NaOD. ....	147
Figure 74: H3 protons from the <sup>1</sup> H spectra of α-ISA (top) and β-ISA (bottom).....	148
Figure 75: <sup>1</sup> H NMR spectra of the fractions collected from the first attempt to isolate β-ISA using automated preparative anion exchange chromatography, the spectrum indicates a mixture of β-ISAL and ISA open-chain form.....	150
Figure 76: Base hydrolysis of β-ISA <sub>L</sub> in the presence of NaOH solution to produce sodium isosaccharinate.....	150

Figure 77: <sup>1</sup> H NMR spectra of the fractions collected from the first attempt to isolate β-ISA using automated preparative anion exchange chromatography. Following a slow evaporation, the collected fractions (pH 7) transformed into the open-chain form of β-ISA, which also contains sodium acetate (bottom). <sup>1</sup> H NMR chromatogram of β-ISA <sub>L</sub> after eluting through a cation exchange column, which also indicates that sodium acetate has been removed (top).....	152
Figure 78: The open-chain form of β-ISA which also contains acetate .....	153
Figure 79: <sup>1</sup> H NMR chromatogram of isolated β-ISA <sub>L</sub> .....	154
Figure 80: <sup>1</sup> H NMR spectrum of the crude material before being applied to short-path distillation, with key resonances labelled. ....	157
Figure 81: The <sup>1</sup> H NMR spectrum of fraction number 1, after short-path distillation of crude β-ISA solution where the maximum temperature was 150 °C (bottom spectrum); which is compared with the spectra of β-ISA <sub>L</sub> (red), α-ISA <sub>L</sub> (green) and 3,4-dihydroxybutano-1,4-lactone (purple).....	159
Figure 82: A section of the <sup>1</sup> H NMR spectrum showing specific resonances which indicate that equal amounts of β-ISA and 3,4-dihydroxybutano-1,4-lactone were present in fraction 2, produced from the short-path distillation of crude β-ISA solution at 150 °C .....	160
Figure 83: <sup>1</sup> H NMR spectrum of fraction 2 collected from the short-path distillation of crude β-ISA solution which indicates a mixture of α- and β-ISA <sub>L</sub> .....	161
Figure 84: HPAEC-PAD chromatogram of β-ISA solution before short-path distillation (left) and fraction two after short path distillation (right) .....	161
Figure 85: Fraction 3 from the 1st short-path distillation attempt indicating that large amounts of 3,4-dihydroxybutano-1,4-lactone was present in the fraction. ....	162
Figure 86: Derivatisation of β-ISA <sub>L</sub> into its tri-acetate or tri-benzoate esters.....	163
Figure 87: <sup>1</sup> H NMR spectrum of the acetylated syrup .....	164
Figure 88: <sup>1</sup> H NMR spectrum of the collected fractions from the first normal phase column (bottom) and the spectrum of the un-fractionated sample (top). ....	165
Figure 89: <sup>1</sup> H NMR of collected fractions 80 - 89 which also indicate that several impurity products are also present (circled resonances). ....	166
Figure 90: COSY NMR spectrum of the collected fractions 80 - 89, which allowed for the identification of two unknown compounds. ....	167
Figure 91: <sup>1</sup> H NMR spectra showing the elution order of five acetylated compounds from the column of the acetylated crude β-ISA solution. ....	169

Figure 92: <sup>1</sup> H NMR spectrum of the combined fractions (90 - 119) showing only minor amounts of THP <sub>L</sub> being present (ringed) and no indication of any DHB <sub>L</sub> .....	170
Figure 93: <sup>1</sup> H NMR spectrum of the β-ISA sodium salt which was isolated using normal phase chromatography.....	172
Figure 94: <sup>1</sup> H NMR spectrum of tribenzoylated α-ISA <sub>L</sub> .....	173
Figure 95: <sup>1</sup> H NMR spectra showing the C3 methylene resonances of tribenzoylated α- and β-ISA <sub>L</sub> .....	174
Figure 96: <sup>1</sup> H NMR spectra of crude benzoylated ISA lactones and the <sup>1</sup> H NMR spectra of benzoic acid, inset.....	175
Figure 97: <sup>1</sup> H NMR spectrum of the isolated mixture of α- and β-ISA tribenzoate esters.....	177
Figure 98: <sup>1</sup> H NMR spectrum of tribenzoylated β-ISA <sub>L</sub> .....	179
Figure 99: COSY NMR spectrum of fractions 5 - 8 indicating the presence of 2,5-dihydropentanoic acid and the tentative indication of 2,3-dideoxypentonic acid. ....	182
Figure 100: <sup>1</sup> H NMR spectrum of crude benzoylated syrup with the resonances representing THP <sub>L</sub> expanded which suggests that two diastereoisomers of THP are present. ....	184
Figure 101: <sup>1</sup> H NMR spectra showing the elution order of seven benzoylated compounds from the column of the benzoylated crude β-ISA solution after the removal of the coloured impurities.....	185
Figure 102: <sup>1</sup> H NMR spectra of un-distilled syrup produced from fractions 220 - 234 (bottom), and the distillate (centre) and the spectrum of a standard sample of benzoylated 3,4-dihydroxybutano-1,4-lactone (top).....	187
Figure 103: COSY NMR spectrum and structure of the dibenzoylated THP <sub>L</sub> .....	188
Figure 104: <sup>1</sup> H NMR spectrum of pure tribenzoylated β-ISA <sub>L</sub> .....	189
Figure 105: <sup>1</sup> H NMR spectra of combined fractions 1 to 4 which contained large amounts of benzoic acid (top spectrum) and following the extraction of the combined fractions using saturated sodium carbonate solution (bottom spectrum). ....	190
Figure 106: Single crystal X-ray structure of tribenzoylated β-ISA <sub>L</sub> (top) and tribenzoylated α-ISA <sub>L</sub> (bottom).....	193
Figure 107: <sup>1</sup> H NMR spectrum of sodium 2-C-(hydroxymethyl)-3-deoxy-D-threopentionate (β-ISA).....	194
Figure 108: <sup>13</sup> C NMR spectrum of a mixed sample of β-ISAH (acid) and β-ISA <sub>L</sub> (lac) ..	196
Figure 109: Structures of β-ISA <sup>-</sup> , β-ILA <sub>L</sub> and XISA.....	198

Figure 110: $^{13}\text{C}$ chemical shifts (ppm) of $\beta\text{-ISA}_L$ (bottom spectrum) and the deprotonated anion of $\beta\text{-ISA}$ (top spectrum).....	198
Figure 111: Variation of the $^{13}\text{C}$ chemical shifts of beta ISA's carbon resonances (C1 – C6) as a function of pD. Solid line represents the fit to the equation: $\delta(\text{pD})=\delta_{\text{acid}}+\delta_{\text{base}}[10^{\text{pD}}/(\text{K}_a+10^{\text{pD}})]$ . .....	201
Figure 112: $^1\text{H}$ NMR spectra showing the conversion of $\text{ISA}_L$ to $\text{ISA}^-$ at pD 8.14 (H3 resonances shown only).....	203
Figure 113: Graph showing the conversion of $\alpha\text{-ISA}_L$ to $\alpha\text{-ISA}^-$ at pD 8.14. ....	204
Figure 114: Normalised plots of the volume of base added (ml) over time (sec) to compensate for the fall in pH due to base hydrolysis of $\beta\text{-ISA}_L$ (top) and $\alpha\text{-ISA}_L$ (bottom). .....	205
Figure 115: Plots of $\ln[\text{Vol}_{\text{base}}]t$ verses time which provide a value of $-k_{\text{obs}}$ as the gradient for the base catalysed hydrolysis of $\beta\text{-ISA}_L$ (left) and $\alpha\text{-ISA}_L$ (right). .....	208
Figure 116: pH verses rate profile for the hydrolysis of $\alpha\text{-ISA}_L$ and $\beta\text{-ISA}_L$ at 25 °C.....	209
Figure 117: Plot of $[\text{OH}^-]$ versus $k_{\text{obs}}$ for the hydroxide catalysed hydrolysis of $\alpha\text{-ISA}_L$ and $\beta\text{-ISA}_L$ .....	210
Figure 118: Structures of valerolactone, butyrolactone and $\text{XISA}_L$ .....	211
Figure 119: Plots of the percentage of $\beta\text{-ISAH}$ (top) and $\alpha\text{-ISAH}$ (bottom) remaining in acidic solution as a function of time. ....	213
Figure 120: A general mechanism for the acid catalysed lactonization of $\text{ISAH}$ and lactone hydrolysis .....	214
Figure 121: Plots of $\ln\{[\text{ISAH}]_t - [\text{ISAH}]_{\text{eq}}/[\text{ISAH}]_0 - [\text{ISAH}]_{\text{eq}}\}$ versus time which provide a value of $-k_{\text{obs}} (k'_{\text{lac}} + k'_{\text{hyd}})$ as the gradient for the acid catalysed hydrolysis of $\alpha/\beta\text{-ISAH}$ . .....	217
Figure 122: pD verses rate profile for the lactonization of alpha and beta $\text{ISAH}$ at 25 °C .....	218
Figure 123: Plot of $[\text{D}^+]$ versus $k'_{\text{lac}}$ for the acid catalysed hydrolysis of alpha and beta $\text{ISA}$ lactones. ....	219

## List of Tables

Table 1: Experimental conditions for the crude $\alpha$ -ISA ethanol solubility experiments .....	55
Table 2: A comparison between experimental and literature NMR chemical shift data for $\alpha$ -ISA .....	76
Table 3: Mass of solid removed from the $\alpha$ -ISA solution as a function of aqueous ethanol concentration (v/v). Each sample (20 ml) contained 2.5 ml of crude $\alpha$ -ISA solution, deionised water and an appropriate volume of ethanol to produce the required concentration .....	87
Table 4: A summary of the cellulose degradation reaction conditions .....	95
Table 5: Summary of results from the degradation of cellulose using NaOH or Ca(OH) <sub>2</sub> as the base catalyst .....	139
Table 6: Summary of collected fractions from the second attempt to isolate triacetylated $\beta$ -ISA <sub>L</sub> using normal phase chromatography .....	169
Table 7: GC-MS results showing the quantity of triacetylated $\alpha$ - and $\beta$ -ISA as a percentage of the total amount of triacetylated ISA .....	170
Table 8: The percentage and magnitude of triacetylated $\alpha$ - and $\beta$ -ISA <sub>L</sub> in collected fractions, determined using GC-MS .....	171
Table 9: Summary of collected fractions from the first attempt to isolate tribenzoylated $\beta$ -ISA <sub>L</sub> using normal phase chromatography .....	178
Table 10: Summary of collected fractions from the second attempt to isolate tribenzoylated $\beta$ -ISA <sub>L</sub> using normal phase chromatography .....	185
Table 11: <sup>13</sup> C chemical shift values (ppm) for carbons 1 - 6 for $\beta$ -ISA as a function of pD .....	199
Table 12: Observed constants for the lactonization of ISAH at various reaction pDs at 25 °C .....	217

# 1 General Introduction

The current worldwide plan for long-term management of radioactive waste is deep geological disposal, with one resulting key area of interest being the interaction of water soluble cellulose degradation products with radioactive isotopes within underground repositories, and how these molecules might affect the safety of a repository after its closure.

This introductory chapter is intended to provide a general background to the properties of cellulose and how its wide spread general use within the nuclear industry has resulted in the accumulation of enormous amounts of cellulose-containing radioactive waste. A summary of the different types of radioactive waste, particularly in the U.K. will follow, and how the Government plans to manage this vast legacy of waste. Previous studies in this emerging field will be discussed, followed by an outline of the aims and objectives of this thesis in contributing to the growing bank of work in this area of research.

## 1.1 Cellulose

After nearly two hundred years of cellulose research, knowledge of its nature still remains incomplete <sup>1</sup>. Cellulose was first discovered and isolated from the cells of various green plants by Anselme Payen in 1838 during his work on plant cell purification. Payen discovered that an insoluble mass would remain after each experiment regardless of plant species; to which the empirical formula  $C_6H_{10}O_5$ , was assigned and the material was subsequently named as cellulose, literally meaning “sugar of cell walls”.

In the vast majority of plant species, cellulose is known to be the main constituent of cell walls, with its primary natural function being the protection of cells and the provision of structure and support (mainly in stalks, stems, trunks and all woody portions).

It was further discovered that cellulose is produced extracellularly, in a very pure form, by various bacterial species, but mainly *Acetobacter xylinum* which is seen to extrude cellulose ribbons into the growth media in cultured bacteria <sup>2-5</sup>. In *Acetobacter xylinum* it is thought that cellulose is produced as a protective shield from substances which may harm the bacteria <sup>2</sup>. Cellulose is also produced in various species of fungi, algae and a group of marine animals called tunicates <sup>3</sup> who secrete a cellulose “house” which the tunicate uses as both a shelter and a food filter. It has even been reported that cellulose is detectable, using

infrared techniques, in the molecular clouds of outer space <sup>4</sup>; with one hypothesis being that its presence is due to the polymerisation of interstellar formaldehyde <sup>4</sup>. So the quantity of cellulose could indeed be endless, but it is definitely the most abundant organic compound on earth; with billions of tonnes being produced in nature by the process of photosynthesis every year <sup>5,6</sup>.

### 1.1.1 Molecular Structure

Cellulose chains are constructed entirely from glucose residues and can be described as an unbranched linear homopolymer of D-anhydroglucopyranose units (AGU); with the repeating unit being the dimer cellobiose <sup>5,7</sup>. Each AGU is rotated by approximately 180 ° relative to the adjacent AGU and are linked together by  $\beta$ -(1-4)-glycosidic bonds <sup>5</sup> with each unit being in the <sup>4</sup>C<sub>1</sub> chair conformation (Figure 1), as determined by NMR measurements <sup>8</sup>.

The free hydroxyl groups and hydrogen atoms of the cellulose molecule are positioned equatorially and axially respectively along the polymer chain; and these and both the ring and bridging oxygen atoms are involved in hydrogen bonding, both intra and inter between adjacent molecules. These bonds form ordered hydrogen bonding systems which are relevant to the single-chain conformation and stiffness of the polymer, making it a water insoluble, tough material <sup>5,6</sup>; with a Young's modulus in the chain direction comparable to Kevlar <sup>9</sup>.

Each cellulose chain is directional, with the terminal AGU on one end being a closed ring (non-reducing end) and the other consisting of a reducing end where the AGU is an aliphatic structure with a carbonyl group in equilibrium with a cyclic hemiacetal <sup>10</sup> (Figure 1).

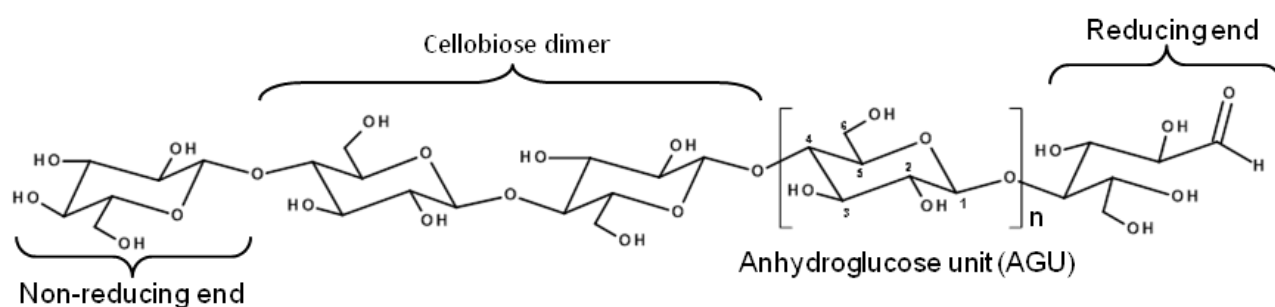


Figure 1: Molecular structure of cellulose, adapted from the work of Klemm *et al.* <sup>5</sup>

Although cellobiose is the repeating unit of cellulose, the molecular size of each chain, the average degree of polymerisation (DP), is actually based on the number of AGUs present; with the average molecular mass being determined by multiplying the DP by the molecular mass of a single AGU. The DP varies depending on, for example, the origin of the cellulose or the industrial treatment applied to it; with typical DPs ranging from hundreds in industrially processed celluloses to over ten thousand units for native cotton cellulose <sup>11</sup>. Commonly, the DP is determined using a viscometer after dissolution in a suitable solvent, with the viscosity of the solution being proportional to the DP <sup>5, 12</sup>; or using size exclusion chromatography (SEC) <sup>13</sup>.

### 1.1.2 Biosynthesis

The complicated process of cellulose biosynthesis is not fully known, however, the current understanding is that it occurs at or outside the plasma membrane <sup>14</sup>. Using scanning electron microscopy and various freeze-fracture <sup>15-17</sup> and immunogold labelling techniques <sup>15</sup>, groups of rosettes of particles with six-fold symmetry (known as terminal complexes, TC) have been witnessed in the plasma membrane (Figure 2).

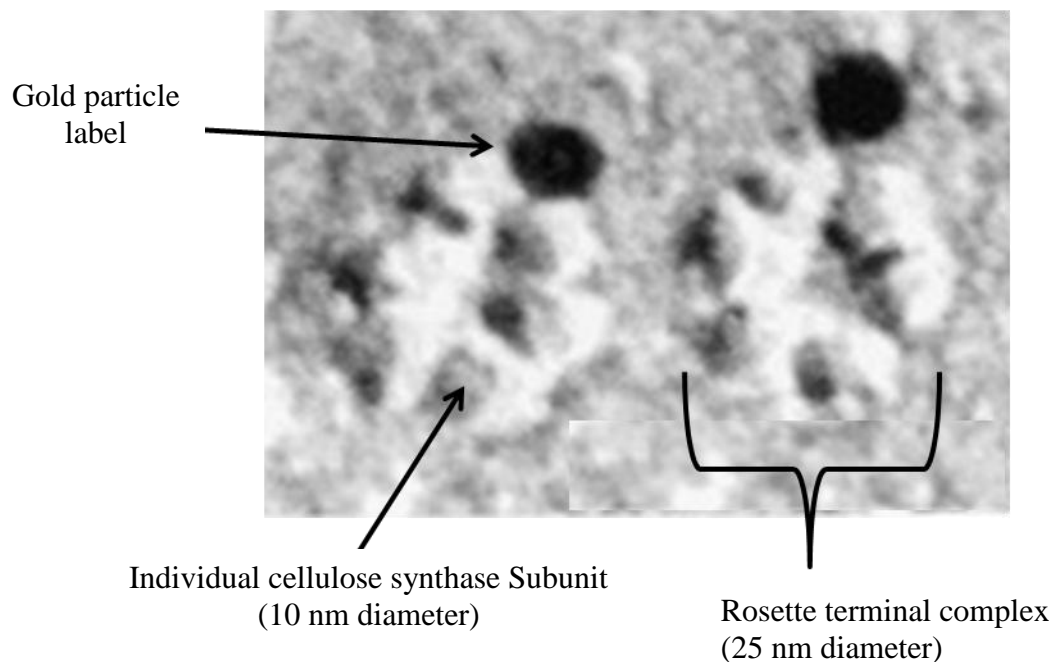


Figure 2: 25 nm diameter rosette terminal cellulose synthesizing complex on the P-fracture face of elongating epicotyls cells of Azuki bean, after immunogold labelling; adapted from the work of Itoh and Kimura <sup>15</sup>.

It is believed that these complexes are associated with the ends of cellulose microfibrils<sup>15</sup>, and it is thought that they are cellulose synthase (CeS) protein complexes, made up of smaller sub-units each of which have multiple catalytic sites able to elongate a single cellulose chain from UDP-glucose which is available from the cytoplasmic side of the membrane<sup>16</sup>. Each sub-unit is thought to synthesize six cellulose chains, which form sheets and the sheets associate to form the basic cellulose microfibril<sup>17, 18</sup> (Figure 3) which are held together by hydrogen bonding and Van der Waals forces<sup>19</sup>.

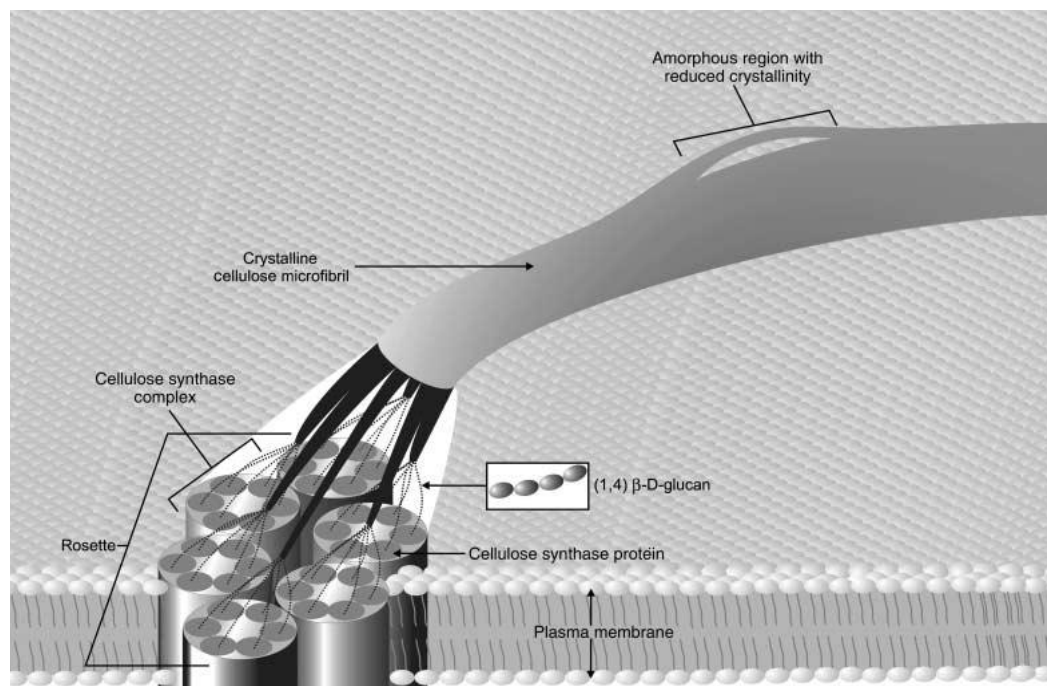


Figure 3: An illustration of the biosynthesis of cellulose, recreated from the review by Gomez *et al.*<sup>16</sup>.

The microfibrils are thought to be the lowest well-defined morphological entity. Research has indicated that the cellulose microfibril can range anywhere between 3 to 35 nm in diameter<sup>20</sup> depending on the source of cellulose. Within plant species the diameter is very constant, with one small angle X-ray scattering study indicating that in sprucewood all microfibrils are  $\approx 2.5$  nm, across hundreds of different tree samples from different locations<sup>21</sup>. Generally, the largest diameter of microfibrils are from animal and algal cellulose which are approximately 20 nm<sup>22</sup>.

Several hundred microfibrils group together to form larger fibril aggregates with a diameter of several micrometers<sup>3</sup>; which aggregate, held together primarily by another cell wall

polymer known as hemicellulose to form cellulose fibres (Figure 4) which are embedded in a matrix of a highly branched polymer of lignin <sup>23</sup>, all of which make what is known as lignocellulose.

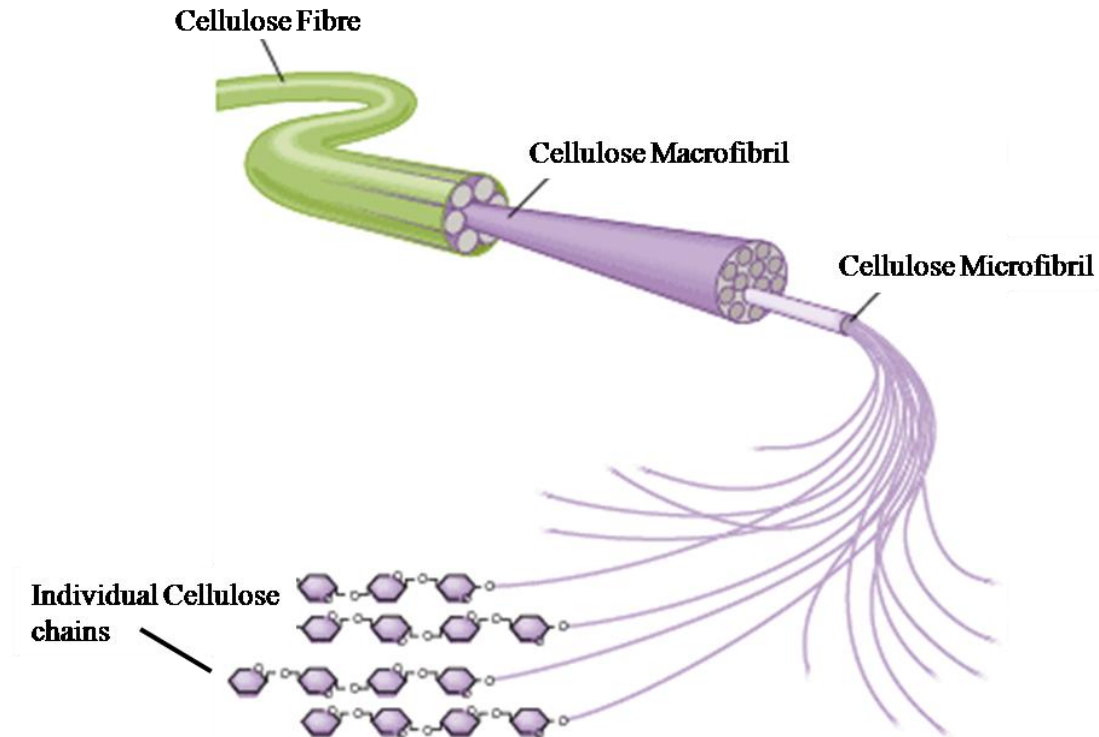


Figure 4: An illustration of the structure of cellulose adapted from the work of Gomez *et al.* <sup>16</sup>; cellulose chains aggregate to form microfibrils; microfibrils aggregate to form macrofibrils and macrofibrils combine to form cellulose fibres.

In plants, cellulose makes up the majority of the cell wall; initially a primary wall layer is formed which stabilises a young plant, whilst allowing continuous growth and development where individual cellulose chains are less ordered and running in all directions encrusted in a lignin matrix <sup>19,24</sup>. After the cell stops growing, a secondary layer is deposited, containing the grouped microfibrils in a parallel, densely packed arrangement, “criss crossing” each over (Figure 5) giving greater tensile strength to the material <sup>24</sup> and providing the mechanical strength and protection against microbial attack <sup>19</sup>.



Figure 5: A freeze-etch of secondary wall microfibrils, reproduced from Brown and Montezinos<sup>18</sup>.

### 1.1.3 Supramolecular Structure

Although cellulose is an unbranched homopolysaccharide, the popular view is that it can exist in varying solid state forms. A widely accepted two phased model “the fringed fibril model” of cellulose fibre morphology was first proposed by Hearle in 1958 in which it was stated that chains of native cellulose have regions of low order (amorphous) and regions of high order (crystalline) i.e. it is a semi-crystalline material (linear chains of cellulose run through several crystalline regions as well as amorphous ones (Figure 6). One research group determined that there were four or five disordered regions for every 300 crystalline ones<sup>25</sup> along the length of fibres. Other researchers claim that the amorphous regions are present on the surface of micro-fibrils and form a so called interface between neighbouring microfibrils<sup>26</sup>. It has been suggested that an intermediate paracrystalline form, which is crystallized, but unordered may also exist between the crystalline and amorphous regions<sup>27</sup>.

<sup>28</sup>.

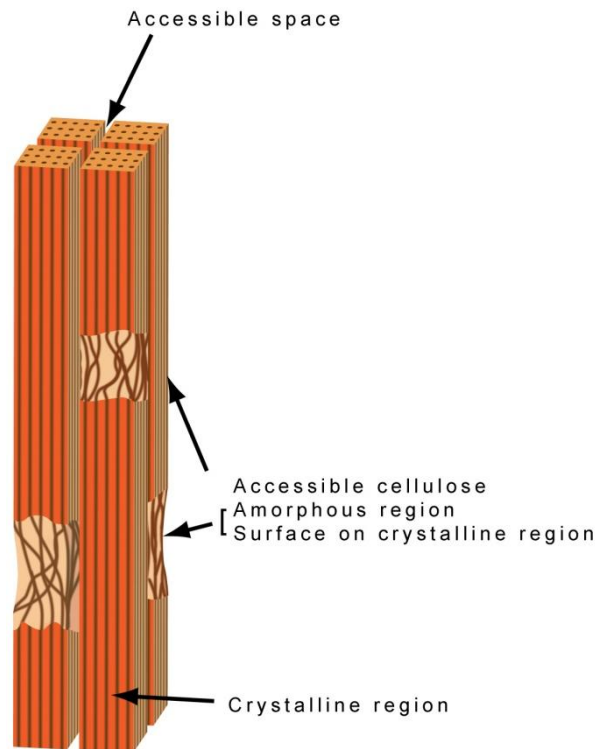


Figure 6: Cellulose microfibril, adapted from the work of Inagaki *et al.*<sup>29</sup>

The fractional amount of high order within cellulose, the crystallinity index (CI) affects the physical properties of the polymer; for example tensile strength, dimensional stability and density<sup>30, 31</sup> increase with a more crystalline form; but a decrease in flexibility, chemical reactivity and swelling due to the tightly packed chains are also observed<sup>32</sup>. The degree of crystallinity is dependent on the method of measurement,<sup>11</sup> previous research has found that various methods of CI determination offer significantly different levels of accuracy<sup>33</sup>, for example, Thygesen *et al.* determined that the CI of Avicel cellulose ranged between 39 % and 67 % depending on the technique of measurement used<sup>34</sup>. The treatment applied to the sample and the origin of the cellulose also affect the CI<sup>35</sup>.

Therefore, the CI has been studied by a number of research groups using a variety of analytical techniques such as: X-ray diffraction (XRD)<sup>33, 34, 36-38</sup>, FT- Raman spectroscopy<sup>32</sup>, FT-IR<sup>39</sup>, wide angle X-ray scattering (WAXS)<sup>40</sup> and solid state NMR<sup>33, 41, 42</sup>, with comparable results seen for all methods<sup>43</sup>. The particular aim of these techniques is to assign bands or peaks for the amorphous and crystalline regions which can then be used to determine a percentage or ratio of the two regions.

The X-ray diffraction “Segal” method (peak height method) is currently the most common method used to determine the degree of crystallinity due to its ease of use<sup>37</sup> and is based on the ratio of the height of the peak at 22.5 ° (2 θ) which represents both the crystalline and amorphous region (002 peak) and the height of the minimum ( $I_{AM}$ ) between the 002 peak and the 101 peak, located at approximately 18 ° (2 θ) which represents the amorphous region. Before calculating the ratio, the peak height which represents only the crystalline region is determined by subtracting, the height of the  $I_{AM}$  from the height of the 002 peak (Figure 7). This method is also criticised however, for being the most inaccurate method due to over estimating the amount of crystallinity<sup>33, 34</sup>.

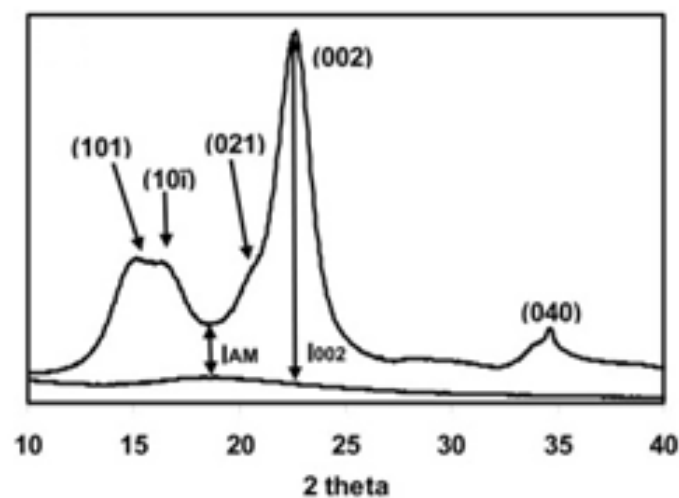


Figure 7: The Segal method  $(I_{002} - I_{AM})/I_{002}$  after subtracting a cellulose free background signal, adapted from the work of Park *et al.*<sup>33</sup>. The ‘peak’ at  $I_{AM}$  represents the amorphous region and the peak at  $I_{002}$  represents the intensity of the combined crystalline and amorphous regions, therefore the height of the  $I_{AM}$  peak must be subtracted from the peak at  $I_{002}$  to determine the intensity of the crystalline peak.

Muller *et al.* and Nishiyama *et al.* studied the amorphous material directly using neutron scattering<sup>25, 26</sup>, they found that the accessible hydroxyl hydrogen atoms of amorphous regions could be exchanged with deuterium ions whereas the OH groups of the crystalline regions were inaccessible to the deuterium. They were then able to distinguish between amorphous and crystalline regions due to the greater contrast between the accessible and crystalline regions due to the large difference in the scattering of neutrons by hydrogen and deuterium. They concluded that the amorphous regions were present on the surface of micro-fibrils and form a so called interface between neighbouring microfibrils<sup>26</sup>.

The fact that amorphous regions exist at all, is still under debate however. One leading cellulose expert (Atalla) hypothesises that native cellulose has right-handed curvature and helical character <sup>1</sup>, and the amorphous regions are actually due to the denaturing of crystalline regions caused by the process of sample preparation, which tightens the curvature, thus causing kinks in the chain <sup>44</sup>. This curvature and helical character has been witnessed in the work of Haigler *et al.* who cultured bacterial cellulose and analysed the fibrils by SEM which provided further evidence to support Atalla's hypothesis <sup>45</sup>.

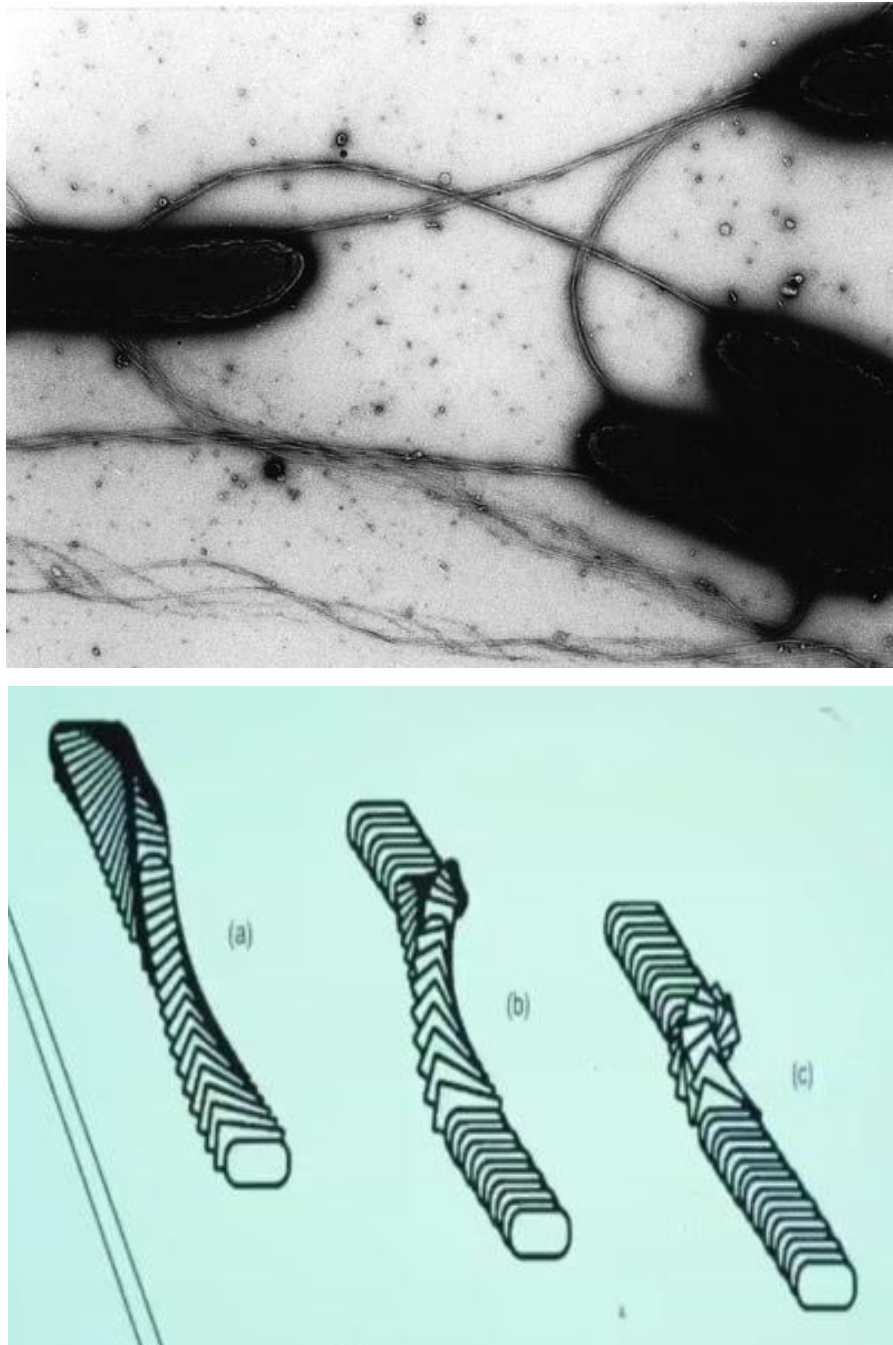


Figure 8: Curvature and helicity witnessed in cultured bacterial cellulose <sup>45</sup> (top) and an illustration of the kinks in the chains caused by the fibril tightening <sup>53</sup>

### 1.1.4 Cellulose polymorphs

Cellulose's linear form and the ability to form hydrogen bonds has enabled the polymer to crystallise in several ways; at the present time there are six known inter-convertible polymorphs of cellulose<sup>24</sup>; these being I, II, III<sub>I</sub>, III<sub>II</sub>, IV<sub>I</sub> and IV<sub>II</sub> based on the way that the individual cellulose polymers are hydrogen bonded together, resulting in differences in unit cell dimensions and chain polarity.

#### 1.1.4.1 Cellulose I

Cellulose I, is the type of cellulose biosynthesized in nature; early SEM studies on dried samples indicated that fibres were ribbon like structures, and not cylindrical (Figure 9)<sup>46</sup>.

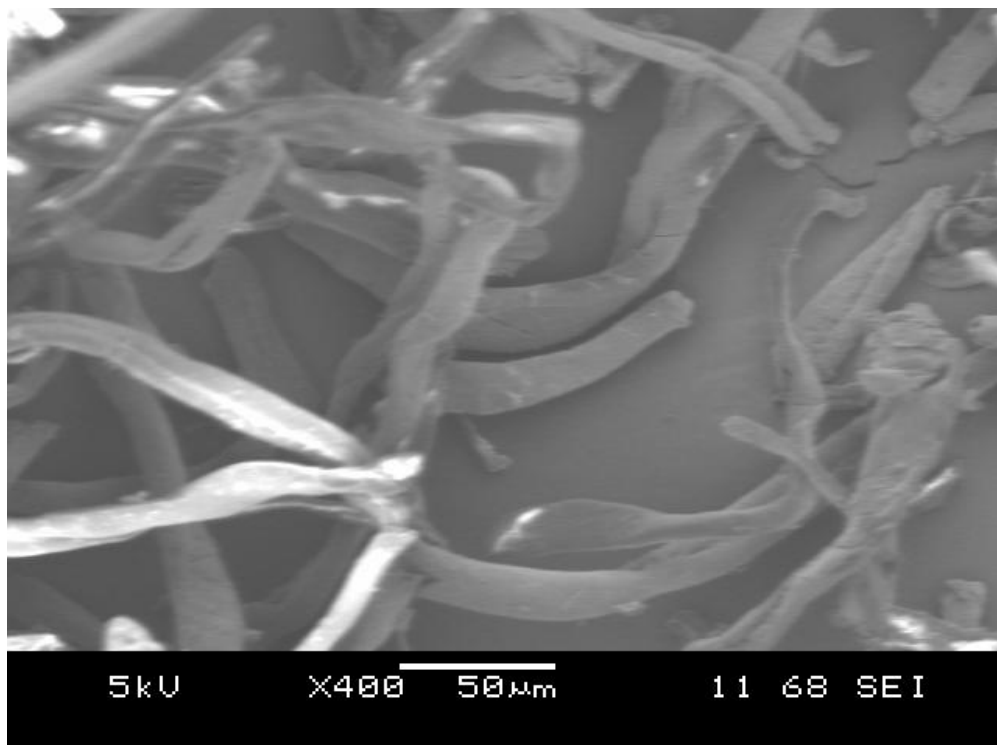


Figure 9: SEM image of cellulose fibres showing their ribbon like structure (original image).

X-ray and electron diffraction studies assumed that cellulose I consisted of parallel chains<sup>47, 48</sup> held together by intra-chain hydrogen bonds at (O3-H $\cdots$ O5) and (O2-H $\cdots$ O6) between adjacent AGUs and an inter-chain bond at (O6-H $\cdots$ O3)<sup>49</sup> between neighbouring chains forming sheets (Figure 10), with no hydrogen bonds between different sheets<sup>50</sup>, instead they are held together by Van der Waal's interactions<sup>47</sup>.

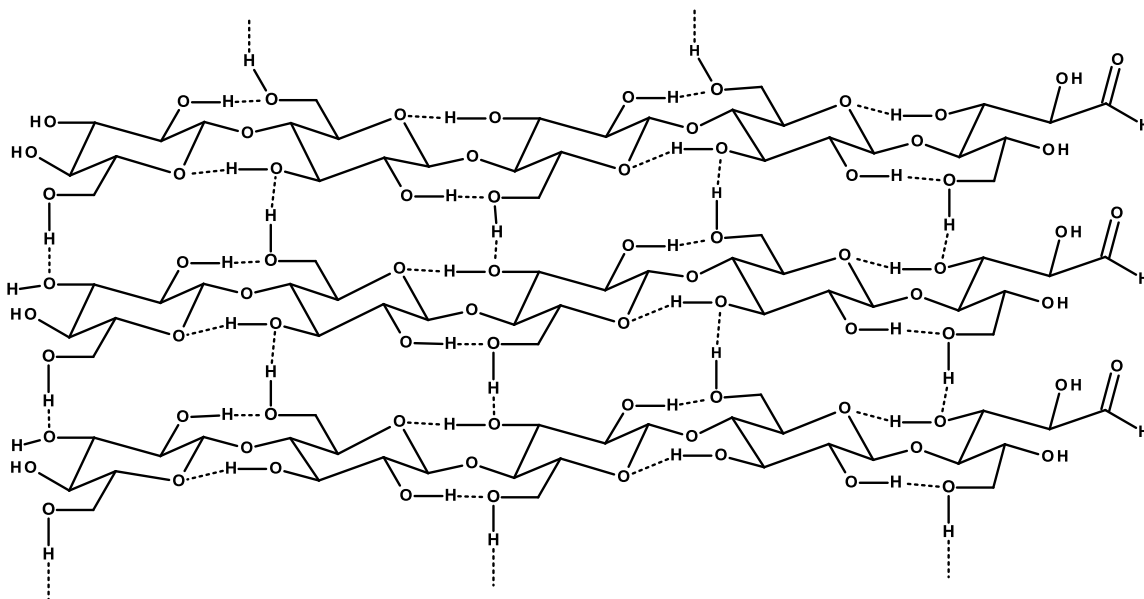


Figure 10: Intra- and inter-chain hydrogen bonding in the parallel cellulose I chains

Inconsistencies existed however between the various unit cell models from early crystal structures and proof of the direction of the chains<sup>47, 48, 51</sup>. The polarity of the chains was solved and determined as being parallel as indicated by the electron microscopy work of Hieta *et al.*<sup>52</sup> who used a staining technique which only reacted with reducing end groups, and discovered that only one end of the microfibril was stained across whole fibres; this was further confirmed by the work of Chanzy and Henrissat<sup>53</sup> who determined that the enzymatic degradation of cellulose only occurred from one end as indicated by the ‘sharpening’ of the ends of fibres as they were being peeled away layer by layer.

The inconsistencies with the crystal structure of cellulose I became clearer largely due to the work of Atalla *et al.* who were the first group to study cellulose by solid-state cross-polarization magic angle spinning carbon-13 nuclear magnetic resonance (CP/MAS <sup>13</sup>C NMR)<sup>7</sup>. In their work it was determined that cellulose I was sub-divided into two separate crystal structures; namely cellulose I $\alpha$  and I $\beta$  mainly due to observations that C-1 carbon atoms of the AGUs were displaying different resonant peaks for chemically equivalent carbons (a singlet for I $\alpha$  and a doublet for I $\beta$ ) indicating magnetically non-equivalent carbons due to a difference in hydrogen bonding in the glycosidic bonds; indicating that two forms were present<sup>54, 55</sup>.

Horii *et al.* further confirmed the presence of the two allomorphs by recording NMR spectra of the crystalline part separate from the amorphous part by using different  $^{13}\text{C}$  spin-lattice relaxation times, which were different for crystalline and non-crystalline portions so the amorphous spectra could effectively be deleted <sup>56</sup>.

The two allomorphs,  $1\alpha$  and  $1\beta$  can be within both the same sample and the same fibril making characterisation difficult <sup>57, 58</sup>, this became clearer however, when it was determined that  $1\alpha$  was meta-stable and could be converted to  $1\beta$ , by annealing at high temperatures in various media <sup>59, 60</sup>. This allowed for electron diffractograms to be obtained for a pure  $1\alpha$  sample (as found in a particular algae species), and then the sample could then be annealed, and a diffractogram of pure  $1\beta$  could be obtained <sup>58</sup>. It is hypothesised that there is more strain in the  $1\alpha$  structure, and that strain is released due to annealing, thus allowing for the  $1\beta$  form to form <sup>57</sup>. Molecular dynamics simulations have also shown that thermodynamically,  $1\beta$  is energetically favoured over  $1\alpha$  <sup>61</sup>.

The presence of the two allomorphs was further supported by the electron diffraction work of Sugiyama *et al.* <sup>57, 58</sup> and more recently by Nishiyama *et al.* using crystallographic studies <sup>22, 62</sup>. It is now commonly accepted that the  $1\alpha$  allomorph consists of a triclinic unit cell composed of one cellulose chain per unit cell and that  $1\beta$  is monoclinic with two cellulose chains per unit cell; with the main difference in the two allomorphs being a unidirectional axial shift between the cellulose sheets in the  $1\alpha$  model <sup>63</sup>.

Both cellulose allomorphs have (O3-H $\cdots$ O5) and (O2-H $\cdots$ O6) intrachain hydrogen bonds and interchain hydrogen bonds at (O6-H $\cdots$ O3) which are of different lengths and angles for both inter and intra chain bonds. There are no inter-sheet (O-H $\cdots$ O) hydrogen bonds for  $1\beta$  or  $1\alpha$  <sup>22, 62</sup>, but there are more inter-sheet (C-H $\cdots$ O) bonds in  $\beta$  than  $\alpha$  making  $\beta$  more stable <sup>62</sup>. Sheets of  $1\beta$  are staggered by half a glucose molecule but  $1\alpha$  sheets are aligned on a constant inclined axis <sup>62</sup>.

It is reported that cellulose produced in the higher plants (such as ramie and cotton) is rich in cellulose  $1\beta$  and that produced by primitive organisms such as bacterial and algal are richer in  $1\alpha$ , but the high ordered portions of all native celluloses are generally made up of varying amounts of the two allomorphs <sup>54</sup>. The relative percentages of each allomorph can now be determined using a variety of techniques such as  $^{13}\text{C}$  NMR <sup>54, 56</sup>, electron diffraction <sup>58, 64</sup> and infrared spectroscopy <sup>64</sup>. In nature, a pure sample of  $1\alpha$  has yet to be discovered, with the highest percentage being that of bacterial cellulose (70 %) <sup>24, 65</sup> however highly

crystalline, almost pure I $\beta$  has been found in the “house” of Tunicates, the only known highly crystalline cellulose produced by animals<sup>3, 54, 66</sup>.

Although cellulose I is the predominate form of cellulose formed by nature, it is however not the most stable form; when cellulose I is recrystallized, it is transformed into cellulose II, and it is thought that this is due to cellulose II being the more thermodynamically stable polymorph<sup>24</sup>.

#### **1.1.4.2 Cellulose II**

Cellulose II has also been reported in the literature to exist in its natural form which is produced by a mutant strain of the bacteria *Acetobacter xylinum* which extrudes the cellulose perpendicular to the bacterial cell as opposed to parallel in the normal strain<sup>13, 67</sup> and also in the algae *Halicystis*<sup>68</sup>; but most cellulose II is generated as a result of man’s activity. Cellulose II is formed, irreversibly from cellulose I ( $\alpha$  and/or  $\beta$ ) by either the regeneration (the solubilisation of cellulose I in appropriate solvent, followed by precipitation of cellulose II by addition of water), which is the typical process involved in the spinning of synthetic cellulose fibres; or mercerization (swelling of cellulose I fibres by addition of concentrated sodium hydroxide, which yields cellulose II on removal of swelling agent) which is generally used to activate the polymer before the production of cellulose ether<sup>6</sup>.

The first unit cell structures of cellulose II were postulated by Kolpak and Blackwell and Stipanovic and Sarko using X-ray diffraction<sup>69, 70</sup>, followed by an updated structure by Langan *et al.* who used neutron fibre diffraction analysis on deuterated cellulose samples<sup>71</sup>. One of the major differences between cellulose I and II is the polarity of individual chains in the unit cell, with cellulose I chains running parallel to one another (all the reducing ends of individual chains are pointing in the same direction, see Figure 11) and cellulose II chains being anti-parallel (the direction of the reducing end of individual chains alternate between adjacent chains, see Figure 12)<sup>48, 70, 72, 73</sup>.

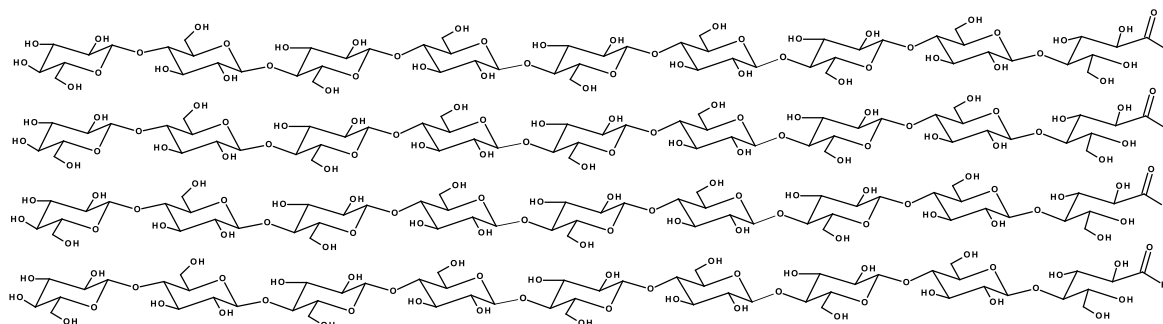


Figure 11: Parallel arrangement of the individual chains of cellulose I, with the reducing ends situated on the right of each chain (hydrogen bonding not shown).

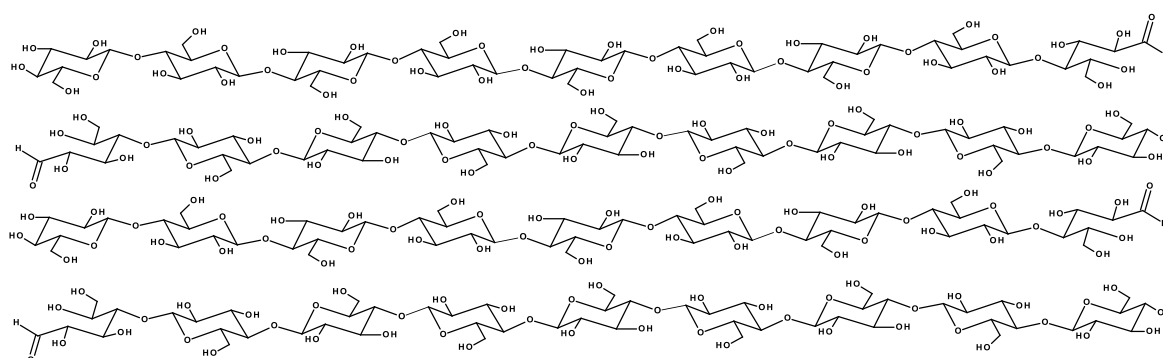


Figure 12: Anti-parallel arrangement of the individual chains of cellulose II. The reducing end of each chain alternates in its direction between adjacent chains (hydrogen bonding not shown).

It is unclear how chains of a parallel polarity could convert into chains of an anti-parallel nature. One theory is that fibrils are actually antiparallel and when fibrils are swollen during the mercerisation process adjacent fibrils can merge into each other thus forming antiparallel chains<sup>74</sup>. Another theory is that chains undergo folding during the mercerisation procedure, due to NaOH disrupting the hydrogen bonds in the swollen fibre and lowering the activation energy allowing chains to fold<sup>48, 69, 75</sup>. It is not known why the so called metastable cellulose I is produced naturally but it is thought that when the chains are all produced at the same time in close proximity the hydrogen bonding may lock them together, providing a high activation energy for the formation of the more stable cellulose II<sup>75</sup>.

The main intra-chain hydrogen bond is the same for both cellulose I and II (O3-H $\cdots$ O5) and (O2-H $\cdots$ O6) which provides the chain its rigid, linear shape and allows it to function as a structural polymer. However, the inter-chain hydrogen bonding is different; in cellulose I

there is an O6-H $\cdots$ O3 inter-chain bond and in cellulose II there is a O6-H $\cdots$ O2 inter-chain bond <sup>10</sup>. Due to the anti-parallel chains in cellulose II, a more complex system of hydrogen bonding is prevalent, where there is not only inter-chain bonding, but also inter-plane hydrogen bonding <sup>72</sup> between (O2-H $\cdots$ O2) thus making it more stable. (Figure 13).

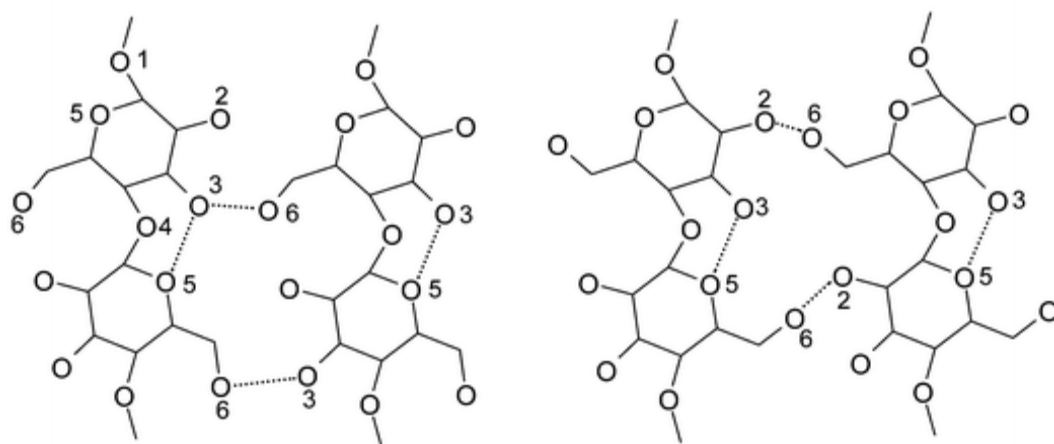


Figure 13: Inter and Intra-chain hydrogen bonding in cellulose I (left) and cellulose II (right), adapted from the review by Kontturi *et al.*<sup>10</sup>

#### 1.1.4.3 Cellulose III and IV

The remaining polymorphs are III and IV, discovered by early diffractometric studies, and they are not as well understood, and will only be very briefly discussed. Polymorphs III and IV can be further classified as either I or II depending on whether their unit cell and polarity was similar to that of cellulose I or cellulose II. Treating cellulose I or II with anhydrous liquid ammonia and evaporation of excess ammonia gas will reversibly form cellulose III<sub>I</sub> and III<sub>II</sub> respectively which can be converted back to its starting material by boiling in water <sup>1</sup>. Heating cellulose III<sub>I</sub> and III<sub>II</sub> at 206 °C whilst immersed in glycerol will produce irreversibly cellulose IV<sub>I</sub> and IV<sub>II</sub> respectively <sup>76</sup> (Figure 14). Cellulose IV can also be produced from the regeneration of cellulose I from solution at elevated temperatures <sup>1</sup>. In cellulose III and IV the only difference is between the crystalline packing of the chains, with each having similar conformation as native cellulose <sup>77</sup>. Cellulose III is assumed to be composed of parallel chains <sup>77</sup>, with the only difference being the position of the sheets <sup>77</sup>. Cellulose IV<sub>I</sub> consists of parallel chains, whilst IV<sub>II</sub> is antiparallel with intersheet hydrogen

bonds in both  $IV_I$  and  $IV_{II}$  making them more stable and dramatic treatment is required to convert them back to cellulose I and II <sup>76</sup>.

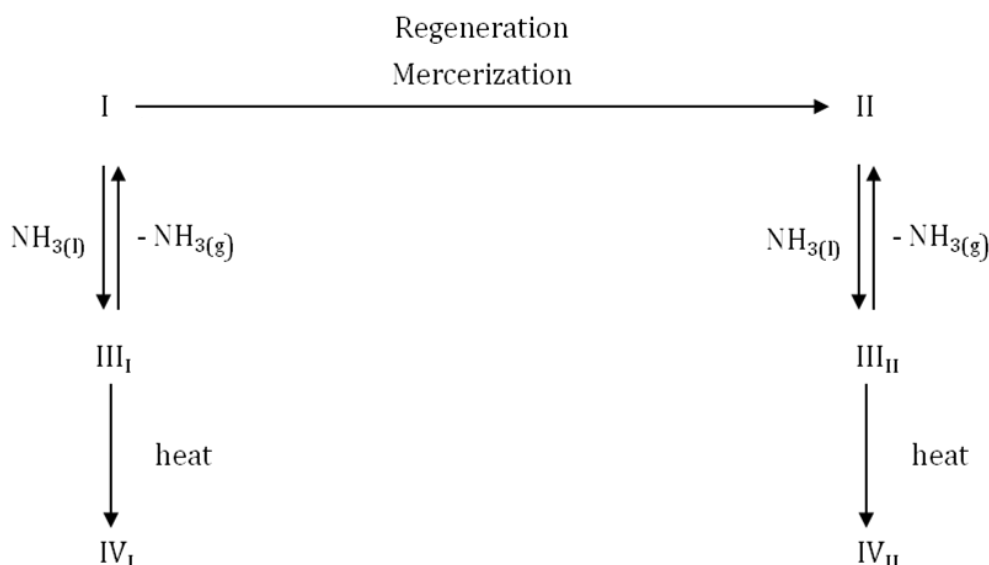


Figure 14: The six known cellulose polymorphs and how they interconvert, adapted from the review by O'Sullivan <sup>32</sup>.

### 1.1.5 Cellulose Utilisation

Cellulose had been utilised by mankind for many centuries before the true identity of the polymer was officially discovered by Payen, initially in its native form e.g. in construction and fuel (wood, charcoal), textiles (cotton, flax) and in the forms of paper and boards. More recently, cellulose has been used as a precursor for chemical modifications such as the development of cellulose nitrate in 1846. Cellulose nitrate is now produced annually in the region of 200,000 tonnes and is widely used in the ammunitions, printing and decorative film industries <sup>78</sup>. The development of cellulose solvents such as Schweitzer's reagent in 1857 allowed for the dissolution of cellulose and the preparation of semi-synthetic regenerated cellulose fibres such as rayon. To this day, approximately three million tons of regenerated cellulose fibres are produced annually using the viscose process <sup>6, 79</sup>. The dissolution of cellulose has led to many more discoveries including the production of cellophane, cellulose acetate, and celluloid, to name but a few <sup>1, 6</sup>.

The enormous use of this renewable polymer has resulted in cellulose based items making up large quantities of waste. In the UK, cellulosic items (paper, cardboard and wood) annually constitute more than 7 million tonnes of household waste<sup>80</sup> and almost 16 million tonnes of industrial waste<sup>81</sup>. One industry producing cellulosic waste is the nuclear power industry which has the added problem that a significant proportion of items used in a nuclear power facility will eventually be classified as radioactive waste, including cellulosic items like papers, packaging, cotton based materials, semi-synthetic items, wood etc. In the UK there is 102,000 tonnes of cellulose containing radioactive waste in storage awaiting disposal<sup>82</sup> and this has hence become an area of interest, in particular (for this thesis) the threat that cellulose waste poses to the integrity of the underground disposal of radioactive waste.

## **1.2 Radioactive waste**

The International Atomic Energy Agency (IAEA) defines radioactive waste as: "Any material that contains or is contaminated by radionuclides at concentrations or radioactivity levels greater than the exempted quantities established by the competent authorities and for which no use is foreseen"<sup>83</sup>.

In the UK, the majority of radioactive waste is generated by the nuclear power industry (approximately 95%), mainly due to the production of nuclear fuel and the decommissioning of old facilities, with the remainder being produced by the Ministry of Defence, hospitals and other educational and research facilities<sup>84</sup>.

Radioactive waste is broadly categorised as being of one of three types: High, Intermediate and Low Level Waste.

High Level Waste (HLW) initially comes in the form of a concentrated nitric acid solution of fission products, primarily produced from the reprocessing of spent nuclear fuel. HLW is highly radioactive and has a thermal output above 2kW per m<sup>3</sup>. It is expected to generate heat for several centuries and its radioactivity is expected to take millions of years to decay back to background levels; therefore great care must be considered in the storage and disposal of the waste. HLW in the liquid form is generally stored in water-cooled stainless steel tanks surrounded by thick-walled concrete containers to protect operators who come into contact with the waste<sup>85</sup>. Liquid HLW commonly undergoes a process of vitrification which involves heating the waste to dryness, and forming a molten mixture with

borosilicate glass in a furnace. The mixture is then poured into steel canisters, sealed and stored in air cooled specially engineered stores<sup>84</sup>.

Intermediate Level Waste (ILW) is less radioactive than HLW and is mainly generated during the process of reprocessing spent nuclear fuel. ILW includes ion exchange resins, sludges from the treatment of liquid effluents and plutonium contaminated materials (PCM). PCMs include things such as paper towels, gloves, filters and other general laboratory equipment. ILW also contains metal objects such as nuclear fuel casings and disassembled nuclear reactor components from nuclear decommissioning<sup>84</sup>. The heat generated by ILW is usually less than 2kW per m<sup>3</sup>, but provisions may be required to control temperature during the storage and disposal of the waste<sup>85</sup>.

Low Level Waste (LLW) is the lowest activity category of radioactive waste. Its radioactivity must not exceed four gigabecquerels per tonne (GBq/te) of alpha or 12 GBq/te of beta/gamma activity. LLW consists of organic waste such as items used within nuclear facilities (operational wastes) such as wipes, paper towels, clothing and other general rubbish; and also heavy items generated from the decommissioning of nuclear power stations such as steel frameworks, building rubble, disused pipe-work, foundations and surrounding soil (decommissioning waste)<sup>84</sup>.

### **1.2.1 Management of Radioactive Waste**

A recent inventory compiled in conjunction with the Department of Energy and Climate Change (DECC) and the Nuclear Decommissioning Authority (NDA) reported that there is approximately 4.7 million cubic meters (or five million tonnes) of radioactive waste in the UK which has been stockpiling since the 1940's; either already in storage or to be generated during the decommissioning process of existing nuclear sites<sup>84</sup>. Of the total waste, 94 % of the volume is due to LLW, 6 % is due to ILW and less than 0.1 % is due to HLW; although HLW accounts for 95 % of the total radioactivity<sup>84</sup>. In 2005, the Nuclear Decommissioning Authority (NDA) was set up to manage the decommissioning and clean-up of the UK's civilian nuclear sites, including the management and disposal of radioactive wastes.

### 1.2.1.1 Current management of HLW

The current practice is to store vitrified HLW for a period of at least fifty years to allow for efficient cooling and a reduction in radiation levels before a long-term management and disposal plan is implemented <sup>84</sup>, however, for the purpose of this thesis, only Low and Intermediate Level Waste will be further discussed.

### 1.2.1.2 Current management of LLW

Due to low radiation levels, most LLW is deemed suitable for disposal in near surface disposal facilities. Since 1959, most of the suitable LLW in the UK has been disposed of in the Low Level Waste Repository (LLWR) based in Cumbria. Current practice is to super-compact steel drums of waste to drastically reduce their volume, and place the drums in large steel containers which are transported to the repository by road or rail. At the repository site, the steel containers are filled with cement to encapsulate and immobilise the waste <sup>86</sup>. Containers are then placed into engineered concrete vaults just below the surface of the site (Figure 15). Since the repository opened, approximately one million cubic meters of LLW have been disposed of in this way, and this waste is in addition to the 4.7 million cubic meters of stockpiled waste, of which 4.4 million cubic meters is LLW.



Figure 15: Low Level Waste Repository (LLWR), Cumbria, England

### 1.2.1.3 Current management of ILW

ILW is generally supercompacted or cut up (if solid) to reduce volume or treated to reduce water content (if sludge or liquid) and then placed in standardised stainless steel drums or boxes which are then filled with a cement based grout to produce an immobilised wasteform.

Packages are prepared at specialised packaging facilities and finally held in specially engineered stores until a long term disposal solution is finalised <sup>87</sup>. These sites are not designed to be long-term and may only have a life span of several decades until a permanent solution is found.



Figure 16: An ILW storage facility <sup>92</sup>

### 1.2.2 Long-term solution for the UK's radioactive waste disposal

The 1976 the “Flower’s Report” identified radioactive waste management as being a significant problem <sup>88</sup>, resulting in the Government’s long-term aim being the deep underground disposal of radioactive waste. In 1982 the Nuclear Industry Radioactive Waste

Management Executive (NIREX) was established with the task of locating, building and running disposal facilities for LLW and ILW with the long-term aim being the establishment of a site for their combined disposal; however, due to some opposed public opinion and a lack of planning permission, a long-term solution failed to materialise. In 1999 the Science and Technology Select Committee suggested a phased approach to waste management, where waste would be stored on the surface until a permanent repository could be established; resulting in NIREX developing the Phased Geological Repository Concept (PGRC) <sup>89</sup>.

### **1.2.3 Phased Geological Repository Concept (PGRC)**

The reversible, phased concept is a multi-barrier approach initially involving the physical containment of waste by producing the immobilised wastefrom and their interim storage in engineered surface stores as previously discussed. The second stage involves transportation of wastefrom packages to the repository and placing the stainless steel, corrosion-resistant packages in engineered vaults located deep underground. The vaults will be excavated from stable “host” rock formations, where the enclosed waste will be allowed to naturally decay over thousands of years beneath hundreds of meters of rock and several man made barriers.

It is planned that a period of monitoring of up to several hundred years will follow, and the decision to backfill the vaults with a highly alkaline cementitious grout would be given to future generations <sup>90</sup>. After the repository is backfilled, it would be closed and sealed to minimise the escape of radioactive material from reaching the biosphere. At this point, re-entrance to the repository would come from conventional mining techniques only <sup>90</sup>.

In 2001 a programme entitled “Managing Radioactive Waste Safely (MRWS)” was initiated with the aim being to find a practicable solution for the UK’s higher activity radioactive wastes. As part of the programme the Committee on Radioactive Waste Management (CoRWM) was established to provide the Government with independent recommendations based on scientific knowledge and public opinion about how best to manage the UK’s radioactive waste. The committee’s conclusions were that interim storage of waste should be implemented, and long-term repository disposal should commence after sufficient research and development has been undertaken to remove any safety concerns and uncertainties. In 2006 NIREX was taken into ownership by a newly created public body; the Nuclear Decommissioning Authority (NDA). The NDA’s purpose is to take responsibility for the UK’s nuclear waste, and following the CoRWM recommendations,

the NDA was given the responsibility for the planning and implementing of geological disposal of the UK's higher activity radioactive waste based on the Phased Geological Repository Concept<sup>91</sup>.

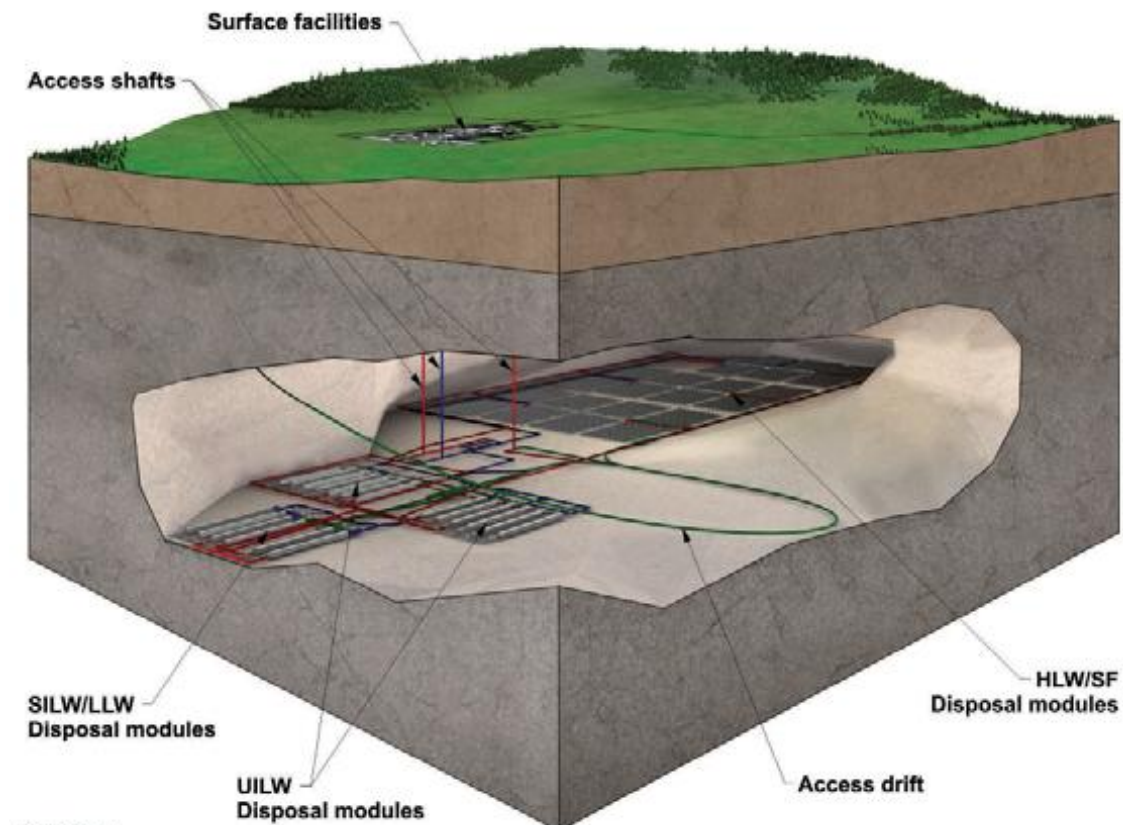


Figure 17: An illustration of a generic deep geological repository designed for the United Kingdom's higher activity radioactive waste<sup>91</sup>

#### 1.2.4 Post-Closure Repository Safety Concerns

Part of the research and development which must be undertaken includes a 'performance assessment' of a repository; i.e. an assessment of how effective the repository would be against preventing radioactive material from leaving the 'near field' of the repository and entering the biosphere. Three main pathways have been identified, these being migration of dissolved radionuclides in groundwater (the groundwater pathway), transport of radionuclide-bearing gas generated in the repository (the gas pathway) and damage to the

repository due to human activity, such as drilling (the human intrusion pathway) allowing radionuclides to escape<sup>90</sup>.

For the purpose of this thesis, the groundwater pathway is of primary importance, in particular the role which cellulose plays in this pathway. However, it must also be noted that the gas pathway is also important in regards to the presence of cellulose in underground repositories<sup>92</sup>. It is expected that the action of microbes and to a lesser extent, the action of radiation on cellulose degradation products will result in the production of carbon dioxide and methane<sup>92</sup>. The significance of this is that both of these gases contain the naturally occurring radioactive carbon-14, and although carbon-14 will only be present in small amounts, due to its low natural abundance, its radioactive nature and long half-life (~ 5730 years) have resulted in a significant amount of research being undertaken to estimate the rate at which carbon-14 will be produced from cellulosic waste under repository conditions and the radiological consequences related to its release into the biosphere<sup>92</sup>.

To decrease the chance of radionuclides escaping the repository and reaching the surrounding environment, the repository is expected to be situated in a rock formation with a long, slow ground water pathway to the surface<sup>90</sup>. The repository is designed to provide both a physical barrier (from the engineered materials and the surrounding geosphere) and also a chemical barrier (provided by the cement backfill). Post-closure ingress of groundwater is expected to partially dissolve the cement backfill, thus creating a high pH environment<sup>93</sup>. The repository is also expected to be anaerobic due to the corrosion of metal packages consuming oxygen. Under these conditions radionuclides are expected to have low water solubility and it is anticipated that there will be high sorption levels of radionuclides onto both the cement based grout (designed to maximise available surface area for sorption) and the surrounding rocks of the geosphere. Therefore, under those conditions, migration due to the groundwater pathway is expected to be minimal.

However, one area of research in the safety assessment of a repository is to investigate any chemicals or processes which could have an inverse affect on the above mentioned chemical barrier; in particular any which affect the solubility and sorption of the radioactive nuclides, with one identified area of research being the effect that cellulose has on the migration of radionuclides through the groundwater pathway<sup>90</sup>.

## 1.3 Past Research

### 1.3.1 Cellulose Degradation

Once the decision is made to backfill the repository, resaturation is expected to occur over several decades, with the pore water in the repository expected to be composed of dissolved NaOH and KOH from the impurities in the cement in a saturated  $\text{Ca}(\text{OH})_2$  solution with the initial pH being 13.4, followed by a second stage where all the NaOH and KOH have leached out and the composition is dictated by  $\text{Ca}(\text{OH})_2$  with the pH falling to 12.5 and remaining there for 100,000 years<sup>94</sup>. Under these conditions, cellulose is known to be unstable<sup>95</sup> and to degrade to form water soluble cellulose degradation products (CDPs)<sup>93</sup>.

Most radionuclides are strongly insoluble under the expected conditions of a repository<sup>96, 97</sup>, but the interest in cellulose degradation products is that they are known to form stable complexes with radioactive nuclides, especially tri- and tetravalent radionuclides such as  $\text{Am}^{3+}$  and  $\text{Pu}^{4+}$ <sup>97-100</sup>, which increases their water solubility and reduces sorption to both mechanical and natural barriers of the repository<sup>96</sup>, this is expected to enhance the mobility of radionuclides within the repository thus increasing their chance of leaving the repository and entering the surrounding environment.

It is known from the pulping industry that the molecular weight of cellulose reduces when boiled in alkaline solutions<sup>93</sup>, however the (1-4) glycosidic linkages in cellulose are thought to be stable at temperatures less than 170 °C under alkaline conditions<sup>93</sup>. This loss in molecular weight can be explained by the peeling reaction which primarily results in the formation of an approximately equal mixture of diastereoisomers: 3-deoxy-2-C-(hydroxymethyl)-erythro-pentanoic acid and 3-deoxy-2-C-(hydroxymethyl)-threo-pentanoic acid which are commonly known as alpha and beta isosaccharinic acids ( $\alpha/\beta$ -ISA)<sup>101, 102</sup>. Under alkaline conditions, cellulose undergoes end-wise degradation of the cellulose chain where individual glucose units are removed from the reducing end one unit at a time, each time generating a new reducing end which allows the reaction to continue<sup>103, 104</sup> (Figure 18). In the cellulose chain, the alkaline induced isomerisation of the aldose (I) to a ketose (IV) initiates the peeling reaction and can be described as the keto-enol tautomerism to form an enolate ion (II), this is followed by isomerisation (III – IV), which can result in the  $\beta$ -alkoxycarbonyl elimination of the cellulose polymer (V) to produce 4-deoxy-2,3-hexodilulose and finally the benzylic acid type rearrangement (VIII) to produce ISA<sup>105</sup> or fragmentation of 4-deoxy-2,3-hexodilulose to produce a number of other smaller organic acids, which are collectively known as cellulose degradation products (CDPs).

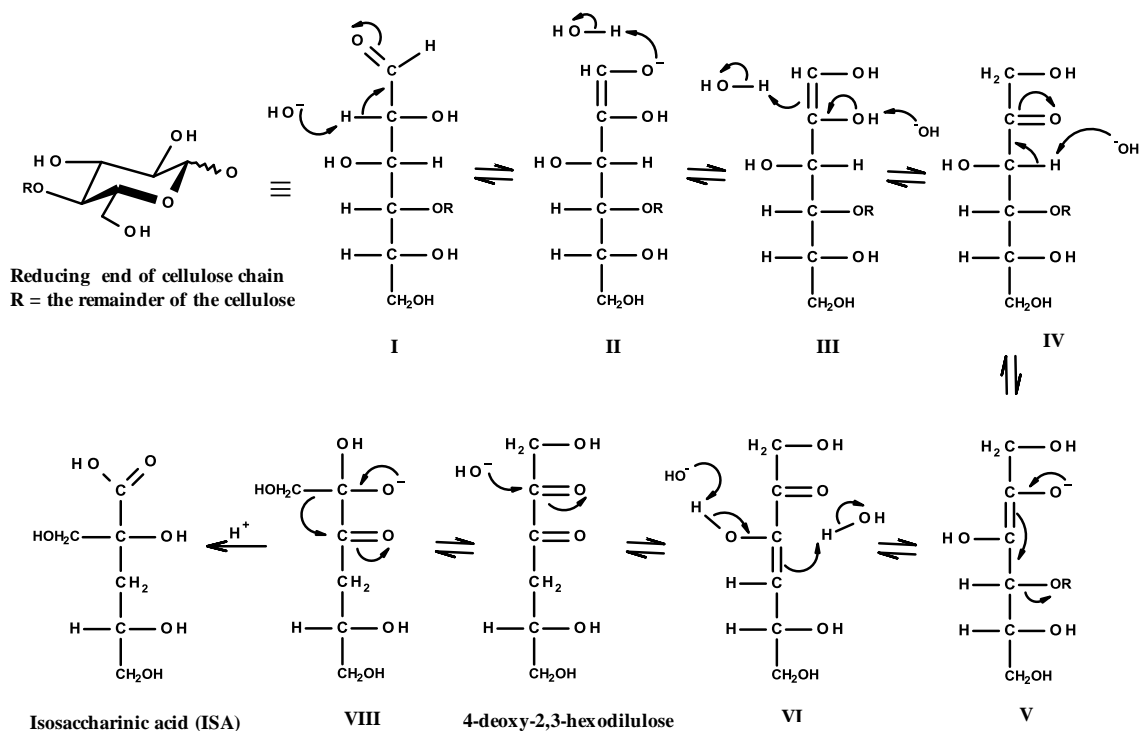


Figure 18: The peeling reaction

The peeling reaction does not completely dissolve cellulose, as competing ‘stopping’ reactions also exist which inhibit chemical peeling and stabilises the cellulose chain<sup>101, 102</sup> due to the formation of alkali-stable end groups (Figure 19). One such pathway, is the occurrence of  $\beta$ -hydroxycarbonyl elimination (II) instead of  $\beta$ -alkoxycarbonyl elimination; and when this happens, it results in the formation of terminal 4-O-substituted 3-deoxy-D-arabino and ribo-hexonic acids (alpha and beta substituted glucometasaccharinic acid, MSA) via a benzilic acid type rearrangement (IV) of the intermediate 3-deoxy-D-glucosone. MSA was initially identified after acid hydrolysis of alkali stable cellulose end groups by Machell and Richards<sup>101</sup>; however, Johansson and Samuelsson have determined that other stopping end groups formed during alkaline degradation also exist<sup>106</sup>.

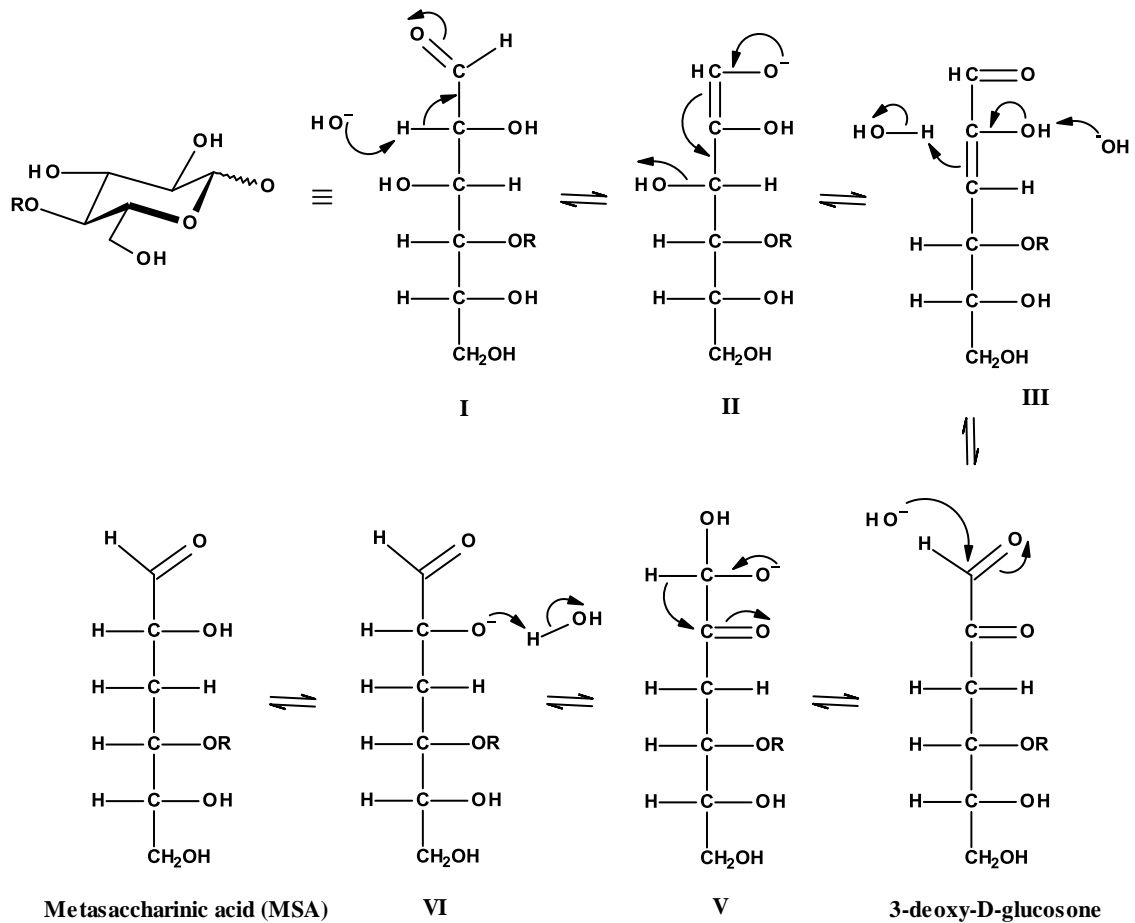


Figure 19: The stopping reaction

To determine the impact that the CDPs have on the safety of the repository, a number of studies have been undertaken to identify the major components that make up the CDPs, to estimate the rates at which they are formed and to determine the effect they have on the solubility and sorption of radionuclides within a repository.

The identification of CDPs has been undertaken by several groups, initially involving the degradation of pure cellulose or cellulosic materials in various alkaline media intended to mimic repository conditions; analytical methods are then utilised to detect the degradation products within the degradation “leachate”. Greenfield *et al.*<sup>107</sup> have identified the mechanisms for the predicted formation of some of the known CDPs with ISA being identified as the most abundant compound.

Commonly, ISA is detected using high performance anion exchange chromatography (HPAEC)<sup>12, 94, 100, 107-112</sup>, and lower molecular weight carboxylic acids such as short chain

fatty acids are detected using high performance ion exclusion chromatography (HPIEC)<sup>12, 94, 108-111, 113, 114</sup>. Other techniques employed include GC-MS (after derivatisation)<sup>94, 96, 107, 110, 112, 115-120</sup>, HPLC<sup>98, 116, 118, 121, 122</sup>, and capillary zone electrophoresis (CZE)<sup>96, 123</sup> with each technique having their own advantages and disadvantages.

A total organic carbon (TOC) analyzer has also been used to determine the total amount of dissolved organic carbon in a degradation leachate<sup>12, 94, 108-110, 115, 124</sup>, and in some studies, the amount of small molecules is said to make up the difference between the dissolved TOC and the amount of ISA<sup>93</sup>.

In low temperature degradation experiments under repository conditions the two major CDPs have consistently been identified as  $\alpha$ - and  $\beta$ -ISA<sup>93</sup>, accounting for between 70 % - 90 % of the degradation products<sup>12, 94, 96, 108, 110, 123</sup> depending on the type of cellulosic product under degradation. However, there are many known alkaline degradation products of cellulose alongside ISA including formic, ethanoic and lactic acid. To date there has been over 65 degradation products reported, an extensive list of which can be found in the review by Knill and Kennedy<sup>93</sup>.

In another study by Hurdus and Pilkington<sup>118</sup>, cellulose was degraded under repository conditions but using cementitious grout, instead of  $\text{Ca}(\text{OH})_2/\text{NaOH}$  to provide the alkaline conditions, with results indicating that ISA was still the major degradation product generated.

The type of CDP formed is related to the experimental conditions. For example, the presence of calcium (a divalent cation) catalyses the alkaline degradation of cellulose<sup>125</sup> and in particular the benzilic acid type rearrangement, thus increasing the amount of ISA produced and reducing the yield of the smaller compounds<sup>102, 107, 126</sup>. The catalysis of the benzilic acid type rearrangement also enhances the formation of metasaccharinic acid (MSA)<sup>127</sup>, which slows down cellulose degradation, this enhancement is greater than the rate of the formation of ISA, so the overall effect of increasing the concentration of  $\text{Ca}^{2+}$  ions is to reduce the rate of degradation<sup>128</sup>.

In experiments where only NaOH was used as the alkali species, additional fragmentation of the intermediate 4-deoxy-2,3-hexodilulose is thought to occur resulting in smaller organic acids constituting a larger percentage of the total CDPs<sup>102, 107, 129-134</sup>. In a set of experiments where either NaOH or  $\text{Ca}(\text{OH})_2$  were used as the alkali species, the amount of ISA produced was 32 % and 63 % of total CDP's respectively<sup>102</sup>. Another interesting result

of using NaOH as the degrading species is that the amount of  $\beta$ -ISA formed is approximately three times greater than the amount of  $\alpha$ -ISA produced<sup>107, 129</sup>.

Temperature is also a factor; under alkaline anaerobic conditions, cellulose is said to favour the formation of the fragmentation products when very high temperatures are observed<sup>113, 135</sup>. For example, Krochta *et al.*<sup>116</sup> studied the degradation of cellulose in NaOH concentrations between 4 – 6 % at a range of temperatures between 240 – 320 °C under anaerobic conditions and observed that the major degradation products were lactic and formic acid with no detection of any ISA; and at temperatures above 200 °C Niemela reported a mixture of 50 hydroxy mono and dicarboxylic acids after the treatment of cotton cellulose with sodium hydroxide (3 M) with ISA only being present in minor amounts and lactic acid being the major product<sup>120</sup>.

The evolving environment of a repository and the variety of alkaline species and types of cellulosic wastes present would make it extremely difficult to predict accurate compositions of the generated CDPs. It has been estimated that peak post-closure repository temperatures would reach no more than 60 °C, and this peak temperature is expected to fall to 35 °C after 10 years<sup>136</sup>. Van Loon and Glaus<sup>94</sup> degraded a range of cellulosic materials at 25 ° under conditions which mimicked an underground repository and found that on average ISA accounted for ~ 80 % of the generated CDPs, with  $\alpha$ - and  $\beta$ -ISA being produced in approximately equal amounts. However, in the present work (see section 3.6) it was determined that when cellulose was degraded using a mixture of Ca(OH)<sub>2</sub> and NaOH under anaerobic conditions, at 90 °C, the amount of  $\beta$ -ISA produced was approximately three times more than the amount of  $\alpha$ -ISA produced. Therefore it is possible that, in an actual repository, at least in the early stages post-closure when both the concentration of NaOH and the temperature of the facility are expected to be at their highest,  $\beta$ -ISA would be produced in larger amounts than the amount of  $\alpha$ -ISA produced.

### **1.3.2 Solubility and Sorption Studies**

As previously discussed, the importance of the CDPs is based on their ability to affect the solubility and sorption of radionuclides within a repository. The complexing power of ISA to radioactive nuclides is well known, backed up by the fact that it is now incorporated into foams and gels and used in the decontamination of materials such as steel and concrete which are contaminated with actinides<sup>97</sup>. A review of the effects of cellulose degradation

products on their ability to influence the solubility and sorption of radionuclides under repository conditions can be found in the report by Heath and Williams<sup>137</sup>.

Glaus *et al.* investigated the complexing properties of CDPs, on Ni<sup>2+</sup>, Eu<sup>3+</sup> and Th<sup>4+</sup> ions sorbed to feldspar at pH 13.3<sup>138</sup> (a material which cellulose degradation products are known not to sorb to), and results indicated that ISA was forming complexes with the nuclides and had an adverse effect on the sorption of Eu<sup>3+</sup> to the feldspar, with  $\alpha$ -ISA having a greater effect than  $\beta$ -ISA: it was determined that the stability of the Eu- $\beta$ -ISA complex was two orders of magnitude lower than the Eu- $\alpha$ -ISA complex; although the  $\beta$ -ISA experiments were performed on a much smaller scale than the  $\alpha$ -ISA due to limiting availability of  $\beta$ -ISA.

Tits *et al.*<sup>100</sup> determined the effect of ISA on radionuclide sorption onto calcite, a stable polymorph of calcium carbonate which will be present in the chemically disturbed zone surrounding a repository<sup>100</sup>, isotopes studied included <sup>152</sup>Eu, <sup>241</sup>Am and <sup>228</sup>Th. The authors found that at concentrations of ISA of more than 10<sup>-5</sup> M, sorption was reduced significantly. Greenfield *et al.* determined that the solubility of plutonium was increased by five orders of magnitude in a mixed  $\alpha$ -ISA and  $\beta$ -ISA solution, and they found that both  $\alpha$ -ISA and  $\beta$ -ISA had an equal effect on the solubility, when measured separately<sup>107</sup>.

Hurdus and Pilkington<sup>118</sup> fractionated a concentrated leachate from their degradation experiment into six portions using semi-preparative HPLC, and determined which fraction had the greatest effect on the solubility of plutonium. GC-MS was used to determine which fraction contained ISA. An equal amount of plutonium nitrate containing <sup>238</sup>Pu was added to each fraction, and the concentration of soluble nuclide was determined after a period of equilibration. It was determined that the solubility increased from 4 x 10<sup>-10</sup> M in a control sample, to 4 x 10<sup>-5</sup> M in the fraction which contained the ISA (which had a concentration of 2.6 x 10<sup>-3</sup> M), hence indicating the potential of ISA to increase the solubility of radionuclides under repository conditions.

Greenfield *et al.*<sup>99</sup> determined the solubility and sorption of various radionuclides in cement equilibrated water, both in the presence of cellulose degradation products and in the cement equilibrated water without degradation products, the results identified that the solubility of uranium increased by three orders of magnitude, and for plutonium a solubility increase of five orders of magnitude was witnessed, in sorption experiments, the sorption of

uranium reduced by one order of magnitude to the cement in cement equilibrated water when in the presence of degradation products.

Various studies have used ISA as a model for CDPs in solubility/sorption studies due to the high percentage of ISA formed; however Warwick *et al.*<sup>121</sup> compared the solubility of thorium in the combined CDPs and pure ISA, at the pH relevant to repository conditions, and indicated that the solubility of thorium was significantly (up to 46 times) greater in the presence of CDPs as when only in an ISA solution of comparative concentration; thus indicating that there are other components which, accumulatively are capable of complexing radionuclides and increasing their solubility. Similar results were observed by Greenfield *et al.*<sup>99</sup> and Glaus *et al.*<sup>138</sup> who determined that the combined leachate had more of an effect on the solubility and sorption respectively of radionuclides than ISA alone.

In general many studies have been carried out which have determined that either ISA<sup>97, 98, 107, 124, 139, 140</sup> or CDPs from degradation experiments<sup>96, 107, 124</sup> are capable of increasing the solubility of radionuclides such as thorium (IV), uranium (IV) and (VI), plutonium (IV) by many orders of magnitude depending on the experimental conditions due to the formation of complexes. Similar results are evident for the reduction in the sorption of radionuclides on to cementitious grouts analogous to the material to be used in repository construction when using ISA<sup>100, 115, 141</sup> or total CDP leachate<sup>94, 99, 119, 124</sup>.

### **1.3.3 Kinetic studies and their use in modelling**

According to Van Loon and Glaus, the assessment of the effect that cellulose degradation has on the migration of radionuclides is essentially based on estimations of the amount of ISA produced due to degradation<sup>128</sup>. To determine this, modelling studies have been performed to estimate the degree of cellulose degradation which is an important parameter in the assessment of the effect that the complexants have on the mobility of radionuclides in a radioactive waste repository<sup>109</sup>. Things that will affect the amount and rate of ISA formed in a repository, will include however: the cellulose loading, the stability of the ISA formed, the sorption of ISA onto cement surfaces, the pH, cations present, temperature and red-ox conditions<sup>94, 115</sup> making accurate estimations a very difficult task.

The degradation of cellulose is also dependent on its morphological structure, a highly crystalline cellulose sample will impede degradation and degrade slower than an unordered

amorphous material<sup>5</sup>. Biddle *et al.* degraded cellulose under alkaline conditions<sup>124</sup> using cotton wool and paper tissues under repository conditions. In their experiments, they concluded that the rate of degradation of the tissues which contained more amorphous cellulose was twice as fast as the cotton wool which contained more crystalline cellulose indicating that amorphous regions react faster than crystalline regions because they are more accessible to reagents<sup>124</sup>. The degree of polymerisation of the cellulose is also important; in one comparative study between the degradation of cotton (DP = 1800) and pure cellulose powder (DP = 117), the degradation was 1 % and 30 % respectively after two years<sup>12</sup>.

Various degradation studies have been carried out to determine the reaction kinetics, and to try to postulate long-term predictions for the time it would take for the complete degradation of cellulose in a radioactive waste repository to occur, with conflicting views existing<sup>94, 108, 109, 123, 127, 128</sup>. The basis of the degradation studies was to measure the conversion of cellulose and cellulose containing materials into soluble organic products and various materials have been employed including cotton, tissue, paper and wood, all of which will have different properties such as the crystallinity and the DP.

In regards to the alkaline degradation of cellulose under repository conditions, a study by Van Loon and Glaus identified four processes<sup>128</sup>:

1. Endwise chain depolymerisation (the peeling reaction)
2. Termination of chain depolymerisation (chemical stopping)
3. Termination of chain depolymerisation (physical stopping)
4. Cleavage of glycosidic bonds in the cellulose chain due to alkaline hydrolysis, leading to new reducing end groups which can undergo depolymerisation by peeling.

Degradation at relatively low temperature has been studied by Hass<sup>127</sup> and Krotcha<sup>116</sup>. Haas<sup>127</sup> used 1.25 M sodium hydroxide and degraded cotton hydrocellulose under anaerobic conditions, at various temperatures ranging from 65 – 131 °C. Haas assigned rate constants for the peeling of reducing end groups ( $k_1$ ), for the chemical stopping by termination due to formation of metasaccharinic acid ( $k_2$ ) and for physical stopping, when peeling is stopped due to chains moving into inaccessible crystalline regions ( $k_{cr}$ ). Haas also determined the activation energies required for the both the peeling (24 kcal mol<sup>-1</sup>) and

stopping reactions ( $32 \text{ kcal mol}^{-1}$ ) indicating that stopping will be more prevalent at higher temperatures.

Models have been developed to account for kinetics of alkaline degradation of cellulose by Van Loon and Glaus<sup>94, 128</sup> and Pavasars<sup>123</sup> and results have allowed for estimates to be made about the degree of degradation over long time scales with estimates suggesting that the initial rate depends on the concentration of reducing ends available, and it is expected that the peeling will eventually cease and what remains will be the inaccessible crystalline cellulose chains<sup>131</sup>. Therefore, the rate limiting step, long-term, will be the generation of new reducing end groups due to mid-chain scission of the chemically stopped chains. The rate of mid-chain scission will therefore be an important parameter.

A mathematical model was proposed by Van Loon and Glaus<sup>94, 128</sup> which was based on both extrapolated results from available literature data and using rate constants proposed by Haas<sup>127</sup> and experimental results where they calculated their own rate constants for comparison; importantly they also introduced a rate for the alkaline hydrolysis of cellulose chains which have been stopped by the formation of metasaccharinic acid. According to Nevell<sup>135</sup>, alkali mid-chain scission (alkaline hydrolysis) of glycosidic bonds does not occur to any significant extent below  $170^\circ \text{C}$  in crystalline material, but a study by Gentile *et al.* who compared the degradation of highly crystalline cellulose to that of amorphous cellulose at relatively low temperatures ( $60 - 80^\circ \text{C}$ ) indicated that random alkaline hydrolysis does occur in amorphous cellulose at both temperatures<sup>142</sup>. Scission can occur in two places, either between the oxygen atom and the glycosyl group or between the oxygen atom and the aglycone, with the former reaction greatly predominating<sup>135</sup>.

In the study of Van Loon and Glaus<sup>94, 128</sup> they developed a model for the degradation of cellulose under the conditions of a repository ( $25^\circ \text{C}$ , anaerobic and  $0.3 \text{ M HO}^-$ ) and extrapolated the rate constants ( $k_1$ ), ( $k_2$ ) and ( $k_{cr}$ ) from those obtained by Haas<sup>127</sup>. In their experiments they degraded pure cellulose and performed other experiments on cellulosic items (Tela tissues, cotton and recycling paper), using artificial cement pore water (ACW-I, NaOH/KOH solution saturated with respect to  $\text{Ca(OH)}_2$ ) under repository conditions and using their results they calculated rate constants for the peeling and stopping reactions which were comparable to the ones which were calculated from the literature data published by Haas. For both the theoretical and experimental results, the alkaline hydrolysis constant ( $k_{obs}$ ) measured at higher temperatures and using larger hydroxide concentrations<sup>143</sup> was extrapolated using the Arrhenius equation resulting in a  $k_{obs}$  of  $5.25 \times 10^{-11} \text{ h}^{-1}$ . Their

calculations indicated that the rate of peeling was  $10^8$  times faster than the rate of alkaline hydrolysis; hence Van Loon and Glaus concluded that the alkaline hydrolysis reaction was of minor importance at ambient temperatures. Therefore, to describe their two-phased model the following kinetic expression was proposed:

$$(\text{cel deg}) = (k_1/k_t)(G_r)_0(1-e^{-k_t t})$$

where: (cel deg) = the mole fraction of cellulose degraded,  $k_1$  = the first order rate constant for the peeling reaction,  $k_t$  = the overall first order rate constant for the stopping reaction,  $(G_r)_0$  = the mole fraction of reducing end groups.

Their reaction model is based on an initial 'fast peeling' stage which is predicted to last for about two years in which 1 – 10 % of cellulose degradation occurs and a maximum of approximately 10 % is degraded after  $10^4$  years. Any further reaction will be governed by the very slow ( $k_{\text{obs}} 5.25 \times 10^{-11} \text{ h}^{-1}$ ) alkaline hydrolysis followed by peeling of the new resulting reduced ends. Based on their model, the cellulose available in a repository would degrade only after  $10^5$  to  $10^6$  years, with the rate of alkaline hydrolysis being the rate limiting factor.

A model by Pavasars *et al.*<sup>123</sup> was also developed to model the degradation of cellulose under repository conditions<sup>123</sup>. Using non-linear analysis to determine kinetic parameters for each reaction phase, they predicted a rate of mid-chain scission (alkaline hydrolysis,  $k_2$ ) which was much larger than the one proposed by Van Loon and Glaus; they determined a value of ( $2-3 \times 10^{-6} \text{ h}^{-1}$ ) and used an extended version of the mathematical model of Van Loon and Glaus to incorporate mid-chain scission:

$$(\text{Cel deg}) = 1 - (1 - (k_1/k_2)(G_r)_0(1 - e^{-k_t t}))e^{-k_{\text{obs}} t}$$

Pavasars proposed a rapid rate of degradation in the first 3 years where 15 – 25 % of cellulose would be degraded by the peeling-off reaction the extent of which was dependent on the concentration of the glucose reducing end groups available. Pavasars also concluded that alkaline cleavage of glycosidic bonds is the rate limiting step over the long-term. The kinetic rate constant, derived from experimental results, for the alkaline hydrolysis were five orders of magnitude larger than the one presented by Van Loon and Glaus extrapolated from the high temperature experiments, resulting in a complete degradation after 150 – 550 years<sup>115</sup>.

A further two year study of the degradation of pure cellulose under repository conditions was performed by Glaus and Van Loon at elevated temperatures (60 °C and 90°C) <sup>109</sup>, with the main purpose being to establish a reliable relationship between the rate constant for the alkaline hydrolysis and temperature; i.e. to determine if the extrapolation of the rate constant for alkaline hydrolysis is accurate over a range of temperatures. They found that at the elevated temperatures, degradation was initially fast for several days, which slowed down over 100 days and eventually stopped with about 60 % of the cellulose degraded. The rate of degradation was the same for both temperatures, with no obvious observation of alkaline hydrolysis. The main finding of the study was that it was not acceptable to extrapolate the data obtained for higher temperatures to data obtained at RT in the determination of rate constants for the alkaline hydrolysis, therefore, they were unable to determine if the second phase of degradation seen in the 60 °C and 90 °C experiments would be witnessed at 25 °C. They concluded that the predictions obtained in the work by Van Loon and Glaus <sup>94, 128</sup> were “not on the safe side”.

To gain a more realistic prediction, a long-term experimental study was performed by Glaus and Van Loon which covered a twelve year period <sup>108</sup>. Various cellulosic materials were reacted in artificial cement pore water under anaerobic conditions at ambient temperature. Their results agreed with the initial fast stage of degradation where peeling predominates, followed by a slow degradation; however previous kinetic models were described as being inadequate at modelling the second slow phase of degradation, with the mid-chain rate constant value proposed by Pavasars shown to be inconsistent (too fast) with the data produced from their long-term study. A new three phase reaction sequence was proposed: 1. an initial rapid peeling off of glucose units of cellulose, 2. slower mid-chain fragmentation catalysed by base which generates new end groups that allow the peeling reaction to continue, 3. complete stopping of the degradation of both the peeling and the mid chain scission, and eventually the rate of mid chain scission reaches zero when there are no more amorphous regions remaining, and for peeling to continue it was hypothesised that a conversion of crystalline to amorphous cellulose must occur by an as yet unknown process.

Van Loon and Glaus concluded that both their own model and the model proposed by Pavasars were inappropriate at estimating the time taken for the complete degradation of cellulose under repository conditions. Pavasars’ estimation of 500 years was considered to be too short due to their adoption of a rate constant for the mid-chain scission reaction

being too high, and Van Loon and Glaus' estimation of  $10^6$  years was deemed to be too slow, due to them not taking into account the new unknown processes which allow the peeling reaction to continue. In conclusion to their long-term study, Glaus and Van Loon estimated that the complete degradation of cellulose would take between one and five thousand years<sup>108</sup>.

Other processes which may allow the degradation to continue include radiolytical and microbial degradation. Baston *et al.*<sup>144</sup> determined the influence of irradiation on cellulose degradation under repository conditions, to determine if radiation can increase degradation after the stopping reactions. To test the effect of radiation, cellulose was degraded under alkaline, anaerobic conditions to initially degrade away any amorphous material, the remaining cellulose was then gamma-irradiated and degraded again and compared with identical un-irradiated experiments and the total organic carbon of the leachate was determined. The sample which had received the highest dose of radiation was a darker colour of yellow, which is related to the number of chain ends under attack and is proportional to the amount of material dissolved and a sign of greater degradation<sup>107</sup>. This was confirmed by measurement of the total organic carbon after the additional experiments, which was higher in the irradiated sample. The solubility of plutonium in the leachate also increased due to an increased concentration of CDPs. However, the dose of radiation in these experiments was far greater than the amount of radiation which is expected to be present in a repository, and only accounted for an additional 4% degradation. Also, in a report by Chambers *et al.* it states that to a limited extent in relation to the overall repository, the irradiation of cellulose causes an increase in disorder, an increase in mid-chain scission and an increased production of ISA<sup>145</sup>. It has also been noted that although radiation may speed up degradation, it may also destroy CDP-radionuclide complexes and in this case may be beneficiary for repository safety<sup>144</sup>.

Microorganisms are also known to degrade cellulose under anaerobic conditions, but a study by Hu and Yu<sup>146</sup> indicated that the optimum conditions for microbial degradation was approximately pH 7, which is a lot lower than the expected pH of a repository which is expected to remain high for thousands of years, also, as in the effect of radiation, a positive effect may also be witnessed as microbial activity could have an enhanced effect of destroying the complexants before they are able to affect radionuclide migration<sup>147</sup>.

### 1.3.4 Stability of ISA

Another important characteristic which will influence the amount of ISA present is the stability of ISA under repository conditions. The degradation of ISA was studied by Greenfield *et al.*<sup>98</sup> by bubbling either O<sub>2</sub>, N<sub>2</sub> and air through saturated Ca(OH)<sub>2</sub> solutions of ISA at RT and 80 °C and the solutions were allowed to equilibrate for periods of up to ten months. After this time, minor, additional peaks were observed in the oxygenated and aerated samples for the RT experiment only and no additional peaks were observed for the anaerobic experiment. However, at 80 °C additional peaks were observed for both aerobic and anaerobic conditions, with much greater degradation being observed for the aerobic experiments, and very little additional degradation was observed for the anaerobic experiment. The results suggested that oxygen was required for any significant degradation of ISA, especially at ambient temperature.

Although, ISA is reported to fragment at high temperatures<sup>109</sup>, it is thought that both  $\alpha$ - and  $\beta$ -ISA are stable at temperatures up to 125 °C<sup>148</sup>. Van Loon and Glaus originally stated that  $\alpha$ - and  $\beta$ -ISA are stable in alkaline solutions at RT<sup>94</sup> however, in a more recent publication, Glaus and Van Loon reported that small losses of  $\alpha$ -ISA were witnessed due to the conversion into smaller chain organic acids (glycolic, formic and lactic acid) under anaerobic conditions at RT where transformations of 1  $\mu$ mol of ISA per gram of solid Ca(OH)<sub>2</sub> or cement were witnessed after 3 years<sup>108</sup>.

### 1.3.5 ISA Sorption

The sorption of ISA onto the cementitious repository will affect its equilibrium concentration in cement porewater and thus the impact that it can have on radionuclide migration, and studies of sorption have therefore also received attention. Sorption of ISA on cement based materials analogous to a repository was studied by Van Loon and Glaus<sup>94</sup>, in their experiments ISA was added to artificial cement pore water and hardened cement was added, the results indicated that both  $\alpha$ - and  $\beta$ -ISA both sorbed at a concentration of approximately 0.3 mol kg<sup>-1</sup> to the cement. Those results predict that the total ISA in solution in a repository may be reduced by three orders of magnitude due to sorption<sup>94</sup>.

Pavasars also witnessed high levels of ISA sorption onto cement vessels during experiments where cellulose was degraded in an encapsulated cement matrix, where the concentration of ISA in solution went from 19.1g/L to 13.8g/L<sup>115</sup>; the solution which

leached out of the cement vessels contained only trace amounts of ISA<sup>115</sup>, indicating that the loss of ISA was due to sorption onto the cement matrix.

Biddle *et al.*<sup>124</sup> also studied sorption of ISA onto the cement of the repository and found that ISA sorbs to the cementitious grout at distribution ratios of  $30 \text{ cm}^3 \text{ g}^{-1}$  for the concentrations of ISA predicted to be present in a repository by Van Loon and Glaus ( $10^{-4}$ – $10^{-5}$  M)<sup>94</sup>. As mentioned, Van Loon and Glaus predict an ISA concentration of  $10^{-4}$ – $10^{-5}$  M in a repository due to the degradation of cellulose and loss of ISA due to sorption, and at that concentration, little effect was seen on the reduction of sorption of radionuclides that they studied<sup>94</sup>. Similar conclusions were made by Pavasars<sup>115</sup>.

### 1.3.6 Previous work on ISA

Because ISA is known to be the major cellulose degradation product under repository conditions, its physical properties have been extensively studied; however the vast majority of this work has only involved  $\alpha$ -ISA, with very little research carried out on  $\beta$ -ISA even though they are both formed in approximately equal amounts under repository conditions and  $\beta$ -ISA is formed in greater amounts in the presence of NaOH.

It is known that each epimer of ISA is present in two forms: at a pH of less than pH 4, the carboxylic acid form of ISA undergoes an acid catalysed transformation to the lactone ( $\alpha/\beta$ -D-isosaccharino-1,4-lactone)<sup>149, 150</sup>.

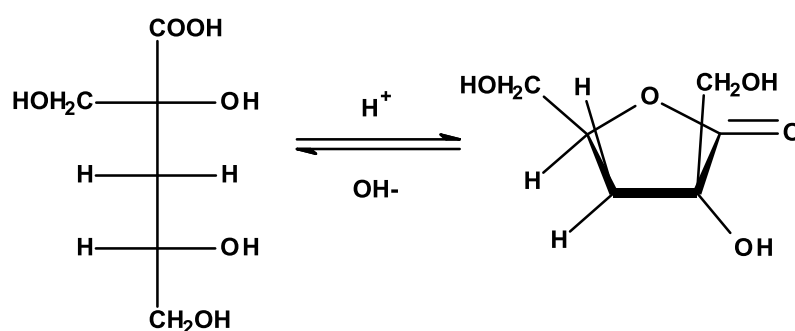


Figure 20: The open-chain and lactone forms of ISA

At acidic pHs Ekberg *et al.*<sup>151</sup> and Brown *et al.*<sup>152</sup> have studied the rates of the transformation between the two forms of  $\alpha$ -ISA using ion chromatography; by placing a

solution of the carboxylic acid into a low pH solution, they determined that the transformation of the carboxylic acid to the lactone took several hours.

For ISA, the acidity of the carboxylate group or the basicity of its conjugate base is an important parameter when trying to investigate its complexing ability in a repository setting; therefore several researchers have investigated the  $pK_a$  of  $\alpha$ -ISA using various analytical methods, this will be further discussed in section 5.1.

### **1.3.7 Preparation of ISA**

#### **1.3.7.1 Preparation of $\alpha$ -ISA**

The primary method used in the literature for the production of  $\alpha$ -ISA is from the method of Whistler and BeMiller<sup>149</sup> which involves the action of lime water on lactose and the precipitation of the calcium isosaccharinate after a few days of reaction; the procedure is straight forward and readily produces  $\alpha$ -ISA in large yields.

#### **1.3.7.2 Previous methods for the production of $\beta$ -ISA**

There are a few methods for the synthesis of  $\beta$ -ISA<sup>94, 107, 110, 148, 153</sup>; the initial method reported for the preparation and isolation of  $\beta$ -ISA was published fifty years ago by Whistler and BeMiller<sup>148</sup> who degraded guaran (a polymer of D-galacto-D-mannoglycan) under anaerobic, alkaline conditions and who experimented with combinations of sodium hydroxide and calcium hydroxide or with saturated calcium hydroxide alone as the base catalyst. Experiments were performed at various temperatures ranging from ambient to autoclaving at 120 °C and they discovered that at higher temperatures a more complex mixture of reaction products was obtained, which at the time, was attributed to the alkaline hydrolysis of glycosidic linkages. This resulted in their final reactions being performed at room temperature, resulting in relatively long reaction times of up to four months, and in the process, setting the trend for future researchers who have subsequently used room temperature for the preparation of crude  $\beta$ -ISA solution.

Several years after Whistler and BeMiller's publication, Feast *et al.*<sup>153</sup> also reported the synthesis of milligram quantities of  $\beta$ -ISA, whose methods, amongst others, also included the alkaline degradation of guaran and other 4-O-substituted D-glucoses analogous to the work of Whistler and BeMiller. However, due to contrasting results between the two sets of authors, doubts were cast as to whether the molecule isolated by Whistler and BeMiller was

indeed  $\beta$ -ISA. Feast *et al.* quantified their (silyated) ISAs using gas-liquid chromatography, and reported that both  $\alpha$ - and  $\beta$ -ISA were produced in approximately equal amounts, whereas, Whistler and BeMiller stated that, for unknown reasons, their reactions, favoured the production of  $\beta$ -ISA. An explanation for this lays in the fact that Whistler and BeMiller added sodium hydroxide to some of their reactions whereas Feast *et al.* only used calcium hydroxide as the alkaline species. It was reported by Alfredsson and Samuelson<sup>129</sup>, a few years after the paper by Feast *et al.* that  $\beta$ -ISA was produced in approximately 3-times the quantity of  $\alpha$ -ISA (188.2 vs. 63 mmol per 100 g) when cellulose was degraded under anaerobic conditions and when sodium hydroxide was used as the alkaline species. It has since been reported by Greenfield *et al.*<sup>107</sup> that when sodium hydroxide is used as the alkaline species a higher proportion of  $\beta$ -ISA is produced and that equal proportions of both epimers are produced when only calcium hydroxide is used. The main controversy, however, was that the molecule reported by Whistler and BeMiller did not lactonize, whereas Feast *et al.* isolated and characterised  $\beta$ -ISA in both the derivatised tri-benzoate form and as the free lactone. Evidence for the lactone came in the form of a strong absorbance at  $1779\text{ cm}^{-1}$  in the infrared spectrum, which is characteristic for a 1,4-linked lactone. Whistler and BeMiller also used infrared spectroscopy, but found no such evidence of lactone carbonyl absorption for the beta epimer, with a strong absorption being present for the alpha counterpart. Whistler and BeMiller failed to lactonize their “ $\beta$ -ISA” with both the use of cation exchange resins and with the addition of hydrochloric acid to lower the pH; both methods which are known, from this work, to force lactonisation of  $\beta$ -ISA. It is now known for definite that  $\beta$ -ISA can lactonize; Glaus *et al.*<sup>110</sup> unequivocally characterised  $\beta$ -ISA lactone using NMR and mass spectrometry techniques; a phenomenon which was also witnessed and studied in this work and will be further discussed in chapter 3.

More recently, methods for the synthesis of  $\beta$ -ISA have come from Greenfield *et al.*<sup>107</sup> and Glaus *et al.*<sup>110</sup> In the report published by Greenfield *et al.* degradation experiments were carried out under various conditions with the aim being the identification of CDPs and the determination of the mechanistic pathways of resulting species which may be produced from cellulosic waste which may be present in a radioactive waste repository. By performing degradation experiments, Greenfield *et al.* were able to determine favourable conditions for the preparation of crude  $\beta$ -ISA solution. Greenfield *et al.* produced crude  $\beta$ -ISA by contacting microcrystalline cellulose with sodium hydroxide solution as base under anaerobic, ambient conditions for thirteen days and to isolate pure  $\beta$ -ISA, small aliquots

were fractionated on a preparative anion exchange column and appropriate fractions collected and combined. Evaporation of the combined fractions produced a syrup which was converted to the calcium salt of  $\beta$ -ISA by precipitation with calcium hydroxide yielding 0.3 g of  $\beta$ -ISA from 50 g of starting material.

Glaus *et al.*<sup>110</sup> have also reported the preparation of  $\beta$ -ISA by contacting microcrystalline cellulose with limewater at ambient temperature under anaerobic conditions for periods of up to six months, and isolation was achieved by passing the crude mixture of products through an analytical HPAEC system and collecting fractions of interest using a fraction collector. After “several” days 1.5 g of crude  $\beta$ -ISA was isolated which was passed through the system again and after 450 injections, 220 mg of pure  $\beta$ -ISA was obtained and characterised using MS/MS, GC-MS and NMR.

It seems obvious from the literature that a significant amount of research is not being undertaken because  $\beta$ -ISA is not readily available in sufficient quantities. One example is highlighted in a report by Chambers *et al.*<sup>145</sup>: they note that solubility data is not available for the calcium salt of  $\beta$ -ISA, they then go on to say that in a repository the solubility of plutonium will be limited by the solubility of ISA in saturated  $\text{Ca}(\text{OH})_2$  solution, so current modelling studies will be more accurate if they involve both  $\alpha$ - and  $\beta$ -ISA; especially when  $\beta$ -ISA is expected to make up at least 50 % of total repository ISA and its solubility is expected to be much greater than that of  $\alpha$ -ISA<sup>149</sup>. Furthermore, in a study by Greenfield *et al.*<sup>99</sup> which investigated the effect of ISA on the solubility of plutonium<sup>99</sup>, it was determined that  $\beta$ -ISA increased the solubility of plutonium slightly more than  $\alpha$ -ISA, however, experiments were limited, in their report the authors state that  $\beta$ -ISA was only available in very small quantities due to the difficulty in isolating the compound.

#### **1.4 Method of analysis used for monitoring ISA production and CDP formation: HPAEC–PAD**

HPAEC-PAD was one of the principle analytical techniques used in this thesis, so its mode of separation will be explained in more detail in the following paragraphs.

The combination of high performance anion exchange chromatography linked with pulsed amperometric detection was first proposed by Rocklin and Pohl<sup>154</sup> and its application for the analysis of carbohydrates was reported by Johnson<sup>155</sup>. HPAEC–PAD is now one of the most established methods for the detection of sugars and related compounds and its uses

include: the analysis of food, beverages and medical samples; an extensive list of these applications and many others can be found in the review by Cataldi *et al.*<sup>156</sup>.

The advantage of using HPAEC–PAD for the analysis of carbohydrates is because it is a very sensitive technique capable of detecting sugars and their derivatives in the picomole level<sup>156</sup> and allows for an analysis requiring very little sample preparation, only filtration and dilution, but more importantly, one which requires no lengthy derivatisation procedure. HPAEC–PAD is selective and specific for the separation and detection of carbohydrates meaning that neutral or cationic species which may be present in the sample quickly pass through the column and elute in or close to the void volume. Furthermore, amperometric detection only detects molecules with oxidizable functional groups<sup>157</sup> so species which cannot be oxidised are not detected, meaning various interfering analytes e.g. small aliphatic acids which may be present in the sample matrix which may otherwise mask valuable analyte peaks, can be ignored.

HPAEC–PAD has previously been used for the detection of  $\alpha$ - and  $\beta$ -ISA<sup>12, 94, 100, 107-112</sup>, however several other instrumental techniques have also been reported for their detection and quantification, all of which have limitations in comparison. As previously mentioned, GC-MS requires sample derivatisation due to the in-volatile nature of ISA, (and carbohydrates in general)<sup>94, 96, 107, 110, 112, 115-120</sup>; traditional reverse phase HPLC has also been used<sup>98, 116, 118, 121, 122</sup>, but due to the near neutral pH of the mobile phases, ISA elutes as a mixture of both lactone and open-chain conformations whereas with the high pH mobile phase used in HPAEC-PAD, ISA is rapidly transformed into the open-chain form, making analysis much less complicated. Capillary zone electrophoresis (CZE)<sup>96, 123</sup> has also been used, but with this technique,  $\alpha$ - and  $\beta$ -ISA remain unresolved and elute as a single peak. PAD does not discriminate between similar carbohydrates; therefore mixtures must be separated prior to detection. With the carbohydrate selective columns utilised with HPAEC-PAD this is achievable, allowing for the separation and quantification of closely related molecules, such as  $\alpha$ - and  $\beta$ -ISA.

#### **1.4.1 Separation mechanism**

In HPAEC-PAD, separation is based on the ionic interactions of the analytes dissolved in the mobile phase ( $A^-$ ) with the positively charged functional group of the stationary phase. Analytes will separate based on their having different levels of interaction with the stationary phase, which will determine the rate at which they migrate through the column.

During analysis the analytes are in equilibrium, partitioning between the stationary phase and the mobile phase, and the position of this equilibrium will depend on the following distribution constant:

$$K_D = \frac{[A_{stationary\ phase}^-]}{[A_{mobile\ phase}^-]}$$

The value of the constant, and hence the affinity of the analyte with the stationary phase will be determined by the charge of the analyte under the conditions of the mobile phase, and hence separations will occur due to differences in the acid dissociation constants ( $K_a$ ) of each analyte, allowing for the separation of the diastereoisomers of  $\alpha$ - and  $\beta$ -ISA with only small differences in  $pK_a$  values.

#### **1.4.2 Mobile phase**

The mobile phase most commonly utilized in HPAEC–PAD is sodium hydroxide solution and this eluent has been used in the vast majority of methods reported in the review by Cataldi *et al.* for the analysis of carbohydrates using this instrumental technique<sup>156</sup>. The high pH of the NaOH mobile phase ensures that carbohydrates, which usually have high  $pK_a$  values, become ionised and are amenable to separation by the anion exchange mechanism. In preparing sodium hydroxide solutions, it is necessary to take precautions to avoid the absorption of atmospheric carbon dioxide, avoiding the formation of sodium carbonate (see experimental section 2.2.1).

#### **1.4.3 Stationary phase**

The high pH environment utilised by HPAEC–PAD is not suitable for traditional silica based HPLC columns, as the silica backbone would dissolve, therefore, with HPAEC-PAD strong anion exchange columns are used which are designed for the separation of carbohydrates. Columns utilise a micro porous polymeric based backbone as an inert support matrix which are covered with a fine latex of microbeads, functionalised with positively charged quaternary ammonium ions which facilitate anion exchange between the counter ions of the mobile phase and negatively charged analytes. Although anion exchange is the major separation mechanism based on differences in  $pK_a$  values, non-polar interactions, due to the hydrophobic backbone of the stationary phase also influence retention. Resins are designed to be stable over the entire pH range, allowing for conditions

which are favourable for the oxidation of carbohydrates at the gold working electrode (in the detector, see next paragraph).

#### **1.4.4 Pulsed Amperometric Detection (PAD)**

For carbohydrate and sugar acid analysis using HPAEC-PAD, detection is performed directly using electrochemical detection in the amperometric detection mode; hence a measurement of current is made between a pair of electrodes in an electrochemical cell, which consists of a gold working electrode, a silver/silver chloride reference electrode and a titanium cell body making up the counter electrode<sup>154, 158</sup>.

In amperometric mode, detection occurs when molecules, containing oxidizable functional groups are oxidized at the gold working electrode by the application of a positive potential, resulting in electrons being transferred from the oxidized species to the surface of the gold electrode. The generated electrical current, which is proportional to the concentration of the analyte is measured by integrating the current over time, known as charge and is measured in coulombs<sup>157</sup>.

#### **1.4.5 Development of pulsed waveforms**

It was initially thought that carbohydrates were not very electro-active at gold working electrodes; however, this was due to early amperometric detection methods using only single potentials, resulting in the products of oxidation sorbing to, and poisoning the electrode surface, thus inhibiting further oxidation<sup>159</sup>.

To avoid this problem, methodologies were developed which applied a series of potentials (waveforms), with the aim being to clean the surface of the electrode. The continuous repeating of the waveform provides the name “pulsed” amperometric detection. Each waveform is split into several potentials applied for given amounts of time, designated E1, E2, etc., in time periods of t1, t2, etc. Potential E1 is the detection potential, whilst the remaining potentials are used to clean the electrode surface of any interfering species and to restore its surface for the next measurement.

In a waveform developed by Rocklin and Pohl<sup>154</sup>, cleaning was achieved by raising the potential after the initial detection period, in what is known as oxidative cleaning. Oxidative cleaning removes the products by desorption, resulting in the formation of a mono layer of

gold oxide on the electrode surface, this is followed by a reductive reactivation of the electrode, resulting in a mono layer of gold oxide being stripped away from the surface of the electrode resulting in the formation of a new gold surface. However, this results in the gradual erosion of the electrode surface over time <sup>160</sup>, which is problematic because with PAD, the measured charge is proportional to the rate of oxidation, and to get reproducible results the rate at which the analytes are transported to the electrode must remain constant; which is proportional to the surface area of the electrode. However, when gold is lost during oxidative cleaning, the surface area is reduced and a decrease in detector response is witnessed, resulting in reduced peak areas over time <sup>161</sup>.

Jenson and Johnson <sup>160</sup> later determined that by avoiding oxidative cleaning, and thus avoiding the formation of gold oxide, dissolution of the electrode could be minimised. This resulted in a quadrupole waveform being developed by Rocklin *et al.* <sup>162</sup> which utilised a negative potential to clean the surface of the electrode, providing less time for gold oxide to form, thus minimising dissolution and recession of the gold electrode, and therefore increasing analyte reproducibility. In optimizing the quadrupole waveform Rocklin *et al.* determined that there was no loss in analyte peak area after two weeks of repeat injections, whilst in contrast, with the waveform developed by Rocklin and Pohl <sup>154</sup> they determined that there was a 45 % loss in peak area over the same time period <sup>162</sup>.

The quadrupole waveform developed by Rocklin *et al.* consists of four pulses which are applied from the potentiostat, termed E1 – E4 in designated time periods of t1 – t4 <sup>154, 161</sup> (Figure 21). Initially, a potential of 0.1 V is applied which is known as the detection potential for a period of 400 ms (E<sub>1</sub>, t<sub>1</sub>) and the resulting current is measured in the last 200 ms of t<sub>1</sub> (t<sub>det</sub>). When changing from one potential to another, for example from E<sub>4</sub> back to E<sub>1</sub> a charging current is produced which is not part of the analyte oxidation current, so during E<sub>1</sub> when the analyte is oxidised and a current produced, a short delay is allowed before any measurement of current is taken to allow for the charge current to dissipate <sup>157</sup>, so the first 200 ms of E<sub>1</sub> is known as a delay period (t<sub>del</sub>), and is ignored. A negative potential of -2.0 V for 10 ms is next applied, which is known as reductive cleaning, which cleans the surface of the electrode (E<sub>2</sub>, t<sub>2</sub>), followed by a potential of 0.6 V (E<sub>3</sub>, t<sub>3</sub>, 10 ms) which forms a small amount of gold oxide on the surface of the electrode, these two steps ensure that the surface of the working electrode remains active, and finally a negative potential of -0.1 V is applied (E<sub>4</sub>, t<sub>4</sub>, 60 ms) which reduces the previously formed gold oxide back to gold resulting in a working electrode ready for the next measurement; with the entire process only taking 500

ms. This process is continuously repeated or “pulsed” to gain multiple data points and hence produce a peak so that the analyte can be detected. As the waveform only takes 500 ms, a frequency of 2Hz can be used, allowing many data points per peak to be collected in a short period of time, allowing for the detection of very sharp early eluting peaks, which may otherwise be missed with slower waveforms.

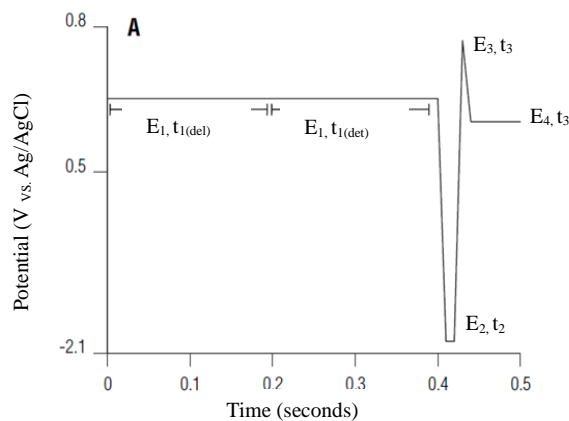


Figure 21: Quadrupole waveform utilized by the ED40 detector, modified from Dionex technical note 21 <sup>161</sup>

## 1.5 Aims and objectives

It was identified in the literature, as previously discussed in chapter 1, that large amounts of research have been performed to study the physical properties of  $\alpha$ -ISA especially in respect to its effect on the safety of a radioactive waste repository post-closure, whereas only limited comparative research has been performed on  $\beta$ -ISA due to the difficulty in obtaining large samples of that compound. With this in mind, the overriding aim of this research is to produce a robust method for the synthesis and isolation of  $\beta$ -ISA.

To accomplish the above aim the key objectives of this research were to develop methods that maximized the production of  $\beta$ -ISA. In chapter 3, the results of degradation experiments to investigate methods of maximizing the production of crude  $\beta$ -ISA solution will be described, with the main aims being to reduce the reaction time and improve yields. To achieve this objective, pure cellulose powder will be degraded at different temperatures and comparisons will be made between sodium hydroxide and calcium hydroxide as the alkaline degradation media. Once an optimal method for producing  $\beta$ -ISA has been determined the next objective will be to develop a method for isolating pure  $\beta$ -ISA. In

chapter 4, the results of experiments which were directed at improving the current methods for the isolation of pure  $\beta$ -ISA will be described. To achieve this objective previously published methods for the synthesis of  $\beta$ -ISA will be investigated and new isolation methods will also be developed.

Another aim of this work is to investigate the chemical properties of  $\beta$ -ISA. In chapter 5, the results of experiments describing the chemical properties of ISA will be described; including determining the solution state properties of both  $\alpha$ - and  $\beta$ -ISA such as measurement of the  $pK_a$  and measurement of the forward and reverse rate constants for the transformation of the carboxylic acid into the cyclic lactone, information which will help to estimate the ability of  $\beta$ -ISA to complex with metals.

## 2 Experimental Methods

### 2.1 General Reagents

The general reagents used in this experimental section were purchased from either Sigma-Aldrich Co. Ltd (Gillingham, Dorset, UK) or Fisher Scientific UK (Loughborough, Leicestershire, UK) unless otherwise stated.

### 2.2 General Analytical Procedures

#### 2.2.1 HPAEC–PAD

Cellulose degradation solutions were analysed by HPAEC–PAD using a Dionex 3000 Ion chromatography system (Dionex, Camberley, UK) which utilised “Chromeleon” software to integrate and process chromatographic data. The system employed an AS50 auto sampler, GS50 gradient pump and an ED50 electrochemical detector using a gold working electrode and an Ag/AgCl reference electrode in the amperometric detection mode which was pre-programmed with a quadrupole waveform. Separation was performed on a Dionex CarboPac PA20 column (6  $\mu\text{m}$  particle size, 250 mm length, 3 mm internal diameter and  $\leq 10 \text{ \AA}$  pore size) and a CarboPac PA20 guard column (3 x 150 mm). Unless otherwise stated, analytes were eluted with a NaOH (50 mM) isocratic mobile phase at a flow rate of  $0.5 \text{ ml min}^{-1}$  and following each analysis, the column was regenerated by eluting with NaOH (200 mM) through the column for 15 minutes.

To obtain optimum results eluents were prepared in a defined manner, for example, when preparing sodium hydroxide stock solution, a strong solution of NaOH (~ 50 %) is used as opposed to using solid sodium hydroxide pellets, as this reduces the chance of carbonate contamination; sodium carbonate is present as a thin layer on solid sodium hydroxide pellets so it should be avoided<sup>157, 163</sup>. With the 50 % solution, any sodium carbonate present is expected to sink to the bottom, so by pipetting the solution from the centre of the container, carbonate contamination can be minimized. Ultra pure water which is free from dissolved carbon dioxide should also be used to dissolve the sodium hydroxide solution, also to prevent carbonate formation. The eluent containers are maintained in an inert atmosphere by blanketing with helium to avoid carbon dioxide absorption from the air which will also introduce carbonate into the mobile phase. Under the high pH conditions of the mobile phase, carbonate becomes a divalent anion, so it binds very strongly to the

column <sup>157</sup>, thus interfering with analyte–stationary phase interactions and decreasing column performance <sup>157</sup>.

### **2.2.2 NMR**

NMR spectra of selected samples were recorded on either a Bruker Avance 400 MHz or 500 MHz spectrometer using Bruker pulse sequences at ambient temperature unless otherwise stated. Samples were dissolved in either D<sub>2</sub>O or CDCl<sub>3</sub> (GOSS Scientific Instruments Ltd, Nantwich, UK) unless otherwise stated and chemical shifts are given in parts per million referenced to acetone (<sup>1</sup>H) or internal CDCl<sub>3</sub> (capillary inset in D<sub>2</sub>O samples).

### **2.2.3 GC–MS**

GC-MS of various samples was performed on an Agilent 7890 gas chromatograph. Typically, 1 µl of sample (100 ppm) was injected into the system and a 50:1 split ratio was applied. Analytes were eluted with a helium carrier gas through an Agilent HP-5MS column consisting of a (5%-phenyl)-methylpolysiloxane non-polar stationary phase. The system employed an Agilent 5975 mass spectrometric detector utilising electron impact ionisation. Unless otherwise stated, a gradient temperature programme was used with an initial temperature of 50 °C (held for 0.5 min), then rising at 10 °C per min until reaching 280 °C and held at 280 °C for a further ten minutes; for a total run time of 33.5 minutes; operating with a flow rate of 1 ml min<sup>-1</sup>.

### **2.2.4 High resolution mass spectrometry (HRMS)**

High resolution mass spectra (HRMS) of synthesised compounds were recorded on a Bruker micrOTOF-Q spectrometer fitted with an ESI interface and operating in either positive or negative ion mode by Dr. Neil McLay at the University of Huddersfield.

### **2.2.5 Total Organic Carbon (TOC)**

The total organic carbon (TOC) of various cellulose degradation samples was determined using a Shimadzu TOC505A analyser. Prior to analysis, samples were diluted 20-fold in deionised water and the pH reduced to pH 2 with the addition of HCl (2 M, 100 µl).

### **2.2.6 Measurement of pH**

Where stated, the pH of solutions was measured using a Beckman ø40 pH Meter (High Wycombe, UK) and to measure the pH directly in NMR tubes, a long reach NMR pH electrode was used (Hanna instruments, Mannheim, Germany).

## **2.3 Degradation Experiments – Investigating methods to maximise the production of crude beta ISA**

Two sets of experiments were carried out to compare the production of crude  $\beta$ -ISA when either sodium hydroxide or calcium hydroxide was used as the alkaline species.

### **2.3.1 Degradation of cellulose in NaOH at RT, 50 °C or 90 °C**

In three separate experiments, cellulose powder (20 g, microcrystalline powder, 20  $\mu$ m particle size) was added to a sodium hydroxide solution (2 M, 200 ml) and the mixture was added to standard quickfit glassware and stirred under an atmosphere of nitrogen at RT, 50 °C or 90 °C for up to two months. Periodically, each experiment was sampled using a syringe and withdrawing an aliquot of the solution through a septum. Samples, (c. 6 ml) were centrifuged (3000 rpm, 30 min) and the resulting supernatants were filtered (Millex, 0.22  $\mu$ m syringe filters) and stored at 4 °C in sealed sample vessels until required for analysis. The remaining undissolved solid was stored in the dark at ambient temperature.

### **2.3.2 Degradation of cellulose in Ca(OH)<sub>2</sub> at RT, 50 °C, and 90 °C**

Experiment 2.3.1 was repeated but substituting NaOH with a saturated calcium hydroxide solution (2 M, 200 ml, Acros Organics).

### **2.3.3 Degradation of cellulose in either Ca(OH)<sub>2</sub>, NaOH or a mixture of Ca(OH)<sub>2</sub> and NaOH at 90 °C**

In a further three separate experiments, cellulose powder (20 g, microcrystalline powder, 20  $\mu$ m particle size) was added to either a calcium hydroxide (200 ml, 2 M), sodium hydroxide (200 ml, 2 M) or a mixed calcium hydroxide and sodium hydroxide solution (200 ml, 2 M of Ca(OH)<sub>2</sub> and 2 M of NaOH) and the mixture was stirred under a stream of nitrogen at 90 °C for up to two months. Periodically, the experiments were sampled using a syringe and withdrawing an aliquot of the solution through a septum. Samples (c. 6 ml)

were centrifuged (3000 rpm, 30 min) and the resulting supernatants were filtered (Millex, 0.22  $\mu\text{m}$  syringe filters). Throughout the experiment, the pH was recorded using a pH meter, and samples were stored at 4  $^{\circ}\text{C}$  in sample vessels until required for analysis. The remaining undissolved solid was stored in the dark at ambient temperature.

### **2.3.4 Extraction of unreacted solid from cellulose degradation experiments**

To investigate the sorption of cellulose degradation products onto the un-reacted solid material (from the experiments in section 2.3.2.), the solids were extracted with a saturated  $\text{NaHCO}_3$  solution as follows:

To each solid sample ( $\text{Ca}(\text{OH})_2$  samples, approximately 2.45 g of hydrated solid was recovered,  $\text{NaOH}$  samples, approximately 1.33 g of hydrated solid was recovered and for the mixed samples, approximately 3.4 g of hydrated solid was recovered),  $\text{NaHCO}_3$  (1 M, 10 ml) was added, and to increase the available surface area, the solid was broken up with a spatula and the sample tube shaken, vortexed and centrifuged (3000 rpm, 30 min). The supernatant was filtered (Millex, 0.22  $\mu\text{m}$  syringe filters) and stored at 4  $^{\circ}\text{C}$  in sample vessels until required for analysis. Prior to extraction, samples were left to air dry for several months.

### **2.3.5 Monitoring cellulose degradation reactions using HPAEC-PAD**

The cellulose degradation reactions were monitored primarily by detecting the amount of  $\alpha$ -ISA and  $\beta$ -ISA produced as a function of reaction time. For a typical analysis, the filtered samples were diluted 40-fold with ultra pure water and D-ribonic acid (25 ppm) was added as an internal standard. Analysis was performed using the HPAEC-PAD conditions as described in section 2.2.1. To quantify  $\alpha$ -ISA and  $\beta$ -ISA in the degradation samples in ppm or mg/l, a series of  $\alpha$ -ISA standards were analysed on the HPAEC-PAD using the same conditions as described above, to generate a calibration curve, and the resulting regression equation describing the line of best fit was used to determine the unknown concentrations.

### **2.3.6 Analysis of cellulose degradation samples using HPIEC**

Various samples from the cellulose degradation experiments were qualitatively analysed by HPIEC for the detection of short-chain aliphatic acids such as formic and lactic acid. Samples were diluted 50-fold in ultra pure water and 2-hydroxyvaleric acid (50 ppm) added

as an internal standard. Analysis was performed on a fully integrated Dionex ICS-1500 Ion Chromatography system based on isocratic separation and comprised of an IonPac ICE-AS6 Analytical Column (8  $\mu\text{m}$  particle size, 250 mm length, 9 mm internal diameter), an AMMS-ICE micro-membrane suppressor and a conductivity detector. The analytes were eluted with a 0.5 mM HFBA (heptafluorobutyric acid) mobile phase at a flow rate of 0.8 ml  $\text{min}^{-1}$  and detected by suppressed conductivity using TBAOH (tetrabutylammonium hydroxide, 5 mM) as an eluent suppressor.

### 2.3.7 Total Organic Carbon Analysis of cellulose degradation samples

To investigate the loss of ISA during the calcium hydroxide degradation experiments, the samples from the experiments described in sections 2.3.2 and 2.3.3 were analysed for their total organic carbon (TOC) content using a Shimadzu TOC505A analyser as described in section 2.2.5. To estimate the accuracy of the instrument, a standard sample of glucose (1000 ppm, 400 mg organic carbon) was analysed and the mean percentage relative error was calculated as  $\pm 2\%$ .

## 2.4 Preparative Methods

To aid in the identification of cellulose degradation products (CDPs) from degradation experiments; the following molecules were prepared for use as analytical standards.

### 2.4.1 Preparation of Calcium 2-C-(hydroxymethyl)-3-deoxy-D-erythro-pentionate $\text{Ca}(\alpha\text{-ISA})_2 - (\alpha\text{-ISA})$

To gain an analytical sample of alpha ISA; calcium 2-C-(hydroxymethyl)-3-deoxy-D-erythro-pentionate,  $\text{Ca}(\alpha\text{-ISA})_2$  was prepared using the established method of Whistler and BeMiller<sup>149</sup> as follows:

Alpha-lactose monohydrate (100 g) was dissolved in distilled water (600 ml), and calcium hydroxide (27 g) was added to the resulting solution. To remove oxygen, the mixture was sonicated for ten minutes and flushed with oxygen free nitrogen. After stirring for three days at ambient temperature, the mixture was heated under reflux for 8 h and then filtered whilst hot. The filtrate was aliquoted into smaller portions, lyophilised and re-dissolved in deionised water (200 ml) resulting in a brown coloured solution which, upon standing for several days results in the sparingly soluble salt of calcium  $\alpha$ -isosaccharinate precipitating

out of solution as a white chalky solid. The brown solution (see section 3.2.3 for analysis of brown solution) was filtered under vacuum, and the resulting precipitated solid was washed with water, ethanol and acetone. The resulting white solid was dried in a desiccator for several days, resulting in a yield of 4.62 g of crude Ca(ISA)<sub>2</sub>.

Crude Ca(ISA)<sub>2</sub> was recrystallized based on the method of Whistler and BeMiller<sup>149</sup>. A saturated calcium isosaccharinate solution was prepared by dissolving the solid Ca(ISA)<sub>2</sub> (4.5 g) in hot water (200 ml) and filtering under gravity to produce an orange solution. A small portion was removed and left to slowly evaporate at 40 °C in an attempt to grow single crystals large enough for single crystal X-ray crystallography. The remaining Ca(ISA)<sub>2</sub> solution was evaporated under reduced pressure until crystallization began; following this the flask was stored in the refrigerator for several days resulting in a white precipitate of the desired product. Decomposition of the resulting filtered product was observed at temperatures above 250 °C in melting point experiments.

To determine if the synthesis was successful, characterisation was carried out using: Gas Chromatography–Mass Spectrometry (GC-MS), Nuclear Magnetic Resonance (NMR), High resolution mass spectrometry (HRMS) and High Performance Anion Exchange Chromatography – Pulsed Amperometric Detection (HPAEC-PAD).

#### **2.4.1.1 GC-MS: determination of fragmentation pattern for characterisation of Ca(ISA)<sub>2</sub>**

Prior to analysis samples were derivatised with the addition of trimethylsilyl groups using the following optimised method of Sweeley *et al.*<sup>164</sup>.

To a boiling tube,  $\alpha$ -ISA (10 mg), dry pyridine (1 ml), hexamethyldisilazane (HMDS, 0.2 ml) and trimethylsilyldisilazane (TMCS, 0.1 ml) were added. The tube was sealed and shaken for 30 seconds and then left to stand for at least five minutes. The silylated material was then diluted 100-fold in acetone and analysed by GC-MS using the instrumental conditions as described in section 2.2.3.

GC–MS EI observed m/z ions (and % relative abundance): 525 (< 1), 510 (< 1), 437 (1), 423 (< 1), 347 (7), 333 (1), 305 (3), 257 (5), 243 (18), 205 (4), 147 (36), 103 (7) and 73 (100).

#### 2.4.1.2 NMR analysis of Ca(ISA)<sub>2</sub>

Both 1D (<sup>1</sup>H, <sup>13</sup>C, DEPT 135 and DEPT 90) and 2D (COSY, HSQC and HMBC) NMR spectra of the synthesised α-ISA were recorded at ambient temperature as described in section 2.2.2. The sample was prepared by dissolving the prepared α-ISA (approximately 20 mg) in D<sub>2</sub>O (700 µl), and chemical shifts were referenced to acetone.

<sup>1</sup>H NMR (500 MHz, D<sub>2</sub>O) 3.79 ppm (m, 1H) 3.63 ppm (d, 1H, *J* = 11.5 Hz) 3.52 ppm (dd, 1H, *J* = 11.7 Hz, 3.8 Hz) 3.44 ppm (d, 1H, *J* = 11.5 Hz) 3.37 ppm (dd, 1H, *J* = 11.7 Hz, 7.0 Hz) 1.76 ppm (dd, 1H, *J* = 14.6 Hz, 8.2 Hz) 1.60 ppm (dd 1H, *J* = 14.6 Hz, 4.5 Hz). <sup>13</sup>C NMR (100 MHz, D<sub>2</sub>O) 180.0 ppm, 77.8 ppm, 68.4 ppm, 67.9 ppm, 66.0 ppm, 37.6 ppm

#### 2.4.1.3 High resolution mass spectrometry (HRMS) of Ca(ISA)<sub>2</sub>

High resolution mass spectra (HRMS) were recorded in negative ion mode using the instrument described in section 2.2.4. The exact mass calculated for α-ISA, C<sub>6</sub>H<sub>12</sub>O<sub>6</sub> [M-H]<sup>-</sup> was 179.0561 and the exact mass found was 179.0568.

#### 2.4.1.4 HPAEC-PAD: – determination of retention time (t<sub>r</sub>) and linear range

Analysis was performed using the Dionex HPAEC-PAD system and employing elution conditions as described in section 2.2.1.

A set of α-ISA standards ranging from 1 ppm to 1000 ppm were prepared by diluting α-ISA in ultra pure water and D-ribonic acid (50 ppm) was added to each standard as an internal standard. Each standard was analysed in duplicate in the order of dilute to concentrated samples.

#### 2.4.2 Preparation of 2-C-(hydroxymethyl)-3-deoxy-D-erythro-pentono-1,4-lactone – (α-ISA<sub>L</sub>)

The preparation of 2-C-(hydroxymethyl)-3-deoxy-D-erythro-pentono-1,4-lactone was modified from the method that was proposed by Greenfield *et al.*<sup>107</sup>, whom had modified their method from the 1961 work of Whistler and BeMiller<sup>149</sup>. Calcium 2-C-(hydroxymethyl)-3-deoxy-D-erythro-pentionate (4.5 g) was suspended in hot water (25 ml) and a hot aqueous solution of oxalic acid dihydrate (1.25 g in 10 ml) was added. The mixture was filtered hot and the filtrate was passed through a column (c. 10 cm<sup>3</sup>) of

Amberlite IR-120 (H<sup>+</sup>) cation exchange resin. The resin was conditioned by passing HCl through it (2 M, 10 ml) and was then flushed with deionised water. The ISA filtrate was eluted through the column, followed by a wash with deionised water. The column effluent and washings were concentrated under reduced pressure to give the desired product as thick, dark orange syrup. The syrup was added to a large beaker and dissolved in water (~ 50 ml), which was left to slowly evaporate at room temperature resulting in the formation of crystalline solid (melting point 95 – 97 °C).

#### 2.4.2.1 NMR analysis of $\alpha$ -ISA<sub>L</sub>

Analysis was performed using the same instrument and conditions as mentioned in section 2.2.2. <sup>1</sup>H, <sup>13</sup>C, DEPT 135, DEPT 90, COSY, HSQC and HMBC spectra were recorded at ambient temperature. The sample was prepared by dissolving ISA<sub>L</sub> (approximately 20 mg) in D<sub>2</sub>O (700  $\mu$ l) and chemical shifts were referenced to CDCl<sub>3</sub> (capillary inset).

<sup>1</sup>H NMR (500 MHz, D<sub>2</sub>O) 4.86 ppm (m, 1H), 3.91 ppm (dd, 1H, *J* = 13.0 Hz, 2.7 Hz), 3.78 ppm (d, 1H, *J* = 11.6), 3.71 ppm (d, 1H, *J* = 11.6 Hz), 3.67 ppm (dd, 1H, *J* = 13.0 Hz, 6.0 Hz) 2.35 ppm (dd, 1H, *J* = 14.3 Hz, 8.4 Hz), 2.29 ppm (dd, 1H, *J* = 14.3 Hz, 7.2 Hz).  
<sup>13</sup>C NMR (100 MHz, D<sub>2</sub>O) 178.6 ppm, 79.6 ppm, 76.6 ppm, 63.3 ppm, 62.5 ppm, 32.9 ppm

#### 2.4.2.2 High resolution mass spectrometry (HRMS) of $\alpha$ -ISA<sub>L</sub>

High resolution mass spectra (HRMS) were recorded on positive ion mode using the instrument as described in section 2.2.4. The exact mass calculated for  $\alpha$ -ISA-lactone, C<sub>6</sub>H<sub>10</sub>O<sub>5</sub> [MNa<sup>+</sup>] was 185.0426 and the exact mass found was 185.0423.

#### 2.4.2.3 HPAEC–PAD analysis of $\alpha$ -ISA<sub>L</sub> – determination of purity

Analysis was performed using the same instrument and conditions as those in section 2.2.1. To prepare the sample the  $\alpha$ -ISA-lactone (2 mg) was diluted in ultra pure water (2000  $\mu$ l) to produce a 1000 ppm stock solution which could be further diluted as required.

#### 2.4.3 Ethanol solubility tests on liquors produced from the preparation of Ca( $\alpha$ -ISA)<sub>2</sub>

The filtrate remaining after the removal of solid Ca( $\alpha$ -ISA)<sub>2</sub> as described in section 2.4.1 was analysed by HPAEC-PAD using the conditions described in section 2.2.1. The filtrate

was lyophilised and a portion of the freeze-dried material was dissolved in D<sub>2</sub>O and was analysed by a combination of 1D and 2D NMR in order to tentatively identify the components of the mixture.

The filtrate was reconstituted in deionised water and, in an attempt to remove coloured impurities the solution was filtered through a thin bed of charcoal. Solubility tests were carried out on a small portion of the charcoaled filtrate to see if any analytes could be precipitated and isolated:

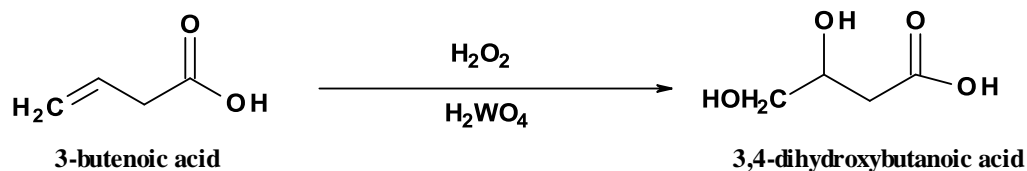
To ten test tubes crude  $\alpha$ -ISA soln. (2.5 ml) was converted into aqueous ethanol solutions ranging from 40 % to 85 % ethanol (see Table 1 for experimental details). The solutions were left to stand overnight resulting in a solid precipitate in each vessel. To remove the solid, each solution was centrifuged (3200 rpm, 30 min) and the solid was dried under a stream of nitrogen. Both the resulting solutions and the precipitated solids were suitably diluted in ultra pure water and analysed by HPAEC-PAD using the conditions as described in section 2.2.1.

Table 1: Experimental conditions for the crude  $\alpha$ -ISA ethanol solubility experiments

Vol. EtOH added (ml)	Vol. $\alpha$ -ISA soln. added (ml)	Vol. H <sub>2</sub> O (ml)	% EtOH soln.
8	2.5	9.5	40
9	2.5	8.5	45
10	2.5	7.5	50
11	2.5	6.5	55
12	2.5	5.5	60
13	2.5	4.5	65
14	2.5	3.5	70
15	2.5	2.5	75
16	2.5	1.5	80
17	2.5	0.5	85

#### 2.4.4 Preparation of 3,4-dihydroxybutanoic acid (DHB)

The preparation of 3,4-dihydroxybutanoic acid was based on the method described by Greenfield *et al.*<sup>107</sup> whom had modified their method from the work of M.A. Asghar<sup>165</sup>.



Tungstic acid (0.2 g) was suspended in a solution of hydrogen peroxide (30 %, 20 ml) and water (50 ml). 3-Butenoic acid (12 ml) was added gradually and the solution was stirred at 70 °C for 48 h. The resulting green solution was filtered through a thin bed of charcoal and the filtrate was extracted with diethyl ether (1 x 100 ml) to remove unreacted starting material. The aqueous phase was concentrated under reduced pressure to produce 3,4-dihydroxybutanoic acid as a yellow syrup (yield = 8.90 g). To determine if the synthesis was successful, characterisation was carried out using GC-MS, NMR and HPAEC-PAD.

#### 2.4.4.1 GC-MS: determination of fragmentation pattern for characterisation of DHB

Prior to analysis 3,4-dihydroxybutanoic acid was derivatised with the addition of trimethylsilyl groups using the method of Sweeley *et al.*<sup>164</sup> as previously described in section 2.4.1.1

GC-MS analysis was performed using the instrument described in section 2.2.3. A gradient temperature programme was utilised with an initial temperature of 80 °C (held for 5 minutes), then rising at 5 °C per min until reaching 280 °C (held at 280 °C for a further five minutes) for a total run time of 50 minutes; operating with a flow rate of 0.83 ml min<sup>-1</sup> and a 25:1 split ratio.

GC-MS EI observed m/z ions (and % relative abundance): 159 (7), 117 (100), 116 (8), 101 (28), 89 (30), 75 (10) and 73 (32).

#### 2.4.4.2 NMR analysis of DHB

NMR spectra of the synthesised 3,4-dihydroxybutanoic acid were recorded using the same instrument and conditions as mentioned in section 2.2.2. <sup>1</sup>H and <sup>13</sup>C spectra were recorded at ambient temperature. The sample was prepared by dissolving approximately 20 mg of 3,4-dihydroxybutanoic acid in D<sub>2</sub>O (700 µl).

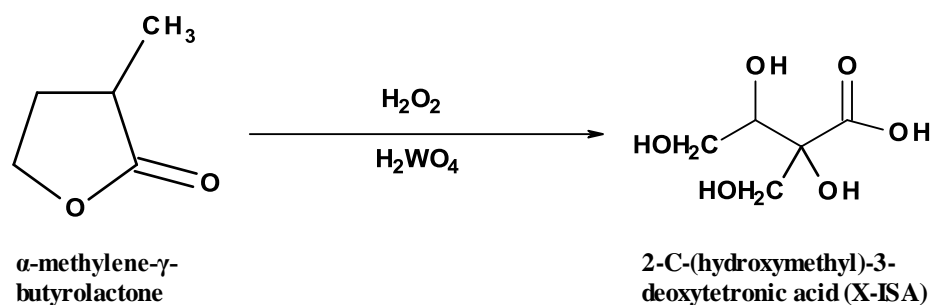
$^1\text{H}$  NMR (400 MHz,  $\text{D}_2\text{O}$ ) 4.65 ppm (m, 1H), 4.48 ppm (dd, 1H,  $J = 10.4$  Hz, 3.7 Hz), 4.29 ppm (d, 1H,  $J = 10.4$  Hz), 2.90 ppm (dd, 1H,  $J = 18.1$  Hz, 5.6 Hz), 2.45 ppm (d, 1H,  $J = 18.1$  Hz).  $^{13}\text{C}$  NMR (100 MHz,  $\text{D}_2\text{O}$ ) 180.2 ppm, 77.0 ppm, 67.2 ppm, 37.2 ppm

#### 2.4.4.3 HPAEC–PAD analysis of DHB – determination of purity and retention time ( $t_r$ )

HPAEC–PAD analysis was performed using the same instrument and conditions as mentioned in section 2.2.1. To prepare the sample, 3,4-dihydroxybutanoic acid (10 mg) was diluted in ultra pure water (10 ml).

#### 2.4.5 Preparation of 2-C-(hydroxymethyl)-3-deoxytetronic acid (xyloisosaccharinic acid, X–ISA)

The preparation of 2-C-(hydroxymethyl)-3-deoxytetronic acid was based on the method described by Greenfield *et al.*<sup>107</sup>.



Tungstic acid (80 mg) was suspended in a solution of hydrogen peroxide (30 %, 800  $\mu\text{l}$ ) and water (2000  $\mu\text{l}$ );  $\alpha$ -methylene- $\gamma$ -butyrolactone (893.6  $\mu\text{l}$ ) was added gradually and the solution was stirred at 70  $^\circ\text{C}$  for 60 h. To this solution, a small amount of charcoal was added and the solution was stirred at 70  $^\circ\text{C}$  for a few minutes. The resulting mixture was filtered hot under gravity through fluted filter paper and the charcoal washed with diethyl ether. The filtrate and washings were evaporated under reduced pressure. Hot ethyl acetate (c. 40 ml) was added to the oily residue resulting in orange coloured solid in the bottom of the flask; the resulting solution was decanted off and concentrated under reduced pressure resulting in the isolation of the desired product as an orange coloured syrup (470 mg). To determine if the synthesis was successful, characterisation was carried out using GC-MS, NMR and HPAEC-PAD.

#### 2.4.5.1 GC-MS: determination of fragmentation pattern for characterisation of X-ISA

Prior to analysis X-ISA was derivatised with the addition of trimethylsilyl groups using the method of Sweeley *et al.*<sup>164</sup> as previously described in section 2.4.1.1. GC-MS analysis was performed using the instrument described in section 2.2.3 and using the gradient programme which was described in section 2.4.4.1.

GC-MS EI observed m/z ions (and % relative abundance): 276 (< 1), 261 (9), 246 (91), 171 (9), 147 (71), 103 (31), 73 (97), 45 (12) and 28 (100).

#### 2.4.5.2 NMR analysis of X-ISA

NMR spectra of the synthesised X-ISA were recorded using the same instrument and conditions as mentioned in section 2.2.2. <sup>1</sup>H and <sup>13</sup>C spectra were recorded at ambient temperature. The sample was prepared by dissolving approximately 20 mg of X-ISA in D<sub>2</sub>O (700 µl) and the pH was increased to pH 14 with the addition of NaOD, and chemical shifts were referenced to acetone.

<sup>1</sup>H NMR (400 MHz, D<sub>2</sub>O/NaOD) 3.86 ppm (d, 1H, *J* = 11.4 Hz), 3.84 ppm (ddd, 1H, *J* = 10.9 Hz, 9.3 Hz, 6.0 Hz), 3.71 ppm (ddd, 1H, *J* = 10.9 Hz, 9.3 Hz, 5.8 Hz), 3.69 ppm (d, 1H, *J* = 11.4 Hz), 2.06 ppm (ddd, 1H, *J* = 13.7 Hz, 9.1 Hz, 5.8 Hz), 1.94 ppm (ddd, 1H, *J* = 13.7 Hz, 9.2 Hz, 6.1 Hz), <sup>13</sup>C NMR (100 MHz, D<sub>2</sub>O/NaOD) 179.7 ppm, 78.1 ppm, 67.5 ppm, 57.7 ppm and 36.6 ppm.

#### 2.4.5.3 HPAEC-PAD analysis of X-ISA – determination of purity and the retention time (*t<sub>r</sub>*)

HPAEC-PAD analysis was performed using the same instrument and conditions as mentioned in section 2.2.1. To prepare the sample, X-ISA (10 mg) was diluted in ultra pure water (10 ml).

## 2.5 Preparation of crude beta ISA ( $\beta$ -ISA)

### 2.5.1 Preparation of crude $\beta$ -ISA using existing methods

For the initial attempt to prepare  $\beta$ -ISA, the following procedure was modified from the method of Greenfield *et al.*<sup>107</sup>. The synthesis was performed several times at different scales; therefore it will only be described once using the largest scale.

Cellulose powder (200 g), deionised water (2000 ml) and sodium hydroxide (40 g) were added to a volumetric flask and the resulting solution was sonicated for ten minutes to remove oxygen bubbles. Nitrogen was bubbled through overnight and the cream coloured solution was sealed and stirred at room temperature for thirteen days. Following this, the solution was centrifuged (12000 rpm (22095 G), 30 minutes) and the supernatant filtered through a number three glass sinter, leaving a pale amber coloured solution. At this point, a portion of the filtrate was diluted in ultra pure water and analysed by the Dionex HPAEC-PAD system using the conditions described in section 2.2.1. To remove sodium ions, the remaining filtrate was passed through a column of Amberlite IR-120 ( $H^+$ ) cation exchange resin (column size 15 cm x 5 cm) after conditioning the resin as described in section 2.4.2 but employing an appropriately larger volume for a larger column. The effluents and washing were lyophilised resulting in a black, sticky crude material (approximately 22.3 g).

### 2.5.2 Preparation of crude $\beta$ -ISA with optimised conditions

From the results of the degradation studies described in section 2.3 it was determined that by increasing the reaction temperature from RT to 90 °C the reaction time could be reduced whilst increasing the production of ISA in the crude solution. Therefore, the reaction described in section 2.5.1 was repeated but with the temperature of the cellulose reaction mixture increased from RT to 90 °C, and the reaction time reduced from 13 days, to 16 h, additionally, an atmosphere of nitrogen was maintained for the duration of the reaction. To determine the time required for optimum reaction, the progress of the reaction was monitored by taking samples every 2 h and analysing them by HPAEC-PAD. Due to the higher temperature, a condenser was attached and the reaction vessel was heated in an oil bath, resulting in the normally white coloured solution turning dark orange/brown. The resulting solution was filtered hot through a number one glass sinter leaving c. 1600 ml of brown coloured solution, and the removal of 142 g of un-reacted starting material. The solution was passed through an Amberlite cation exchange column (as described in section

2.4.2) in order to exchange sodium ions for hydrogen ions reducing the pH of the solution and lactonizing the  $\alpha$ - and  $\beta$ -ISA. The effluent and washings were evaporated under reduced pressure resulting in a “tar” (57 g) which was ready for use in the isolation procedures.

### **2.5.3 Preparation of crude $\beta$ -ISA using microwave heating**

To further reduce reaction time, a small scale experiment was investigated using microwave heating:

Cellulose powder (20 g), deionised water (200 ml) and sodium hydroxide (4 g) were added to a standard round-bottom flask and the resulting solution was refluxed in a microwave oven and heated on full power (750 W). The microwave oven was adapted with a built in magnetic stirrer and a condenser attachment so that reactions could be safely controlled. The experiment was stopped and sampled every minute for 16 minutes and the reaction monitored by HPAEC-PAD using the conditions described in section 2.2.1. No attempts were made to isolate the products of the reaction.

### **2.5.4 Preparation of crude $\beta$ -ISA using microwave heating using either 0.5 M or 5.0 M NaOH**

To investigate the effect of swelling of cellulose fibres on the rate and yield of  $\beta$ -ISA production, an additional small-scale microwave experiment was performed:

To two separate standard round-bottom flasks, cellulose powder (20 g) and sodium hydroxide solution (200 ml, 0.5 M or 5.0 M) were refluxed in a microwave oven using the settings and instrument described in section 2.5.3. The experiment was stopped after 12 minutes and the entire solution were filtered under vacuum through a sintered glass funnel to remove the unreacted cellulose. The cellulose was washed with deionised water (300 ml) and the resulting liquor and washings were further diluted ten-fold and analysed by HPAEC-PAD using the conditions described in section 2.2.1. No attempts were made to isolate the products of the reaction.

## 2.6 Isolation of 2-C-(hydroxymethyl)-3-deoxy-D-threo-pentanoic acid ( $\beta$ -ISA)

### 2.6.1 Soxhlet Extraction followed by short-path distillation

Initial attempts were made to isolate  $\beta$ -ISA using a combination of Soxhlet extraction and short-path (Kugelrohr) distillation.

A portion of crude  $\beta$ -ISA (as described in section 2.5.1, 500 ml) was removed from the reaction prior to passage through the Amberlite column. Instead of passing the solution through the Amberlite column, the pH was reduced to  $< 2$  with the addition of concentrated HCl and the resulting solution was lyophilised overnight resulting in a brown solid (14.10 g). The solid was applied to a Soxhlet extraction thimble and the solid was continuously extracted with refluxing ethanol (500 ml) for 16 h. Following this, there remained a white solid in the sock (10.79 g) and in the round-bottom flask the ethanol was now a dark brown colour.

Following the extraction, the brown ethanol solution was evaporated under reduced pressure resulting in a syrup and a small portion was directly applied to a short path distillation using four bulbs. Approximately 5 ml of sample was applied to the first bulb and was distilled for approximately 1 h under a strong vacuum ( $\sim 1$  mmHg). The distillation temperature was increased gradually to maximum temperatures ranging from 150 - 250°C which resulted in the presence of small amounts of liquid in each of the 3 bulbs (several  $\mu$ l). The colour of the liquid in each bulb ranged from dark brown in the first bulb to pale yellow in the final bulb. Samples were dissolved in D<sub>2</sub>O and analysed by NMR and also by HPAEC-PAD using the conditions as described in section 2.2.

### 2.6.2 Isolation of $\beta$ -ISA using preparative anion exchange chromatography

To isolate small amounts of  $\beta$ -ISA, aliquots (1 ml or 3 ml) of the crude  $\beta$ -ISA solution as described in section 2.5.1 were dissolved in NaOH (0.1 M,  $\sim 100$  ml) and separated on a column of anion exchange resin based on the method of Greenfield *et al.*<sup>107</sup> as follows:

A standard chromatography column (25 x 2 cm) was filled with anion exchange resin (Dowex, 1-X8, 200-400 mesh, chloride form) to a depth of approximately 160 mm using a resin/water slurry. The resin was preconditioned into the acetate form by eluting with

sodium acetate (2 M, 150 ml) followed by deionised water (c. 100 ml) to wash away excess sodium acetate and sodium chloride. The crude  $\beta$ -ISA sample (initially 3 ml, and then 1 ml on subsequent columns) was eluted through the column with a linear gradient of sodium hydroxide (25 ml x 20, 40, 60, 80, 100 mM). The column was repeated several times, each time adjusting the mobile phase conditions by varying the gradient as necessary. Collected fractions (2 ml) were diluted two-fold and screened for  $\beta$ -ISA using HPAEC-PAD using the conditions as described in section 2.2.1. Fractions containing  $\geq 90$  %  $\beta$ -ISA in relation to  $\alpha$ -ISA were combined, lyophilised, diluted in D<sub>2</sub>O (20 mg in 700  $\mu$ l) and analysed by NMR using the conditions as described in section 2.2.2. To simplify the resulting NMR spectra, the  $\geq 90$  % fractions were analysed by NMR again, but this time a few drops of NaOD were added to the D<sub>2</sub>O sample to encourage a complete conversion of the lactone to the open-chain form.

### **2.6.3 Isolation of $\beta$ -ISA using automated preparative anion exchange chromatography**

To increase the yield of isolated  $\beta$ -ISA, a method was developed which utilised an automated preparative anion exchange chromatography set-up. The instrument used was a BioCAD SPRINT, Perfusion Chromatography System, utilising an Amersham Biosciences column (200 or 300 mm x 30 mm). The column was packed with a slurry of anion exchange resin (Dowex, 1-X8, 200-400 mesh, chloride form), which was preconditioned prior to analysis by passing sodium acetate (2 M, 200 ml) and then deionised water (200 ml) through the column.

Crude  $\beta$ -ISA solution was prepared as described in section 2.5.2 and reconstituted in NaOH (0.1 M, 75 ml). For the initial separation, 0.5 ml of sample was injected onto the column using a manual sample injection valve (Rheodyne, LLC, California, USA) and the column was eluted with a linear gradient of 10 – 50 mM NaOH over 50 minutes, and held at 50 mM with a flow rate of 4 ml min<sup>-1</sup> using an automated fraction collector (Pharmacia Biotech Frac-100) until 50 fractions had been collected. Each fraction was screened using HPAEC-PAD (as described in section 2.2.1) and fractions which contained  $\geq 90$  %  $\beta$ -ISA in relation to  $\alpha$ -ISA were combined, lyophilised and analysed by NMR.

To isolate a larger sample of  $\beta$ -ISA, crude  $\beta$ -ISA solution was prepared as described in section 2.5.2 and reconstituted in NaOH (0.1 M, 75 ml) and a further addition of deionised

water (75 ml) was added to reduce the thickness of the solution and in an attempt to reduce the problem of fouling of the anion exchange resin the brown solution was boiled in charcoal (2 %) for several minutes and filtered under gravity resulting in a visibly cleaner solution. For the separation of the crude solution 5 ml of sample was injected onto the column and the column was eluted with a linear gradient of 20 – 40 mM NaOH over 50 minutes with a flow rate of 2 ml min<sup>-1</sup>. Altogether, the column was run 23 times and 79 × ≥ 90 % fractions were collected providing 158 ml of material which after lyophilisation provided β-ISA as a white solid (~ 250 mg). The method of Greenfield *et al.*<sup>107</sup> was used to form the calcium salt of β-ISA: the solid was dissolved in warm deionised water (~ 50 ml) and saturated Ca(OH)<sub>2</sub> solution was added until the mixture reached pH 9, the resulting solution was left to stand at 4 °C for several days to encourage precipitation. After this time a very small amount of white material had precipitated. A portion of the solution was removed (300 µl) and dissolved in D<sub>2</sub>O (300 µl) and analysed by NMR, which indicated β-ISA, but also calcium acetate. In an attempt to isolate β-ISA free from the calcium acetate, the remaining solution was converted into a 90 % ethanol solution and stored at 4 °C for several days. Following this, the sample was filtered under vacuum resulting in the removal of a small amount of brown coloured impurity (14 mg). The remaining filtrate was evaporated under reduced pressure to remove ethanol producing a small amount of white material (~ 200 mg), this was dissolved in deionised water (25 ml) and was then passed through a column of Amberlite resin (as previously described in section 2.4.2) and the eluent and washings were evaporated under reduced pressure to produce orange syrup (163 mg), the sample was submitted for NMR analysis.

To further increase the yield of β-ISA, a larger column was used (300 mm x 30 mm) which was filled with 100 g of Dowex resin. For these runs, new chromatography conditions were applied. Portions of the crude solution (5 ml) were injected onto the column and eluted with a gradient of 10 – 100 mM NaOH over 100 minutes with a flow rate of 2 ml min<sup>-1</sup>. Fractions collected were screened using HPAEC-PAD and fractions containing ≥ 90 % β-ISA were collected as previously described. This operation was repeated (17 times) eluting approximately 85 ml of crude β-ISA and resulting in 232 fractions being suitable for collection; these were lyophilised and analysed by NMR. The NMR analysis indicated that the fractions predominantly contained β-ISA which was present as a mixture of its acid and lactone forms, a large amount of sodium acetate was also present. The material collected was passed through the Amberlite column as described in section 2.4.2 with the intention of

converting the sodium acetate into acetic acid and converting all of the  $\beta$ -ISA into the lactone form. Following the column, the eluent and washings were evaporated under reduced pressure and run on NMR in  $D_2O$  which indicated highly pure  $\beta$ -ISA (c. 1000 mg).

## **2.6.4 Isolation of $\beta$ -ISA using derivatisation followed by normal phase chromatography**

### **2.6.4.1 Acetylation of crude $\beta$ -ISA**

A portion of crude  $\beta$ -ISA-rich syrup (32 g), prepared as described in section 2.5.2 was dissolved in pyridine (200 ml) and a catalytic amount of DMAP (4-N,N-dimethylaminopyridine, 1 g, 8.2 mmol) was added, followed by a gradual addition of acetic anhydride (100 ml) whilst the mixture was stirring in an ice bath. After one and a half hours the mixture was poured onto crushed ice and chloroform (200 ml) was added to extract the acetylated material. The mixture was transferred to a separating funnel and the two layers separated; the organic layer was removed and dried with anhydrous sodium sulphate, the mixture was filtered under gravity and rotary evaporated under reduced pressure resulting in a further syrup (36.56 g), a small portion of which was dissolved in  $CDCl_3$  and analysed by NMR.

### **2.6.4.2 Normal phase chromatography**

To separate the acetylated mixture of  $\alpha$ - and  $\beta$ -ISA and other impurities, the syrup was dissolved in a minimum of ethyl acetate (30 ml) and applied to a normal phase silica column. Prior to the column, a small amount was analysed by TLC using ethyl acetate as eluent (100 %) which, after sulphuric acid staining (20 % concentrated sulphuric acid in ethanol) and heating with a hot air gun to reveal any spots yielded one predominant spot with Rf value 0.46 and at least two minor spots with Rf values of 0.28 and 0.20; and the column was used to isolate the predominate spot. Half of the syrup (16 g) was applied to a silica column (50 x 5 cm bed size) which was eluted with ethyl acetate (100 %). Collected fractions were analysed by TLC and appropriate fractions which had an Rf value of 0.46 were combined, evaporated and analysed by NMR in  $CDCl_3$ . The collected fractions produced 9 g of syrup which were rich in peracetylated  $\beta$ -ISA, but also contained significant amounts of peracetylated  $\alpha$ -ISA. An attempt was made to crystallise the peracetylated  $\beta$ -ISA by dissolving the syrup in acetonitrile (30 ml) adding water as a

counter solvent until the solution was fully saturated and leaving the solution to stand for several days; however, this was unsuccessful.

To gain a purer sample of the peracetylated  $\beta$ -ISA free of the peracetylated  $\alpha$ -ISA, the column was repeated and this time petroleum ether: ethyl acetate (50:50) was used as mobile phase to slow down elution. TLC of the crude syrup prior to the column using the same ether: ethyl acetate (50:50) mobile phase resulted in a predominant spot which had an  $R_f$  value of 0.33. The column was monitored using TLC and appropriate fractions which also contained a spot with the same  $R_f$  value were combined, evaporated under reduced pressure and analysed by NMR. NMR analysis indicated that a better screening technique was required and those fractions rich in total peracetylated ISA (alpha and beta) were analysed by GC-MS using the instrument described in section 2.2.3. A gradient temperature programme was utilised with an initial temperature of 95 °C (held for 1 minute), then rising at 1 °C per min until reaching 120 °C (held at 120 °C for a further five minutes) for a total run time of 31 minutes; operating with a flow rate of 0.84 ml min<sup>-1</sup> and a 10:1 split ratio. GC-MS analysis allowed the percentage of peracetylated  $\beta$ -ISA in collected fractions to be determined, those fractions containing greater than 80 %  $\beta$ -ISA were pooled and the solvent evaporated to give triacetylated  $\beta$ -ISA as a yellow syrup resulting in the pooling of 6 g of syrup containing  $\geq 80$  %  $\beta$ -ISA. The  $\geq 80$  % purity syrup was applied to a second silica column using slower elution conditions; and every 5<sup>th</sup> fraction (20 ml, undiluted) was analysed by GC-MS using the same conditions as described above, allowing for the collection of samples which contained  $\geq 90$ % peracetylated  $\beta$ -ISA. All fractions which contained  $\geq 90$ %  $\beta$ -ISA were pooled and taken forward to the next reaction step i.e. removal of the acetyl groups (deacetylation).

The  $\geq 90$ % peracetylated  $\beta$ -ISA syrup was rotary evaporated under reduced pressure to produce a syrup (2.51 g) which was expected to be in the 2,5,6-tri-*O*-acetyl- $\beta$ -isosaccharino-1,4-lactone conformation.

#### **2.6.4.3 Removal of acetyl groups**

The syrup was dissolved in acetonitrile and water (12:4 v/v) and sodium hydroxide solution (2 M) was added drop-wise to maintain the pH between 12 and 13, this was continued until the reaction had consumed one equivalent of base and the pH remained constant. Following this a small amount of acetic acid (10  $\mu$ l) was added to neutralize the solution. The majority

of the solvent was removed by rotary evaporation under reduced pressure and the sample was finally lyophilised overnight resulting in a white solid (2.28 g), a small portion of which was dissolved in D<sub>2</sub>O and analysed by NMR.

To deacetylate the 2,5,6-tri-*O*-acetyl- $\beta$ -isosaccharino-1,4-lactone, the white solid was dissolved in methanol (7.5 ml) and sodium methoxide (1 g) was added as base catalyst. The mixture was stirred for 2 h and then neutralized and rotary evaporated under reduced pressure to give the sodium salt of  $\beta$ -ISA of  $\geq 90$  % purity as a white solid (2.09 g).

#### 2.6.4.4 Benzoylation of crude $\beta$ -ISA – final procedure

Crude  $\beta$ -ISA was prepared as described in section 2.5.2 and the ISA epimers were converted into their tribenzoate esters based on the method of Whistler and BeMiller<sup>148</sup>:

Crude  $\beta$ -ISA (55 g) was dissolved in pyridine (300 ml) and a catalytic amount of DMAP (1 g, 8.2 mmol) was added before the solution was cooled to 0 °C and then an excess amount of benzoyl chloride (150 g, 1.2 mol) was gradually added whilst stirring. After 2 h of stirring at 0°C and then 16 h at room temperature the mixture was poured onto an equal volume of water to hydrolyse excess benzoyl chloride. Chloroform (500 ml) was added to the reaction mixture and the products extracted. The 2 layers were separated and the chloroform layer dried with anhydrous sodium sulphate. The solution was filtered and the solvent removed under reduced pressure, resulting in a “tacky” dark brown solid (c. 170 g). To remove excess benzoic acid from the tar, it was back extracted from chloroform with a saturated sodium carbonate solution (3 x 50 ml) and the resulting organic layer was filtered and dried with anhydrous sodium sulphate, filtered and evaporated under reduced pressure resulting in a brown solid (76.08 g), a portion of which was dissolved in CDCl<sub>3</sub> and analysed by NMR.

#### 2.6.4.5 Purification of the 2,5,6-tri-*O*-benzoyl-isosaccharino-1,4-lactones

Highly coloured polar impurities were removed by eluting the mixture through a crude silica column using the following method:

The brown solid (76.08 g, from section 2.6.4.4) was dissolved in chloroform (200 ml) and dry silica (approximately 100 g) was added to the round-bottom flask and the mixture was rotary evaporated under reduced pressure to produce a dry crude/silica mix. The mixture

was added dry to a bed of dry silica in a large column (5 cm depth x 30 cm diameter) and coarsely fractionated with a linear gradient which started at 75 % petroleum ether and 25 % ethyl acetate (2000 ml) and rising to 50 % (2000 ml) and finally 100 % ethyl acetate (2000 ml). Altogether, eight large fractions were collected (c. 500 ml each) which were screened by TLC and NMR spectroscopy for 2,5,6-tri-*O*-benzoyl- $\beta$ -isosaccharino-1,4-lactone. NMR analysis indicated that all the collected fractions contained approximately 60 – 70 % of the  $\beta$ -tribenzoate and 30 – 40 %  $\alpha$ -tribenzoate and a small amount of impurities consisting of similar sugar type cellulose degradation products; the identification of which has been investigated and will be further discussed in chapter 5.

Each of the fractions contained approximately the same amount of ISA; therefore, they were combined and evaporated resulting in translucent pale yellow syrup (25.57 g). A large number of coloured impurities were retained by the silica.

To separate and isolate the derivatised ISA isomers, the entire syrup was dissolved in a minimum of ethyl acetate (c. 20 ml) and was applied to a large normal phase silica column (55 cm x 7 cm bed size) which was eluted very slowly with a linear gradient which started at 95 % petroleum ether and 5 % ethyl acetate (2000 ml) rising by 5 % after every 2000 ml was added to the column until 30 % ethyl acetate was used (excess). The eluting fractions were monitored by TLC, and selected fractions were rotary evaporated and analysed by NMR after being suitably dissolved in  $\text{CDCl}_3$ .

Fractions which contained only 2,5,6-tri-*O*-benzoyl- $\beta$ -isosaccharino-1,4-lactone were pooled together and allowed to slowly evaporate resulting in the formation of single crystals suitable for single-crystal X-ray crystallography. Pooled fractions, rich in 2,5,6-tri-*O*-benzoyl- $\alpha$ -isosaccharino-1,4-lactone failed to produce suitable crystals therefore, for the alpha isomer; crystals were grown by experimenting with various binary solvent systems using a “vapour diffusion” method. After testing several solvent systems, it was determined that by dissolving a small amount of the alpha epimer (c. 20 mg) in chloroform (solvent, c. 1 ml) and allowing petroleum ether (counter solvent, 40 – 60°, c. 2 ml) to slowly diffuse into the sample vial, crystals suitable for single crystal X-ray analysis could be produced over a period of days.

#### 2.6.4.6 NMR analysis of 2,5,6-tri-*O*-benzoyl- $\beta$ -isosaccharino-1,4-lactone ( $\beta$ -ISA tribenzoate)

NMR spectra of 2,5,6-tri-*O*-benzoyl- $\beta$ -isosaccharino-1,4-lactone were recorded using the same instrument and conditions as mentioned in section 2.2.2.  $^1\text{H}$  and  $^{13}\text{C}$  spectra were recorded at ambient temperature. The sample was prepared by dissolving approximately 20 mg of the  $\beta$ -ISA tribenzoate in  $\text{CDCl}_3$  (700  $\mu\text{l}$ ) and chemical shifts were referenced to acetone.

$^1\text{H}$  NMR (400 MHz,  $\text{CDCl}_3$ ) 8.17 – 8.04 ppm (m, 6H), 7.72 – 7.60 ppm (m, 3H), 7.52 – 7.44 ppm (m, 6H), 5.00 – 4.94 ppm (m, 1H), 4.92 ppm (d, 1H,  $J = 11.1$  Hz), 4.73 ppm (d, 1H,  $J = 11.1$  Hz), 4.74 – 4.65 ppm (m, 2H). 2.56 ppm (d,  $J = 8.1$  Hz).  $^{13}\text{C}$  NMR (100 MHz,  $\text{CDCl}_3$ ) 171.7 ppm, 166.3 ppm, 165.7 ppm, 164.8 ppm, 134.1 ppm, 133.9 ppm, 133.4 ppm, 130.1 ppm, 130.0 ppm, 129.8 ppm, 128.8 ppm, 128.7 ppm, 128.5 ppm, 128.3 ppm, 78.7 ppm, 74.4 ppm, 65.6 ppm, 65.4 ppm, 32.2 ppm

#### 2.6.4.7 High resolution mass spectrometry (HRMS) of 2,5,6-tri-*O*-benzoyl- $\beta$ -isosaccharino-1,4-lactone ( $\beta$ -ISA tribenzoate)

High resolution mass spectra (HRMS) were recorded in positive ion mode using the instrument described in section 2.2.4. The exact mass calculated for  $\beta$ -ISA-tribenzoate,  $\text{C}_{27}\text{H}_{22}\text{O}_8$  [ $\text{MNa}^+$ ] was 497.1213 and the exact mass found was 497.1222.

#### 2.6.4.8 NMR analysis of 2,5,6-tri-*O*-benzoyl- $\alpha$ -isosaccharino-1,4-lactone ( $\alpha$ -ISA tribenzoate)

NMR spectra of 2,5,6-tri-*O*-benzoyl- $\alpha$ -isosaccharino-1,4-lactone were recorded using the same instrument and conditions as mentioned in section 2.2.2.  $^1\text{H}$  and  $^{13}\text{C}$  spectra were recorded at ambient temperature. The sample was prepared by dissolving approximately 20 mg of the  $\alpha$ -ISA tribenzoate in  $\text{CDCl}_3$  (700  $\mu\text{l}$ ) and chemical shifts were referenced to acetone.

$^1\text{H}$  NMR (400 MHz,  $\text{CDCl}_3$ ) 8.11 – 8.03 ppm (m, 6H), 7.67 – 7.56 ppm (m, 3H), 7.52 – 7.42 ppm (m, 6H), 5.42 – 5.34 ppm (m, 1H), 4.91 ppm (d, 1H,  $J = 11.8$  Hz), 4.68 ppm (d, 1H,  $J = 11.8$  Hz), 4.64 ppm (dd, 1H,  $J = 12.3$  Hz, 3.4 Hz), 4.51 ppm (dd, 1H,  $J = 12.3$  Hz, 6.4 Hz), 2.82 ppm (dd, 1H,  $J = 15.0$  Hz, 8.6 Hz), 2.61 ppm (dd, 1H,  $J = 15.0$  Hz, 7.0 Hz).

$^{13}\text{C}$  NMR (100 MHz,  $\text{CDCl}_3$ ) 172.1 ppm, 166.3 ppm, 165.9 ppm, 165.6 ppm, 134.4 ppm, 134.0 ppm, 133.7 ppm, 130.3 ppm, 130.0 ppm, 129.9 ppm, 128.9 ppm, 128.7 ppm, 78.6 ppm, 75.6 ppm, 66.2 ppm, 65.5 ppm, 32.9 ppm.

#### **2.6.4.9 High resolution mass spectrometry (HRMS) of 2,5,6-tri-*O*-benzoyl- $\alpha$ -isosaccharino-1,4-lactone ( $\alpha$ -ISA tribenzoate)**

High resolution mass spectra (HRMS) were recorded in positive ion mode using the instrument described in section 2.2.4. The exact mass calculated for  $\alpha$ -ISA-tribenzoate,  $\text{C}_{27}\text{H}_{22}\text{O}_8$  [ $\text{MNa}^+$ ] was 497.1213 and the exact mass found was 497.1170.

#### **2.6.4.10 Removal of benzoyl groups**

In a typical example, the  $\beta$ -tribenzoate syrup which was isolated from the column as described in section 2.6.4.5, (10 g) was dissolved in an acetonitrile water mix (100:30 v/v) and the pH of the solution was maintained at pH 12 – 13 with the addition of sodium hydroxide solution (2 M), until the reaction had consumed one equivalent of base and the pH remained constant. Following this a small amount of acetic acid (220  $\mu\text{l}$ ) was added to neutralize the solution and finally the solution was filtered. The filtrate was rotary evaporated under reduced pressure to produce a white gum (9.16 g). The white gum was dissolved directly into methanol (500 ml) and to remove the benzoate groups a catalytic amount of sodium methoxide (1 g) was added and the mixture was stirred for 2 h, following which the mixture was filtered and rotary evaporated under reduced pressure to produce a solid white product (12.17 g). The solid was dissolved in deionised water and was extracted with diethyl ether to remove residual methyl benzoate and finally water was removed by rotary evaporation to provide sodium 2-*C*-(hydroxymethyl)-3-deoxy-*D*-threo-pentionate ( $\beta$ -ISA) in greater than 95 % purity (3.82 g, 94 %) which was analysed by NMR and HRMS (ESI).

#### **2.6.4.11 NMR analysis of sodium 2-*C*-(hydroxymethyl)-3-deoxy-*D*-threo-pentionate ( $\beta$ -ISA)**

NMR spectra of the sodium salt of  $\beta$ -ISA were recorded using the same instrument and conditions as mentioned in section 2.2.2.  $^1\text{H}$  and  $^{13}\text{C}$  spectra were recorded at ambient temperature. The sample was prepared by dissolving approximately 20 mg of the  $\beta$ -ISA sodium salt in  $\text{D}_2\text{O}$  (700  $\mu\text{l}$ ) and chemical shifts were referenced to acetone.

$^1\text{H}$  NMR (400 MHz,  $\text{D}_2\text{O}$ ) 3.99 ppm (m, 1H), 3.85 ppm (d, 1H,  $J = 11.5$  Hz), 3.73 ppm (d, 1H,  $J = 11.5$  Hz), 3.67 ppm (dd, 1H,  $J = 11.7$  Hz, 3.8 Hz), 3.57 ppm (dd, 1H,  $J = 11.7$  Hz, 6.8 Hz), 1.97 ppm (dd, 1H,  $J = 14.7$  Hz, 3.5 Hz), 1.84 ppm (dd, 1H,  $J = 14.7$  Hz, 8.5 Hz).  $^{13}\text{C}$  NMR (100 MHz,  $\text{D}_2\text{O}$ ) 180.0 ppm, 77.8 ppm, 68.4 ppm, 67.9 ppm, 66.0 ppm, 37.6 ppm

#### **2.6.4.12 High resolution mass spectrometry (HRMS) of sodium 2-C-(hydroxymethyl)-3-deoxy-D-threo-pentionate ( $\beta$ -ISA)**

High resolution mass spectra (HRMS) were recorded in negative ion mode using the instrument described in section 2.2.4. The exact mass calculated for the sodium salt of  $\beta$ -ISA,  $\text{C}_6\text{H}_{12}\text{O}_6$   $[\text{M}-\text{H}]^-$  was 179.0561 and the exact mass found was 179.0554.

#### **2.6.4.13 Preparation of 2-C-(hydroxymethyl)-3-deoxy-D-threo-pentono-1,4-lactone – ( $\beta$ -ISA<sub>L</sub>)**

To prepare a pure sample of  $\beta$ -ISA-lactone, the sodium salt of 2-C-(hydroxymethyl)-3-deoxy-D-threo-pentionate (3.5 g) was passed through a column of Amberlite cation exchange resin using the procedure described in section 2.4.2. Following the Amberlite column, the eluent and washing were evaporated to produce crude  $\beta$ -ISA-lactone as orange syrup (c. 3 g) which contained small amounts of impurities, which were removed by diluting the syrup in water and extracting with ethyl acetate. Evaporation of the aqueous layer produced pure  $\beta$ -ISA-lactone in greater than 95 % purity (2.65 g) which was analysed by NMR and HRMS (ESI).

#### **2.6.4.14 NMR analysis of 2-C-(hydroxymethyl)-3-deoxy-D-threo-pentono-1,4-lactone – $\beta$ -ISA<sub>L</sub>**

NMR spectra of the  $\beta$ -ISA-lactone were recorded using the same instrument and conditions as mentioned in section 2.2.2.  $^1\text{H}$  and  $^{13}\text{C}$  spectra were recorded at ambient temperature. The sample was prepared by dissolving approximately 20 mg of  $\beta$ -ISA-lactone in  $\text{D}_2\text{O}$  (700  $\mu\text{l}$ ) and chemical shifts were referenced to acetone.

$^1\text{H}$  NMR (400 MHz,  $\text{D}_2\text{O}$ ) 4.52 ppm (m, 1H), 3.72 ppm (dd, 1H,  $J = 13.0$  Hz, 2.6 Hz), 3.61 ppm (d, 1H,  $J = 11.7$  Hz), 3.49 ppm (dd, 1H,  $J = 13.0$  Hz, 5.6 Hz), 2.43 ppm (dd, 1H,  $J = 13.5$  Hz, 6.7 Hz), 1.98 ppm (dd, 1H,  $J = 13.5$  Hz, 9.2 Hz).  $^{13}\text{C}$  NMR (100 MHz,  $\text{D}_2\text{O}$ ) 179.8 ppm, 79.0 ppm, 77.0 ppm, 64.9 ppm, 62.7 ppm, 34.0 ppm.

#### **2.6.4.15 High resolution mass spectrometry (HRMS) of 2-C-(hydroxymethyl)-3-deoxy-D-threo-pentono-1,4-lactone – $\beta$ -ISA<sub>L</sub>**

High resolution mass spectra (HRMS) were recorded in positive ion mode using the instrument described in section 2.2.4. The exact mass calculated for  $\beta$ -ISA-lactone, C<sub>6</sub>H<sub>10</sub>O<sub>5</sub> [MNa<sup>+</sup>] was 185.0426 and the exact mass found was 185.0474.

#### **2.6.4.16 Preparation of Calcium 2-C-(hydroxymethyl)-3-deoxy-D-threo-pentionate Ca( $\beta$ -ISA)<sub>2</sub> – ( $\beta$ -ISA)**

To produce the calcium salt of  $\beta$ -ISA,  $\beta$ -ISA-lactone (1.5 g) was dissolved in hot water (15 ml) and the pH was increased to pH 9 with the addition of aqueous calcium hydroxide (160 ml) and the mixture was left to cool over night. The following day, the entire solution was filtered to remove excess Ca(OH)<sub>2</sub> and the filtrate was rotary evaporated under reduced pressure to produce a white solid of the desired product (1.5 g) which was analysed by NMR and HRMS (ESI).

#### **2.6.4.17 NMR analysis of Calcium 2-C-(hydroxymethyl)-3-deoxy-D-threo-pentionate Ca( $\beta$ -ISA)<sub>2</sub> – ( $\beta$ -ISA)**

NMR spectra of the calcium salt of  $\beta$ -ISA were recorded using the same instrument and conditions as mentioned in section 2.2.2. A <sup>1</sup>H spectrum was recorded at ambient temperature. The sample was prepared by dissolving approximately 20 mg of the  $\beta$ -ISA calcium salt in D<sub>2</sub>O (700  $\mu$ l) and chemical shifts were referenced to acetone.

<sup>1</sup>H NMR (400 MHz, D<sub>2</sub>O) 3.68 ppm (m, 1H), 3.55 ppm (d, 1H, *J* = 11.5 Hz), 3.42 ppm (d, 1H, *J* = 11.5 Hz), 3.37 ppm (dd, 1H, *J* = 11.7 Hz, 3.8 Hz), 3.26 ppm (dd, 1H, *J* = 11.7 Hz, 6.9 Hz), 1.67 ppm (dd, 1H, *J* = 14.7 Hz, 3.5 Hz), 1.54 ppm (dd, 1H, *J* = 14.7 Hz, 8.5 Hz).

#### **2.6.4.18 High resolution mass spectrometry (HRMS) of Calcium 2-C-(hydroxymethyl)-3-deoxy-D-threo-pentionate Ca( $\beta$ -ISA)<sub>2</sub> – ( $\beta$ -ISA)**

High resolution mass spectra (HRMS) were recorded in negative ion mode using the instrument described in section 2.2.4. The exact mass calculated for the calcium salt of  $\beta$ -

ISA,  $C_6H_{12}O_6 [M-H]^-$  was 179.0561 and the exact mass found was 179.0571, which represent the deprotonated free acid form of  $\beta$ -ISA.

A flow chart summarizing the final isolation procedure is presented in Figure 22, below.

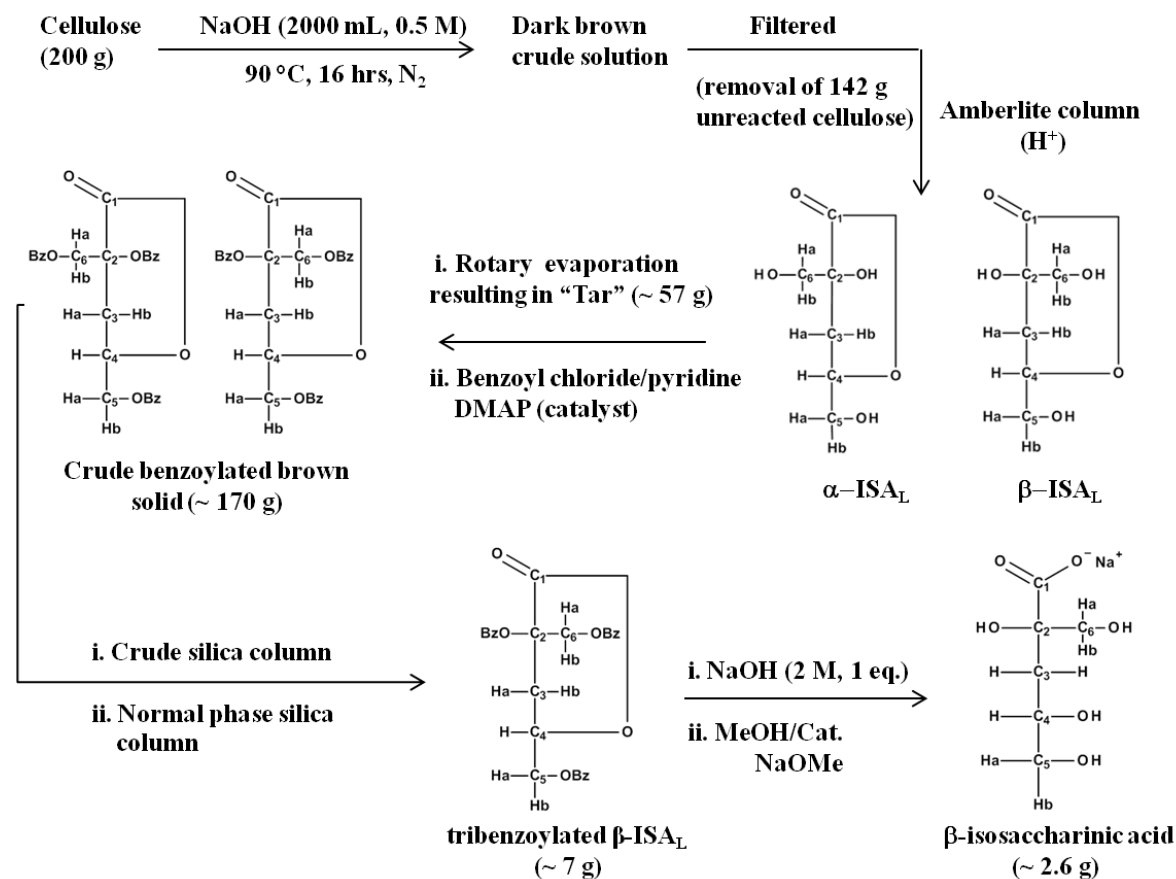


Figure 22: Synthesis and isolation of the sodium- $\beta$ -isosaccharinate

## 2.7 Investigating the physical properties of $\beta$ -ISA and $\alpha$ -ISA in aqueous solution

### 2.7.1.1 Determination of the aqueous $pK_a$ of $\beta$ -ISA using $^{13}C$ NMR spectroscopy

The calcium salt of  $\beta$ -ISA (30 mg, 7.5 mmol) was dissolved in  $D_2O$  (1 mL) and the pH of the solution was varied between pD 2 and pD 9 using either  $DNO_3$  or  $NaOD$  and reporting the pD as the measured pH + 0.4. Samples were quickly transferred to NMR tubes and spectra were recorded on a Bruker Avance 500 MHz (125 MHz  $^{13}C$ ) spectrometer using

quantitative carbon pulse programmes. Each spectrum was recorded using 4000 scans employing a wait time of 12 s between scans. A capillary insert, containing  $\text{CDCl}_3$ , was used as an internal reference. The solution pH was measured in the NMR tube using a Beckman  $\varnothing 40$  pH Meter (High Wycombe, UK) in combination with a Hanna instruments glass long reach NMR pH electrode (Mannheim, Germany). The  $pK_a$  of the acid was determined using the Henderson–Hasselbach equation:  $pK_a = pD + \log\{[AD]/[A^-]\}$ .

### 2.7.2 Determination of the rate of the base catalysed conversion of $\text{ISA}_L$ to $\text{ISAH}$

A stock solution of ISA lactone was prepared by dissolving  $\alpha/\beta$ - $\text{ISA}_L$  (20 mg) in HCl (100  $\mu\text{l}$ , 0.1 M). Kinetic runs were initiated by adding the  $\text{ISA}_L$  stock solution (50  $\mu\text{l}$ ) to ultrapure water (65 ml) in a round bottom flask and the solution was stirred under an atmosphere of nitrogen. The reaction vessel was attached to a Metrohm autotitrator (Titrano model 857, Metrohm, Runcorn, UK) and was maintained at 25 °C throughout the experiments. Fresh sodium hydroxide solutions were used as the titrant, these were prepared from a volumetric standard prior to the reaction and the titrant was flushed with nitrogen to avoid absorption of carbon dioxide. The appropriate start pH was selected and the volume of titrant added as a function of time was recorded. All pH measurements were recorded in-situ using a Unitrode combined glass pH electrode equipped with a built-in PT1000 temperature sensor (Metrohm, Runcorn, UK).

### 2.7.3 Determination of the rate of the acid catalysed conversion of $\text{ISAH}$ to $\text{ISA}_L$

The kinetics for the lactonisation of  $\text{ISAH}$  was followed using NMR spectroscopy using the instrument described in section 2.2.2. Samples of the calcium salt of  $\alpha/\beta$ - $\text{ISA}_L$  were dissolved in  $\text{D}_2\text{O}$  (20 mg/ml) and the samples were adjusted to the required pD (1 – 2.5, pH + 0.4) through the addition of  $\text{DNO}_3$ . Samples were immediately transferred to the NMR spectrometer and spectra were recorded at regular periods over a period of several days or until no further reaction was observed. When spectra were not being recorded samples were stored at 25 °C and the pD of the reaction solution was monitored throughout the course of the reaction using the long reach NMR pH electrode which was described in section 2.2.6.

### **3 Degradation of cellulose: attempts to maximise the solution concentration of $\beta$ -ISA solution**

#### **3.1 Introduction**

This section will primarily discuss cellulose degradation experiments which were undertaken to investigate ways of maximising the production of  $\beta$ -ISA, initially by maximising the production of  $\beta$ -ISA present in solution. The actual isolation of  $\beta$ -ISA from the crude solution, which also contains  $\alpha$ -ISA and other CDPs, will be discussed in chapter 4. A secondary aim of this chapter was to identify other CDPs which were produced and in order to confirm their identification several compounds were prepared in the laboratory for use as analytical standards.

There are a few reports of the synthesis of  $\beta$ -ISA<sup>94, 107, 110, 148, 153</sup>, and they have been described in chapter 1. Those methods have taken advantage of the “peeling reaction” (see chapter 1), which predominantly generates ISA when cellulose or other 1-4 linked glucose derivatives are contacted with alkali under anaerobic conditions. It is evident from the literature, that there are advantages and disadvantages of using either calcium or sodium hydroxide as the alkaline species. When cellulose is degraded using calcium hydroxide solution, research has shown that high percentages of the converted cellulose constitutes ISA of which approximately an equal proportion of  $\alpha$ - and  $\beta$ -ISA are produced, with smaller fragmentation products constituting only a minor proportion of the degradation mixture. When sodium hydroxide is used, more fragmentation occurs and ISA makes up a lesser proportion of the total degradation products; however, a key advantage of using sodium hydroxide is that the amount of  $\beta$ -ISA produced is greater than the amount of  $\alpha$ -ISA produced.

In this work the degradation of cellulose was investigated under anaerobic conditions using either sodium hydroxide or calcium hydroxide as the degrading species, and in order to determine optimum conditions, a range of temperatures (RT, 50 °C and 90°C) and different reaction times (1 – 52 days) were investigated. To monitor the progress of reactions, experiments were sampled periodically through a rubber septum and the concentration of  $\alpha$ - and  $\beta$ -ISA in the samples was determined using analytical HPAEC–PAD.

## 3.2 Preparation of an analytical standard of $\alpha$ -ISA and characterisation of $\alpha$ -ISA using HPAEC–PAD, NMR, GC–MS and HRMS

In order to allow us to follow the progress of the degradation reactions using analytical HPAEC–PAD a pure sample of  $\alpha$ -ISA was required. To obtain an analytical sample of  $\alpha$ -ISA; calcium 2-C-(hydroxymethyl)-3-deoxy-D-erythro-pentionate,  $\text{Ca}(\alpha\text{-ISA})_2$  was prepared using the established method of Whistler and BeMiller<sup>149</sup> (see section 2.4.1).

### 3.2.1 Characterisation of $\alpha$ -ISA

#### 3.2.1.1 Characterisation of $\alpha$ -ISA by NMR

To confirm that the correct product was synthesised it was characterised using both 1D ( $^1\text{H}$ ,  $^{13}\text{C}$ , DEPT 135 and DEPT 90) and 2D (COSY, HSQC and HMBC) NMR spectroscopy, see Figure 23 for the  $^1\text{H}$  spectra, which indicates high purity  $\alpha$ -ISA was obtained (> 95 %), and Table 2 which indicates a good comparison between the chemical shifts and peak multiplicities obtained in this work with those of previously published results<sup>110</sup>.

Throughout this work, the location of specific resonances will be used to identify the presence of  $\alpha$ -ISA in solution and the conformation adopted. Of note are the C3-methylene protons which are present as AMX splitting patterns centered at 1.76 and 1.60 ppm and are located up-field of the other signals because they are the only detectable protons which do not have electron withdrawing hydroxyl groups attached to the carbon atom to which they are bonded to. Also of note is that the single methyne proton (H4) resonates as a multiplet at 3.8 ppm in  $\alpha\text{-Ca}(\text{ISA})_2$ .

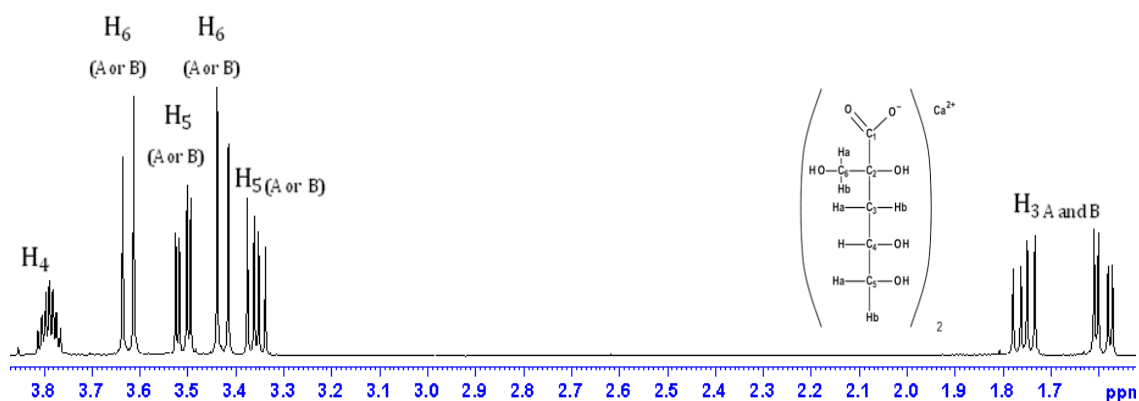


Figure 23:  $^1\text{H}$  NMR spectrum of the calcium salt of  $\alpha$ -ISA

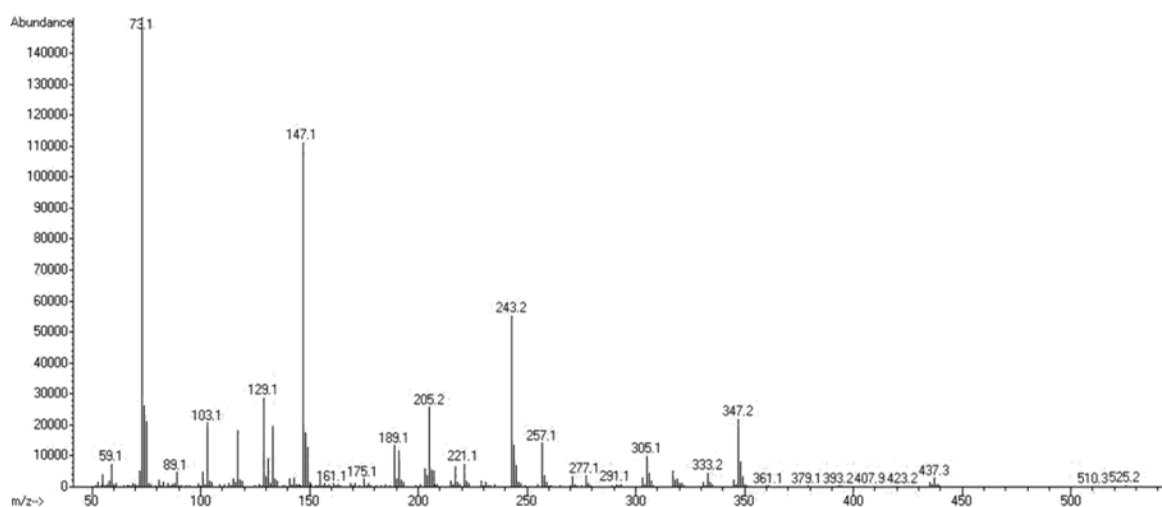
Table 2: A comparison between experimental and literature NMR chemical shift data for  $\alpha$ -ISA

Proton	Multiplicity	Chemical shift (ppm) From literature <sup>110</sup>	Chemical shift (ppm) Experimental
H3a or H3b	dd/dd	1.61/1.76	1.60/1.76
H4	M	3.79	3.79
H5a or H5b	dd/dd	3.37/3.53	3.37/3.52
H6a or H6b	d/d	3.43/3.63	3.44/3.63

### 3.2.1.2 Characterisation of $\alpha$ -ISA by GC-MS

The synthesised  $\alpha$ -ISA was further characterised using GC-MS after derivatisation with the addition of trimethylsilyl (TMS) groups. The reason for derivatisation is to increase the volatility of the ISA, thus making it more amenable to analysis by gas chromatography. The TMS method optimised by Sweeley *et al.* <sup>164</sup> is quick and simple and complete in less than 30 minutes (see section 2.4.1.1) and results in the proton of every –OH group of the compound being replaced with a TMS group.

The GC-MS spectra of the silyated  $\alpha$ -ISA produced in this work is presented in Figure 24 and is similar to that published by Greenfield *et al.* for the same compound <sup>107</sup>. Routes for the production of each major fragment ion have previously been determined and can be found in the work of Petersson <sup>166, 167</sup>.


 Figure 24: GC-MS electron impact ionisation spectrum of  $\alpha$ -ISA

### 3.2.1.3 Characterisation of $\alpha$ -ISA by HPAEC–PAD

To establish if  $\alpha$ -ISA could be detected using HPAEC–PAD, a sample was analysed using the conditions described in section 2.4.1.4 resulting in a peak with a retention time of approximately 8.4 minutes (Figure 27, left). The minor peak with a retention time of 11.7 minutes represents an impurity, which was later determined to be  $\beta$ -ISA, and accounts for 2.6 % of the total peak area. To further purify the product, an attempt was made to convert the chalky calcium salt of  $\alpha$ -ISA into the lactone conformation ( $\alpha$ -ISA<sub>L</sub>) using the method of Whistler and BeMiller<sup>149</sup> (see section 2.4.2) which, in the first conversion attempt, inadvertently resulted in the isolation of the free acid form of  $\alpha$ -ISA ( $\alpha$ -ISAH) as a highly soluble white crystalline solid (807 mg).

### 3.2.2 Preparation and characterisation of $\alpha$ -ISAH and $\alpha$ -ISA<sub>L</sub>

Initial experimental evidence that the free acid and not the lactone had been produced came from a melting point determination of 139 – 141 °C, which is considerably higher than the value presented by Whistler and BeMiller<sup>148</sup> (95 - 96 °C) for the  $\alpha$ -ISA<sub>L</sub> and coincides with the free acid, being a carboxylic acid having a higher melting point than the lactone, which is an ester. Further evidence came from infrared analysis of the crystalline solid which showed a strong absorbance at 1684 cm<sup>-1</sup> which is characteristic of a carboxylic acid functional group, as opposed to an absorbance at 1779 cm<sup>-1</sup> which is characteristic for the carbonyl group of a 1,4-linked lactone<sup>153</sup>.

The  $\alpha$ -ISAH was analysed using both 1D (<sup>1</sup>H, <sup>13</sup>C, DEPT 135 and DEPT 90) and 2D (COSY, HSQC and HMBC) NMR which provided further evidence that the free acid and not the lactone had been produced. Of note was the HMBC spectrum which showed no evidence of coupling between the C1 and H4 atoms, an indication of this coupling would be expected if an ester linkage between C1 and the oxygen attached to C4 had formed. A comparison of the <sup>1</sup>H NMR spectrum of the crystalline solid with <sup>1</sup>H NMR data published by Glaus *et al.*<sup>110</sup> for  $\alpha$ -ISA<sub>L</sub> further concluded that the lactone had not been produced, with the major difference being the chemical shift of the methyne proton (H4) resonating significantly more downfield in the lactone (4.79 ppm<sup>110</sup>) than the H4 methyne of the free acid (3.93 ppm) due to the de-shielding effect of the oxycarbonyl in the lactone<sup>110</sup>.

A comparison of the NMR spectra of the  $\alpha$ -Ca(ISA)<sub>2</sub> and  $\alpha$ -ISAH (Figure 25) indicated that they both contain the same resonances, with the position of methyne proton (H4) being very

similar indicating that both compounds are in the open-chain conformation, however various signals have shifted position, with the main difference being the downfield shift of one of the H5 methylene signals of the free acid. In an NMR study by Cho *et al.*<sup>150</sup> it was determined that the resonances of ISA are pH dependent due to ISA being present in one of three forms depending on the pH of the solution (the free acid, the conjugate base and the lactone). In this study, when  $\text{Ca}(\text{ISA})_2$  was dissolved in  $\text{D}_2\text{O}$  (20 mg in 1 ml) its measured pH was 8.2 whereas an equivalent sample of the free acid had a pH of 2.4. The  $\text{pK}_a$  of  $\alpha$ -ISA was calculated as being 3.36 by Cho *et al.*<sup>150</sup>, so at pH 8.2 the calcium salt will be present as a deprotonated anion, whereas at pH 2.4, the ISA will be a protonated free acid; this difference in species results in a shift in the position of the chemical shifts.

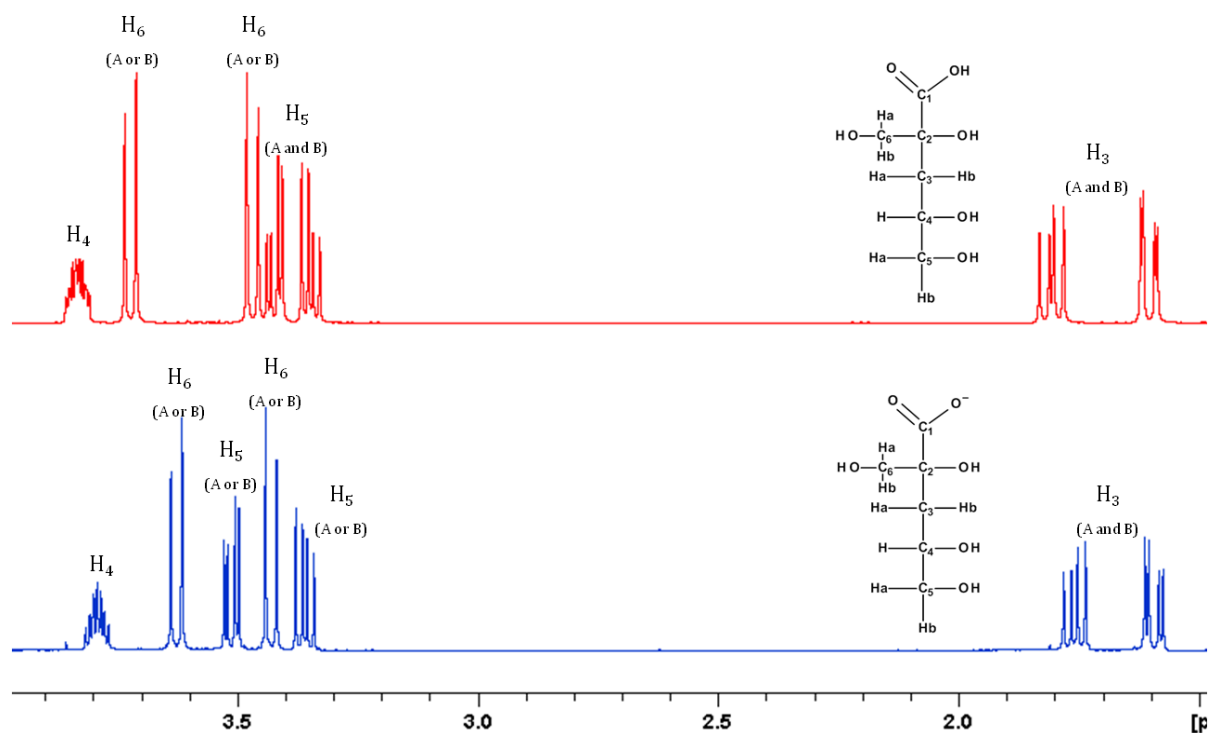


Figure 25:  $^1\text{H}$  NMR spectra of  $\alpha\text{-Ca}(\text{ISA})_2$  (bottom) and  $\alpha\text{-ISAH}$  (top)

As previously discussed in chapter 1, ISA undergoes an acid catalysed transformation to the lactone at pH units less than 4<sup>149, 150</sup>. However, depending on the pH, this conversion can be very slow; for example, results to be discussed in section 5.2.2 have indicated that at pH 1.07 this conversion takes approximately 10 h and it can be estimated that it would take over 500 days at pH 4. This slow transformation provides a possible explanation as to why the free acid and not  $\alpha\text{-ISA}_L$  was initially isolated: in the production of  $\alpha\text{-ISA}_L$ , oxalic acid was added to a solution of  $\text{Ca}(\text{ISA})_2$  to remove calcium ions, and then the free acid was

eluted through a column of cation exchange resin in the  $H^+$  form to encourage lactone formation, after conditioning the resin with HCl as described in section 2.4.2. It is possible that the column was not conditioned adequately due to the volume or the concentration of the HCl being insufficient, or the elution of the ISA through the column may have been too fast, which could result in the ISA passing through the column before lactonisation had time to take place.

By repeating the procedure as described in section 2.4.2, for the production of  $\alpha$ -ISA<sub>L</sub> but using an excess of HCl (2 M) to condition the column and employing slower elution conditions (c. 1 ml min<sup>-1</sup>) a syrup of the desired  $\alpha$ -ISA<sub>L</sub> was produced, which was crystallized by slow evaporation of the syrup from water. NMR analysis of the resulting product confirmed that high purity  $\alpha$ -ISA<sub>L</sub> (> 95 %) had been produced, and a comparison of experimental NMR results with the <sup>1</sup>H and <sup>13</sup>C NMR data from the work of Glaus *et al.*<sup>110</sup> and Cho *et al.*<sup>150</sup> respectively for the same compound indicated that on this occasion the correct product had been isolated (Figure 26).

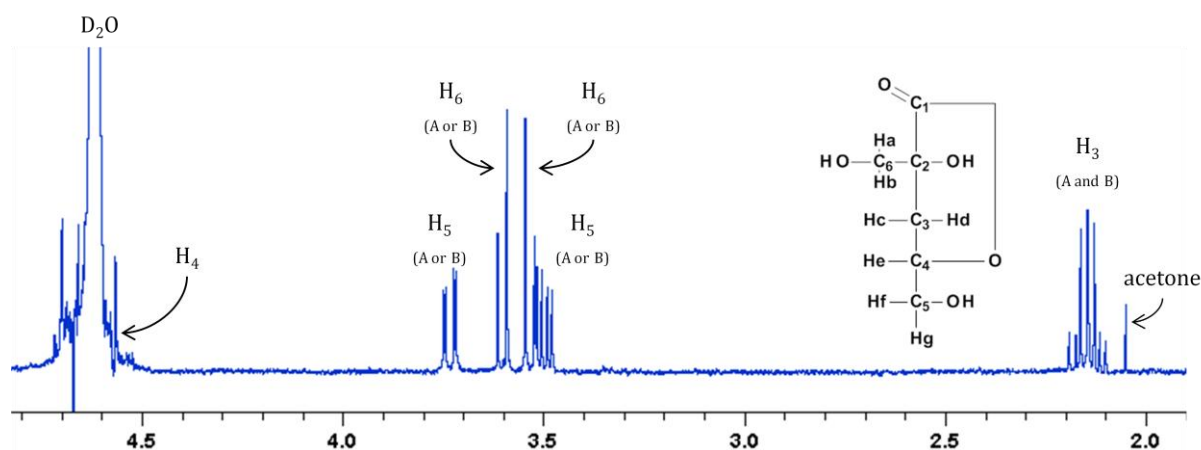


Figure 26: <sup>1</sup>H spectrum of  $\alpha$ -ISA<sub>L</sub>

Particular characteristics in the <sup>1</sup>H spectrum of the lactone are the significant down-field shift, due to the de-shielding of the methyne proton (H4), which is concealed by the signal from the D<sub>2</sub>O, but whose presence was determined using the HSQC spectrum. Also, the chemical shifts of the up-field C3-methylene protons are now much closer together in comparison to the C3-methylene signals in the free acid and the calcium salt, which is probably related to the increased torsion angle introduced due to the formation of the lactone, as indicated by the similar vicinal coupling constants of the C3 protons with the C4 methyne proton indicating that the dihedral angle between each C3 proton and the C4

proton are similar indicating that the two protons are now more magnetically equivalent than when they are in the open-chain forms. Further characterisation of the lactone came from melting point measurements (95 – 97 °C) which are comparable to literature values 107, 149, 153 and an IR absorbance of 1754  $\text{cm}^{-1}$  being characteristic of an ester carbonyl stretch and close to the value quoted by Feast *et al.* for the absorbance of a 1,4-lactone<sup>153</sup>.

### 3.2.2.1 HPAEC-PAD analysis of $\alpha$ -ISAH and $\alpha$ -ISA<sub>L</sub>

In addition to the HPAEC-PAD analysis of  $\text{Ca}(\text{ISA})_2$  (section 3.2.1.3), the remaining two synthesised species of  $\alpha$ -ISA (ISAH and ISA<sub>L</sub>) were individually analysed by HPAEC-PAD using the conditions described in section 2.4.1.4. Analysis of each individual species resulted in a single, sharp peak with a similar retention time to the one produced for the  $\text{Ca}(\text{ISA})_2$  sample, also in both the ISAH and ISA<sub>L</sub> samples there was no sign of the impurity  $\beta$ -ISA peak which was present in the  $\text{Ca}(\text{ISA})_2$  trace (Figure 27, centre). With the 50 mM mobile phase utilised with HPAEC-PAD (pH 12.7), an almost instantaneous transformation to the open-chain anion will occur, irrespective of the type of ISA species, due to base catalysed hydrolysis, ensuring that all the ISA is in the same form. To confirm that  $\alpha$ -ISA<sub>L</sub> and the  $\text{Ca}(\text{ISA})_2$  sample were co-eluting at the same retention time, a mixed sample was prepared (125 ppm of each species, total 250 ppm) and analysed using the same conditions, resulting in a single peak which had a similar peak area as the 250 ppm  $\text{Ca}(\text{ISA})_2$  sample which was described in section 3.2.1.3 (Figure 27, right).

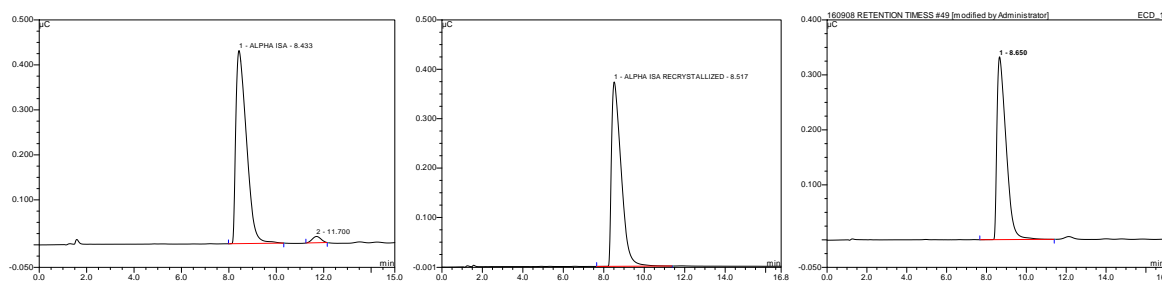


Figure 27: HPAEC-PAD chromatograms of the  $\text{Ca}(\alpha\text{-ISA})_2$ , (left), the crystalline  $\alpha$ -ISAH (centre) and a combined sample of  $\text{Ca}(\text{ISA})_2/\text{ISA}_L$  (250 ppm) indicating a single peak, (right).

Using the crystalline  $\alpha$ -ISAH sample a calibration graph was constructed by preparing and running a series of standards of known concentration, as described in section 2.2.1 (Figure 28)

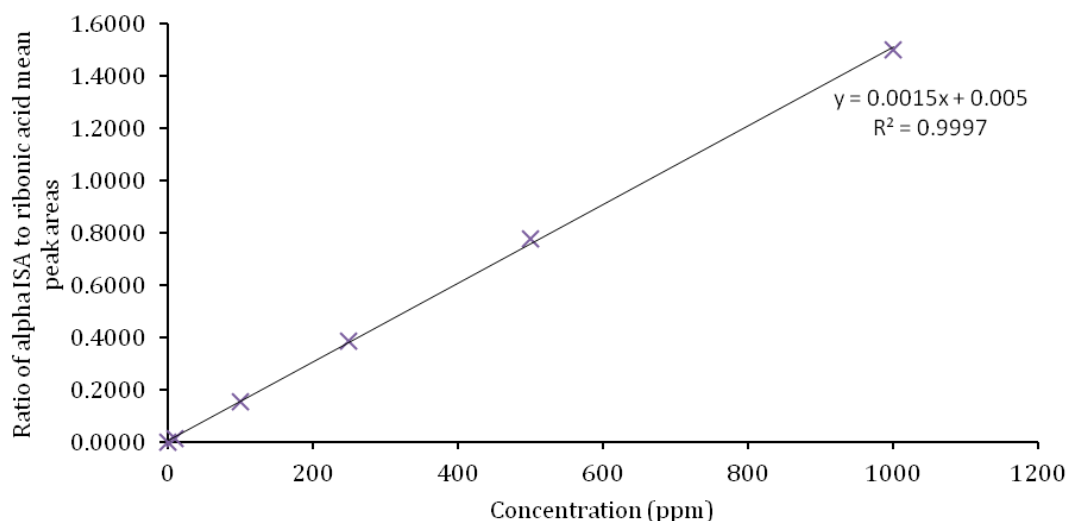


Figure 28: Calibration curve of  $\alpha$ -ISA using HPAEC-PAD

One problem which was encountered with HPAEC-PAD was that retention times can fluctuate slightly if the anion exchange capacity of the column does not remain constant, which may be affected by carbonate or other strongly retained analytes being bound to the column, resulting in an inconsistent number of sites being available for anion exchange. To prevent this from occurring, the column was regenerated by eluting the mobile phase stock solution (200 mM NaOH) through the column after each run for a short period of time. Another problem which was encountered was a fluctuation in the size of peak areas, which is probably related to problems with the electrode within the detector. To counter these problems, D-ribonic acid (50 ppm) was added as an internal standard to each ISA standard and, to generate the calibration graph, the ratio of analyte peak area to internal standard peak area was plotted against analyte concentration (Figure 28); therefore by using a ratio as opposed to absolute readings, any fluctuations in peak area or retention time were minimized.

D-ribonic acid was established as a suitable internal standard, as it gave a retention time within a few minutes of the analyte peaks, whilst still providing adequate resolution so as not to interfere with the other peaks. D-ribonic acid has been reported as being a cellulose degradation product in the review by Knill and Kennedy<sup>93</sup>. However, the original literature source from that review states that only trace amounts (< 0.5 %) of ribonic acid was produced in their degradation reactions<sup>106, 131</sup>, and this trace amount was not present in the degradation liquor, rather it was one of the minor alkali stable stopping groups, and only

released into solution after acid hydrolysis treatment of the alkali stable cellulose, so D-ribonic acid is not expected to be present in our degradation solutions. This was further confirmed when preliminary analysis of degradation samples produced in this work showed no sign of the presence of any D-ribonic acid.

From the calibration graph in Figure 28 it can be seen that there is a good linear range over the entire series of concentrations, also the intercept is close to zero indicating very little leverage or bias in the results. The correlation coefficient is close to 1 indicating a strong correlation between the X and Y values indicating that the intensity of the signal is directly proportional to the concentration of the analyte; therefore, the regression equation can reliably be used to calculate unknown concentrations of ISA.

### 3.2.3 Analysis of crude $\alpha$ -ISA solution

To further understand the reaction which was used to produce calcium  $\alpha$ -isosaccharinate, the crude brown solution produced from the degradation of lactose (see section 2.4.1) was analysed using HPAEC-PAD both before and after the precipitation and removal of  $\alpha$ -ISA. Analysis prior to the precipitation of the calcium salt indicated that the solution contained four major degradation products and assuming that each analyte gives an equal detector response, each was present in approximately equal amounts (peak 1, 25 %; peak 2, 27 %; peaks 3 and 4 were unresolved accounting for 48 % of the total peak area), (Figure 29).

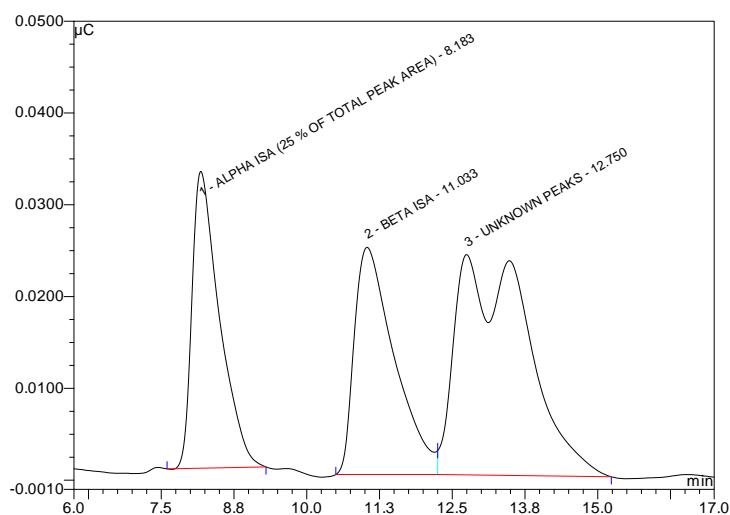


Figure 29: HPAEC-PAD chromatogram of the crude  $\alpha$ -ISA solution before the removal of any  $\text{Ca}(\alpha\text{-ISA})_2$ .

The peak at 8.2 minutes represents  $\alpha$ -ISA, and can be identified by comparing its retention time with that of the synthesised product. The peak at 11 minutes, which matches the impurity peak in the calcium  $\alpha$ -ISA chromatogram represents  $\beta$ -ISA; the retention time of which became known during the course of this work when a pure sample became available; in agreement with literature, when calcium hydroxide is used as the degrading species, both analytes are present in approximately equal amounts<sup>153</sup>. The remaining two unresolved peaks were tentatively assigned as alpha and beta (galacto)–metasaccharinic acid because these two compounds were isolated from lactose in the work of Feast *et al.*<sup>153</sup>. When lactose (or other 4-O-derivatised glucoses) undergo alkaline peeling, the substituent which is attached at the 4 position is eliminated, which in this case is galactose, and is free to react further. Treatment of galactose with lime water is known to produce metasaccharinic acid, via the formation of a dicarbonyl intermediate (3-deoxy-D-glucosone)<sup>130</sup> which undergoes a benzylic acid type rearrangement resulting in the formation of a new asymmetric centre at C2, allowing for the production of alpha and beta metasaccharinic acid<sup>149</sup>. Metasaccharinic acid is isomeric in nature to the starting material so in this case the metasaccharinic acid is known as galacto–metasaccharinic acid<sup>168</sup>, whereas from the degradation of cellulose, which consists entirely of glucose-linked monomers, the resulting MSA is known as gluco-metasaccharinic acid with the only difference between the two forms of MSA being that they are C4 epimers. In a calcium hydroxide environment, there is a preference for the production of the  $\alpha$ -MSA as opposed to the beta epimer<sup>153</sup>; however, unlike alpha and beta isosaccharinic acid which do not interconvert (at least at temperatures of up to 125 °C)<sup>148</sup>, upon heating the epimers of metasaccharinic acid do interconvert through an epimerisation reaction<sup>106, 169</sup>. Therefore, during the eight hour reflux, an equilibration occurs resulting in the production of equal proportions of  $\alpha$ - and  $\beta$ -MSA<sup>169</sup>, which is in agreement with the peaks on the chromatogram being approximately equal in size.

Tentative attempts were made to separate the components of the crude mixture; the aim being to confirm the literature assignment of MSA. The separation was performed using an automated preparative anion exchange chromatography system using similar conditions as those described in section 2.6.3., small amounts of the brown crude  $\alpha$ -ISA solution (5 ml) were eluted through an anion exchange column and the fractions collected were screened on the HPAEC–PAD system. In this process, only a partial separation was achieved, but fractions were obtained which contained greater proportions of the probable MSA peaks than in the original un-fractionated sample (the initial MSA content of the solution was ~

50 %, and after the chromatography a fraction was collected which contained  $\sim 78$  % MSA) which could then be analysed by NMR. Selected fractions were lyophilised and dissolved in  $D_2O$  and analysed by a combination of 1D ( $^1H$ ,  $^{13}C$ , DEPT 135 and DEPT 90) and 2D (COSY, HSQC and HMBC) NMR, with results confirming that the crude reaction mixture contained  $\alpha$ - and  $\beta$ -ISA and  $\alpha$ - and  $\beta$ -MSA in approximately equal concentrations. NMR analysis also indicated the presence of lactic acid in the crude alpha ISA sample (see Figure 30 for the  $^{13}C$  NMR spectrum).

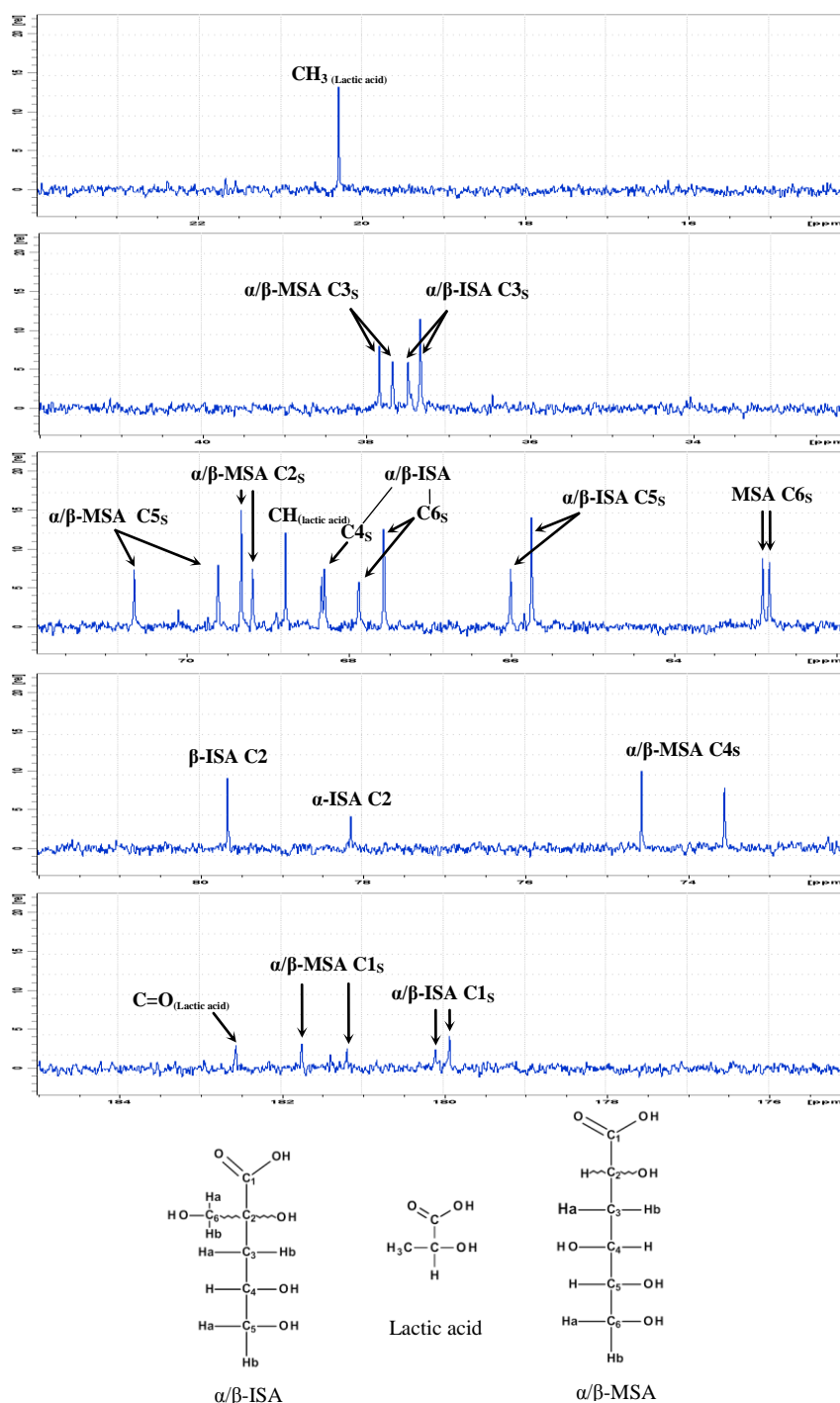


Figure 30:  $^{13}C$  NMR spectrum of the crude alpha ISA sample

The precipitation of  $\alpha$ -ISA from the crude material did not eliminate the entire  $\alpha$ -ISA content from the crude solution. Re-analysis of the crude material after the removal of the precipitated  $\text{Ca}(\alpha\text{-ISA})_2$  using HPAEC-PAD indicated that there was still a large quantity of  $\alpha$ -ISA remaining in the solution; accounting for approximately 14 % of the total peak area (Figure 31).

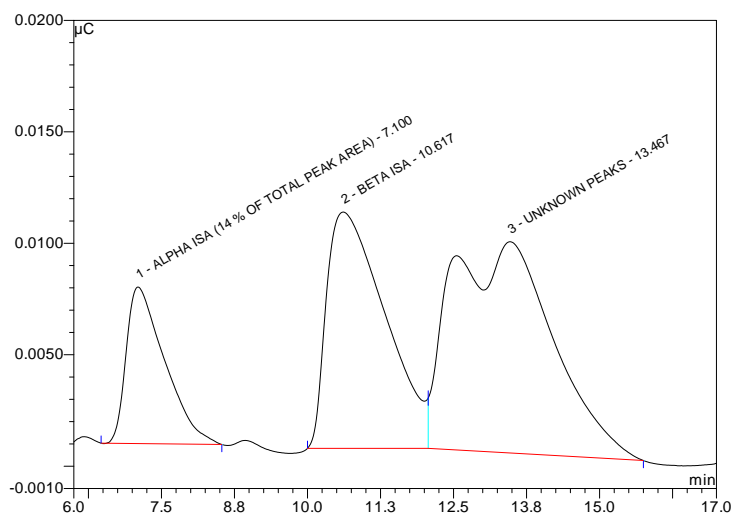


Figure 31: HPAEC-PAD chromatogram of the filtrate following the precipitation of  $\alpha$ -ISA, showing that large quantities of  $\alpha$ -ISA are still present in the solution

Further attempts to precipitate the remaining  $\text{Ca}(\alpha\text{-ISA})_2$  by lyophilising the crude solution and repeating the previously described process resulted in only minor additional precipitation; thus indicating the difficulty in isolating the highly soluble  $\beta$ -ISA from the degradation mixtures which contain residual  $\alpha$ -ISA and other degradation products.

### **3.2.4 Ethanol solubility experiments – Attempts to preferentially precipitate one of the saccharinic acids using fractional precipitation**

Whistler and BeMiller reported that the products of the alkaline degradation of guaran were only partially soluble in 70 % ethanol solutions<sup>148</sup>, so with this in mind some preliminary solubility studies were performed on small portions of the crude  $\alpha$ -ISA solution after the precipitation of the majority of the  $\alpha$ -ISA (see section 2.4.3). As stated above, after the removal of the  $\text{Ca}(\alpha\text{-ISA})_2$ , the composition of the solution consisted of  $\alpha$ -ISA (14 %),  $\beta$ -ISA (22 %) and MSA (64 %, combined, unresolved). The crude solution was a very dark brown colour, so prior to any solubility tests the solution was boiled in the presence of

activated charcoal (2 %) in an attempt to remove coloured impurities; however, it was questionable if this method had any visual effect on the appearance of the solution.

To perform the solubility tests, portions of crude ISA solution (2.5 ml) were added to test tubes and converted into aqueous ethanol solutions ranging from 40 % to 90 % ethanol (v/v). The initial ISA/ethanol solutions were dark brown in appearance, but as the concentration of ethanol increased, the colour of the solution became clearer indicating that coloured material was precipitating out of the solution, and this effect was more noticeable with an increase in the ethanol content of the solution. The identification of the brown coloured material has previously been studied by Ziderman *et al.*<sup>170</sup> who indicated that the material is converted from a proportion of the 4-deoxy-2,3-hexodiulose intermediate and using ultraviolet and I.R. spectroscopy it was concluded that the chromophore was a  $\beta$ -diketone which in basic solutions forms enolates to produce a yellow anion<sup>170</sup> (Figure 32). Lewin *et al.*<sup>171</sup> also studied the chromophore produced from the degradation of cellulose solutions and using dialysis they determined that the responsible molecule had a low molecular weight and found that the absorbance shifted with the addition of acid or base, and determined that the product was a simple conjugated carbonyl, as previously suggested by Ziderman *et al.*

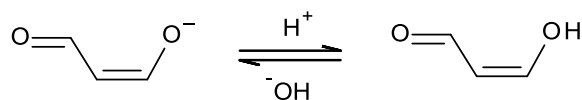


Figure 32: The proposed yellow anion produced in cellulose degradation reactions.

The ethanol solutions were left to stand overnight at room temperature, which resulted in visible amounts of solid precipitating from each solution, and again, this was also related to the concentration of the ethanol (see Table 3).

Table 3: Mass of solid removed from the  $\alpha$ -ISA solution as a function of aqueous ethanol concentration (v/v). Each sample (20 ml) contained 2.5 ml of crude  $\alpha$ -ISA solution, deionised water and an appropriate volume of ethanol to produce the required concentration

Ethanol concentration (%)	Mass of collected solid (mg)
40	6
50	6
60	19
70	18
80	64
90	81

The solid was removed from each test tube by transferring into a suitable vessel and centrifuging the contents (3200 rpm, 30 min), the resulting pellet was dried under a stream of nitrogen, and each solid sample was analysed by HPAEC–PAD at a concentration of approximately 100 ppm. At the same time the remaining solutions were appropriately diluted (100–fold) and were also analysed by HPAEC–PAD and the peak area of each sample was determined, however no attempt was made to quantify the analytes present in solution. HPAEC-PAD analysis of the solutions indicated that between the concentrations of ethanol of 40 % to 60 % there was little effect on the solubility of both the ISA and the MSA as both remained in solution with the exception of a small amount of precipitate; but above 60 % ethanol concentration, there was a noticeable reduction in peak area for both ISA and MSA (Figure 33), with a greater loss observed for MSA, at the same time the mass of the solid removed from each test tube increased from 19 mg in the 60 % ethanol test tube to 81 mg in the 90 % test tube.

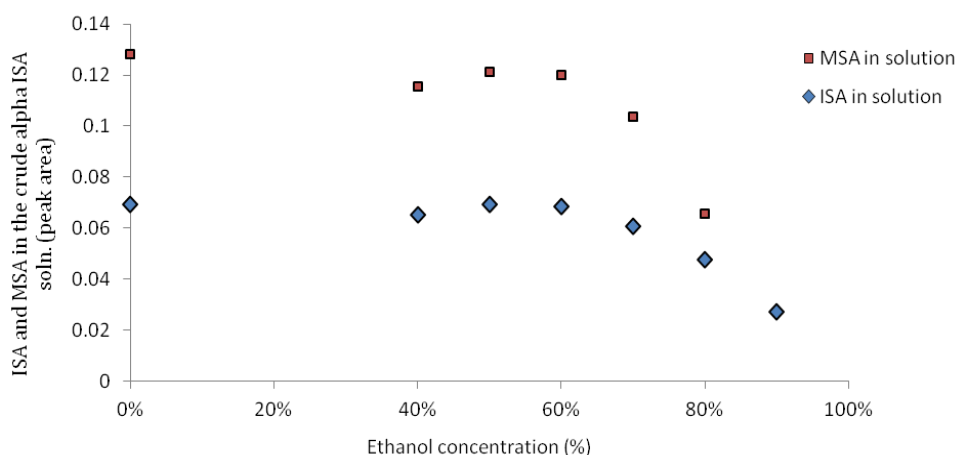


Figure 33: Graph showing ISA and MSA peak areas as a function of ethanol concentration in the remaining crude  $\alpha$ -ISA solution

The results of these preliminary solubility tests indicated that the effect of the addition of ethanol was greater on the solubility of MSA than the ISA indicating that MSA has a lower solubility in aqueous ethanol than ISA; between the ethanol concentrations of 40 % - 60 % MSA accounted for 64 % of the total peak area, however, between 60 % - 90 % ethanol the MSA content fell to about 50 % of the total peak area (Figure 34), and this was mirrored by the percentage of MSA found in the precipitated solid samples increasing from 65 % of the peak area in the 40 % ethanol samples to 72 % of the total peak area in the 90 % ethanol sample.

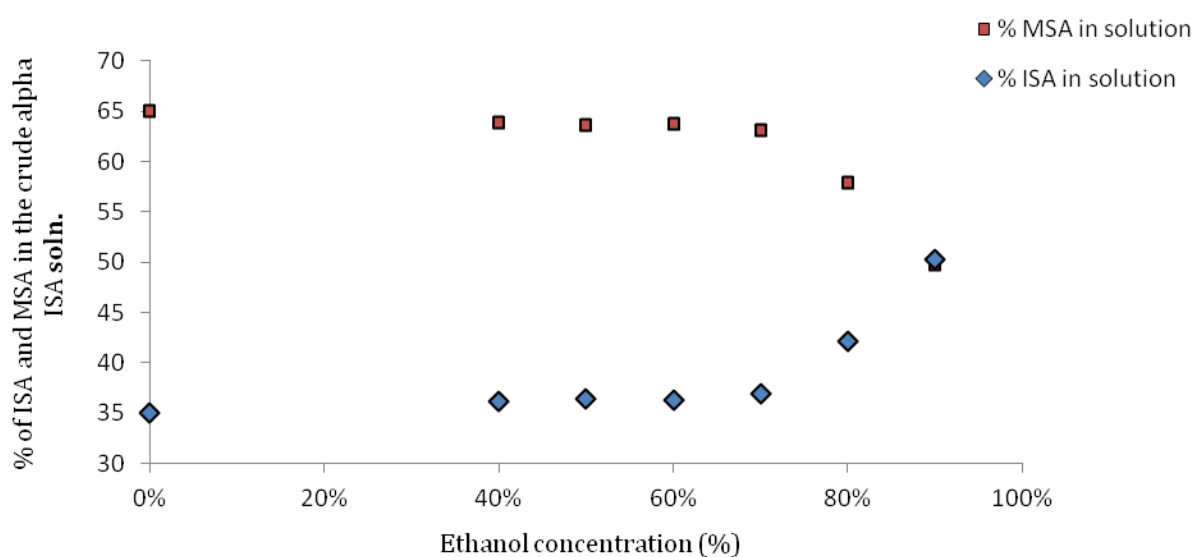


Figure 34: Graph to show the ratio of MSA to ISA against % ethanol solution

The HPAEC-PAD analysis indicated that the ratios of the amount of  $\alpha$ -ISA to  $\beta$ -ISA and  $\alpha$ -MSA to  $\beta$ -MSA in the initial crude solution was very similar to their respective ratios in the final 90 % ethanol solution, indicating that there was no significant difference in the effect of the ethanol on the solubility of alpha or beta forms of either molecule. The 90 % ethanol solution still contained both ISA and MSA, with the combined ISA now accounting for slightly more than 50 % of the total peak area, as opposed to 36 % in the initial crude solution. The results indicated that although neither ISA nor MSA were completely removed from the crude solution through the action of ethanol, further development of these types of experiments may produce methods to remove unwanted MSA or other unwanted impurities from the degradation media; there was however a clear effect that the addition of ethanol to the crude solution gave a visibly cleaner solution, which may be useful when applying crude solutions to chromatographic isolation methods; fouling of

anion exchange columns was a significant problem encountered in this work when attempting to isolate  $\beta$ -ISA from crude brown-coloured degradation solutions using anion exchange chromatography. However, for this work, no further attempt was made to remove MSA from degradation mixtures using fractional precipitation with ethanol, the overriding conclusion is that to maximise the chances of gaining an isolated sample of pure  $\beta$ -ISA, a starting material should be used that does not produce MSA in the degradation solution in the first instance so its removal would not be required. In all future experiments cellulose will be used as a substrate for the production of  $\beta$ -ISA.

### **3.3 Optimisation of reaction conditions for the production of $\beta$ -ISA using cellulose as a substrate**

The production of ISA is influenced by the quantity and type of substrate used, the type of alkali used, the pH of the solution and the reaction temperature<sup>172</sup>. As discussed in the previous section, lactose was deemed as an undesirable starting material for the production of crude  $\beta$ -ISA because it results in the production of large amounts of metasaccharinic acid being released into the degradation solution. Also, it has been reported by Greenfield *et al.*<sup>107</sup> that lactose and cellobiose give rise to a greater amount of side reactions which results in a wider range of degradation products, thus making isolation of  $\beta$ -ISA more difficult. Guaran was also deemed unsuitable, because at higher temperatures, according to Whistler and BeMiller, it produces a complex mixture of degradation products<sup>148</sup>; which is problematic when one of the key aims of this work was to reduce the reaction time by increasing the reaction temperature. With cellulose however, any MSA produced is expected to remain attached to the cellulose chain as alkali stable end-groups which do not enter the degradation solution. For this reason cellulose has been used in the most recent published methods for the preparation of  $\beta$ -ISA<sup>107, 110</sup> and was also used in this work.

#### **3.3.1 Type of cellulose**

Previous studies have compared the degradation of a variety of cellulosic materials and results have indicated that the type of cellulose used affects the amount of ISA being produced. Glaus *et al.*<sup>110</sup> compared the degradation of different types of cellulosic materials, including microcrystalline cellulose, cotton, paper and tissues, under repository conditions and found that with pure microcrystalline cellulose there was a higher percentage of ISA being produced as opposed to a wider range of smaller products in the

other substrates. In another study, Van Loon and Glaus<sup>12</sup> found that with pure cellulose powder, ISA accounted for ~ 80 % of total degradation products whereas with Tela tissues, ISA accounted for ~ 50 % of the degradation products and with paper, ISA accounted for ~ 30 % of the degradation products. The lower amounts of ISA being produced in the degradation of paper and tissues can be explained because they also contain hemicellulosic items which will contribute to the overall cellulose degradation products.

Biddle *et al.*<sup>124</sup> compared the degradation of cotton and tissues and found that because cotton was more crystalline it degraded at half the rate of tissue paper, although other factors such as the hemicellulose content of the tissues would also increase the rate of degradation. Greenfield *et al.*<sup>107</sup> also degraded a range of cellulosic materials and found that the hemicellulose containing materials produced a wider range of degradation products when compared with the degradation of pure cellulose.

When comparing different cellulosic materials which are described as highly pure by cellulose content, such as cotton and cellulose powder, the extent of degradation under repository conditions depends on both the number of reducing end groups in the cellulose chain and the accessibility of the alkaline reagent to the cellulose fibres<sup>12</sup>. If cellulose of equivalent crystallinity is used, the rate of peeling is proportional to the number of reducing end groups<sup>12, 131</sup>. The degree of polymerisation of the cellulose can be used to predict, quite accurately the number of reducing end groups of a given cellulose chain i.e. by calculating the reciprocal of the degree of polymerisation<sup>12</sup>. Hence the smaller the degree of polymerisation, the more reducing end groups will be available for end-wise attack per mole of cellulose. The degree of polymerisation is important because under various conditions only 50 – 70 glucose residues are removed before the cellulose chain becomes stabilised to further attack<sup>127, 143, 173</sup>; if very long cellulose chains are used, the vast majority of the polymer will remain un-degraded. An example of this can be seen in the work of Van Loon and Glaus, who compared different types of pure cellulose<sup>12</sup> each having a different DP and found that cellulose with a DP of 117 degraded 30 times more than a cellulose with a DP of 1800, culminating in 65 times more ISA being produced from the DP 117 cellulose.

The ability of reagents to access the cellulose fibres also affects cellulose degradation. It is thought that the anaerobic, alkaline degradation of cellulose only occurs in the amorphous regions of the cellulose fibre<sup>12, 127</sup>, therefore the extent of degradation is linked to the

accessibility of alkali to the amorphous fibres. Interestingly though, microcrystalline cellulose undergoes cellulose degradation, as mentioned above, but it is claimed by Sigma Aldrich that microcrystalline cellulose is crystalline with all amorphous regions being removed by acid hydrolysis. If this is correct, it cannot be true that cellulose degradation only occurs at the amorphous regions of the cellulose chain. However, Atalla and Isogai<sup>174</sup> determined using XRD that microcrystalline cellulose from several different brands only contains about 80 % crystalline material, which explains why only 20 – 30 % degradation takes place, and that this is probably a result of degradation taking part in the amorphous parts of the cellulose and the amorphous/crystalline bordering regions. Furthermore, evidence exists that degradation takes place in crystalline regions; Ziderman and Perel<sup>175</sup> studied the crystallinity of microcrystalline cellulose after alkaline degradation in refluxing sodium hydrogen carbonate and found that the crystallinity index actually reduced suggesting that cellulose chains located within the crystalline areas were also being eroded.

Based on the above information, it was decided that degradation experiments would be performed on pure microcrystalline cellulose (Avicel, Sigma-Aldrich, catalogue number 310697), which has a degree of polymerisation of approximately 117<sup>12</sup> which provides a large number of reducing end groups available for alkaline attack.

### 3.3.2 Cellulose loading

The ratio of the mass of solid cellulose to the amount of alkaline solution is known as the cellulose loading and also affects the amount of ISA produced. Pavasars *et al.*<sup>123</sup> performed some cellulose degradation experiments which compared a cellulose loading of 100 g per litre with a cellulose loading of 5 g per litre and found that with the higher loading, ISA contributed to a higher percentage of the total organic carbon produced (83 % and 75 % respectively). It was further determined that whether 100 g or 5 g of cellulose was degraded, the total percentage of the degraded cellulose was the same, so by using a 20 times higher cellulose loading, at least 20 times more ISA would be produced; therefore in our experiments a 100 g per litre cellulose loading was used. Furthermore, when calcium hydroxide is used as the alkaline reagent, the limiting effect of the lower cellulose loading is further exacerbated as some of the cellulose is expected to get trapped in the insoluble calcium hydroxide<sup>123</sup> so this cellulose would be unavailable to react, whereas this would not be such a significant problem when a large excess of cellulose is used, as in the 100 g per litre loading.

### 3.3.3 Reaction temperature

Relatively recent methods for the isolation of  $\beta$ -ISA which were published by Greenfield *et al.*<sup>107</sup> and Glaus *et al.*<sup>110</sup> used RT in their degradation reactions, and in early cellulose degradation reactions in this work, RT was also used; however, in addition further reactions at 50 °C and 90 °C were also performed to investigate the effects of temperature on the production of crude  $\beta$ -ISA solution. There are a number of reports that claim that using very high temperatures have negative effects on the amount of ISA produced. Krochta *et al.*<sup>116</sup> and Niemela<sup>120</sup> reported that at temperatures above 200 °C a complex mixture of degradation products was produced due to fragmentation reactions of intermediate products, and ISA was either not detected or only present in minor amounts. Another concern of raising the reaction temperature too high is that it has previously been shown<sup>127</sup> that the activation energy for the degradation of cellulose is less than the activation energy for the stopping reaction, so the extent of stopping increases with an increase in temperature. However, results from previous work suggest that at the intermediate temperatures employed in this study, ISA will be the major product of alkaline, anaerobic, degradation of cellulose. For example, Alfredsson and Samuelson degraded pure cotton cellulose over the range of temperatures from 20 °C – 100 °C<sup>129</sup> using various NaOH solutions and found that ISA was the major product of their reactions and Whistler and BeMiller used 80 °C for the majority of their reactions in the preparation of small quantities of beta ISA<sup>148</sup>. Even at temperatures between 170 °C and 190 °C, using NaOH solution under anaerobic conditions, ISA was reported to be the major CDP, however only accounting for 30 % of the total CDPs<sup>120</sup>. It should be noted that in a similar study, which also included the presence of oxygen, only traces of ISA were observed<sup>176</sup>, indicating the importance of the anaerobic conditions.

### 3.3.4 Anaerobic conditions

In the current study of the degradation reactions of cellulose, anaerobic conditions were maintained by continuously flushing reaction vessels with a stream of nitrogen. This was important because the presence of oxygen in the reaction system is known to reduce the concentration of ISA being produced. Previous studies have indicated that higher yields of ISA are produced under anaerobic conditions<sup>107, 177</sup>. Kolmodin and Samuelson<sup>177</sup>, treated hydrocellulose with 0.5 % sodium hydroxide at 95 °C under either aerobic or anaerobic conditions and found that twice as much degradation occurred in the anaerobic reaction,

indicating that the overall effect of oxygen in the reaction system reduces degradation; however, they determined that the main degradation pathway under both aerobic and anaerobic conditions was still end-wise peeling<sup>177</sup>.

The reason for the reduced production of ISA when oxygen is present is that the intermediate dicarbonyl moieties formed during the peeling reaction are very sensitive to oxygen, resulting in fragmentation reactions and the generation of smaller water soluble degradation products<sup>129, 177</sup>; the reason for a general reduction in cellulose degradation is because oxygen in the system can oxidise the reducing ends of the cellulose chains resulting in the generation of alkali stable aldonic acid end groups, thus rendering the ends stable to further alkali attack and the termination of the peeling reaction<sup>131, 178, 179</sup>.

### 3.3.5 Concentration of alkaline solution

The alkaline degradation of cellulose under anaerobic conditions is pH dependent so the amount of ISA produced will be related to the concentration of the alkali in the degradation reaction.

According to the results of other authors, cellulose rapidly undergoes alkaline peeling at pHs as low as 7<sup>180</sup> and the rate of peeling is invariable up to pH 8.5<sup>125</sup>. Above pH 8.5, Ziderman and Bel-ayche<sup>125</sup> and Chiang and Sarkanen<sup>180</sup> determined that the rate of peeling increases until pH 11. Furthermore, Pavasars *et al.*<sup>123</sup> determined that the rate of degradation was greater for a solution of pH 13.3 compared to a solution of pH 12.7 and Colbran and Davidson found that the amount of degradation increased from 0.1 M (pH 13) to 0.5 M (pH 13.7) HO<sup>-</sup> concentration when either sodium hydroxide or calcium hydroxide was used<sup>181</sup>. Lai and Sarkanen<sup>182</sup> found similar results with the degradation of amylose, which reacts in a very similar manner to cellulose<sup>183</sup>.

The pH dependency of the rate of peeling can be explained by the ionisation of the substrate at the reducing end to generate an anion<sup>182</sup> (Figure 35). Ziderman and Bel-ayche found that the rate of peeling was directly correlated to the concentration of the ionized end groups<sup>125</sup> and that there is no further reported increase in the rate of peeling above pH 13.7 because at that pH the hydroxyl group which has a pK<sub>a</sub> of 11.7<sup>180</sup> is fully ionised<sup>182</sup>.

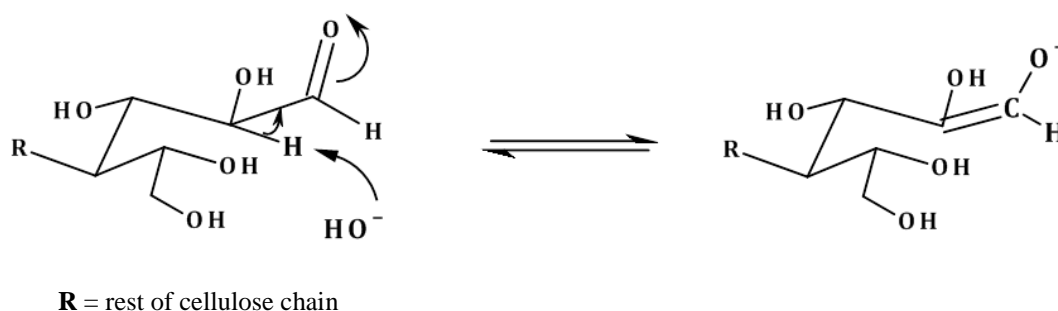


Figure 35: The formation of the cellulose enolate anion

The cellulose I structure is unaffected morphologically by the action of base below the concentration which swells cellulose fibres, therefore if reactions are allowed to run to completion the number of glucose residues peeled off should be independent of temperature and base concentration below 2.5 M (mercerization strength)<sup>184, 185</sup> because at lower base concentrations the base will not be able to access the tightly packed cellulose fibres i.e. the extent of reaction should not be influenced by the base concentration. However, because there is a correlation between pH and the rate of degradation, for short term reactions a higher pH of at least pH 13.7 (0.5 M) should be used to maximise the amount of degradation.

To further increase degradation beyond this point, the alkaline concentration must be above the swelling concentration, which will allow the  $\text{HO}^-$  to freely access all fibres and degradation will be allowed to continue<sup>184</sup>. Machell and Richards found that with sodium hydroxide concentrations of 2.5 M to 5 M degradation increases resulting in more weight loss of cellulose<sup>184</sup>. However, in the swelling range, caution must be applied, as the stopping reaction also occurs more readily<sup>184</sup>. It is thought that above 6 M NaOH, the extent of degradation rapidly falls<sup>185</sup>. Lai and Ontto<sup>185</sup> degraded hydrocellulose under anaerobic conditions in sodium hydroxide concentrations ranging from 0.05 M (pH 12.7) to 18.6 M (pH 15.3) and determined that at temperatures similar to the ones used in this work (120 °C) that degradation increased up until 6 M (pH 14.8) where swelling is thought to be at its maximum<sup>186</sup> and then the amount of cellulose degradation drastically decreased between 6 M and 18 M<sup>185</sup>. Therefore, as far as the NaOH concentration is concerned, the amount of degradation will be linked to the accessibility of the reagent with the base, i.e. there should be no difference below 0.5 M, increase until 6 M and then a decrease due to an enhanced rate of the stopping reactions<sup>185</sup>.

In the presented study, we wanted to maximise degradation whilst remaining below the swelling concentration of the cellulose fibres so as to minimise the stopping reaction. Greenfield *et al.*<sup>107</sup> degraded their cellulose using 0.5 M NaOH (pH 13.7) which is the pH required for optimal degradation. However, the formation of ISA and other cellulose degradation products is known to lower the pH of degradation solutions; one author reported that the pH was lowered from 12.36 (start, day zero) to 6.77 in anaerobic biogas reactions due to the production of ISA and other degradation products<sup>187</sup>. To prevent this from happening in the present reactions a 2 M NaOH concentration was used to ensure that the pH remained constant especially, in the higher temperature reactions where degradation is expected to increase. In calcium hydroxide reactions, a pH of 13.7 is not attainable, due to the low solubility of calcium hydroxide, so to ensure as high a pH as possible, a saturated calcium hydroxide solution was used (2 M by mass).

The conditions used in this work for the cellulose degradation reactions are summarised in Table 4 as follows:

Table 4: A summary of the cellulose degradation reaction conditions

Alkaline species	NaOH	Ca(OH) <sub>2</sub>
Substrate	Micro crystalline cellulose dp ~ 117	
Cellulose loading (g L <sup>-1</sup> )	100	
Reaction temperature (°C)	RT, 50 and 90	
Reaction conditions	A continuous stream of nitrogen applied to each reaction to maintain anaerobic conditions, standard glassware	
Base concentration (M)	2	Saturated (2 by mass)

### 3.4 Degradation of cellulose using sodium hydroxide solution

#### 3.4.1 Identification of degradation products

Three experiments were performed at RT, 50 °C and 90 °C and reactions were performed under a stream of nitrogen to maintain anaerobic conditions and, as previously discussed, reactions were monitored using HPAEC–PAD for periods of up to 35 days. A sample chromatogram representing each reaction is displayed in Figure 36, and results indicate that at each temperature the degradation reactions generate four HPAEC–detectable products, as indicated by the four peaks (labelled 1 – 4 in Figure 36).

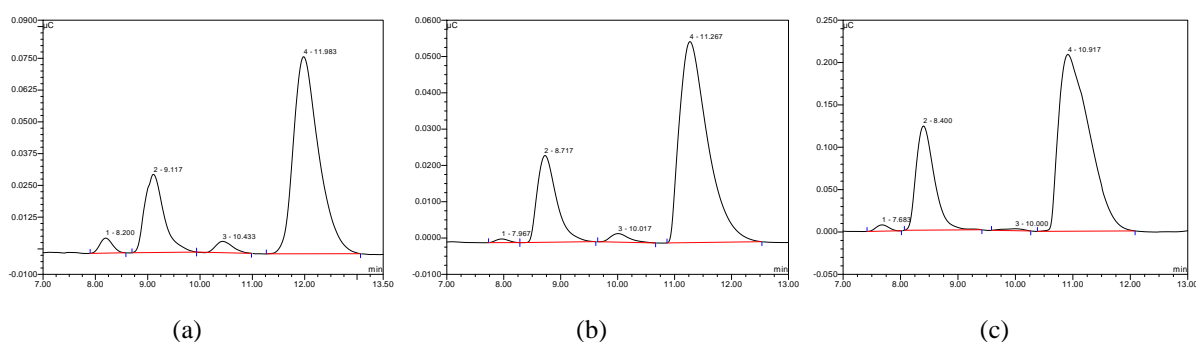


Figure 36: HPAEC-PAD chromatograms of (a) RT, (b) 50 °C and (c) 90 °C sodium hydroxide reactions.

Peak 2 was assigned as  $\alpha$ -ISA by comparisons with the retention time of the  $\alpha$ -ISA prepared in section 2.4.1 and the identity was confirmed by spiking one of the degradation samples with a pure  $\alpha$ -ISA sample. Peak 4 was assigned as  $\beta$ -ISA as it is a known degradation product under the reaction conditions and it is produced in greater yields than  $\alpha$ -ISA when sodium hydroxide is used as the alkaline species,  $\beta$ -ISA corresponds to the largest peak, and it was found that it was approximately 3 times larger than the alpha ISA peak for all reaction temperatures.

To confirm the assignment of peak 4, a crude  $\beta$ -ISA solution prepared as described in section 2.5.1 was passed through a preparative anion exchange column and fractions were screened using HPAEC–PAD resulting in the partial isolation of the peak (see Figure 37 for an example chromatogram). Selected fractions were lyophilized, their  $^1\text{H}$  NMR spectrum were recorded and the spectra were compared with  $^1\text{H}$  NMR data from the literature <sup>110</sup>. When a pure sample of  $\beta$ -ISA became available as the project progressed, the retention time was then determined and the identity of the peak was confirmed.

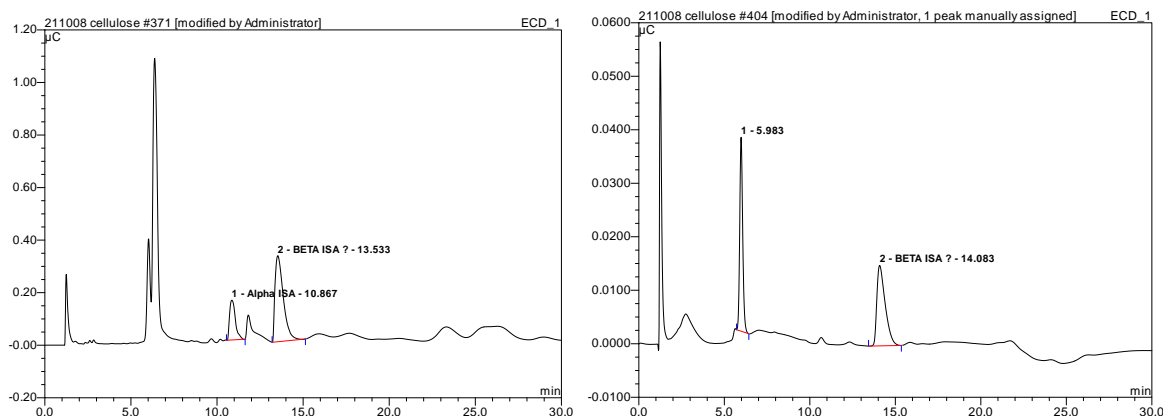


Figure 37: HPAEC-PAD chromatogram of crude  $\beta$ -ISA solution (left) and the same solution after being eluted through a preparative anion exchange column resulting in the partial isolation of  $\beta$ -ISA (right).

The fractionation and NMR analysis of the crude solution also allowed for the tentative identification of peak 3 as belonging to 3,4-dihydroxybutanoic acid (DHB). A HPAEC-PAD chromatogram published by Glaus *et al.* of a similar cellulose degradation sample shows a similar peak located between the  $\alpha$ -ISA and  $\beta$ -ISA peaks, but in their work the peak is assigned as an unknown<sup>110</sup> (Figure 38).

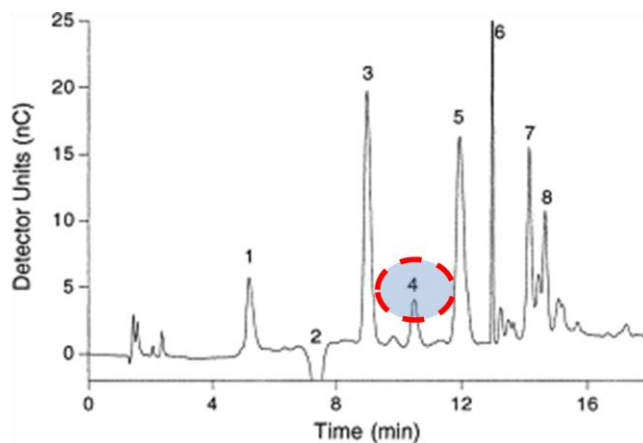


Figure 38: HPAEC chromatogram from Glaus *et al.* of the degradation of cellulosic materials with unknown peak No.4

$^1\text{H}$  NMR analysis of one particular fraction indicated that  $\beta$ -ISA was present, but also several additional proton environments were visible (Figure 39). Further 2D and Dept  $^{13}\text{C}$  NMR analysis of this sample indicated that all the additional peaks were coupled indicating one compound (3,4-dihydroxybutanoic acid, DHB) which was present in the 1,4-lactone conformation ( $\text{DHB}_L$ ) (Figure 40).

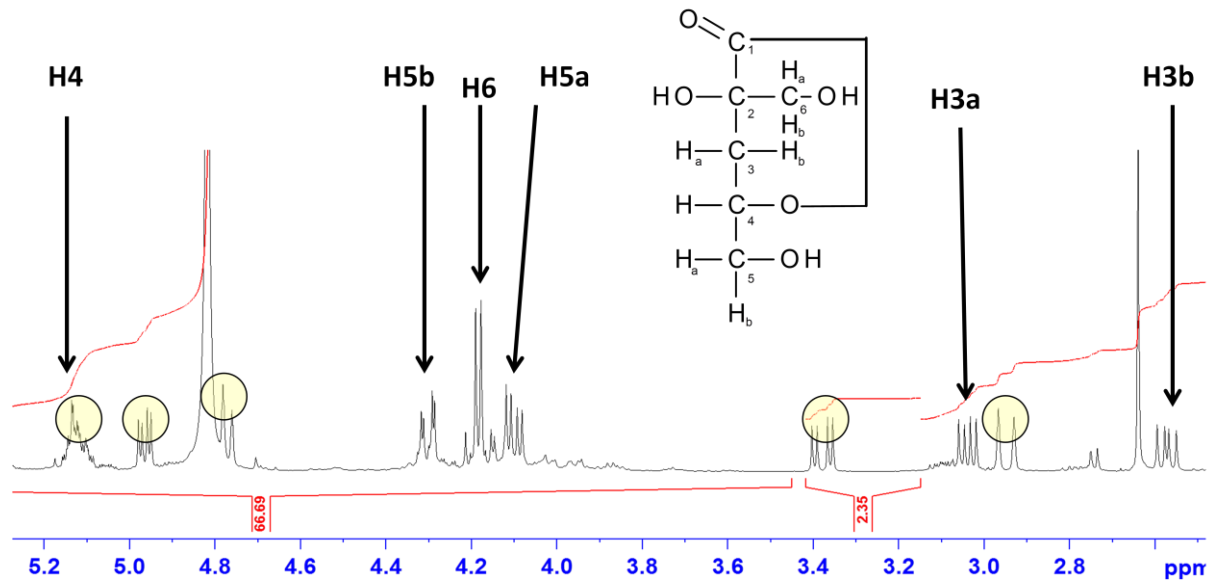


Figure 39:  $^1\text{H}$  NMR spectrum of partially separated  $\beta$ -ISA (labelled peaks) and also the presence of additional peaks (yellow circles).

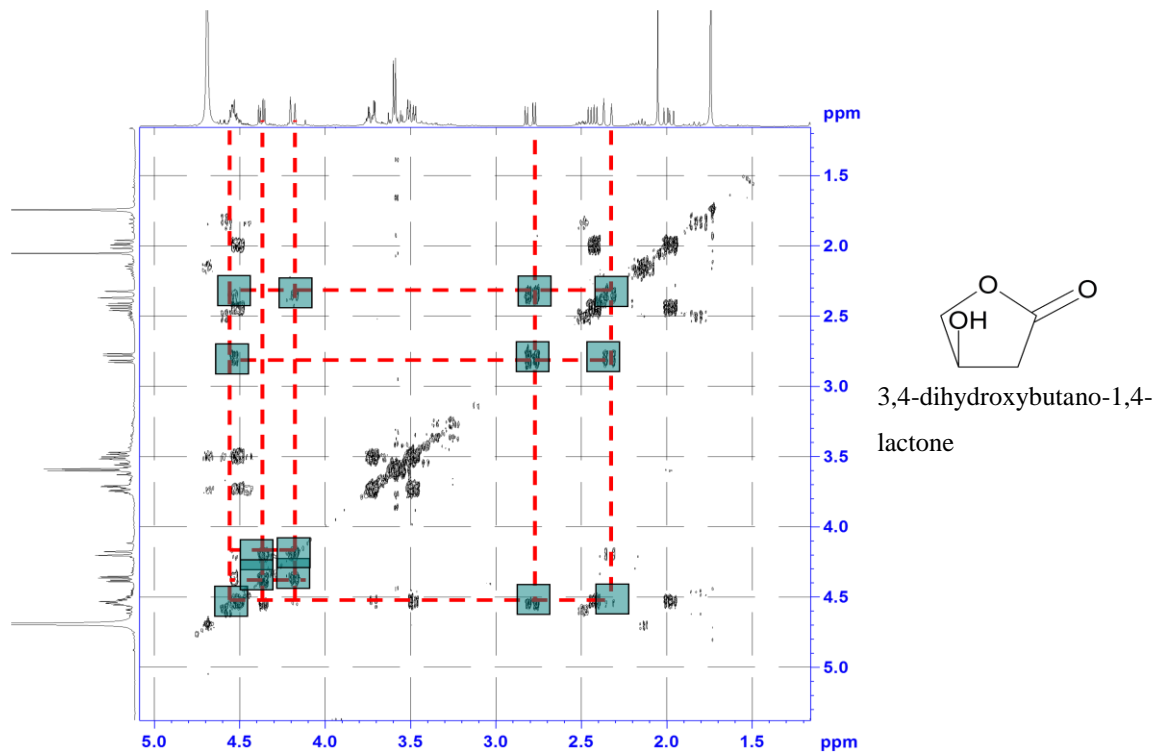


Figure 40: COSY NMR spectrum allowing for the identification of 3,4-dihydroxybutano-1,4-lactone

DHB is an expected product of the degradation of cellulose. When sodium hydroxide is used as a base, one of the major reaction mechanisms is the scission between the C2 and C3 bond of the dicarbonyl intermediate (4-deoxy-2,3-hexodiulose) resulting in the formation of DHB and glycolic acid (Figure 41) and also the production of formic acid and other volatile acids due to other fragmentation<sup>129-132</sup>. The potential for this scission to occur was proven by Machell and Richards<sup>133</sup> when the intermediate was isolated<sup>133, 134</sup> and reacted with sodium hydroxide solution at 25 °C under anaerobic conditions and the resulting major products were ISA, DHB, glycolic acid, formic acid and minor amounts of other volatile acids<sup>133</sup>.

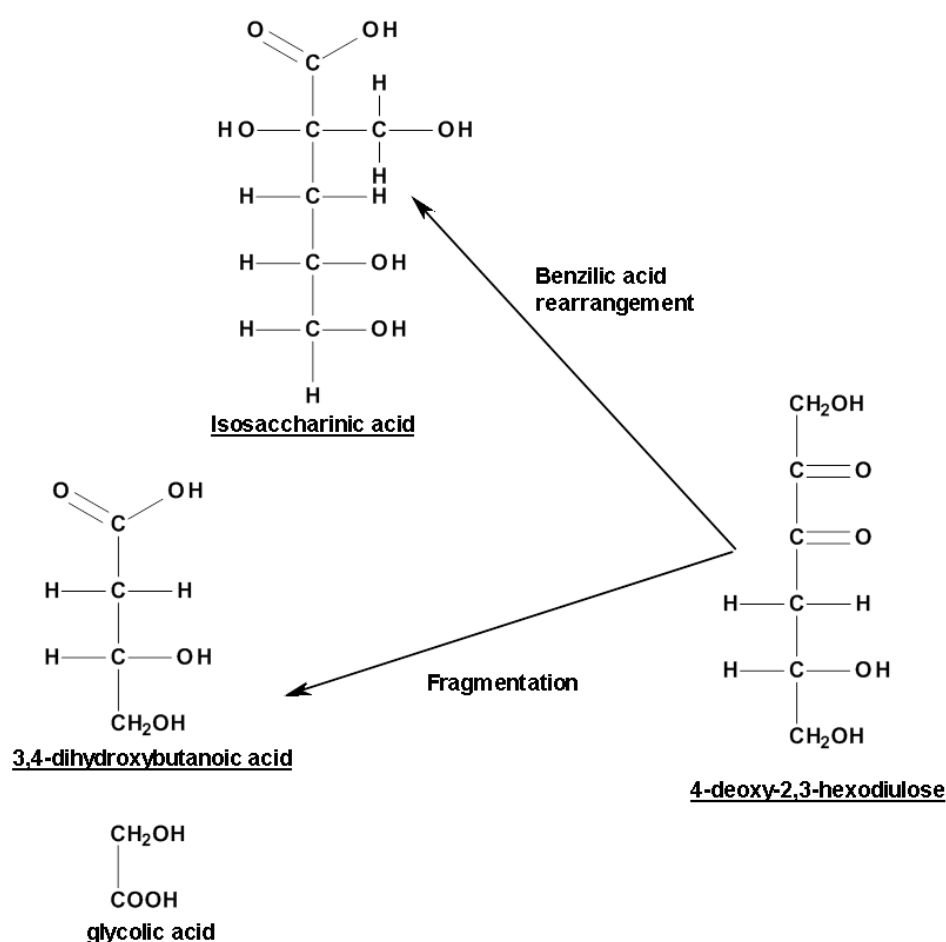


Figure 41: Diagram showing the action of NaOH on 4-deoxy-2,3-hexodiulose, adapted from the results of Machell and Richards<sup>130</sup>.

In the present work, to confirm the assignment of DHB, a sample was synthesised using the method of Greenfield *et al.*<sup>107</sup> by the peroxidation of 3-butenic acid using a tungstic acid catalyst<sup>188</sup>. The synthesised product was characterised using GC-MS and NMR and as can be seen in Figure 42, the  $^1\text{H}$  NMR spectrum of the synthesised product is in good agreement with the unknown peaks in the original NMR spectrum (Figure 39); additionally, when one of the degradation samples was spiked with the synthesised DHB, peak 3 dramatically increasing in size, confirming the assignment (Figure 43).

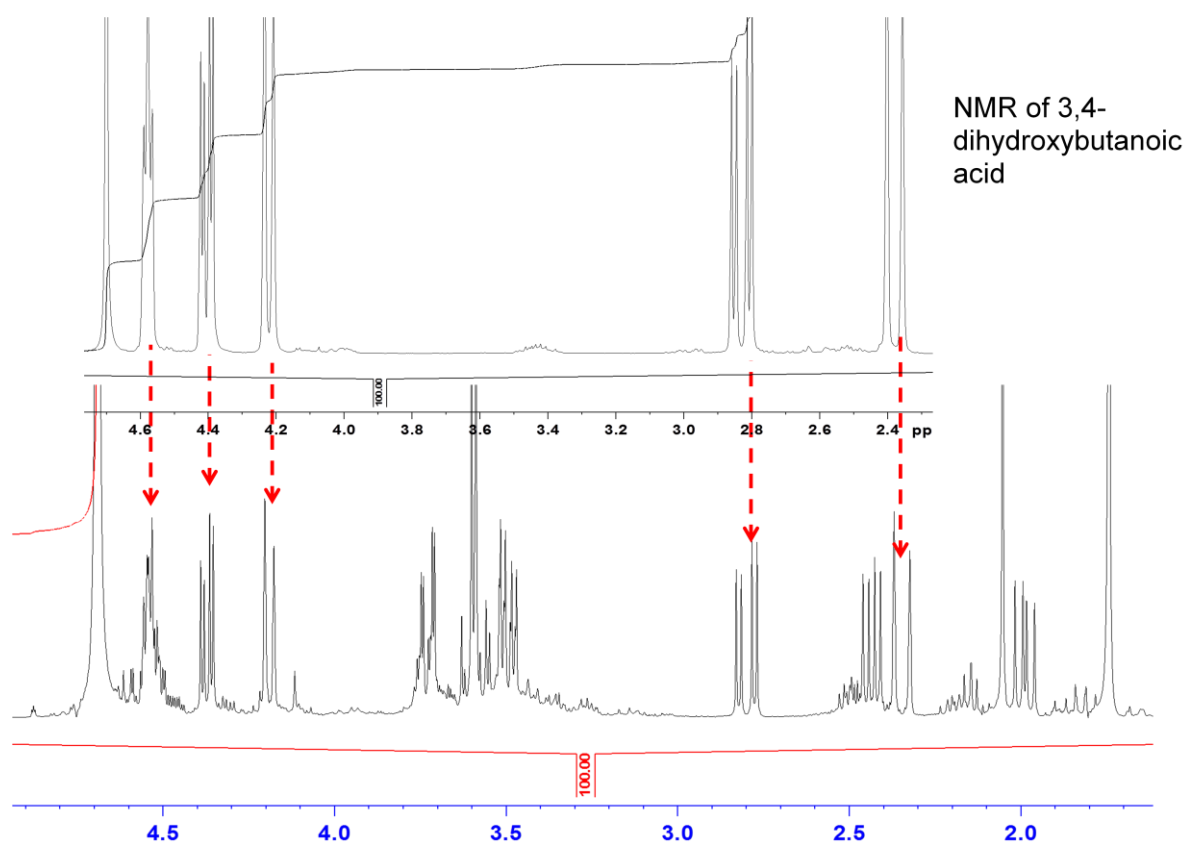


Figure 42: Comparison between the  $^1\text{H}$  NMR spectrum of the synthesised 3,4-dihydroxybutanoic acid and the additional peaks in the cellulose degradation sample.

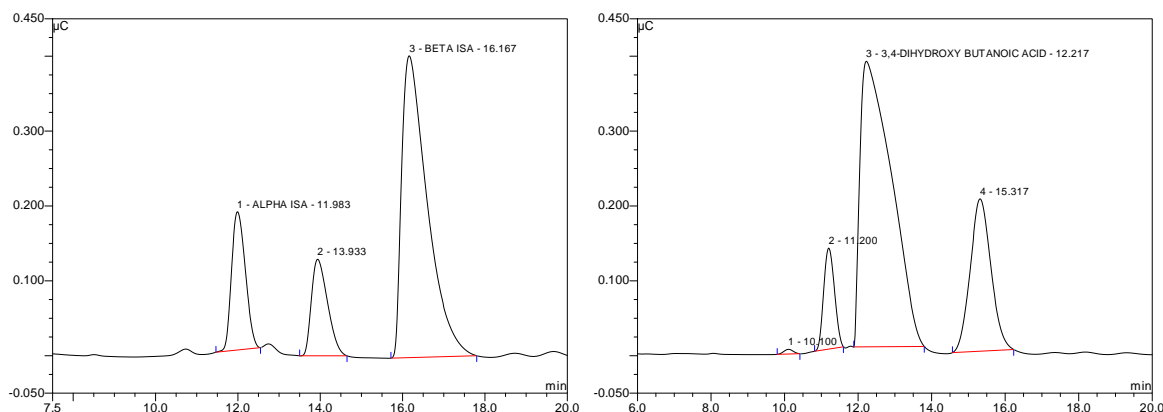


Figure 43: Cellulose degradation sample before (left) and after being spiked with 3,4-dihydroxybutanoic acid.

Previous results in the literature indicate that the reaction temperature has an effect on the production of DHB. Machell and Richards determined that when they degraded 4-deoxy-2,3-hexodilulose in NaOH solution at RT, DHB was produced in greater amounts than ISA, however, at 100 °C ISA was produced in greater yields than DHB<sup>133</sup>. Alfredsson and Samuelson<sup>129</sup> degraded cellulose in NaOH (0.5 M) at various temperatures and found that as the temperature of the degradation reaction increased from 20 °C to 100 °C the molar % of DHB and glycolic acid present in relation to the relative amount of ISA formed significantly decreased, whereas the relative amount of formic acid significantly increased. Richards and Sephton and Machell and Richards<sup>102 126</sup> also degraded cellulose in NaOH (0.5 M) at 100 °C and determined that ISA and formic acid were the major products and, due to the higher temperature, only trace amounts of DHB and glycolic acid were produced.

As can be seen in Figure 36, the DHB peak is small in comparison to the ISA peaks and accounts for less than 3 % of the combined ISA peak area in the RT reaction, and it is evident that the ISA peaks increase in size relative to the DHB peak as the reaction temperature increases from RT to 90 °C; at 90 °C the DHB peak only accounts for 0.5 % of the peak area, indicating that, in agreement with the literature, its production is not favoured at the higher temperatures.

It is also possible that the production of DHB may have resulted from the presence of traces of oxygen in our degradation reactions as it was not possible to operate in strictly anaerobic conditions i.e. no use of a glove box. The possible production of DHB by oxidation was highlighted by Machell and Richards<sup>133</sup> who isolated the 4-deoxy-2,3-hexodilulose

intermediate and oxidized it with hydrogen peroxide in the absence of alkali to generate DHB and glycolic acid in high yield and in equimolar amounts.

To investigate the efficacy of the anaerobic conditions used in the present work, two additional short-term reactions were performed in which cellulose was degraded in sodium hydroxide solution (2 M, 90 °C), using either anaerobic or aerobic conditions. After 72 h both reactions were stopped and analysed by HPAEC–PAD (Figure 44) and results indicated that a noticeable increase in the amount of DHB was occurring in the aerobic reaction, where its peak constituted 5 % of the total peak area as compared to 1.3 % in the anaerobic reaction, therefore indicating the importance of flushing degradation reactions with nitrogen. It is possible that a further decrease in the production of DHB may be achieved if more stringent anaerobic conditions were adhered to, for example if the degradation reactions had been performed in a glove box as opposed to using standard laboratory conditions.

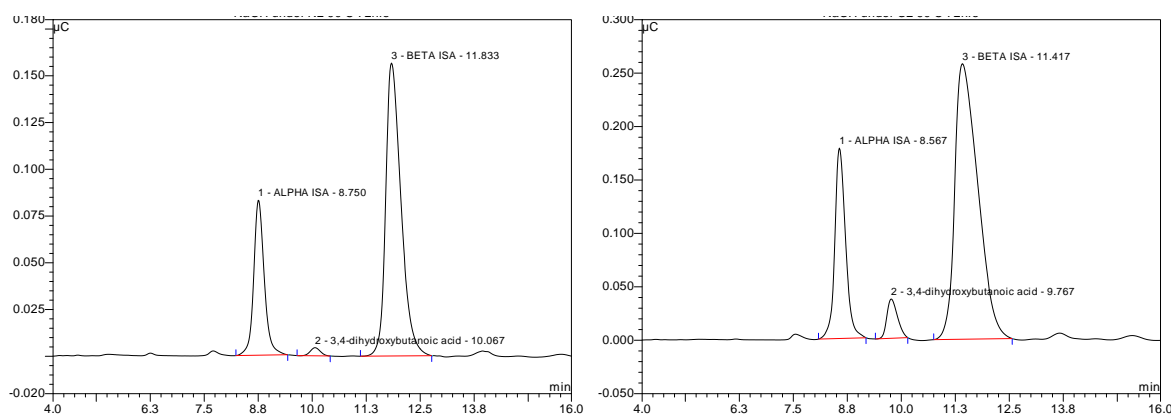


**Figure 44:** HPAEC-PAD chromatograms comparing the production of DHB under anaerobic (left) and aerobic conditions (right) when cellulose is degraded using NaOH (2 M) at 90 °C for 72 h.

A comparative set of anaerobic versus aerobic reactions were also undertaken using  $\text{Ca}(\text{OH})_2$  instead of NaOH as the base; when using  $\text{Ca}(\text{OH})_2$  as the base, the results indicated that there was no significant difference between the amount of DHB produced (Figure 45) when either aerobic or anaerobic conditions were used, in both reactions DHB only accounted for about 1 % of the total peak area.

The percentage of the intermediate lost to fragmentation reactions can be reduced by favouring the benzilic acid type rearrangement reaction. A number of authors have reported that  $\text{Ca}^{2+}$  promotes the benzilic acid type rearrangement. Machell and Richards indicated

that under anaerobic conditions at 25 °C when calcium hydroxide is used as the base, the isolated 4-deoxy-2,3-hexodilulose intermediate is converted into ISA in yields of up to 90 %<sup>133</sup> with no DHB being detected, indicating the catalytic effect of calcium ions on the benzilic acid type rearrangement. However, Greenfield *et al.* degraded cellulose, using  $\text{Ca}(\text{OH})_2$  as a base for longer periods of time (7 days) at RT, but they used aerobic conditions and in their reactions DHB accounted for approximately a third of the degradation products indicating that at RT, under aerobic conditions the catalytic effect of  $\text{Ca}(\text{OH})_2$  on promoting the benzilic acid type rearrangement is less prevalent which allows more scission of the 4-deoxy-2,3-hexodilulose intermediate to take place. Whereas the results of the present short-term study (Figure 45) indicate that when reactions are carried out at 90 °C and employing calcium hydroxide, the benzilic acid type rearrangement occurs too fast to allow scission to significantly take place whether anaerobic or aerobic conditions are used and it can be said that in relation to maximising the production of ISA, there is no clear advantage to performing experiments under anaerobic conditions.

The speed of the conversion of the intermediate to ISA in the presence of calcium hydroxide was evident in the work of both Machell and Richards and Whistler and BeMiller. The intermediate was first identified as being 4-deoxy-2,3-hexodilulose by Machell and Richards<sup>102</sup> and also later isolated by Machell and Richards<sup>133</sup>, and characterised using UV, elemental analysis, optical rotation, and derivative preparation; Whistler and BeMiller also isolated and characterised the intermediate at around the same time<sup>134</sup>. In the case of Whistler and BeMiller, isolation was attempted by degrading cellobiose under anaerobic conditions using calcium hydroxide; they found that the benzilic acid type rearrangement occurred too rapidly to allow any isolation to take place. However, when they repeated the experiment using potassium hydroxide, isolation of the intermediate was achieved. Likewise, Machell and Richards<sup>133</sup> also achieved isolation by degrading cellobiose using sodium hydroxide. The results of both sets of authors further indicates the catalytic effect of calcium ions, resulting in the occurrence of the benzilic acid type rearrangement<sup>134</sup>; their results indicate that when using sodium hydroxide to degrade cellulose, anaerobic conditions are important as there is more time for fragmentation of the intermediate to occur.

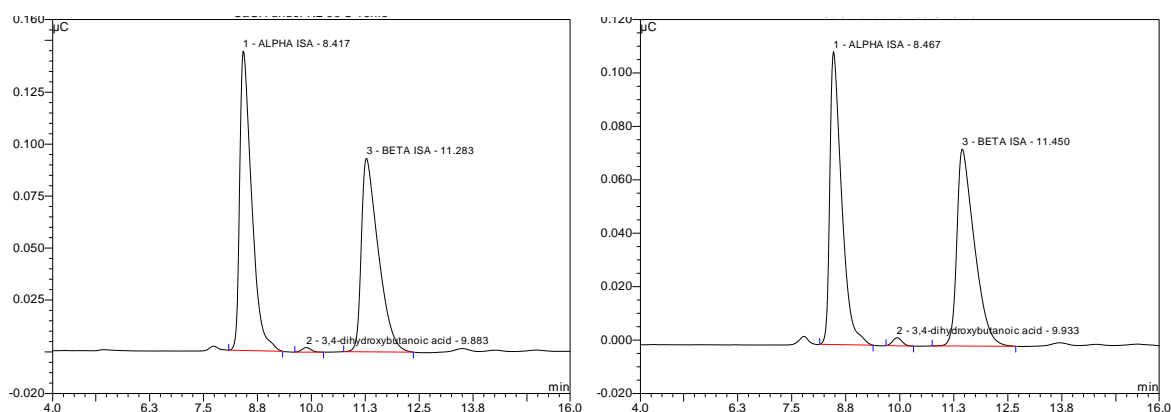


**Figure 45: HPAEC chromatograms comparing the production of 3,4-dihydroxybutanoic acid under anaerobic (left) and aerobic conditions (right) when cellulose is degraded using  $\text{Ca}(\text{OH})_2$  (saturated soln.) at 90 °C for 16 h.**

Finally, an attempt was made to identify the 1<sup>st</sup> peak from the chromatograph displayed in Figure 36. NMR analysis of one of the degradation samples suggested that peak number 1 was 2-C-(hydroxymethyl)-3-deoxytetronic acid (xyloisosaccharinic acid, XISA, Figure 46). XISA is the major product of the alkaline degradation of xylose, which is the major monomer present in xylan<sup>189</sup>, which is itself the major component of hemicellulose; XISA is listed as a significant product (1 – 10 %) in the alkaline degradation of cellulose under similar reaction conditions, see the review by Knill and Kennedy<sup>93</sup>.

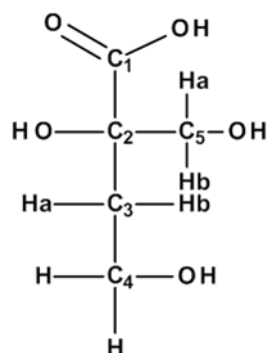


Figure 46: Structure of X-ISA

In an attempt to confirm the assignment of peak 1, XISA was synthesised in the laboratory using the method of Greenfield *et al.*<sup>107</sup> and was characterised by NMR. The synthesised XISA was used to spike one of the degradation samples containing the unknown peak, but rather than seeing an increase in height of the unknown peak, an additional peak was observed indicating that the compound was not responsible for the unknown peak as it

possessed a clearly different retention time (Figure 47), thus highlighting the importance of using more than one chemical technique when identifying unknowns.

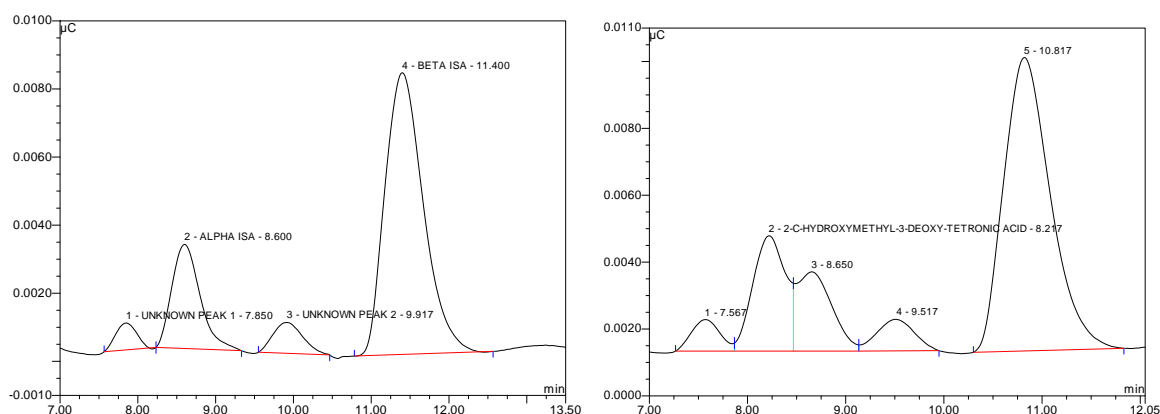


Figure 47: HPAEC chromatogram of a cellulose degradation sample (left) and after being spiked with xyloisosaccharinic acid (XISA).

In the work of Greenfield *et al.*<sup>107</sup> and Pavasars<sup>115</sup> they predicted that XISA was produced from the hemicellulose containing substrates in their degradation reactions, with XISA arising from the degradation of xylan; in an analogous way to the production of ISA from peeled off glucose units in cellulose degradation. In the present study, pure cellulose was degraded which contained little, if any hemicellulose, so it is understandable that XISA was not present in our degradation solutions. No further attempts were made to identify peak number 1, as its identification was not a major aim of this work.

An interesting observation came out of these results however; in Greenfield *et al.*<sup>107</sup> they determined that with their method of analysis, the peaks representing XISA and  $\beta$ -ISA were co-eluting and shared the same retention times, so it was hypothesised that that was the reason why  $\beta$ -ISA's peak area was larger than  $\alpha$ -ISA's; however, in our work we have shown that XISA and  $\beta$ -ISA are completely resolved under the applied HPAEC-PAD conditions and the  $\beta$ -ISA peak is still larger than the  $\alpha$ -ISA peak even when XISA is absent, indicating that the presence of sodium ions or the absence of calcium ions is the reason for the preference of the production of excess  $\beta$ -ISA.

### 3.4.2 Monitoring the production of $\alpha$ -ISA and $\beta$ -ISA using HPAEC-PAD

The pure  $\alpha$ -ISAH sample, as described in section 3.2.2 was used to quantify both  $\alpha$ - and  $\beta$ -ISA because no sample of  $\beta$ -ISA was available at the time of analysis. It was deemed

acceptable to use  $\alpha$ -ISA for the quantification of both  $\alpha$ - and  $\beta$ -ISA because they both were expected to give an equal detector response factor in terms of peak area, whilst having different retention times, allowing for adequate peak resolution. However, it is interesting to note that each analyte possesses quite a different peak shape; with  $\alpha$ -ISA having a taller, narrower peak than  $\beta$ -ISA, indicating that both analytes interact differently within the column. Using the “Chromeleon” software which was used with the HPAEC-PAD system, it was determined that the peaks of both analytes have an asymmetry factor of 1.2 indicating that they have very similar, but small levels of peak tailing which indicates that the same retention mechanisms are occurring for both analytes; however the calculated number of theoretical plates for the  $\alpha$ -ISA peak (4031) is more than that of the  $\beta$ -ISA peak (3465) which indicates that  $\beta$ -ISA is retained more strongly by the stationary phase resulting in a broader peak shape (see Figure 48, for illustration purposes only), most probably due to  $\beta$ -ISA having a lower  $pK_a$  value (see section 5.1.2 for discussion of  $pK_a$  results).

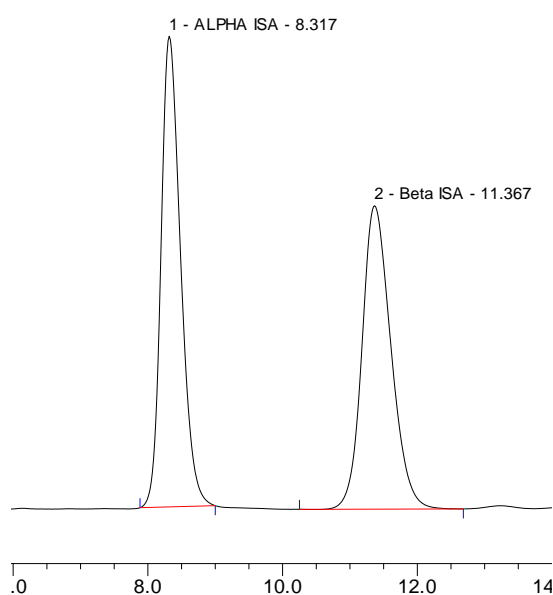


Figure 48: HPAEC-PAD chromatogram of alpha and beta ISA (both 50 ppm).

### 3.4.3 Determination of solution concentrations of $\alpha$ - and $\beta$ -ISA

The production of  $\beta$ -ISA and  $\alpha$ -ISA in ppm as a function of time are shown in Figure 49 and Figure 50 and they were produced from the sodium hydroxide catalysed cellulose

degradation reactions, which were performed using the conditions as described in section 2.3.5.

The time courses for the production of ISA produced in this work follow similar trends to those reported by Glaus and Van Loon<sup>108</sup>, which, in this work is most visible in the 90 °C reaction due to the faster rate of ISA production; that is there is an initial fast stage of ISA production, linked to the alkaline peeling of the available reducing end groups of the amorphous regions in the cellulose fibres. This initial stage lasts for approximately 24 h in the 90 °C reaction and seven days in the 50 °C reaction. In the RT reaction, the initial fast stage of peeling was still ongoing for the duration of the reaction; it was reported in the work of Van Loon *et al.*<sup>12</sup>, that when degrading pure cellulose at RT, the rate of degradation does not plateau until periods of more than one year. In the 90 °C and 50 °C reactions, following the initial fast stage of peeling, the production of ISA begins to slow down due to a combination of the formation of alkali stable end groups (chemical stopping)<sup>101, 184</sup> or due to the inaccessible crystalline regions preventing access to the base (physical stopping)<sup>127, 181, 184</sup>. Following the termination of the degradation reactions after 35 days, there still appears to be a slow production of ISA for all reaction temperatures. According to Hass *et al.*<sup>127</sup> degradation does not instantly stop when a crystalline region is entered, more likely it drastically slows down as reagents struggle to access fibres. It was reported by Biddle *et al.*<sup>124</sup> that when cellulose was degraded at 80 °C under anaerobic, alkaline conditions, degradation continued at a slow but measurable rate for a period of up to two years. For peeling to continue following the completion of the initial stage of peeling, mid chain scission due to alkaline hydrolysis is required, resulting in the formation of new reducing end-groups which are available for further peeling. Alkaline hydrolysis is a known process at high temperatures<sup>190</sup>, but at the temperatures employed in this work it is said to be insignificant<sup>143</sup>.

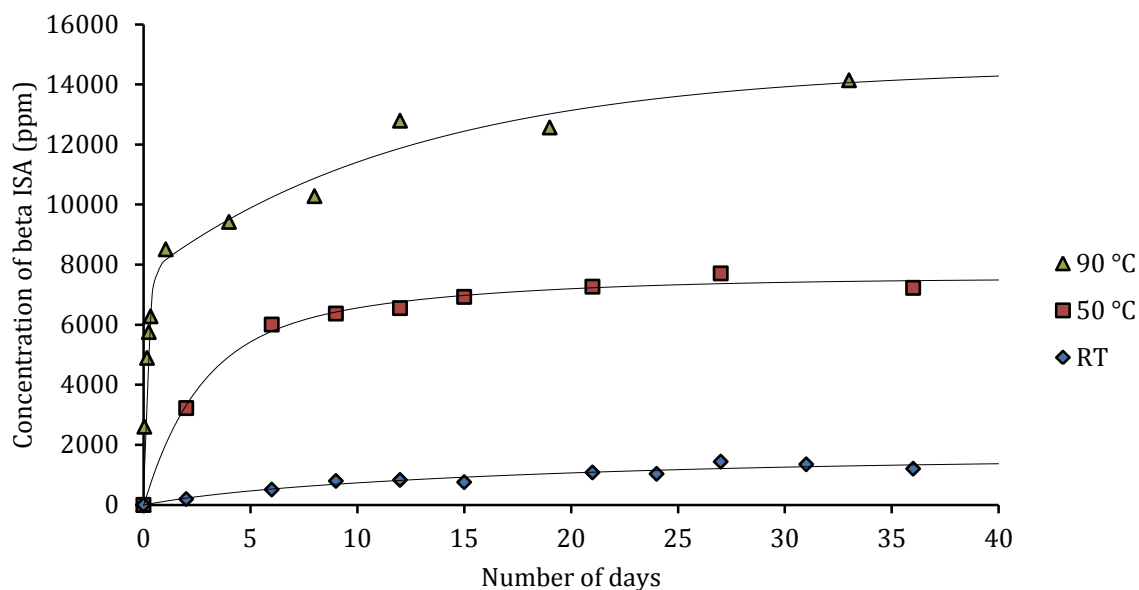


Figure 49: Time course for the production of  $\beta$ -ISA (ppm) for the sodium hydroxide catalysed degradation of cellulose at RT, 50 °C and 90 °C (lines are a guide for the eye only).

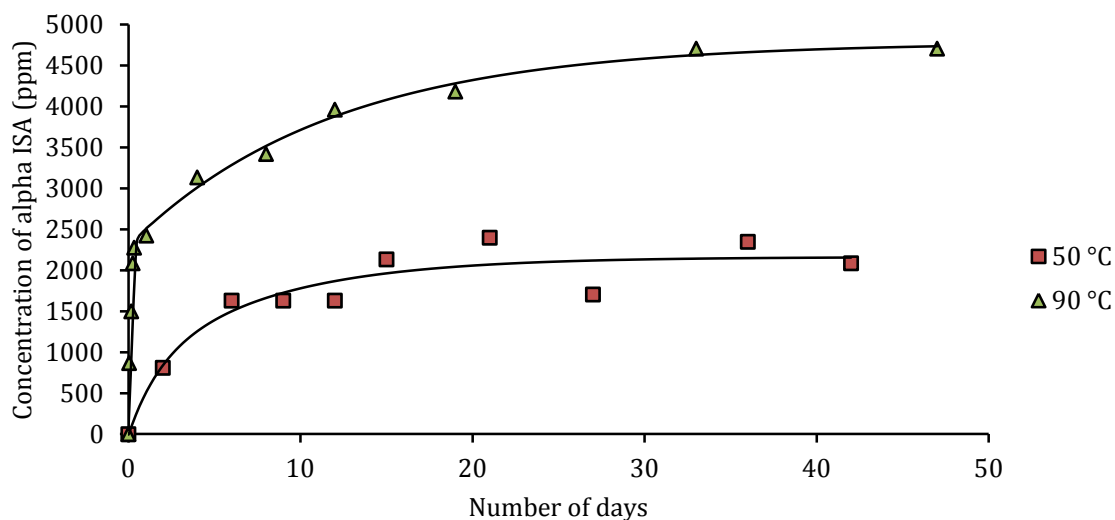


Figure 50: Time course for the production of  $\alpha$ -ISA (ppm) for the sodium hydroxide catalysed degradation of cellulose at 50 °C and 90 °C (lines are a guide for the eye only).

A further observation regarding the degradation reactions carried out in this work was the colour of the solutions, which is an indicator of the progression of cellulose degradation reactions. The amount of chromogen produced is related to the extent of end-wise

degradation due to beta elimination<sup>107</sup>, the darker the colour of the reaction the more the cellulose has been degraded due to the number of reducing end groups undergoing end-wise peeling. Albeck *et al.*<sup>191</sup> determined using colorimetry that the absorbance of water soluble products formed during cellulose degradation has a linear relationship with the amount of material degraded. Further studies by Ziderman *et al.*<sup>170</sup> and Ziderman and Belayche<sup>192</sup> monitored the progression of degradation reactions using either cellulose or amylose as the substrate by measuring the absorbance of the resulting degradation solution<sup>192</sup> using U.V. spectrometry and found a linear correlation between the weight loss of the substrate and the absorbance of the degradation mixture. In the present study, the initial colour of all the reactions was creamy white, but over time, depending on temperature, there was an obvious colour change between the different reaction temperatures as the reactions proceeded. The room temperature reaction remaining creamy white for the duration of the reaction, the 50 °C reaction turned a dark yellow/pale brown colour after several hours and the 90 °C reaction was very dark brown after several hours. An indication of the species which is responsible for the brown colouration has previously been discussed in section 3.2.4.

In agreement with the observed colour of the reaction solutions, the concentration of ISA generated from each reaction increased with the temperature of the reaction. After 36 days of reaction, approximate final solution concentrations of  $\beta$ -ISA were 1.2 g L<sup>-1</sup> for the RT reaction, 7.2 g L<sup>-1</sup> for the 50 °C reaction and 14 g L<sup>-1</sup> for the 90 °C reaction; and for  $\alpha$ -ISA, concentrations of 2.3 g L<sup>-1</sup> for the 50 °C reaction and 4.7 g L<sup>-1</sup> for the 90 °C reaction were observed. A visual comparison of the generated  $\alpha$ - and  $\beta$ -ISA concentrations produced at either 50 °C or 90 °C are presented in Figure 51, which clearly indicate the preference for the production of  $\beta$ -ISA when NaOH is used as the degrading alkaline species. However, due to an unforeseen problem encountered with the HPAEC-PAD system, an accurate measurement of the  $\alpha$ -ISA peak areas for the RT reaction could not be made, so the RT concentrations are not reported, however, throughout the entirety of this work, when cellulose was degraded using sodium hydroxide, the concentration of  $\alpha$ -ISA was consistently three times less than the concentration of  $\beta$ -ISA, so the concentration of  $\alpha$ -ISA produced in the RT reaction can be estimated as being approximately 0.4 g L<sup>-1</sup>.

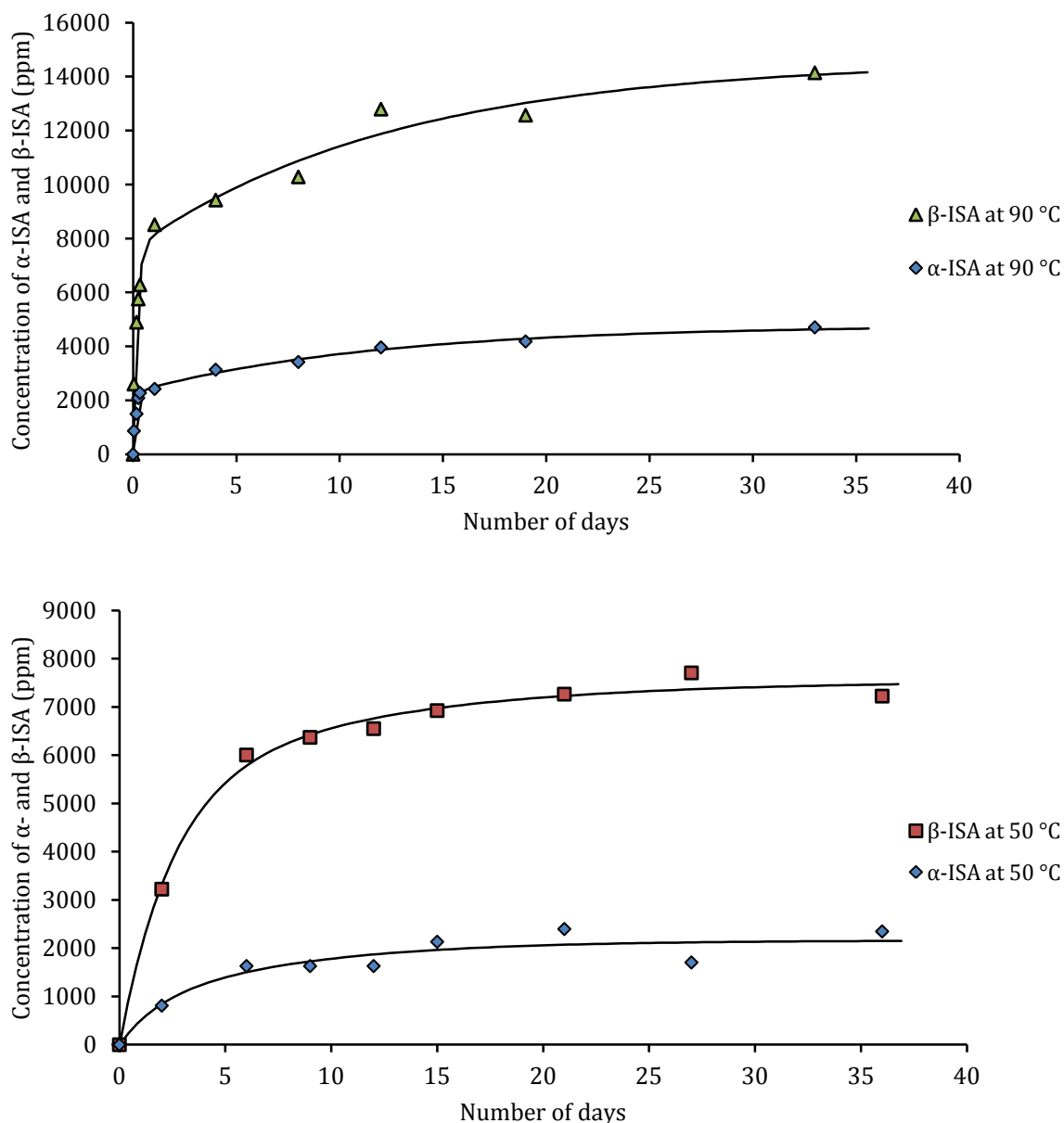


Figure 51: Time course for the production of  $\alpha$ -ISA and  $\beta$ -ISA (ppm) for the sodium hydroxide catalysed degradation of cellulose at either 90 °C (top) or 50 °C (bottom) (lines are a guide for the eye only).

To determine the ISA content of the 90 °C reaction solution as a percentage of the total generated CDPs, the final solution from the 90 °C reaction was analysed for its total organic carbon (TOC) content using the conditions described in section 2.3.7. Results indicated that the organic carbon content of the 90 °C reaction was  $13.2 \pm 0.264 \text{ g L}^{-1}$  after 33 days reaction time. The total  $\alpha + \beta$ -ISA concentration of  $18.8 \text{ g L}^{-1}$  equates to  $7.5 \text{ g L}^{-1}$  of carbon (40 % of  $180 \text{ g mol}^{-1}$ ), so the total amount of ISA accounts for ~ 57 % of the TOC in the 90 °C reaction after 33 days, of which  $\beta$ -ISA and  $\alpha$ -ISA account for ~ 42 % and ~ 14 % of the TOC respectively.

Further qualitative analysis of the 90 °C degradation solution using HPIEC, using the conditions described in section 2.3.6, indicated that after ISAs, the second most abundant CDP was formic acid, which accounted for 41 % of the total peak area, minor amounts of acetic acid, propanoic acid and glycolic acid were also indicated by comparisons of the retention times with analytical standards. Several other studies have also reported that formic acid was the second most abundant CDP produced under similar reaction conditions; small amounts of lactic acid, DHB and glycolic acid were also reported<sup>102, 126, 129, 133</sup>.

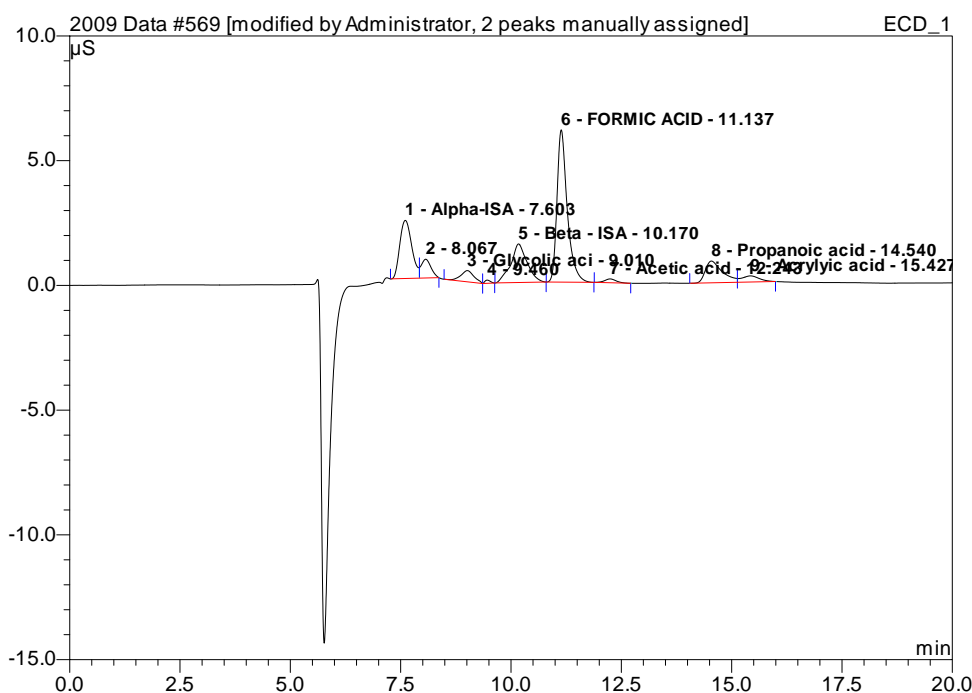


Figure 52: HPIEC chromatogram of the solution produced from the degradation of cellulose at 90 °C using NaOH (2 M) solution.

It is expected that at the base strength employed in this work, the same amount of degradation would be achieved for all three reaction temperatures if the reactions were allowed to proceed until completion. In a paper by Lai and Ontto<sup>185</sup> it was reported that with cellulose, the number of total glucose units peeled off is almost independent of temperature and base concentration up to 2 M<sup>185</sup> due to the crystalline cellulose being inaccessible to the base below this concentration. However, for the short term reactions, as can be seen from Figure 49 there is clear advantage to using higher temperatures of up to 90 °C as opposed to RT due to a larger production of  $\beta$ -ISA at that temperature.

The initial results of this study indicated that by using 90 °C as opposed to RT, approximately a twelve-fold increase in  $\beta$ -ISA solution concentration was achieved after 35 days, and the maximum  $\beta$ -ISA concentration achieved at room temperature (1.2 g L<sup>-1</sup>), was achieved in less than one hour at 90 °C (2.6 g L<sup>-1</sup> after 1 h). For those reasons, larger scale degradation reactions for the production of crude  $\beta$ -ISA solution employed a 90 °C reaction temperature, and it was decided that an approximate reaction time of 24 h would be employed, as that period of time the rate of production of  $\beta$ -ISA was at a maximum.

### **3.5 Degradation of cellulose in calcium hydroxide solution**

#### **3.5.1 Identification of degradation products**

The experiments discussed in section 3.4 were repeated but instead of using NaOH as the base, saturated solutions of Ca(OH)<sub>2</sub> were used (see section 2.3.2). Three experiments were performed at RT, 50 °C and 90 °C and each was performed under anaerobic conditions and the reactions were monitored using HPAEC–PAD.

A sample chromatogram produced from the Ca(OH)<sub>2</sub> reactions is presented in Figure 53; for all reaction temperatures two major peaks representing  $\alpha$ - and  $\beta$ -ISA were present and these were assigned by comparison with the retention time of analytical standards. For each reaction temperature the concentrations of  $\alpha$ - and  $\beta$ -ISA were very similar, which is as expected when calcium hydroxide is used as base, however, in agreement with the results published by Greenfield *et al.*<sup>107</sup>, the amount of  $\alpha$ -ISA present in degradation solutions slightly predominated. In the present work, the  $\alpha$ -ISA peak appears to be closely eluting with two smaller peaks, signs of those additional peaks were visible on both sides of the base of the  $\alpha$ -ISA peak, and these may account for the slightly larger peak area. The small additional peaks probably represent the same two small peaks which were present in the NaOH reactions (DHB and an unknown compound). In all of the chromatograms produced from the Ca(OH)<sub>2</sub> samples, the minor peaks are significantly smaller in relation to the peak areas of the ISA peaks which is consistent with Ca<sup>2+</sup> ions catalysing the benzilic acid type rearrangement in preference to fragmentation reactions resulting in ISA making up larger proportions of the total CDPs.

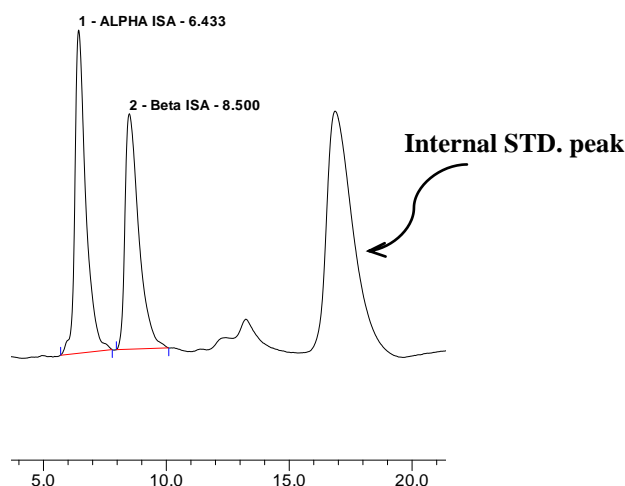


Figure 53: Example of a HPAEC-PAD chromatogram produced from the degradation of cellulose using saturated calcium hydroxide solution.

It was also evident from the  $\text{Ca}(\text{OH})_2$  reactions, that there was an additional two small unresolved peaks which had a retention time of 12 and 13 minutes (Figure 53), and the location of these peaks coincided with those for  $\alpha$ - and  $\beta$ -MSA (see section 3.2.3); these peaks were also possibly present in the NaOH reactions (described in section 0), but they were less prominent, (< 1 % of the size of the ISA peaks).

It is understandable why MSA may be produced at chain ends, particularly during the  $\text{Ca}(\text{OH})_2$  reactions: because  $\text{Ca}(\text{OH})_2$  promotes the mechanism which forms MSA i.e. the benzilic acid type rearrangement, in a comparable way to the formation of ISA. Machell and Richards<sup>130</sup> isolated the intermediate precursor for the generation of MSA, known as 3-deoxy-D-glucosone<sup>130</sup> by degrading 3-O-benzyl-D-glucose in solutions of sodium hydroxide and it was determined that when the intermediate was degraded with either sodium hydroxide (0.05 M) or saturated calcium hydroxide solution an almost quantitative yield of MSA was achieved, however, the formation was faster in lime water indicating the catalytic effect of  $\text{Ca}(\text{OH})_2$  on the benzilic acid type rearrangement (see Figure 54 for scheme). Colbran and Davidson<sup>181</sup>, also compared the effect that NaOH and  $\text{Ca}(\text{OH})_2$  had on the weight loss of cellulose when comparable reaction conditions were used; they determined that a greater weight loss was observed when NaOH was used. When  $\text{Ca}(\text{OH})_2$  was used as the base there was an increase in the carboxyl content in the remaining unreacted cellulose fibres which was attributed to the formation of alkali stable end-groups, indicating that more MSA was being produced in the  $\text{Ca}(\text{OH})_2$  reaction.

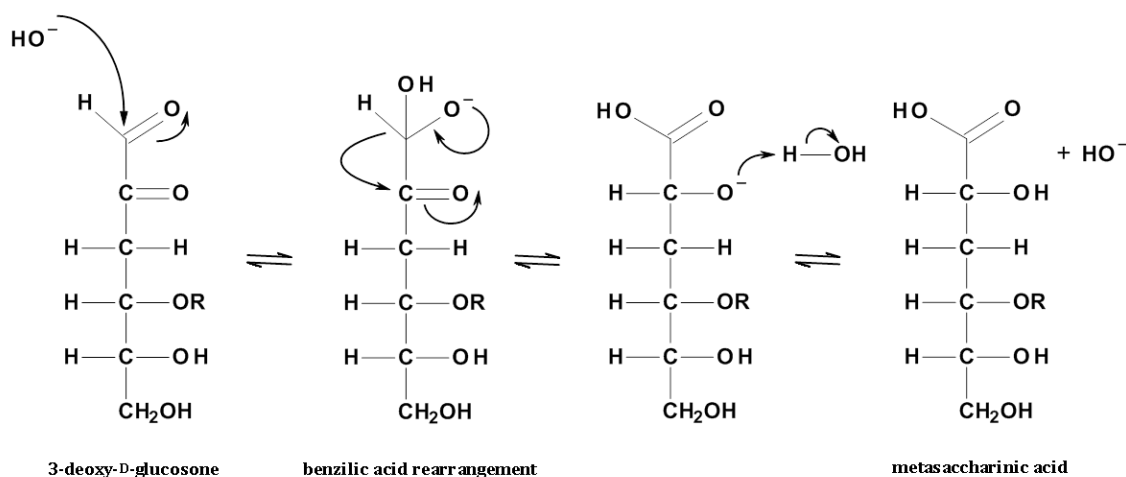


Figure 54: The base catalysed formation of MSA from the 3-deoxy-D-glucosone intermediate, R = the cellulose chain

It is known that the majority of MSA remains attached to the cellulose polymer as alkali-stable end-groups (chemical stopping), however, small amounts of MSA were reported as being present in cellulose degradation solutions in the work of Alfredsson and Samuelson<sup>129</sup>. It can be seen in the chromatogram which is presented in Figure 53 that the amount of MSA produced is small in comparison to the amount of ISA produced and there are several possible mechanisms which could account for this small amount of free MSA. One such mechanism involves the reducing end of a cellulose fibre being completely depolymerised, resulting in the removal of all of the AGUs until only the terminal AGU remains at the non-reducing end of the cellulose chain, which would then be released into the degradation solution; under alkaline conditions it is known that glucose is converted into MSA<sup>93, 103</sup> (amongst other products including ISA and lactic acid)<sup>193</sup>. Indeed, a published method by Diehl and Fletcher<sup>194</sup>, for the preparation of crude MSA involved the degradation of glucose using solid calcium hydroxide. Furthermore, Yang and Montgomery have identified MSA as being one of a complex mixture of products produced from the degradation of glucose when calcium hydroxide solution was used as the alkaline species. It is unlikely, however, that large amounts of glucose would be released in this way due to the onset of both physical and chemical stopping reactions retarding the complete peeling of the cellulose chain. A second possible mechanism could occur via the alkaline hydrolysis of glycosidic linkages either at the non-reducing end of the cellulose chain, releasing the terminal glucose monomer, which could further react and produce MSA as previously discussed; alternatively, hydrolysis at a chain end which has been made stable to alkali due

to the formation of a MSA end group (chemical stopping) would directly release MSA into the solution (Figure 55). However, as previously discussed, at the reaction temperatures applied in the present work, alkaline hydrolysis is thought to be a very insignificant process 93, 135

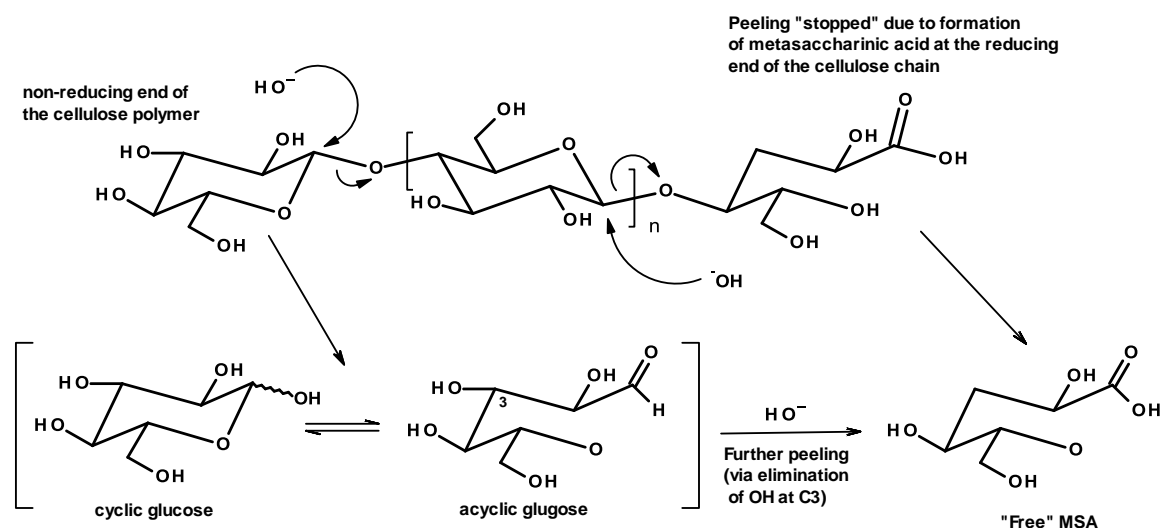


Figure 55: Possible methods for the release of MSA into solution: via alkaline hydrolysis at the non-reducing end of the cellulose chain (top, left), resulting in the release of a glucose monomer which can react with base to produce MSA, or hydrolysis at the glycosidic linkage of an alkali stable end-group (top, right), directly releasing MSA into solution.

It is also possible that some of MSA could be produced during the peeling reaction itself, in competition with the other, more favourable mechanistic pathways. One such pathway for the production of free MSA from either 4-*O*-methylglucose or cellobiose was published by MacLeod and Schroeder<sup>193</sup>. Both of those compounds are 1,4-linked glucose derivatives, therefore, it is likely that cellulose would also produce free MSA in the same way. In the proposed mechanism, published by MacLeod and Schroeder<sup>193</sup>, but replacing 4-*O*-methylglucose or cellobiose with cellulose (Figure 56), the same initial steps (I – IV) as those which were described for the stopping reaction in Figure 19 are followed resulting in the elimination of the hydroxide group which is attached to carbon 3 and the formation of the 3-deoxy-D-glucosone intermediate (which remains attached to the cellulose chain). However, in this alternative pathway, hydroxide ion then removes an alpha hydrogen at C3 as opposed to attacking the carbonyl group at C1 (in the stopping reaction), resulting in the migration of the double bond down the carbon chain and the  $\beta$ -elimination of the remainder

of the cellulose chain at C4 (V) and the formation of a diketone intermediate (3,4-dideoxy-D-hex-3-enosulose) (VI). Nucleophilic conjugate addition of hydroxide at C4 (VI) is facilitated due to the conjugated vinyl ketone structure to re-produce the 3-deoxy-D-glucosone intermediate which is now unattached to the cellulose chain. The benzilic acid type rearrangement (IX) can then occur to yield MSA, however, the MSA is now free in solution.

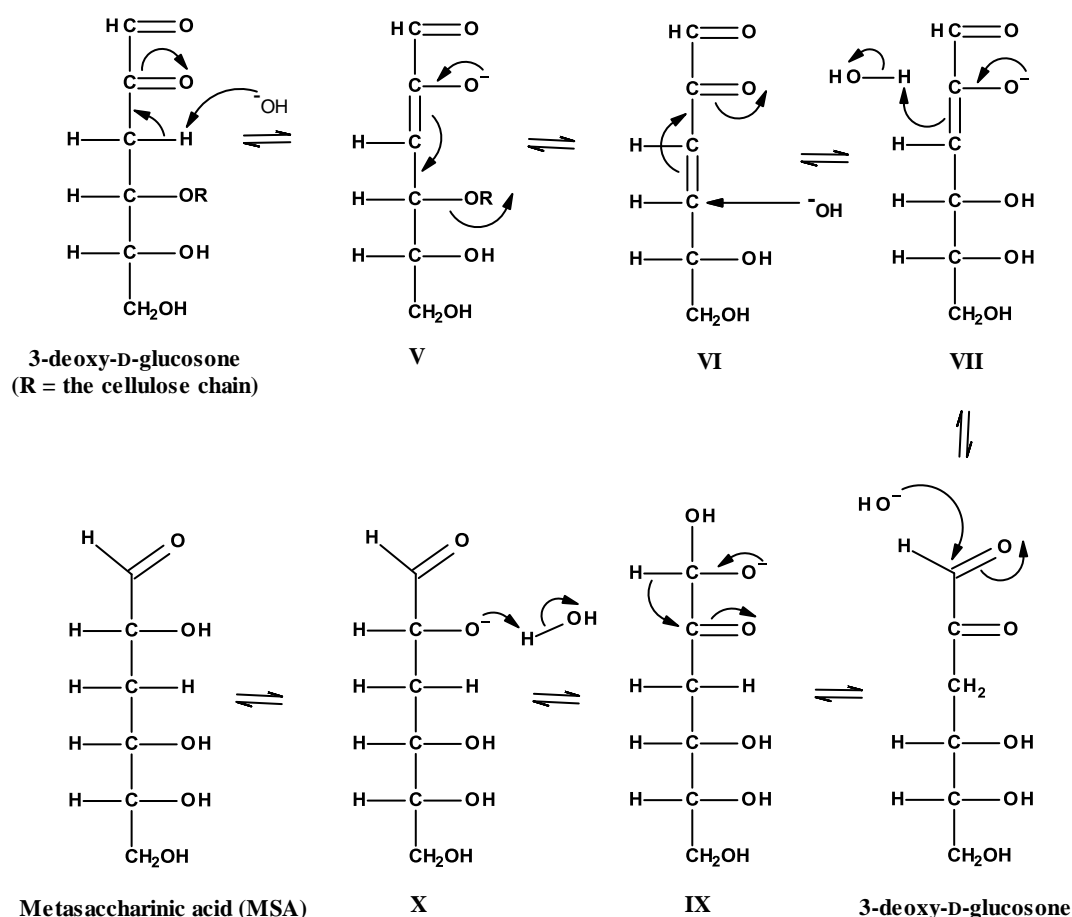


Figure 56: Mechanism to account for the production of free MSA during the peeling reaction <sup>193</sup>

The chemical stopping reaction, and hence the production of MSA is enhanced at higher temperatures because the activation energy of the chemical stopping reaction is greater than the activation energy required for the peeling reaction <sup>127</sup>. This was evident in the present work: the combined MSA peaks were plotted as a function of time, and to gain an estimation of the concentration of MSA produced at each reaction temperature, the pure  $\alpha$ -

ISAH sample, as described in section 3.2.2 was used for quantification. The  $\alpha$ -ISAH was used because no standard sample of MSA was available at the time of analysis and allowed an estimate of the concentration of MSA to be determined. The production of MSA in ppm as a function of time is shown in Figure 57, and the time course follows a similar profile to the production of ISA which was generated during the same  $\text{Ca}(\text{OH})_2$  reactions, (which will be discussed in section 3.5.2), which suggests that the majority of the free MSA was produced during the peeling reaction itself (Figure 56, above), i.e. an initial rapid production of free MSA, related to the availability of reducing end groups on the cellulose chains, followed by a much slower production due to the combined effect of chemical and physical stopping reactions (Figure 57), although the observed concentrations of MSA were much smaller than the concentrations of ISA produced, indicating that the production of MSA due to peeling is only of minor importance. For the RT reaction there was a slow, continual increase in the MSA concentration for the duration of the reaction and after 35 days a maximum concentration of  $\sim 0.2 \text{ g L}^{-1}$  was achieved; for the  $50 \text{ }^\circ\text{C}$  reaction, there was an initial fast production of MSA which reached a maximum concentration of  $\sim 0.5 \text{ g L}^{-1}$  after four days, and then the MSA concentration appears to slowly increase for the remainder of the reaction; finally, for the  $90 \text{ }^\circ\text{C}$  reaction, there was also an initial rapid production of MSA, followed by a much slower production (Figure 57); however, in the  $90 \text{ }^\circ\text{C}$  reaction, the solution concentration of MSA reached a maximum of approximately  $0.7 \text{ g L}^{-1}$  after ten days but then gradually began to fall; a similar observation was witnessed for the production of ISA in the same  $\text{Ca}(\text{OH})_2$  reactions, at the same temperature, and this will be discussed in section 3.5.2.

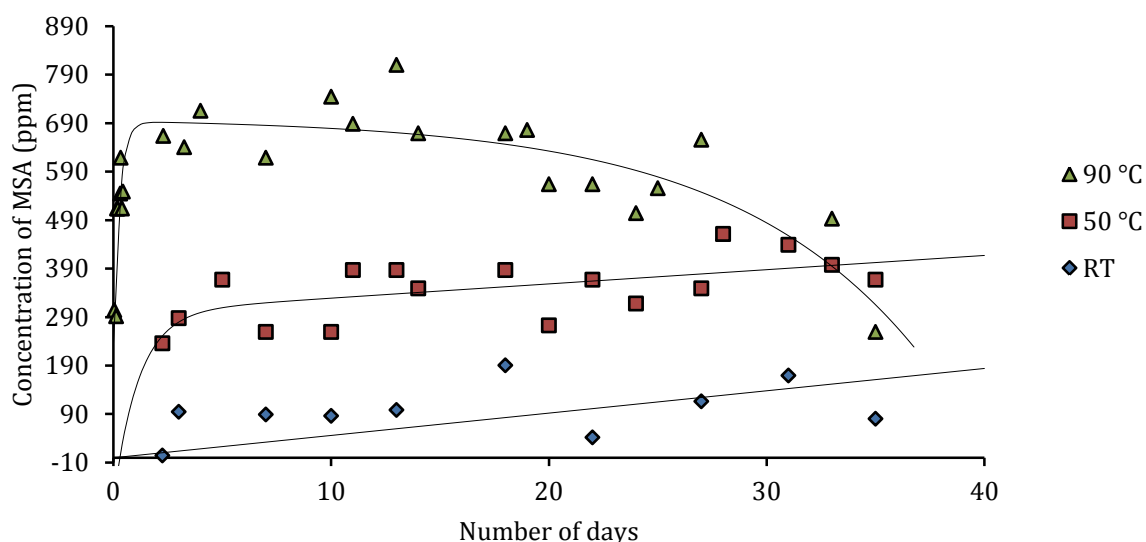


Figure 57: Time course for the production of MSA (ppm) for the calcium hydroxide catalysed degradation of cellulose at RT, 50 °C and 90 °C (lines are a guide for the eye only).

### 3.5.2 Monitoring the production of $\alpha$ -ISA and $\beta$ -ISA using HPAEC-PAD due to the $\text{Ca}(\text{OH})_2$ catalysed hydrolysis of cellulose

As with the NaOH reactions which were described in section 3.4 (and for the quantification of MSA, above), the pure  $\alpha$ -ISAH sample was used to quantify both  $\alpha$ - and  $\beta$ -ISA which was produced from the degradation of cellulose using saturated  $\text{Ca}(\text{OH})_2$  solution. The production of  $\beta$ -ISA and  $\alpha$ -ISA in ppm as a function of time are shown in Figure 58 and Figure 59. For the RT and 50 °C reactions, the time courses for the production of ISA follow similar trends to those produced in the NaOH reactions but with  $\alpha$ - and  $\beta$ -ISA being generated in equal quantities. The most striking difference between the results of the NaOH and  $\text{Ca}(\text{OH})_2$  reactions were those produced from the 90 °C reaction; with the concentration of both  $\alpha$ - and  $\beta$ -ISA initially increasing and then decreasing.

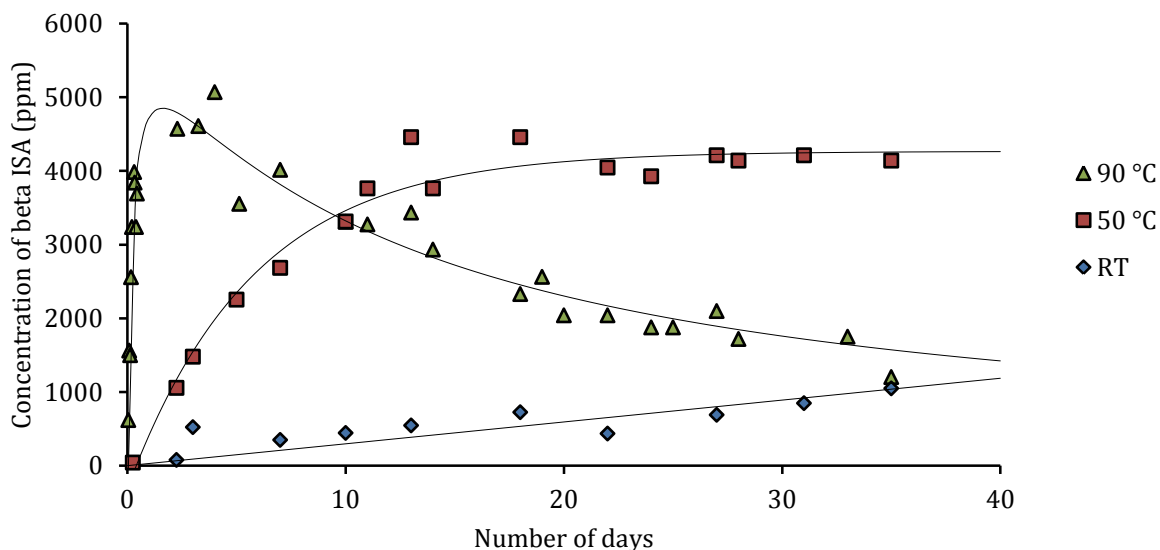


Figure 58: Time course for the production of  $\beta$ -ISA (ppm) for the calcium hydroxide catalysed degradation of cellulose at RT, 50 °C and 90 °C (lines are a guide for the eye only).

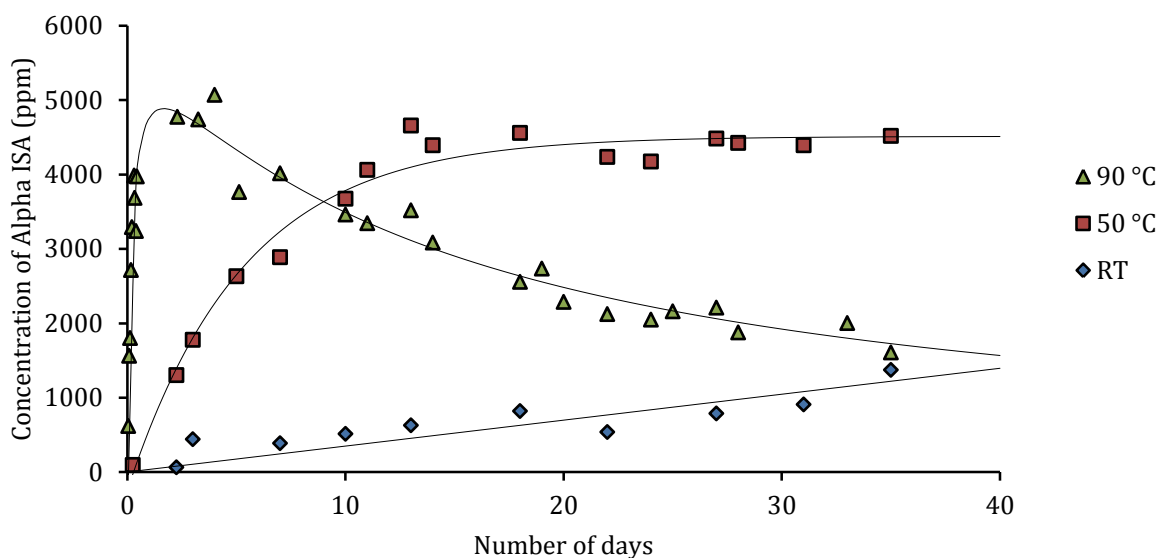


Figure 59: Time course for the production of  $\alpha$ -ISA (ppm) for the calcium hydroxide catalysed degradation of cellulose at RT, 50 °C and 90 °C (lines are a guide for the eye only).

Analogous to the NaOH reaction, the production of ISA at RT continued for the duration of the reaction and following the termination of the reaction after 35 days, the final solution

concentration of  $\alpha$ -ISA was  $1.4 \text{ g L}^{-1}$  (56 %) and the final concentration of  $\beta$ -ISA was  $1.1 \text{ g L}^{-1}$  (44 %). These results indicate that the concentration of  $\beta$ -ISA produced using  $\text{Ca}(\text{OH})_2$  was slightly less than the  $\beta$ -ISA produced in the NaOH reaction ( $1.2 \text{ g L}^{-1}$ ) but the total ISA produced in the  $\text{Ca}(\text{OH})_2$  reactions ( $2.5 \text{ g L}^{-1}$ ) was greater than the total amount of ISA produced in the equivalent NaOH reactions ( $1.6 \text{ g L}^{-1}$ ). The solubility of  $\text{Ca}(\text{OH})_2$  at RT is approximately  $1.56 \text{ g L}^{-1}$ <sup>195</sup> so at RT, the pH of the  $\text{Ca}(\text{OH})_2$  reaction solution could not be more than 12.6, so the initial rate of cellulose degradation will be faster in the NaOH reaction. However, as previously discussed, a greater percentage of cellulose is converted into ISA when  $\text{Ca}(\text{OH})_2$  is used as the base due to  $\text{Ca}^{2+}$  ions catalysing the benzylic acid type rearrangement, and this may account for greater amounts of ISA being produced at this reaction temperature when  $\text{Ca}(\text{OH})_2$  is used as base.

In the  $50 \text{ }^\circ\text{C}$   $\text{Ca}(\text{OH})_2$  reaction, the results indicate that the initial fast stage of peeling lasts for approximately 13 days compared to approximately 7 days in the equivalent NaOH reaction, again indicating that the higher pH of the NaOH reaction promotes a faster initial rate of peeling. In the  $\text{Ca}(\text{OH})_2$  reaction, after 35 days the concentration of  $\alpha$ - and  $\beta$ -ISA was  $4.5 \text{ g L}^{-1}$  and  $4.1 \text{ g L}^{-1}$  respectively, giving a total ISA concentration of  $8.6 \text{ g L}^{-1}$ . For the NaOH reaction, the total ISA concentration was similar, at  $9.5 \text{ g L}^{-1}$  but much greater concentrations of  $\beta$ -ISA were produced for the NaOH reaction ( $7.2 \text{ g L}^{-1}$ ) due to the preference of the production of  $\beta$ -ISA when NaOH is used as the base. The production of ISA appears to have stopped after 13 days in the  $\text{Ca}(\text{OH})_2$  reaction whereas in the  $50 \text{ }^\circ\text{C}$  NaOH reaction the production of ISA appears to continue at a slower rate indicative of secondary peeling. A second phase of peeling in the  $\text{Ca}(\text{OH})_2$  reaction may also be occurring but at an even slower rate due to the lower pH of the  $\text{Ca}(\text{OH})_2$  reaction, longer time periods may be required to witness any further degradation. Also, as previously discussed, the chemical stopping reaction is enhanced when  $\text{Ca}(\text{OH})_2$  is used as the base, so it may be possible that degradation has stopped due to a predominance of physical and chemical stopping reactions in the  $50 \text{ }^\circ\text{C}$  reaction. Furthermore, it is possible that the further slow phase of ISA production observed in the NaOH reaction may be a result of the 2 M NaOH solution allowing a limited swelling of the cellulose fibres to occur, which may allow additional further degradation to slowly proceed, at the lower pH of the  $\text{Ca}(\text{OH})_2$  reaction solution swelling of cellulose fibres will not occur.

Unlike the RT and  $50 \text{ }^\circ\text{C}$  results, the time course for production of  $\alpha$ - and  $\beta$ -ISA at  $90 \text{ }^\circ\text{C}$  for the NaOH and  $\text{Ca}(\text{OH})_2$  reactions are different. In the NaOH reaction there was an

initial rapid rate of ISA production during the first 24 h, following this, the rate of ISA production began to slow down. With the 90 °C  $\text{Ca}(\text{OH})_2$  reaction there was also an initial rapid production of ISA in the first 24 h and then the amount of ISA fell. A maximum concentration of 5.1 g L<sup>-1</sup> for  $\alpha$ -ISA and 5.1 g L<sup>-1</sup> of  $\beta$ -ISA was achieved after 4 days of reaction. This maximum concentration was similar to those achieved for the 50 °C  $\text{Ca}(\text{OH})_2$  reaction indicating that, under the present reaction conditions, approximately 5 g L<sup>-1</sup> is the maximum solution concentration of  $\alpha/\beta$ -ISA that can be achieved regardless of reaction temperature before stopping reactions slow down or stop further cellulose degradation. In comparison, the 90 °C NaOH reaction produced 3.1 g L<sup>-1</sup> of  $\alpha$ -ISA and 9.4 g L<sup>-1</sup> of  $\beta$ -ISA after 4 days of reaction, resulting in a total ISA concentration of ~ 12.5 g L<sup>-1</sup>, which was greater than the total ISA produced for the  $\text{Ca}(\text{OH})_2$  reaction (~ 10.2 g L<sup>-1</sup>). This can be explained due to the known preference of the chemical stopping reaction in  $\text{Ca}(\text{OH})_2$  catalysed cellulose degradation reactions, and as previously discussed, greater maximum concentrations of ISA may be achieved in the NaOH reactions due to the possibility that the onset of swelling may be occurring at the higher pH.

The major difference between the two sets of results however, was that for the  $\text{Ca}(\text{OH})_2$  reaction, for both  $\alpha$ - and  $\beta$ -ISA, after the maximum concentration was achieved, it then began to fall to levels similar to the final concentrations produced in the RT reaction. A similar observation was witnessed in the results of Glaus and Van Loon<sup>109</sup> when they also degraded cellulose at 90 °C using  $\text{Ca}(\text{OH})_2$  and they assumed that the loss of ISA was due to the occurrence of an unknown fragmentation of ISA which they related to the presence of  $\text{Ca}(\text{OH})_2$  in their reactions. It was also hypothesised by Pavasars *et al.*<sup>123</sup>, after they performed similar degradation reactions, that it may be possible that ISA could degrade in solution faster than it was being produced during long term reactions at ambient temperatures. However, this is unlikely because it was reported by Whistler and BeMiller<sup>148</sup> that ISA is relatively stable at temperatures of up to 125 °C under alkaline conditions. Glaus and Van Loon<sup>114</sup> studied the effect of solid  $\text{Ca}(\text{OH})_2$  on the disappearance of ISA from cellulose degradation reactions by treating  $\alpha$ -ISA with excess  $\text{Ca}(\text{OH})_2$  under various reaction conditions. They determined that the major cause for the loss of ISA from solution was the chemical transformation into glycolic, formic and lactic acid by unknown mechanisms. It was determined that under anaerobic conditions, approximately 1  $\mu\text{mol}$  of  $\alpha$ -ISA is transformed into smaller fragmentation products per gram of solid  $\text{Ca}(\text{OH})_2$  present in reaction vessels. In the present work, 30 g of solid  $\text{Ca}(\text{OH})_2$  were added to the 90 °C degradation reaction and because the solubility of  $\text{Ca}(\text{OH})_2$  at 90 °C is only 0.81 g L<sup>-1</sup>,

the vast majority of the added  $\text{Ca(OH)}_2$  will have been present as solid. In a worst case scenario, according to the results of Glaus and Van Loon, if all of the solid  $\text{Ca(OH)}_2$  was available to react with ISA, a total of 30  $\mu\text{mol}$  of ISA could be transformed into fragmentation products, a minor amount compared to the 10.2  $\text{g L}^{-1}$  of ISA produced in the 90 °C  $\text{Ca(OH)}_2$  degradation reaction. It was determined by Glaus and Van Loon<sup>114</sup> that any additional ISA above 30  $\mu\text{mol}$  was stable to degradation for periods of several months. When the experiments of Glaus and Van Loon were repeated under aerobic conditions, they determined that ISA was converted quantitatively to smaller fragmentation products, suggesting that the fragmentation reaction is an oxidative process with stoichiometric amounts of an oxidant being required for complete reaction, therefore it can be expected that in the present work slightly higher amounts of the transformation of ISA into smaller organic acids may occur due to the fact that the reactions described here were not performed under glove box conditions.

Another reason for the loss of ISA could be sorption onto solid phases which are present in the reaction system; various studies have determined that ISA sorbs significantly on to cement based materials<sup>94, 115, 124, 196</sup>, however, in several studies, Glaus and Van Loon have determined that the loss of ISA due to sorption onto solid  $\text{Ca(OH)}_2$  was of minor importance, and was of lesser significance than the loss of ISA due to chemical transformation<sup>94, 109, 114</sup>.

### **3.5.3 Monitoring the production of total organic carbon from the $\text{Ca(OH)}_2$ reactions**

To further understand why the concentrations of  $\alpha$ - and  $\beta$ -ISA reached a maximum and then fell in the 90 °C  $\text{Ca(OH)}_2$  reaction, the samples produced from all 3 temperature  $\text{Ca(OH)}_2$  reactions were analysed for their TOC content, using the conditions described in section 2.3.7. Analysis of the TOC would allow any fragmentation products that were not detected by HPAEC-PAD to be quantified. The production of TOC, in  $\text{mg L}^{-1}$  as a function of time, which was produced from the RT, 50 °C and 90 C ° reactions is presented in Figure 60.

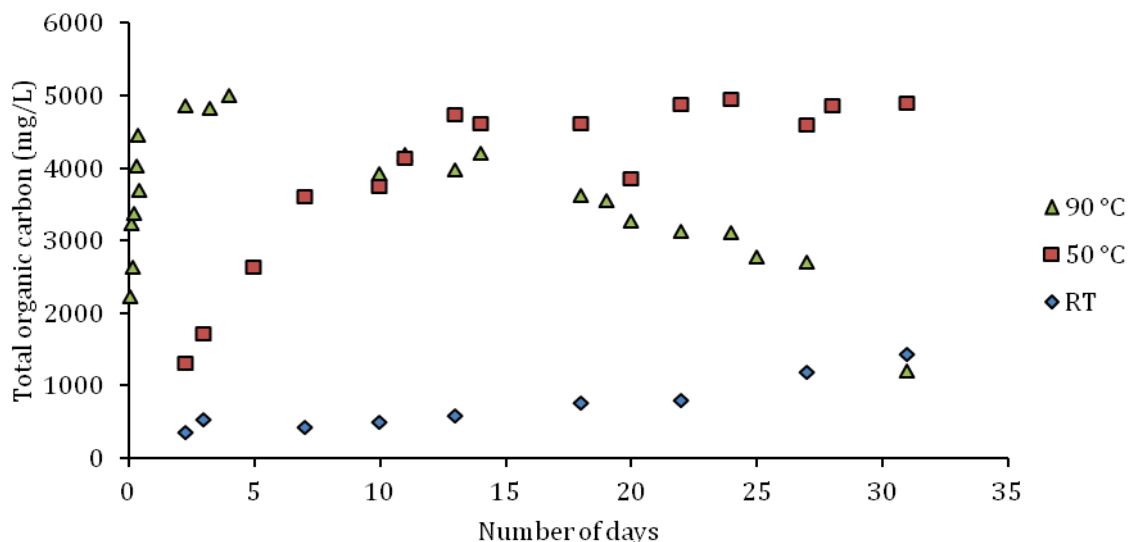


Figure 60: Time course for the production of TOC ( $\text{mg L}^{-1}$ ) produced from the calcium hydroxide catalysed degradation of cellulose at RT, 50 °C and 90 °C.

The results of the TOC experiments indicate that the maximum organic carbon content of the  $\text{Ca}(\text{OH})_2$  reactions was:  $5.0 \pm 0.10 \text{ g L}^{-1}$  for the 90 °C reaction, which was achieved after 4 days. For the 50 °C reaction a value of  $4.9 \pm 0.10 \text{ g L}^{-1}$  was measured and for the RT reaction a value of  $1.4 \pm 0.03 \text{ g L}^{-1}$  was measured. The TOC results indicate that the ISA produced in the RT and 50 °C reactions accounted for approximately 70 % of the TOC and the ISA produced in the 90 °C reaction accounted for approximately 82 % of the TOC. The results of the present study are in agreement with previously reported results<sup>110, 123</sup>, as it has been reported that ISA accounts for between 70 – 85 % of degradation products when  $\text{Ca}(\text{OH})_2$  is used as the alkaline species.

It was expected that if ISA was being converted into smaller organic acids, the concentration of TOC would remain relatively constant due to any new organic products contributing to the TOC. However, the time courses for the HPAEC-PAD (Figure 58 and Figure 59) and TOC (Figure 60) follow very similar trends indicating that no appreciable amount of ISA were being transformed into smaller organic compounds; unless the formed products were being removed from the bulk solution. The drop in ISA concentration was only witnessed in the 90 °C reaction and not in the 50 °C or RT reactions; therefore, it is possible that some of the volatile fragmentation products, which may have been formed due the oxidation of the ISA, may have escaped from the reaction vessel as vapour through the

open topped condenser. This would be more likely in the 90 °C reaction as opposed to the 50 °C and RT reactions due to the higher temperature and would account for the drop in both TOC and ISA concentrations. Another possible reason for the drop in ISA concentration could be due sorption processes of either ISA and/or fragmentation products onto unreacted solid materials which may be present in the reaction vessel: either solid calcium hydroxide or unreacted cellulose fibres. It is possible that these sorption processes would be more evident in the highest temperature reaction, which would account for greater losses of ISA from bulk solutions.

### **3.6 Degradation of cellulose using either $\text{Ca}(\text{OH})_2$ , NaOH or a mixture of $\text{Ca}(\text{OH})_2$ and NaOH at 90 °C**

To investigate why the concentrations of  $\alpha$ - and  $\beta$ -ISA reached a maximum and then fell in the 90 °C  $\text{Ca}(\text{OH})_2$  reaction, 3 additional experiments were performed, as described in section 2.3.3. The first additional experiment was a repeat of the 90 °C  $\text{Ca}(\text{OH})_2$  reaction which was carried out to judge the repeatability of that experiment. The second additional experiment was a repeat of the 90 ° NaOH experiment, the reason for this was to determine if residual oxygen in the 90 °C  $\text{Ca}(\text{OH})_2$  reaction may have resulted in the observed loss of ISA concentration, as similar anaerobic environments are expected to be present in both the NaOH and  $\text{Ca}(\text{OH})_2$  reaction systems. A third additional reaction was performed, with the only difference to the previous two reactions being that the cellulose was degraded in a mixture of NaOH and  $\text{Ca}(\text{OH})_2$ , this reaction was performed to increase the pH of the  $\text{Ca}(\text{OH})_2$  reaction. Each reaction was sampled periodically and the samples were analysed by HPAEC-PAD and for their TOC content using the conditions described previously. It is also worth noting that any losses of material due to evaporation from the reaction systems are expected to be negligible as any condensate produced was returned to the reaction vessel due to condenser glassware being attached to each vessel; if any evaporation did occur, it is expected that losses would be similar for all three experiments.

#### **3.6.1 Monitoring the production of $\alpha$ -ISA and $\beta$ -ISA using HPAEC-PAD and the determination of the TOC**

The production of  $\beta$ -ISA and  $\alpha$ -ISA in ppm as a function of time for the additional  $\text{Ca}(\text{OH})_2$ , NaOH and mixed  $\text{Ca}(\text{OH})_2$ /NaOH reactions are presented in Figure 61 and Figure 62. The  $\text{Ca}(\text{OH})_2$  results were very similar to those obtained in the initial 90 °C

$\text{Ca}(\text{OH})_2$  reaction: there being a maximum concentration of approximately  $5 \text{ g L}^{-1}$  of  $\alpha$ - and  $\beta$ -ISA being achieved after 4 days of reaction, which then began to fall for the remainder of the reaction. The reproducibility of the results indicate that the results produced in the initial  $90^\circ\text{C}$   $\text{Ca}(\text{OH})_2$  experiment were reliable.

The repeated  $90^\circ\text{C}$   $\text{NaOH}$  reaction also produced similar results to the initial  $90^\circ\text{C}$   $\text{NaOH}$  reaction which was discussed in section 3.4, with no indication of a fall in ISA concentration being observed for the duration of the reaction. This indicates that low levels of oxygen in the reaction system are not the reason why the ISA concentration fell in the  $90^\circ\text{C}$   $\text{Ca}(\text{OH})_2$  reaction (unless fragmentation via oxidation is catalysed by  $\text{Ca}(\text{OH})_2$ ); the method to maintain anaerobic conditions was the same in both reactions, with a constant stream of nitrogen being applied to both reaction vessels. The results suggest that it is very unlikely that losses of ISA are due to evaporation of volatile fragmentation products through the condenser funnel, as no similar losses were witnessed in the  $\text{NaOH}$  reaction which was performed under identical conditions. The results suggest that the presence of  $\text{Ca}(\text{OH})_2$  in the reaction system is related to the observed fall in ISA concentration.

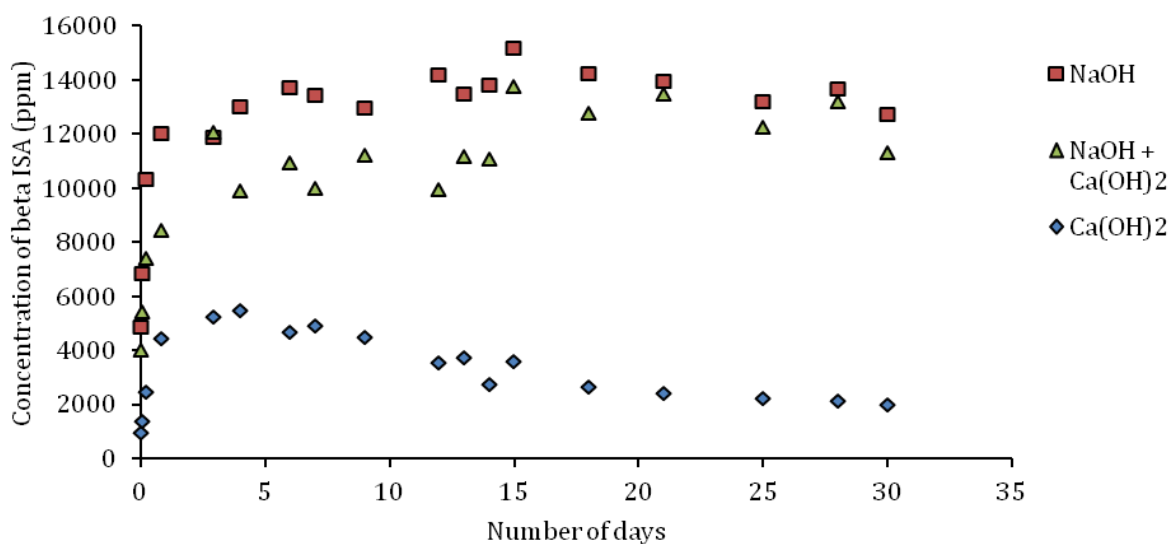


Figure 61: Time course for the production of  $\beta$ -ISA (ppm) generated from the degradation of cellulose at  $90^\circ\text{C}$  using either saturated  $\text{Ca}(\text{OH})_2$  soln.,  $\text{NaOH}$  (2 M) or using both saturated  $\text{Ca}(\text{OH})_2$  soln. and  $\text{NaOH}$  (2 M).

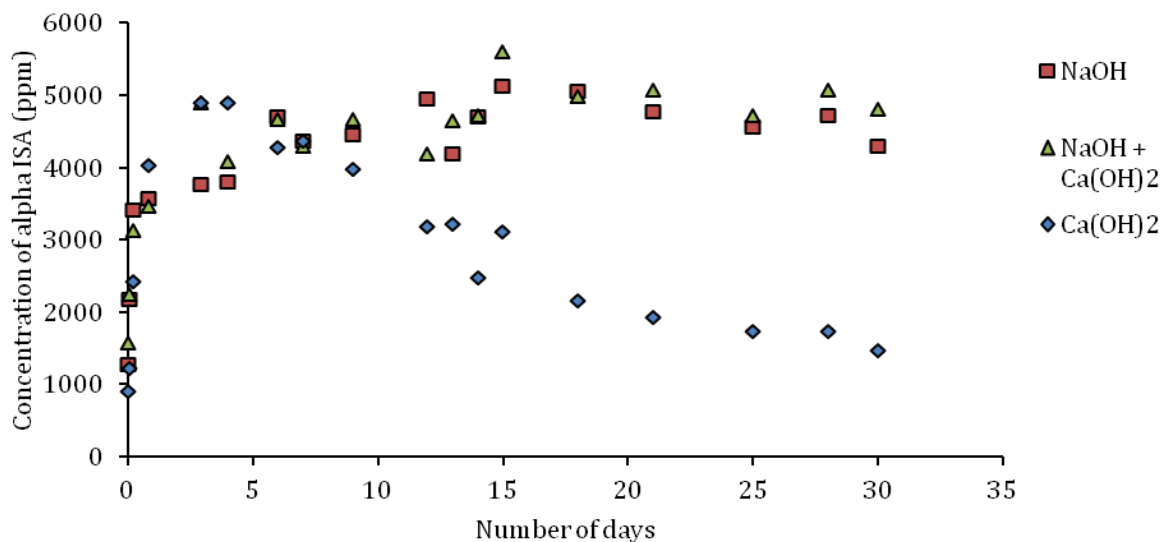


Figure 62: Time course for the production of  $\alpha$ -ISA (ppm) generated from the degradation of cellulose at 90 °C using either saturated  $\text{Ca}(\text{OH})_2$  soln., NaOH (2 M) or using both saturated  $\text{Ca}(\text{OH})_2$  soln. and NaOH (2 M).

The concentration versus time profile for the ISA produced in the mixed  $\text{Ca}(\text{OH})_2/\text{NaOH}$  reaction is interesting because for both  $\alpha$ - and  $\beta$ -ISA their production follows a similar pattern to that of the ISA produced in the NaOH reaction. The rate of production of  $\alpha$ -ISA is very similar for both reaction systems, whereas the initial rate of  $\beta$ -ISA production appears to be slightly less in the mixed alkaline system. That was probably because  $\text{Ca}^{2+}$  ions are present in that system, and as previously discussed,  $\text{Ca}^{2+}$  ions promote the production of equal quantities of  $\alpha$ - and  $\beta$ -ISA whereas  $\text{Na}^+$  ions favour the production of  $\beta$ -ISA resulting in a slower production of  $\beta$ -ISA in comparison to the 90 °C reaction where only NaOH is present. The final concentration of both  $\alpha$ - and  $\beta$ -ISA produced from both the NaOH and the  $\text{Ca}(\text{OH})_2/\text{NaOH}$  reactions was very similar; and the subsequent TOC analysis of the NaOH and  $\text{Ca}(\text{OH})_2/\text{NaOH}$  reactions (Figure 63) indicated more clearly, that the TOC produced and its rate of production was very similar from both reactions. The observed pH of all the samples produced from both the NaOH reaction and the mixed  $\text{Ca}(\text{OH})_2/\text{NaOH}$  reaction was  $\sim 14$ , whereas the average pH of the samples produced from the  $\text{Ca}(\text{OH})_2$  reaction was 12.6 indicating that, in those reactions, the base concentration and not the presence of solid  $\text{Ca}(\text{OH})_2$  in the reaction system dictates the solution concentration of ISA produced.

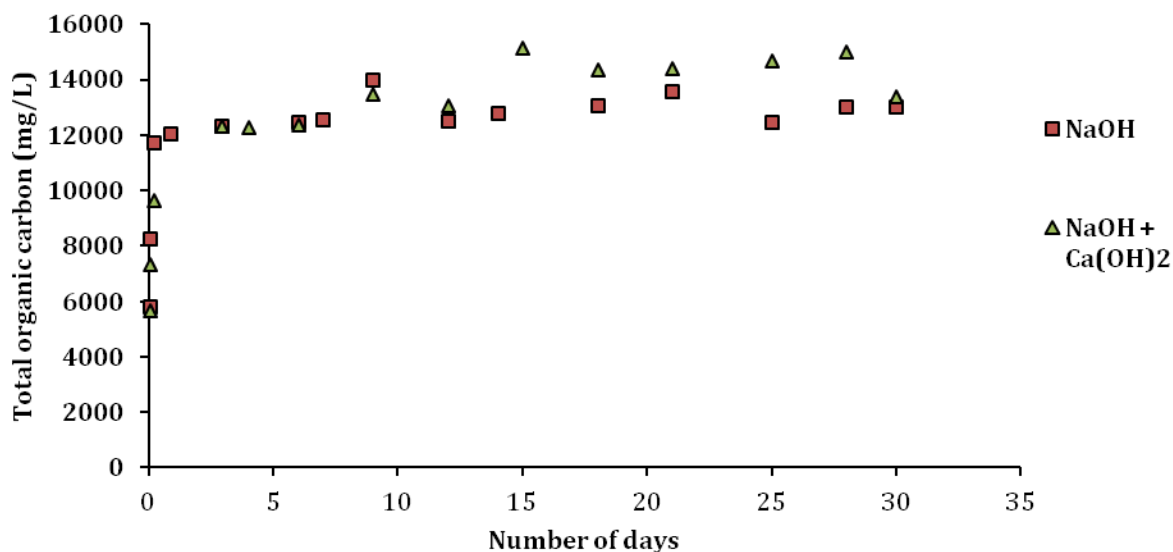


Figure 63: Time course for the production of TOC ( $\text{mg L}^{-1}$ ) produced from the degradation of cellulose at 90 °C using either NaOH (2 M) or using both saturated  $\text{Ca}(\text{OH})_2$  soln. and NaOH (2 M).

One of the most important results from this series of experiments was the observation that there was no obvious loss of ISA from the mixed  $\text{Ca}(\text{OH})_2/\text{NaOH}$  reaction due to sorption. This was unusual because the solubility of  $\text{Ca}(\text{OH})_2$  sharply decreases in the presence of NaOH due to the common ion effect of  $\text{HO}^-$ <sup>195</sup>. For example, Yuan<sup>195</sup> indicated that, at 76 °C, the solubility of calcium hydroxide reduced from  $0.9 \text{ g L}^{-1}$  to  $0.03 \text{ g L}^{-1}$  with the addition of 0.5 M NaOH solution. This suggests that there should be more undissolved solid  $\text{Ca}(\text{OH})_2$  able to act as an absorbent in the mixed  $\text{Ca}(\text{OH})_2/\text{NaOH}$  reaction than in the  $\text{Ca}(\text{OH})_2$  reaction and this is in agreement with the observed average mass of the unreacted solid which was present in the samples produced from the  $\text{Ca}(\text{OH})_2/\text{NaOH}$  reaction (3.4 g in 6 ml samples) being more than the average mass of the unreacted solid in the samples which were produced from the  $\text{Ca}(\text{OH})_2$  reaction (2.4 g in 6 ml samples). In comparison, the average mass of the unreacted solid which was observed in the samples produced from the NaOH reaction, which contained no  $\text{Ca}(\text{OH})_2$  was 1.3 g (in the 6 ml samples). The larger quantity of solid  $\text{Ca}(\text{OH})_2$  in the mixed  $\text{Ca}(\text{OH})_2/\text{NaOH}$  reaction in combination with the fact that there was no indication of any loss of ISA from that reaction suggests that sorption onto solid  $\text{Ca}(\text{OH})_2$  was not the reason for the observed loss of ISA from reaction solutions.

### 3.6.2 Extraction of unreacted solid produced in the cellulose degradation reactions

To further investigate if ISA or other CDPs were sorbing onto the unreacted solid materials, the solid which was present in the samples from the 90 °C  $\text{Ca}(\text{OH})_2$ , NaOH and mixed  $\text{Ca}(\text{OH})_2/\text{NaOH}$  reactions were extracted with a saturated solution of sodium hydrogen carbonate using the method which was described in section 2.3.4; sodium hydrogen carbonate has previously been used in a method reported by Glaus and Van Loon<sup>114</sup> for the extraction of ISA which was sorbed to hardened cement paste. The extracts were filtered and analysed by HPAEC-PAD using the conditions described in section 2.3.5 and their TOC content was determined using the conditions described in section 2.3.7.

#### 3.6.2.1 HPAEC-PAD analysis of extracted samples

The concentration of the extracted  $\alpha$ - and  $\beta$ -ISA in ppm as a function of time from the  $\text{Ca}(\text{OH})_2$  reaction is presented in Figure 64. The results show that following the extraction procedure, the 10 ml of extractant contained a maximum ISA concentration of  $3.5 \text{ g L}^{-1}$ , which consisted of  $\sim 1.8 \text{ g L}^{-1}$  of  $\alpha$ -ISA and  $\sim 1.8 \text{ g L}^{-1}$  of  $\beta$ -ISA, equating to  $\sim 7.4 \text{ mg}$  of  $\alpha$ -ISA and  $\sim 7.4 \text{ mg}$  of  $\beta$ -ISA per gram of unreacted solid material, in agreement with equal proportions of both isomers being produced when  $\text{Ca}(\text{OH})_2$  is used as the base in cellulose degradation reactions. Interestingly, the results indicate that the sorption process has no preference for the removal of the sparingly soluble  $\text{Ca-}\alpha(\text{ISA})_2$ , which has a reported solubility of approximately 0.2 M at pH 12<sup>197</sup> in comparison to the removal of  $\text{Ca-}\beta(\text{ISA})_2$  which is highly soluble in aqueous solutions<sup>148</sup>; however, the solubility of  $\text{Ca-}\alpha(\text{ISA})_2$  is known to increase above pH 12 due to the precipitation of  $\text{Ca}(\text{OH})_2$ <sup>197</sup> and may explain why equal amounts of both isomers were lost from solution due to sorption processes. Interestingly, the results of the extraction of the 90 °C NaOH samples (Figure 65) indicated that similar amounts of ISA were being recovered from the unreacted solid as to the amount of ISA recovered from the solids from the  $\text{Ca}(\text{OH})_2$  reaction, this being  $\sim 2.8 \text{ g L}^{-1}$  being present in the 10 ml of extractant, of which there was approximately 3 times more  $\beta$ -ISA ( $2.1 \text{ g L}^{-1}$ ) than  $\alpha$ -ISA ( $0.74 \text{ g L}^{-1}$ ) analogous to the observed 3 : 1 solution concentration of  $\beta$ - and  $\alpha$ -ISA. However, in the samples produced from the NaOH reaction, each sample contained less unreacted solid, therefore, the amount of solid ISA present per gram of unreacted solid was greater, this being approximately 22 mg (16 mg of  $\beta$ -ISA and 5.7 mg of  $\alpha$ -ISA) per gram of unreacted solid; and as there was no solid  $\text{Ca}(\text{OH})_2$  present in the NaOH

reactions, it can be assumed that in both the  $\text{Ca}(\text{OH})_2$  and  $\text{NaOH}$  reactions, the loss of ISA was primarily due to the sorption onto unreacted cellulose and not solid  $\text{Ca}(\text{OH})_2$ .

The concentration of the ISA observed from the extraction of solids from the mixed  $\text{Ca}(\text{OH})_2/\text{NaOH}$  reaction (Figure 66) was lower than the concentration of ISA observed for both the  $\text{NaOH}$  and the  $\text{Ca}(\text{OH})_2$  reactions. The maximum concentration of  $\alpha$ -ISA present in the 10 ml of extractant from the mixed reaction was  $0.25 \text{ g L}^{-1}$  (0.74 mg of  $\alpha$ -ISA per gram of unreacted solid) and the concentration of  $\beta$ -ISA was  $0.55 \text{ g L}^{-1}$  (1.6 mg of  $\beta$ -ISA per gram of unreacted solid). As previously discussed, it was expected that more solid  $\text{Ca}(\text{OH})_2$  should be present in the samples produced from the mixed  $\text{Ca}(\text{OH})_2/\text{NaOH}$  reaction, as the concentration of ISA sorbed to that solid was less than in the  $\text{NaOH}$  and  $\text{Ca}(\text{OH})_2$  reactions, this is further evidence that ISA was not sorbing to solid  $\text{Ca}(\text{OH})_2$ .

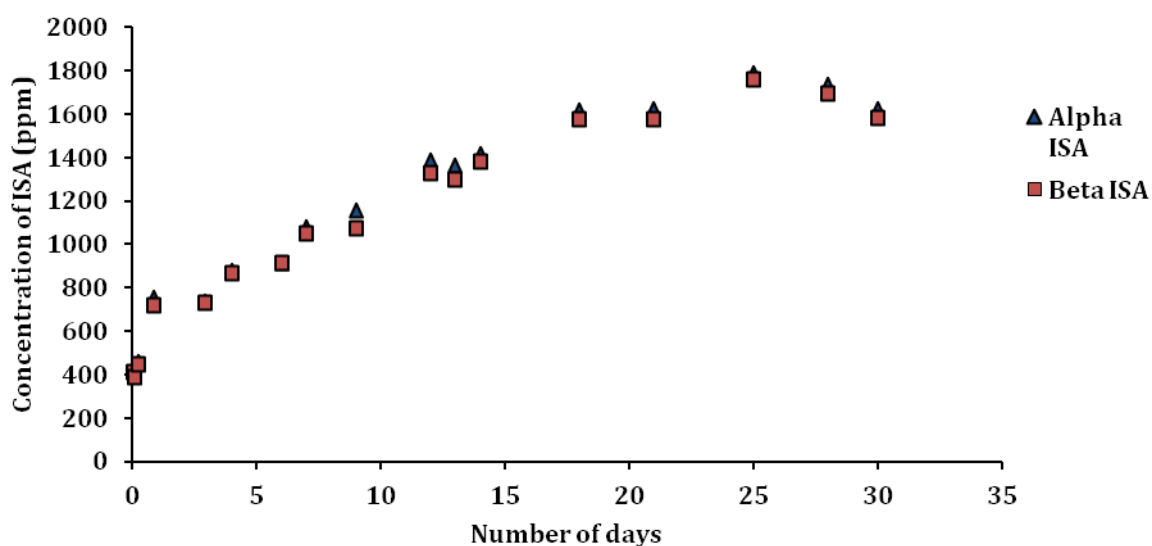


Figure 64: HPAEC-PAD generated time course for the concentration of ISA which was extracted from unreacted solid material present in samples produced from the  $\text{Ca}(\text{OH})_2$  catalysed degradation of cellulose at  $90^\circ\text{C}$ .

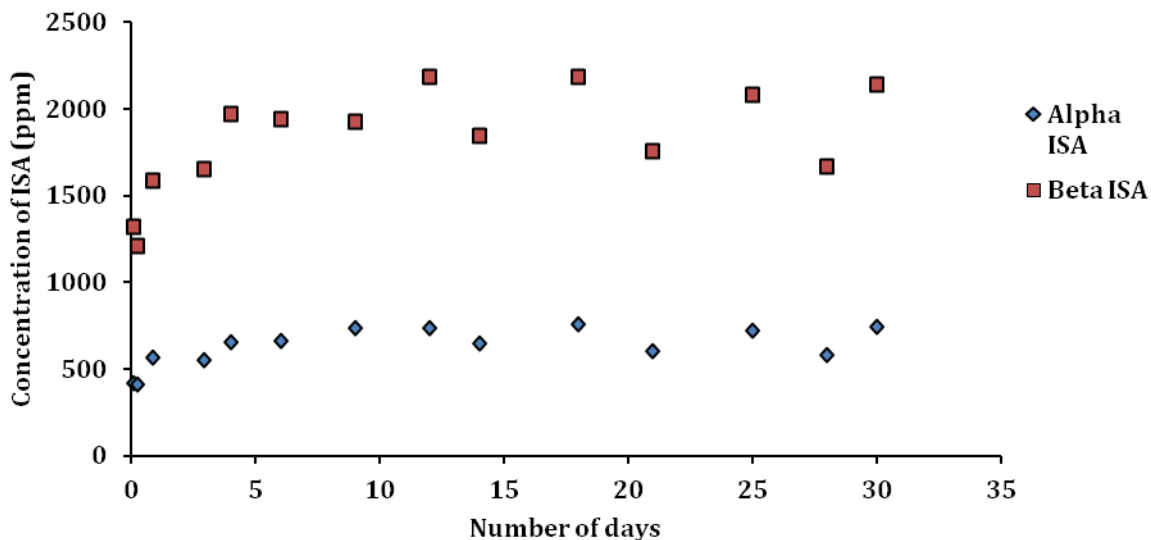


Figure 65: HPAEC-PAD generated time course for the concentration of ISA which was extracted from unreacted solid material present in samples produced from the NaOH catalysed degradation of cellulose at 90 °C.

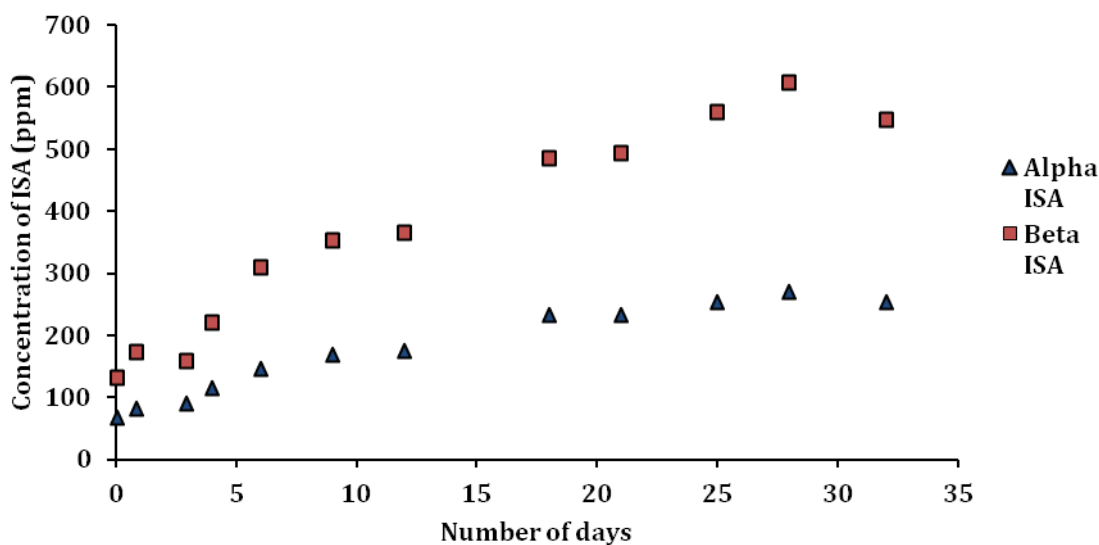


Figure 66: HPAEC-PAD generated time course for the concentration of ISA which was extracted from unreacted solid material present in samples produced from the mixed  $\text{Ca}(\text{OH})_2/\text{NaOH}$  catalysed degradation of cellulose at 90 °C.

The time courses for the extracted  $\beta$ -ISA (and also  $\alpha$ -ISA) from the unreacted solids produced from each degradation reaction ( $\text{Ca}(\text{OH})_2$ , NaOH or mixed hydroxides) were

plotted on the same graph so that comparisons could be made between the rate at which ISA was being removed from the solution in each of the degradation reactions (Figure 67).

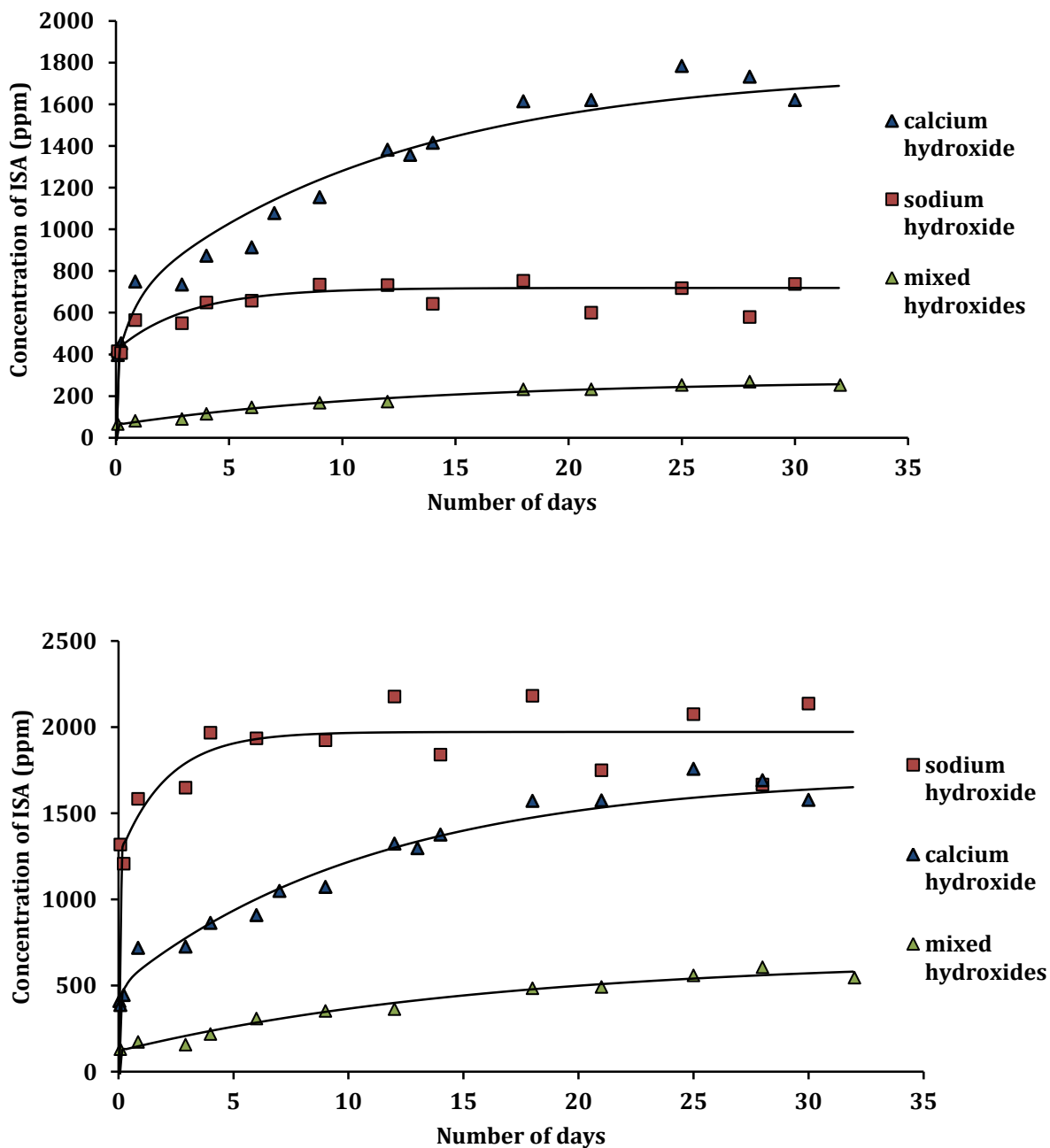


Figure 67: HPAEC-PAD generated time courses for the concentration of  $\beta$ -ISA (top) and  $\alpha$ -ISA (bottom) which was extracted from unreacted solid material present in samples produced from the  $\text{Ca}(\text{OH})_2$ ,  $\text{NaOH}$  or mixed  $\text{Ca}(\text{OH})_2/\text{NaOH}$  catalysed degradation of cellulose at  $90^\circ\text{C}$  (lines are a guide for the eye only).

The plots (in Figure 67) illustrate that it is possible that insoluble  $\text{Ca}(\text{OH})_2$  prevents, or reduces the rate that ISA is lost from reaction solutions. As previously discussed, cellulose can get trapped in insoluble  $\text{Ca}(\text{OH})_2$ <sup>123</sup> resulting in the trapped cellulose being inaccessible, or in this case being unable to take part in the removal of ISA due to sorption mechanisms. In the NaOH reaction no solid  $\text{Ca}(\text{OH})_2$  was present and as can be seen in Figure 65 and Figure 67, in comparison to the  $\text{Ca}(\text{OH})_2$  and mixed  $\text{Ca}(\text{OH})_2/\text{NaOH}$  reactions, the loss of ISA due to sorption occurs rapidly as indicated by a maximum concentration of recovered ISA being observed from the solid taken from the samples which were produced in the first few days of the degradation reaction, and following this only a negligible increase in recovered ISA concentration was observed. This indicates that when there is no solid  $\text{Ca}(\text{OH})_2$  in the reaction vessel, sorption occurs quickly and it appears that once the sorption capacity of the available cellulose is reached no further sorption can take place, as indicated by the levelling off of the concentration of the ISA in the extracts produced from the NaOH reaction. In the 90 °C NaOH reaction, because the loss of ISA due to sorption occurs quickly, before maximum ISA solution concentrations are reached, there was no obvious indication in the HPAEC-PAD time courses (Figure 61 and Figure 62) that any ISA was being removed from the solution phase. However, the opposite is true for the 90 °C  $\text{Ca}(\text{OH})_2$  reaction, where a fall in ISA concentration was observed for the duration of the reaction after the maximum concentrations of ISA were observed. The results of the extraction of the solid material from the samples from that reaction indicate that the sorption of ISA onto the unreacted solid occurs at a slower rate than in the 90 °C NaOH reaction (Figure 64 and Figure 67), as indicated by the concentration of ISA recovered from the solid increasing as a function of time, indicating that loss due to sorption was gradually occurring for the duration of that reaction. The time course for the production of ISA in the original 90 °C  $\text{Ca}(\text{OH})_2$  reaction (Figure 58 and Figure 59) indicated that the initial fast stage of ISA production was complete after approximately 4 days, and because no significant amounts of ISA was being produced after this time, and because the loss of ISA due to sorption was continuing for the duration of the reaction, a fall in ISA concentration was clearly evident in that reaction. This suggests that the presence of solid  $\text{Ca}(\text{OH})_2$  in the reaction system inhibits contact with the cellulose, which makes the loss of ISA due to sorption a much slower process. In the mixed  $\text{Ca}(\text{OH})_2/\text{NaOH}$  reaction the loss of ISA due to sorption was also a slow process and was ongoing for the duration of the reaction (Figure 66 and Figure 67). The additional solid  $\text{Ca}(\text{OH})_2$  in that reaction system, being greater than the amount of solid  $\text{Ca}(\text{OH})_2$  in the 90 °C  $\text{Ca}(\text{OH})_2$

reaction may account for the much lower amounts of ISA being lost due to sorption, a possible reason being that that the ISA cannot easily come into contact with the cellulose chains.

### 3.6.2.2 TOC analysis of extracted samples

The TOC ( $\text{mg L}^{-1}$ ) which was recovered from the extracted solid material produced from the  $90\text{ }^\circ\text{C}$   $\text{Ca}(\text{OH})_2$ , NaOH and mixed  $\text{Ca}(\text{OH})_2/\text{NaOH}$  reactions as a function of time is presented in Figure 68. The results indicate that the total amount of TOC lost due to sorption onto unreacted solids was quiet similar regardless of the solid  $\text{Ca}(\text{OH})_2$  content of the reaction, further suggesting that the loss of ISA and other CDPs is primarily due to sorption onto unreacted cellulose and not  $\text{Ca}(\text{OH})_2$ . The material constituting the TOC which was recovered from the unreacted solid after 30 days of reaction time was  $2.1\text{ g L}^{-1}$  for the  $\text{Ca}(\text{OH})_2$  reaction,  $2.4\text{ g L}^{-1}$  for the NaOH reaction and  $2.6\text{ g L}^{-1}$  for the mixed  $\text{Ca}(\text{OH})_2/\text{NaOH}$  reaction. The similar TOC contents further suggest that cellulose has a given sorption capacity, and when this is reached no further sorption can take place.

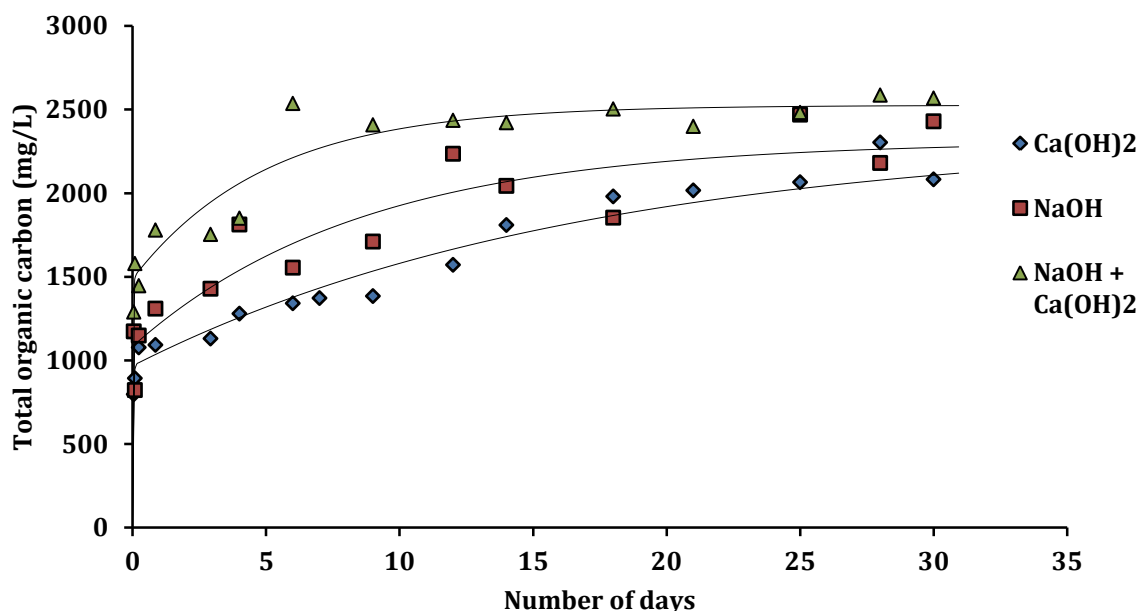


Figure 68: Time course for the production of TOC ( $\text{mg L}^{-1}$ ) from the extraction of unreacted solid material which was produced from the degradation of cellulose at  $90\text{ }^\circ\text{C}$  using either saturated  $\text{Ca}(\text{OH})_2$  soln., NaOH (2 M) or using both saturated  $\text{Ca}(\text{OH})_2$  soln. and NaOH (2 M) (lines are a guide for the eye only)

Now, the final TOC absorption again follows ISA (CDP) production with there being an initial rapid phase followed by a slower second phase of absorption, suggesting that a dynamic equilibrium between aqueous phase CDP components and solid phase. Interestingly, in the mixed  $\text{Ca}(\text{OH})_2/\text{NaOH}$  system, the amount of TOC observed after 5 days is greater than that observed in both the individual  $\text{NaOH}$  or  $\text{Ca}(\text{OH})_2$  reactions despite low levels of ISA being absorbed. This suggests that a lot of small acids are being produced and absorbed in the first day. This may suggest that solid calcium hydroxide catalyses the oxidation of some of the ISA that is produced in the first 24 h of reaction when residual oxygen levels are likely to be at their highest.

The final TOC content of the extracts from the solids from the mixed  $\text{Ca}(\text{OH})_2/\text{NaOH}$  reaction indicated that ISA accounted for only approximately 12 % of the TOC which was lost due to sorption, with the remainder assumed to be small organic acids. In comparison, for the extracts from the solid from the  $\text{Ca}(\text{OH})_2$  reaction, ISA accounted for approximately 61 % of the TOC and in the  $\text{NaOH}$  reaction ISA accounted for approximately 48 % of the extracted TOC. In the  $\text{NaOH}$  reaction, the percentage of ISA present in the TOC which was extracted from the unreacted solid material was very similar to the percentage of ISA present in the TOC in the original sample solutions ( $48 \pm 2$  % vs.  $52 \pm 2$  %). The similarities in those percentages, in conjunction with the rapid rate at which sorption occurred in the  $\text{NaOH}$  reaction suggests that the observed sorption was primarily a physical process. Cellulose fibres are reported to partially swell in 2 M  $\text{NaOH}$ <sup>198</sup> due to the hydrated alkali ions in aqueous systems penetrating into the cellulose fibres, also, the swelling stress inside the fibres can cause fibres to split into smaller microfibrils<sup>198</sup>, and as there was no large excess of solid  $\text{Ca}(\text{OH})_2$  present in the reaction mixture, this would allow the CDP solution to readily access the cellulose chains, allowing a portion of the CDP solution to become “soaked” up by the hydrated cellulose. Whereas, with the reaction where only  $\text{Ca}(\text{OH})_2$  was present, the percentage of ISA in the TOC of the extracts was much lower than the percentage of ISA in the TOC of the original sample solutions ( $\sim 61$  % vs.  $\sim 84$  %) which further suggests that solid  $\text{Ca}(\text{OH})_2$  in the reaction may prevent ISA sorbing onto the cellulose. The lower pH of the  $\text{Ca}(\text{OH})_2$  reaction will prevent swelling from occurring, which, in combination with the large excess of solid calcium hydroxide being present, could possibly prevent the reaction solution from significantly penetrating the crystalline cellulose fibres, making ISA sorption a slower process and preventing sorption from rapidly occurring in the same manner as which was observed in the  $\text{NaOH}$  reaction; however, for the smaller organic acids which are present in the solution, the cellulose fibres may be more

accessible, as indicated by the percentage of ISA in the extracts (~ 61 %) being lower than the percentage of ISA present in the bulk solutions (~ 84 %), however, the plot of the recovered combined TOC as a function of time (Figure 68) indicated that the sorption of both ISA and the other fragmentation products was a slow and gradual process, and this is probably as a result of the combination of the solid calcium hydroxide and the lack of swelling of the cellulose fibres slowing down the sorption process. In the  $\text{Ca}(\text{OH})_2$  reaction, it is also likely that other sorption processes are occurring. In basic pH environments, cellulose binds  $\text{Ca}^{2+}$  ions by a cation exchange mechanism<sup>198</sup>, indeed, cellulose has been used as an ion exchange material for the removal of calcium ions (and other cations) from wastewaters<sup>199</sup>. Although, cellulose is known to have little affinity for calcium ions in comparison to other heavier metal cations and complexation is not thought to occur with the hydroxyl groups of the cellulose<sup>200</sup> but with carboxylates generated by partial oxidation of cellulose; the uptake of calcium ions is limited by the carboxyl content of the cellulose; with an exchange occurring between accessible carboxylic hydrogens, exchanging with any available  $\text{Ca}^{2+}$  ions<sup>198, 201</sup>. Previous research has indicated that the molar ratio being one calcium ion to each available carboxylate group<sup>201, 202</sup>, resulting in a net positive charge of the cellulose, which will be neutralised by the binding of a negatively charged counter ion. In the  $\text{Ca}(\text{OH})_2$  reaction, the ISA will be present as its calcium salt, with each calcium ion being associated with two ISA molecules, therefore, a cation exchange is likely to occur between the calcium of  $\text{Ca}(\text{ISA})_2$  and the proton of the cellulose carboxylate group, binding  $^+\text{Ca-ISA}$  to the cellulose and releasing free protonated ISA into the reaction solution. Other CDPs present in the reaction solution, also present as their calcium salts will also be able to bind to the cellulose in the same way, in competition with the binding of the ISA, thus lowering the percentage of ISA in recovered extracts. In the mixed  $\text{Ca}(\text{OH})_2/\text{NaOH}$  reaction, the difference between the percentage of ISA which consists of the TOC in the solution and solid phases was even greater; the percentage of ISA in the TOC of the extracts was four times less than the percentage of the ISA in the TOC of the original sample solutions (~ 12 % vs. ~ 48 %) indicating that the small fragmentation products were binding to the cellulose in preference to the ISA. In both the NaOH and mixed  $\text{Ca}(\text{OH})_2/\text{NaOH}$  reactions, the concentration and rate of ISA production (Figure 61 and Figure 62), the concentration and the rate of production of the combined TOC (Figure 63) and the percentage of ISA present in the TOC (~ 50 %) were very similar, indicating that the presence of the NaOH or the high pH dictates the type of CDP and the rate of their production. However, the percentage of ISA in the extracts was four times lower in the

mixed reaction in comparison to the NaOH reaction, the only difference being the large excess of solid calcium hydroxide being present in the mixed reaction, suggesting that the difference in the percentages was either due to the  $\text{Ca}(\text{OH})_2$  blocking access of the ISA to the cellulose fibres or catalysing its oxidation to smaller organic acids, resulting in a lower percentage of ISA in the extracts of the mixed reaction. Interestingly, however, the time course for the production of TOC from the extracted solids from all three reactions (Figure 68) indicates that the sorption of the TOC was occurring the fastest in the mixed reaction, indicating that, in that reaction the small organic acids were being rapidly absorbed onto the cellulose, in spite of the presence of the solid calcium hydroxide.

An alternative explanation is as follows: calcium ions are the most effective cation for aiding in the dissolution of cellulose<sup>203</sup> because they introduce large amounts of bound water molecules into the cellulose chains; in aqueous systems disassociation of  $\text{Ca}(\text{OH})_2$  allows free calcium ions to form calcium–water clusters which contain up to ten complexed water molecules per calcium ion<sup>204-207</sup>. Therefore, in the high pH of the mixed reaction, the hydrated calcium ions will be able to penetrate the cellulose matrix, resulting in enhanced swelling, and the cellulose chains becoming highly hydrated, which may allow for a rapid absorption of the smaller fragmentation products to occur in a similar manner to the way that the ISA was “soaked up” in the NaOH reaction, and by cation exchange at the carboxyl groups, whereas the excess solid calcium hydroxide in the system will possibly hinder the larger ISA molecules from binding in the same manner, as indicated by the low amount of ISA recovered from the unreacted solid material.

It is clear that further experiments are required to fully understand the processes which are occurring in these reactions which result in the loss of ISA and other CDPs from the reaction solutions. Understanding of these processes was complicated due to the continual production of ISA which was occurring in conjunction with the losses due to the absorption processes. The main aim of this work was to maximize the production of  $\beta$ -ISA; therefore no further experiments were performed to further investigate the observed losses of ISA from reaction solutions, however, the results of these experiments suggest that loss of ISA from degradation solutions onto unreacted cellulose may be of similar importance to the sorption of ISA onto cement based materials and is therefore of importance in respect to the safety assessment for the proposed repository for radioactive waste. For example, Van Loon and Glaus<sup>94</sup> determined that both  $\alpha$ - and  $\beta$ -ISA sorbed on to cement in the quantity of  $0.3 \text{ mol kg}^{-1}$ , and from those results they predicted that, due to that sorption, the total ISA in

solution in a repository may be reduced by three orders of magnitude<sup>94</sup>. In the present study, the extracted unreacted cellulose from the 90 °C NaOH reaction contained 2.84 g L<sup>-1</sup> of ISA, therefore, as there was initially 50 g L<sup>-1</sup> of cellulose in the above degradation reaction, and the molecular mass of ISA is 180 g mol<sup>-1</sup>, it can be roughly estimated that under the present reaction conditions, cellulose is capable of removing ISA due to sorption also in the region of 0.3 mol kg<sup>-1</sup>; suggesting that additional research is required on the effect of the sorption of ISA onto cellulose under repository conditions.

### **3.7 Summary and conclusion of results: production of ISA from the NaOH and Ca(OH)<sub>2</sub> reactions**

As discussed in section 3.4.2 when using NaOH as the alkaline species, 90 °C was the preferred reaction temperature for production of the ISAs: at that temperature the largest concentrations of  $\beta$ -ISA were produced and its rate of production was also faster in comparison to that in the other reactions. Therefore, to determine which base is preferred for the production of  $\beta$ -ISA to be used in a standard optimised synthesis, a comparison was made between the use of NaOH at 90 °C and Ca(OH)<sub>2</sub> at 90 °C. By combining the ISA and TOC concentrations recovered from the extracted solids (as described in section 3.6.2) with the ISA and TOC concentrations from solution, a comparison could be made between NaOH or Ca(OH)<sub>2</sub> solutions.

In the NaOH reaction the fastest rate of ISA production was within the first 24 h and after 30 days of reaction the concentration of TOC produced was ~ 13 g L<sup>-1</sup>. The ISA content of the TOC was ~ 53.2 % with  $\alpha$ -ISA (4.3 g L<sup>-1</sup>) accounting for ~ 14 % of the TOC and  $\beta$ -ISA (12.7 g L<sup>-1</sup>) accounting for ~ 39 % of the TOC. In the equivalent Ca(OH)<sub>2</sub> reaction, a maximum TOC concentration of ~ 5 g L<sup>-1</sup> was produced after 4 days with ISA accounting for ~ 82 % of the TOC with  $\alpha$ -ISA (5.1 g L<sup>-1</sup>) accounting for ~ 41 % and  $\beta$ -ISA (5.1 g L<sup>-1</sup>) also accounting for ~ 41 %. After the maximum concentrations were witnessed, an obvious fall in both ISA and TOC concentrations were witnessed for the Ca(OH)<sub>2</sub> reaction and the extraction of the unreacted solids from that reaction resulted in the recovery of 2.1 g L<sup>-1</sup> of TOC which contained ~ 1.8 g L<sup>-1</sup> of  $\alpha$ -ISA and ~ 1.8 g L<sup>-1</sup> of  $\beta$ -ISA. There was no obvious indication of a fall in the ISA concentration in the NaOH reaction, but the extraction of the solids from that reaction resulted in similar recoveries of TOC (2.4 g L<sup>-1</sup>), which contained ~ 0.74 g L<sup>-1</sup> of  $\alpha$ -ISA and ~ 2.1 g L<sup>-1</sup> of  $\beta$ -ISA. When the extracted concentrations were added to the original solution concentrations, the maximum TOC produced from the NaOH

reaction was now  $15.4 \text{ g L}^{-1}$  and this contained  $\sim 39 \%$  of  $\beta$ -ISA ( $14.9 \text{ g L}^{-1}$ ) and  $\sim 13 \%$  of  $\alpha$ -ISA ( $5.0 \text{ g L}^{-1}$ ). A plot of the combined TOC concentrations produced from the extraction of the unreacted solids and the original solution concentrations shows only a small drop in TOC concentration for the  $\text{Ca}(\text{OH})_2$  reaction after the maximum amount of TOC is observed after 4 days, indicating that most of the TOC lost due to sorption was recovered in the extraction procedure (Figure 69). When the  $\text{Ca}(\text{OH})_2$  results were combined, the maximum TOC was  $6.3 \text{ g L}^{-1}$ , and this contained  $\sim 43 \%$  of  $\beta$ -ISA ( $6.8 \text{ g L}^{-1}$ ) and  $\sim 44 \%$  of  $\alpha$ -ISA ( $6.9 \text{ g L}^{-1}$ ).

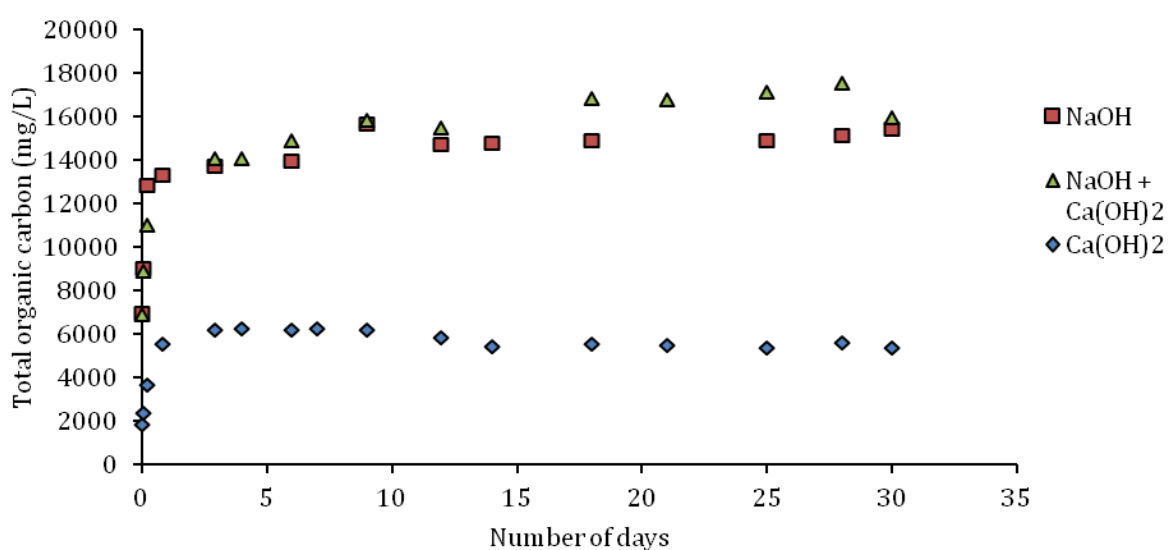


Figure 69: Time course for the production of TOC ( $\text{mg L}^{-1}$ ) from the degradation of cellulose at  $90 \text{ }^\circ\text{C}$  using either saturated  $\text{Ca}(\text{OH})_2$  soln., NaOH (2 M) or using both NaOH and saturated  $\text{Ca}(\text{OH})_2$  soln. with the extraction results also added

The results indicate that in the NaOH reaction after 30 days,  $\sim 35 \%$  of the cellulose had been converted into organic products and  $\sim 15 \%$  of which was converted directly into  $\beta$ -ISA. In comparison, in the  $\text{Ca}(\text{OH})_2$  reaction,  $\sim 14 \%$  of the cellulose was converted into organic products and  $\sim 6.8 \%$  of the cellulose was converted directly into  $\beta$ -ISA. The results are similar to the findings of Colbran and Davidson<sup>181</sup> who determined that the weight loss of cellulose was  $32 \%$  after being degraded in  $0.5 \text{ M}$  NaOH at  $100 \text{ }^\circ\text{C}$  and when the experiment was repeated with saturated  $\text{Ca}(\text{OH})_2$  solution, a weight loss of  $16 \%$  was observed. Colbran and Davidson concluded that the smaller weight loss of the  $\text{Ca}(\text{OH})_2$

degraded cellulose was due to the increased prevalence of the chemical stopping reaction when  $\text{Ca}(\text{OH})_2$  was used as the base, making cellulose stable to further degradation.

One of the aims of this work was to reduce the reaction time and increase the yield of  $\beta$ -ISA; therefore from the generated results, NaOH is the preferred base to be used as the degrading species for the production of  $\beta$ -ISA and further experiments incorporated NaOH as base. In the 90 °C NaOH reaction maximum concentrations of  $\beta$ -ISA were greater than the maximum concentration achieved in the 90 °C  $\text{Ca}(\text{OH})_2$  reaction ( $\sim 15 \text{ g L}^{-1}$  vs.  $\sim 7 \text{ g L}^{-1}$ ) and those concentrations were achieved in less time in the NaOH reaction (1 day vs. 4 days). A further drawback of the  $\text{Ca}(\text{OH})_2$  reaction was that  $\sim 26 \%$  of the produced  $\beta$ -ISA was lost due to sorption, whereas only  $\sim 14 \%$  of the  $\beta$ -ISA was lost due to sorption in the NaOH reaction (see Table 5 for a summary of the results).

Table 5: Summary of results from the degradation of cellulose using NaOH or  $\text{Ca}(\text{OH})_2$  as the base catalyst

Degradation of cellulose (20 g) under anaerobic conditions at 90 °C, for 30 days. Alkaline species:	NaOH (2M)	$\text{Ca}(\text{OH})_2$ (Saturated soln.)
Approximate % of cellulose degraded after 30 days	35	14
Maximum TOC concentration after 30 days ( $\text{g L}^{-1}$ )	15	6.3
% of total ISA in the TOC	52	87
% of $\beta$ -ISA in the TOC	39	43
Approximate % of cellulose added to the reaction converted into $\beta$ -ISA	15	6.8
Maximum $\beta$ -ISA concentration after 30 days ( $\text{g L}^{-1}$ )	$15 \text{ g L}^{-1}$	$6.8 \text{ g L}^{-1}$

### 3.8 Large scale cellulose degradation reaction using optimized conditions

To generate crude  $\beta$ -ISA solution for use in isolation procedures, a large scale cellulose degradation reaction was performed, as described in section 2.5.2 using a ten-fold scale-up. However, because it has been suggested that sodium ions promote the cleavage of the 4-deoxy-2,3-hexodilulose intermediate<sup>107, 172</sup>, and that the generated crude solution is passed through a cation exchange column to remove sodium ions; to minimise the amount of excess sodium ions in the reaction solution, the larger reaction used a 0.5 M sodium hydroxide solution instead of the 2 M solution. At that pH the amount of degradation is expected to be very similar because, as previously discussed, the rate of peeling is not expected to increase after pH 13.7 (0.5 M)<sup>107</sup>. To monitor the progress of the reaction and to gain a more precise reaction end-time, the reaction was sampled every two hours and each sample was analysed by HPAEC-PAD using the conditions described in section 2.2.1.

The results of the HPAEC-PAD analysis indicated that the most rapid stage of  $\beta$ -ISA production was complete after 16 h, following this period of time the rate of  $\beta$ -ISA production subsides as indicated by the levelling-off of the time course (Figure 70). After 16 h the solution concentration of  $\beta$ -ISA was  $8.1 \text{ g L}^{-1}$  and the concentration of  $\alpha$ -ISA was  $2.7 \text{ g L}^{-1}$ , these concentrations are in agreement with those obtained in the small scale NaOH reactions described above, after equivalent time periods, indicating that there is no significant difference between using 0.5 M and 2.0 M NaOH as the base concentration. Following the 16 h reaction time there remained 142 g of un-reacted starting material indicating that 29 % of the cellulose had been converted into soluble products or 8.1 % of the initial cellulose had been directly converted into  $\beta$ -ISA. These results are similar to those of Lai and Ontto<sup>185</sup> who determined that between 20 and 30 % of cellulose chains were degraded before the substrate becomes inert to any significant further degradation when treating cellulose using sodium hydroxide concentrations between 0.5 – 4 M.

### **3.9 Ongoing and future work to further reduce reaction time and increase solution concentration of $\beta$ -ISA using microwave heating**

As previously discussed, when the peeling reaction is hindered due to the physical stopping process, it may be continued by swelling the cellulose fibres, a process which is known as mercerization, as this allows  $\text{HO}^-$  to access previously inaccessible cellulose fibres allowing further degradation to occur. Traditionally, this requires the use of sodium hydroxide concentrations greater than 2.5 M, however a study by Moharram and Mahmoud<sup>208</sup> indicated that the mercerization process occurs when more dilute sodium hydroxide concentrations are used and in shorter periods of time if cellulose fibres are irradiated with microwave radiation. With this in mind, in an attempt to further reduce the reaction time and increase the solution concentration of  $\beta$ -ISA, a small scale reaction was performed using microwave heating, as described in section 2.5.3. Unfortunately, no further increase in  $\beta$ -ISA solution concentration was observed indicating that enhanced swelling was not occurring under the reaction conditions. However, according to Moharram and Mahmoud, the enhanced effect of swelling due to microwave irradiation is related to carefully controlling the power output of microwave reactions, this was not possible with the microwave equipment available in the present work due to only one power setting being available (750 W), but significantly, results indicated that the  $\beta$ -ISA concentration achieved

after 15 min of microwave heating equalled the concentration obtained after 16 h of conventional heating (Figure 70).

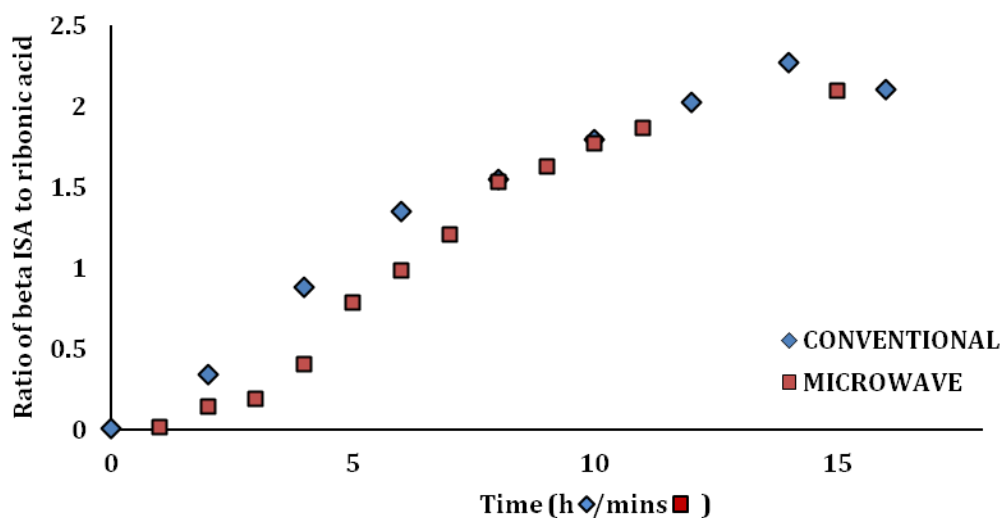


Figure 70: Time course for the production of  $\beta$ -ISA, as indicated by the ratio of  $\beta$ -ISA peak area to ribonic acid (IS) peak area for the sodium hydroxide catalysed degradation of cellulose using conventional heating at 90 °C (diamonds) and microwave heating at reflux (squares).

To investigate the effect of swelling on enhancing cellulose degradation, a further exploratory microwave reaction was undertaken, which utilised sodium hydroxide concentrations above those required for mercerization to take place. It was previously discussed in the present work that when sodium hydroxide concentrations between 2.5 M and 5 M are used, total cellulose degradation increases resulting in more weight loss of cellulose<sup>184</sup>, however it was unclear in the report by Machell and Richards if the reactions with higher NaOH concentrations resulted in the formation of greater amounts of ISA. To investigate this, an experiment was performed which compared the effect of 0.5 M and 5.0 M NaOH solutions on  $\beta$ -ISA production using the conditions as described in section 2.5.4. Preliminary results indicated that with the 5.0 M base concentration, approximately 3-times more  $\beta$ -ISA production was achieved and using  $\alpha$ -ISA standards, calculated  $\beta$ -ISA solution concentrations of 6.8 g L<sup>-1</sup> and 19.6 g L<sup>-1</sup> were achieved respectively after only 12 min of reaction time. In comparison only 14.1 g L<sup>-1</sup> of  $\beta$ -ISA was produced after 36 days of reaction at 90 °C using conventional heating, which indicates the great potential that microwave heating offers in increasing  $\beta$ -ISA yields in vastly shorter reaction times; microwave studies are ongoing at the University of Huddersfield.

## 4 Isolation of $\beta$ -ISA

### 4.1 Introduction

This chapter will primarily discuss methods which were developed to isolate pure  $\beta$ -ISA from solutions of crude  $\beta$ -ISA which also contain  $\alpha$ -ISA and other CDPs; the preparation of the crude solution was discussed in chapter 3. A secondary aim of this chapter was to identify other CDPs which were present in the crude solution.

As discussed in section 1.3.7.2 there are a few reported methods for the isolation of  $\beta$ -ISA<sup>94, 107, 110, 148, 153</sup>. Whistler and BeMiller<sup>148</sup> and Feast *et al.*<sup>153</sup> used cellulose column chromatography to partially separate  $\beta$ -ISA from crude degradation mixtures. Whistler and BeMiller then isolated pure  $\beta$ -ISA using paper chromatography, the  $\beta$ -ISA was then converted into its tetrabenzoate (Figure 71,  $\beta$ -ISA-tetrabenzoate) and recrystallized from 75 % aqueous ethanol. Feast *et al.*<sup>153</sup> isolated a mixture of  $\alpha$ - and  $\beta$ -ISA lactone using cellulose column chromatography, the mixture was then converted into their corresponding tribenzoate esters (Figure 71,  $\beta$ -ISA<sub>L</sub>-tribenzoate) and small amounts of  $\beta$ -ISA tribenzoate was isolated using preparative TLC. In more recent methods, Greenfield *et al.*<sup>107</sup> and Glaus *et al.*<sup>110</sup> isolated small amounts of  $\beta$ -ISA by passing crude mixtures of CDPs through anion exchange columns. Greenfield *et al.* used preparative anion exchange chromatography to purify small quantities of  $\beta$ -ISA and precipitated the calcium salt of  $\beta$ -ISA by adding calcium hydroxide to their pooled fractions. Glaus *et al.* isolated the sodium salt of  $\beta$ -ISA using an analytical HPAEC system; collected fractions were converted into  $\beta$ -ISA<sub>L</sub> using the established procedures described by Whistler and BeMiller<sup>149</sup>.

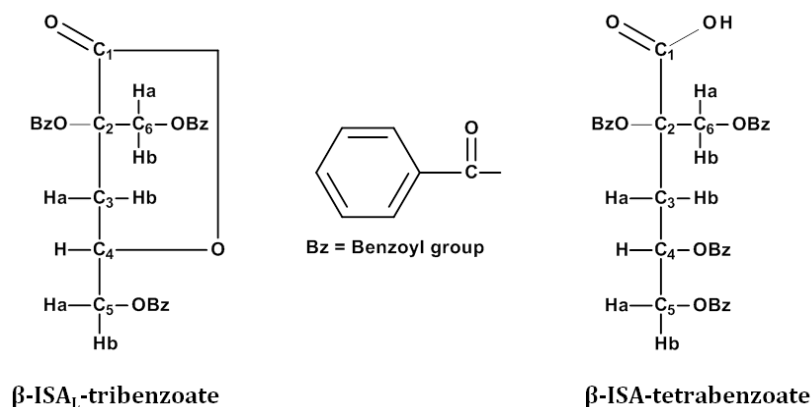


Figure 71: The tribenzoate lactone which was isolated by Feast *et al.* (left) and the open-chain tetrabenzoate which was isolated by Whistler and BeMiller (right).

## 4.2 Isolation of $\beta$ -ISA using preparative anion exchange chromatography

Initial attempts to isolate  $\beta$ -ISA free from  $\alpha$ -ISA and other cellulose degradation products were based on the work reported by Greenfield *et al.*<sup>107</sup> and resulted in only limited success. The method (described in section 2.6.2) involved applying crude cellulose degradation solution directly to a column of anion exchange resin. One of the major limitations of the procedure was that coloured substances which were present in the crude material were strongly retained by the column, resulting in an impaired separation performance; this was indicated by the majority of the crude material eluting through the column un-fractionated and this was evident when eluting samples through either new or regenerated resin. Similar problems were reported by Glaus *et al.*<sup>110</sup> who isolated  $\beta$ -ISA directly from crude cellulose degradation solutions using analytical anion exchange chromatography (HPAEC). In their method, crude solutions were eluted twice through an anion exchange column and steps were included after each run to remove impurities from the column.

In the present work, fractions collected from isolation attempts were screened for their  $\beta$ -ISA content using HPAEC-PAD and employing the conditions described in section 2.3.5, with the exception that samples were diluted two-fold. To identify  $\beta$ -ISA, a sample of the un-fractionated solution was also analysed; to identify  $\alpha$ -ISA in the collected fractions, its retention time was compared with that of an analytical standard, the synthesis of which was described in section 3.2.2.

HPAEC-PAD analysis of the crude solution indicated that the major components were  $\beta$ -ISA (~ 60 %),  $\alpha$ -ISA (~23 %) and DHB (~ 17 %) with other minor peaks representing less than 1 % of the total peak area. It is worth noting that the crude  $\beta$ -ISA solution used in this initial isolation procedure was prepared by degrading cellulose at RT, furthermore, the reaction mixture was only flushed with nitrogen for the first 24 h as instructed by the method of Greenfield *et al.*<sup>107</sup>. It was discussed in section 3.4.1 that the production of DHB is temperature and oxygen dependent. In latter reactions, when the reaction system was continuously flushed with nitrogen, DHB accounted for less than 3 % of the total peak area and when cellulose was degraded at 90 °C, in the presence of nitrogen, DHB accounted for only 0.3 % of the peak area. The large amounts of DHB present in the crude solution used in the present isolation procedure suggest that significant amounts of oxygen were present

in the reaction vessel, indicating that continuous flushing of the reaction with nitrogen is required to reduce the production of DHB.

In the initial attempt to isolate  $\beta$ -ISA, 3 ml aliquots of crude  $\beta$ -ISA solution which contained approximately  $20 \text{ g L}^{-1}$  of total  $\alpha$ - and  $\beta$ -ISA ( $\sim 60 \text{ mg}$ ) were applied to the column and the products were eluted using a linear gradient starting from 10 mM NaOH and slowly increasing until a maximum concentration of 100 mM NaOH. The HPAEC-PAD results of the first column indicated that only a partial separation of  $\beta$ -ISA was achieved, with several fractions containing  $\beta$ -ISA with a sample purity of greater than 60 %. The column was repeated several times with various mobile phase gradients, each time producing similar results. The elution of the column was extremely slow, however HPAEC-PAD analysis indicated that all of the ISA was eluting from the column within the first ten fractions. The elution order was relatively consistent for each column: the early eluting fractions contained minor impurity peaks; only one or two of the subsequent collected fractions was rich in  $\beta$ -ISA in comparison to the amount of  $\alpha$ -ISA, where the  $\beta$ -ISA peak was approximately ten-times larger than the  $\alpha$ -ISA peak, and the remaining fractions contained relatively un-fractionated crude material. It was unusual that the  $\beta$ -ISA was eluting before the  $\alpha$ -ISA because it is known from both the present work, and the work of Greenfield *et al.*<sup>107</sup> and Glaus *et al.*<sup>110</sup> that  $\beta$ -ISA usually elutes after  $\alpha$ -ISA when using anion exchange chromatography. The anion exchange capacity of the wetted bed volume of the column was  $1.2 \text{ eq/L}$ <sup>209</sup> indicating that the number of moles available for anion exchange ( $\sim 0.06$ ) was significantly greater than the number of moles of ISA applied to the column ( $\sim 0.00033$ ). The results suggest that the polar impurities which were present within the solution were binding to, and blocking the sites of anion exchange, thus reducing the anion exchange capacity of the column, effecting both the separation performance and elution order of the analytes. It is possible that any separation was actually due to absorption processes other than anion exchange, such as non-polar interactions.

In an attempt to improve the isolation procedure, further attempts were made using a larger column (50 x 4 cm as opposed to the 25 x 2 cm). The crude  $\beta$ -ISA solution applied to the column was produced from the degradation of cellulose at 90 °C as opposed to RT, and in agreement with the findings discussed in section 3.4.1, the DHB content of the crude material now accounted for only 8 % of the crude material as opposed to 17 %. To minimise column overloading, the volume of the sample, which now contained

approximately  $80 \text{ g L}^{-1}$  of total  $\alpha$ - and  $\beta$ -ISA was reduced from 3 ml to 2 ml (~160 mg of ISA).

With the larger column the best results were produced when a mobile phase utilising a linear gradient starting from 10 mM NaOH and slowly increasing to 30 mM was used, followed by the elution with an excess of 100 mM NaOH in an attempt to elute strongly retained impurities. In a typical example, 35 x 2 ml fractions were collected and compared with the reference un-fractionated sample. In general, the ISAs were eluting from the column after approximately the 20<sup>th</sup> fraction; the first of these fractions were rich in  $\beta$ -ISA with minor amounts of  $\alpha$ -ISA and other impurities, in subsequent fractions the amount of  $\alpha$ -ISA increased, and in the final collected fractions approximately equal amounts of  $\alpha$ - and  $\beta$ -ISA were present and other smaller impurity peaks; the best results were achieved when 5 of the fractions that were collected contained  $\geq 90 \%$   $\beta$ -ISA. The  $\beta$ -ISA-rich fractions were pooled and lyophilised and the resulting material was dissolved in  $\text{D}_2\text{O}$  and was analysed by 1D ( $^1\text{H}$ ,  $^{13}\text{C}$ , DEPT 135 and DEPT 90) and 2D (COSY, HSQC and HMBC) NMR spectroscopy. The  $^1\text{H}$  NMR spectrum (Figure 72) confirmed that the major component was  $\beta\text{-ISA}_\text{L}$ , as indicated by the chemical shifts and multiplicities being very similar to those published by Glaus *et al.*<sup>110</sup> for the same compound (literature values are displayed in brackets in Figure 72). The NMR also indicated that several other peaks were present, suggesting that the isolated  $\beta$ -ISA sample was not of high purity. 2D and DEPT NMR analysis of the sample indicated that the other major peaks were coupled indicating that only one additional major compound was present. The position of the chemical shifts and multiplicities of the peaks were similar to those of the open-chain form of  $\alpha$ -ISA, suggesting that the NMR spectra presented in Figure 72 was a mixture of the lactone and open-chain forms of  $\beta$ -ISA.

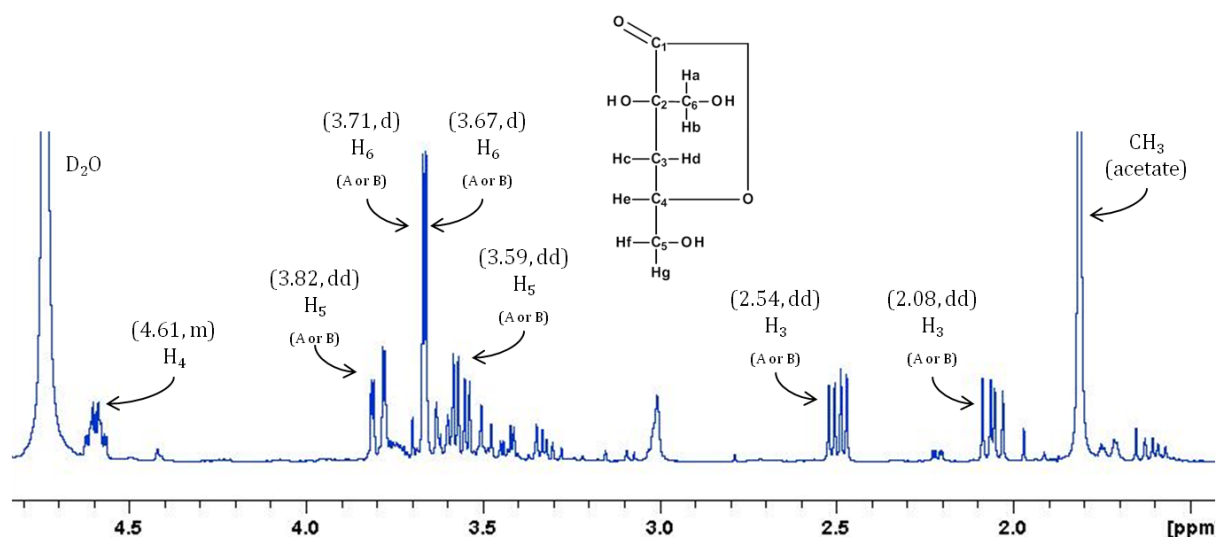


Figure 72:  $^1\text{H}$  NMR spectrum of lyophilised fractions which were collected from the preparative anion exchange chromatography of crude  $\beta$ -ISA solution.

To further investigate if the NMR sample was a mixture of  $\beta$ -ISA<sub>L</sub> and  $\beta$ -ISA, the pH of the sample was increased with the addition of 10  $\mu\text{l}$  aliquots of 10 M NaOD, resulting in the pH of the NMR sample increasing to  $\sim 13$ . At that pH it is known that a rapid ring opening of ISA<sub>L</sub> occurs due to base hydrolysis (see section 5.2.1). After each addition of NaOD a  $^1\text{H}$  NMR spectrum was recorded, which showed a rapid decrease in the size of the  $\beta$ -ISA<sub>L</sub> resonances and an increase in the size of the other major peaks. To gain a complete transformation, an equivalent amount of base was required, so several aliquots of NaOD were added until all of the  $\beta$ -ISA<sub>L</sub> resonances had disappeared and the seven resonances representing  $> 90\%$  pure  $\beta$ -ISA remained (see Figure 73, for the  $^1\text{H}$  NMR spectra).

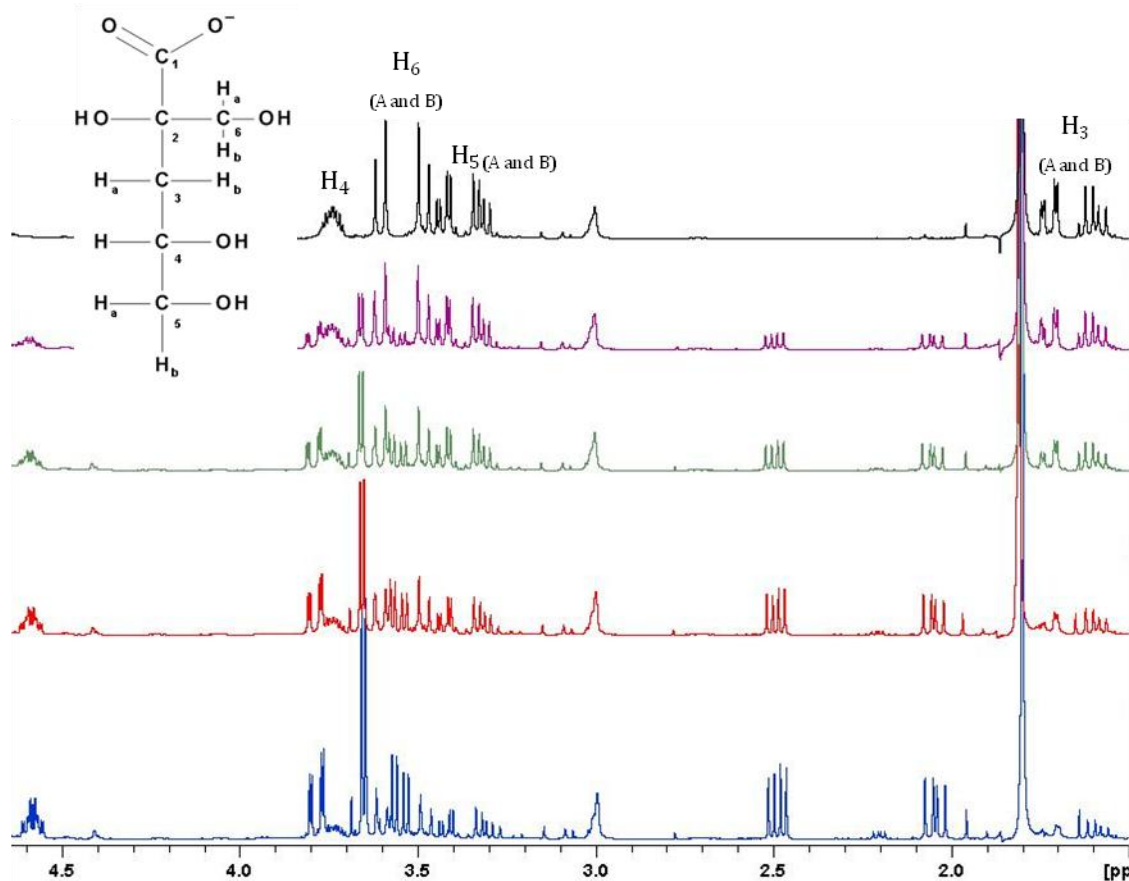


Figure 73:  $^1\text{H}$  NMR spectra showing the base catalysed transformation of  $\beta\text{-ISA}_L$  (bottom spectrum) to the open-chain form of  $\beta\text{-ISA}$  (top spectrum) due to the addition of NaOD.

The  $\text{pK}_a$  of  $\beta\text{-ISA}$  was determined as being 3.61<sup>210</sup> so at pH 13, the  $\beta\text{-ISA}$  will be present as its deprotonated open-chain anion. In agreement with what is observed for the  $\alpha\text{-ISA}$  anion, the single methyne proton (H4) has shifted up-field (4.6 ppm to 3.8 ppm) and this is a key indication that ring opening has occurred. The splitting patterns of the resonances in the  $^1\text{H}$  NMR spectra of the deprotonated  $\alpha$ - and  $\beta\text{-ISA}$  are very similar, however, a key difference which allows an easy differentiation between the spectra of the two isomers are the splitting patterns of the C3-methylene protons which are located furthest up-field for both  $\alpha$ - and  $\beta\text{-ISA}$ . In the  $\alpha\text{-ISA}$  sample the vicinal coupling between the most up-field H3 proton and the H4 proton (1.60 ppm, 3.5 Hz) is smaller than the vicinal coupling constant of the second-most up-field H3 proton with the H4 proton (1.76 ppm, 8.2 Hz). Whereas, with  $\beta\text{-ISA}$ , the vicinal coupling of the most up-field H3 proton with the H4 proton is larger than the vicinal coupling of the second-most up-field H3 proton with the H4 proton (Figure 74). The differences in the splitting patterns of the C3-methylene protons can be related to the

differences in the configuration of the C2 chiral centres of each isomer, resulting in different magnetic environments of the protons on adjacent carbons (see section 4.5.4.5).

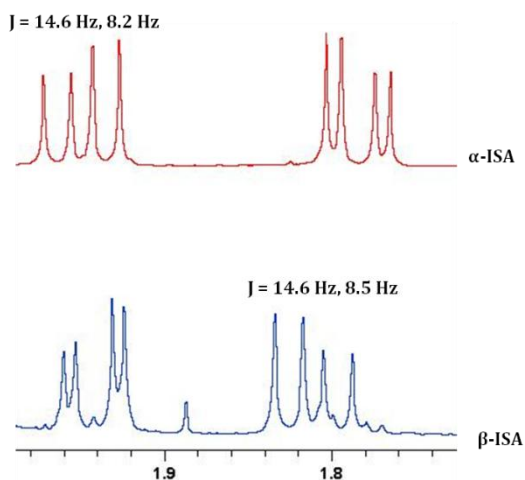


Figure 74: H3 protons from the  $^1\text{H}$  spectra of  $\alpha$ -ISA (top) and  $\beta$ -ISA (bottom)

In this method only a small amount of  $\beta$ -ISA was isolated, but importantly the NMR spectrum of the open-chain form of  $\beta$ -ISA was obtained for the first time, which allows for the identification of  $\beta$ -ISAH in solutions and for studies of the conformation adopted (see section 2.6.4.11 for NMR data).

Isolating large amounts of  $\beta$ -ISA using the manual anion exchange column proved to be very difficult, one of the main reasons, apart from the fouling of the resin was the very slow flow rate of the column. The flow rates used in the method of Glaus *et al.* ranged from  $4 \text{ ml min}^{-1}$  in the first elution of their crude solution to  $2 \text{ ml min}^{-1}$  for the second elution with several hundred injections being required for them to isolate 220 mg of  $\beta$ -ISA. In the method described above, the flow rate of the anion exchange column was  $< 0.1 \text{ ml min}^{-1}$  due to the gravity elution and atmospheric pressure conditions of the column, which resulted in very long periods of time being required to run a single column. The resin used in each column was 200-400 mesh size, which is the finest resin in the Dowex range and was chosen because it was used in the method of Greenfield *et al.*<sup>107</sup> In future work, resins may be used with a larger particle size, which would increase the flow rate of the column, however, the limited separation performance may deteriorate as a result. In an attempt to increase the yield of  $\beta$ -ISA, a method was developed which utilised an automated preparative anion exchange chromatography system which utilised pressurised columns and allowed increased flow rates to be applied, whilst maintaining the use of the fine resin.

### 4.3 Isolation of $\beta$ -ISA using automated preparative anion exchange chromatography

Several attempts were made to isolate  $\beta$ -ISA using an automated preparative anion exchange chromatography system which was described in section 2.6.3. Various parameters were explored, such as changing the sample size, experimenting with different mobile phase gradients and using different flow rates in an attempt to maximise the amount of  $\beta$ -ISA isolated. In the initial attempt, 0.5 ml of crude  $\beta$ -ISA solution was filtered and injected onto the column (20 cm x 3 cm). The crude solution was prepared using the method described in section 2.5.2 and when reconstituted in 75 ml of NaOH it contained approximately 80 g L<sup>-1</sup> (0.44 M) of total  $\alpha$ - and  $\beta$ -ISA of which approximately 60 g L<sup>-1</sup> (0.33 M) was  $\beta$ -ISA, therefore there was approximately 4.5 g of  $\beta$ -ISA in the reconstituted solution. In the first isolation attempt, the products were eluted with a linear gradient starting at 10 mM NaOH and rising to 50 mM over 50 minutes and the initial flow rate applied to the column was 4 ml min<sup>-1</sup>. From the initial column, 41 x 2 ml fractions were collected and screened for their  $\beta$ -ISA content using HPAEC-PAD and employing the conditions described in section 4.2. For convenience, collection fractions were diluted directly in the fraction collector prior to HPAEC-PAD analysis. The HPAEC-PAD results indicated that the elution order of the components was similar to that of the previous manual column, as described in section 4.2. The early eluting fractions contained impurity peaks; minor amounts of  $\alpha$ - and  $\beta$ -ISA were visible after approximately the 20<sup>th</sup> fraction; the amount of  $\beta$ -ISA present in the fractions increased in relation to the amount of  $\alpha$ -ISA in the subsequent fractions and eventually, the amount of  $\beta$ -ISA decreased and after the 35<sup>th</sup> fraction, the amount of  $\alpha$ -ISA was greater than the amount of  $\beta$ -ISA present. From the first column, eight fractions were collected that contained a sample of  $\beta$ -ISA of greater than 90 % purity; these fractions were combined and a small volume was removed and lyophilised and the resulting solid material was dissolved in D<sub>2</sub>O and analysed by NMR. The <sup>1</sup>H NMR results indicated that the sample was rich in  $\beta$ -ISA; however, in agreement with the results from the manual column in section 4.2, the sample still contained a mixture of the open-chain and lactone forms of  $\beta$ -ISA. Integration of the resonances for the respective C3-methylene protons determined that the mixture consisted of approximately twice as much of the open-chain form as was present as the lactone.

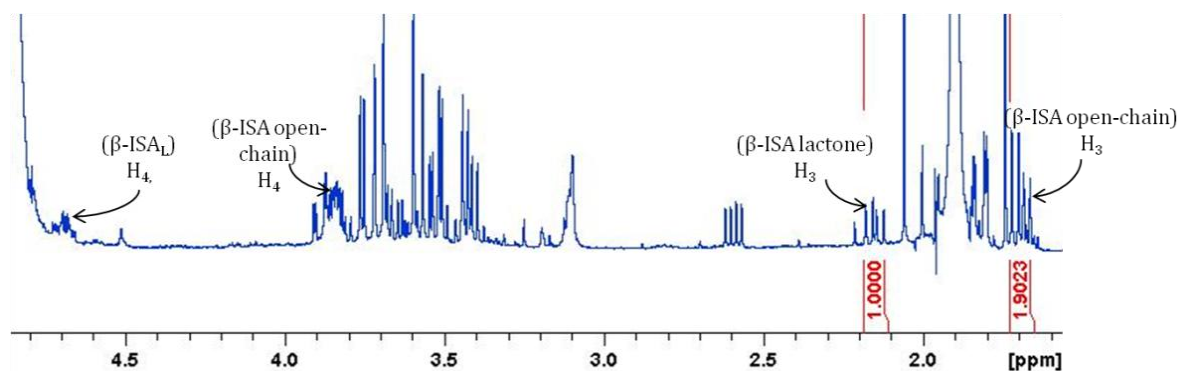


Figure 75:  $^1\text{H}$  NMR spectra of the fractions collected from the first attempt to isolate  $\beta$ -ISA using automated preparative anion exchange chromatography, the spectrum indicates a mixture of  $\beta$ -ISAL and ISA open-chain form

Initially, it was unexpected that a mixture of the two forms of  $\beta$ -ISA were present, because as discussed in section 3.2.2.1, when mixtures of  $\text{ISA}_L$  and  $\text{ISAH}$  are analysed by HPAEC-PAD, the 50 mM mobile phase results in an instantaneous transformation from the lactone to the open-chain anion which results in single peaks being observed; this is as a result of base hydrolysis of the  $\text{ISA}_L$  (Figure 76) and results in all the ISA being present in the open-chain de-protonated form.

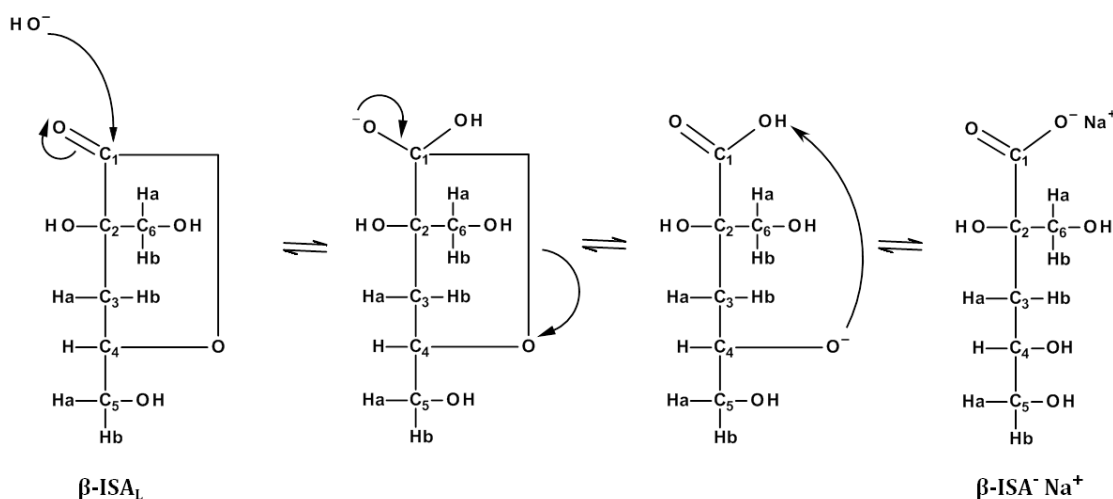


Figure 76: Base hydrolysis of  $\beta$ - $\text{ISA}_L$  in the presence of NaOH solution to produce sodium isosaccharinate

In the present work, the isolation of a mixture of  $\text{ISAH}$  and  $\text{ISA}_L$  was unexpected but can be explained as follows: in the preparation of the crude  $\beta$ -ISA solution, the degradation mixture was eluted through a cation exchange column (see section 2.5.2) to remove the sodium ions and, due to the low pH environment of the column, the resulting protonated

free acids are converted into their corresponding lactones. The lactone mixture, was then lyophilised and, according to the method of Greenfield *et al.*<sup>107</sup>, the freeze-died material was reconstituted in NaOH (0.1 M, 75 ml). The base hydrolysis of the lactone at pH 13 is rapid (see section 5.2.1), but the base is consumed in the reaction so a molar equivalent of base is required to convert all the ISA<sub>L</sub> into the free acid; however, it was estimated that the crude material contained ~ 6 g (0.033 mol) of ISA, and this was dissolved in 75 ml of NaOH (0.1 M, 0.0075 mol) so in the crude solution to be applied to the column only about a quarter of the ISA<sub>L</sub> could have been converted into the open-chain form. It had been hoped that as the column was eluted with a NaOH solution mobile phase, that any lactone present in the sample would rapidly be converted to the ring opened acid (as was observed with the analytical system).

In the preparative system, described above, the flow rates are many times faster (4 ml min<sup>-1</sup>) than those used in HPAEC-PAD (0.5 ml min<sup>-1</sup>), so it is likely that the mixed ISAH/ISA<sub>L</sub> solution injected onto the preparative column, (0.5 ml, ~2 x 10<sup>-4</sup> mol of ISA), passed through the column before a conversion of the lactone to the open-chain form could take place, which was in agreement with the NMR results which indicated a mixture of ISAH and ISA<sub>L</sub> was isolated (Figure 75). Whereas, when the corresponding fractions are screened using HPAEC-PAD, much smaller amounts of sample are injected onto the system. For example, in an extreme scenario, if all of the ISA which was injected onto the preparative column was present in a single collected fraction (~2 x 10<sup>-4</sup> mol), each fraction is diluted two-fold (1 x 10<sup>-4</sup> mol, 4 ml total volume) and only 20  $\mu$ l of that sample is injected onto the HPAEC-PAD column, so < 5 x 10<sup>-7</sup> moles of ISA would be injected onto the column. Therefore, any ISA<sub>L</sub> present would be quickly converted into the open-chain form due to a combination of the relatively slow flow rates being applied and an excess of high pH base being present in the mobile phase.

The pH of the combined diluted fractions obtained from the anion exchange column was 7, at that pH, the ring opening of the lactone is expected to be extremely slow (see section 5.2.1), further explaining why a mixture of ISAH and ISA<sub>L</sub> was observed. The combined fractions were allowed to stand for several weeks which resulted in the solvent slowly evaporating, producing a small amount of white solid. The solid was dissolved in D<sub>2</sub>O and analysed by <sup>1</sup>H NMR, and the results indicated that all the ISA was now present in the open-chain form, indicating that even at near neutral pHs a slow transformation of ISA<sub>L</sub> to ISAH occurs. The NMR spectrum also indicated the presence of sodium acetate, due to the

large resonant peak which was present as a singlet at 1.9 ppm, representing the methyl group of acetate (Figure 77, bottom spectrum). To convert the acetate into acetic acid, the collected fractions were reconstituted in deionised water and eluted through a cation exchange column using the method described in section 2.4.2. The effluent and washings were rotary evaporated under reduced pressure to remove the acetic acid and  $^1\text{H}$  NMR analysis of the resulting syrup (several mg) indicated the presence of highly pure  $\beta\text{-ISA}_L$  with no indication of the acetate peak at 1.9 ppm (Figure 77, top spectrum).

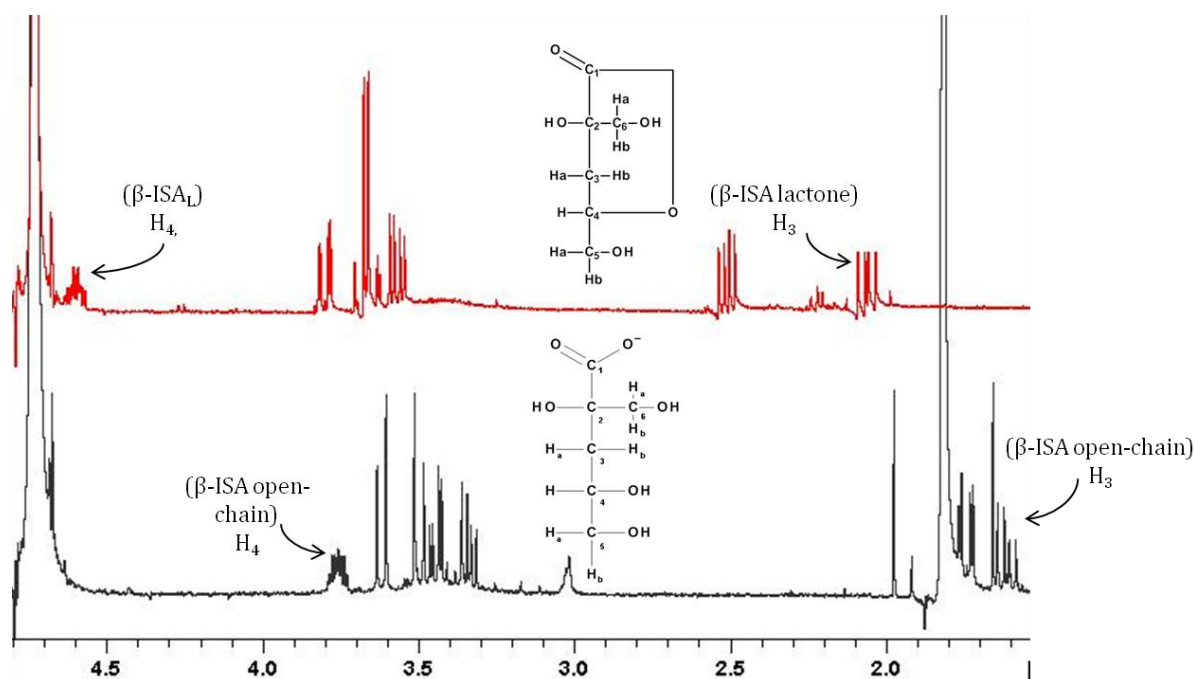


Figure 77:  $^1\text{H}$  NMR spectra of the fractions collected from the first attempt to isolate  $\beta$ -ISA using automated preparative anion exchange chromatography. Following a slow evaporation, the collected fractions (pH 7) transformed into the open-chain form of  $\beta$ -ISA, which also contains sodium acetate (bottom).  $^1\text{H}$  NMR chromatogram of  $\beta\text{-ISA}_L$  after eluting through a cation exchange column, which also indicates that sodium acetate has been removed (top).

Given that the separation procedure worked, in an attempt to isolate larger amounts of  $\beta$ -ISA a new crude solution was produced using the conditions described in section 2.5.2, and to reduce the viscosity of the un-fractionated solution, an additional 75 ml of water was added to the reconstituted 75 ml of NaOH/ $\beta$ -ISA solution, resulting in a total volume of 150 ml. Also, in an attempt to remove coloured impurities and reduce the problem of column fouling, the crude solution was boiled with activated charcoal (2 %) which appeared to produce a visibly cleaner solution. The crude solution was applied to a column which utilised a gradient starting at 20 mM NaOH and rising to 40 mM NaOH over a 50 minute

period with a flow rate of  $2 \text{ ml min}^{-1}$  being applied. Also in these runs, 5 ml aliquots of the crude sample were injected onto the column and any fractions containing  $\geq 90 \%$   $\beta$ -ISA were combined. Altogether, the column was repeated 23 times, resulting in the collection of 79 fractions and as with the previous isolation attempt, NMR analysis of the collected fractions indicated a mixture of lactone and open-chain forms of  $\beta$ -ISA. Following the freeze-drying of the collected fractions there was  $\sim 250 \text{ mg}$  of white solid and at this point an attempt was made to precipitate the calcium salt of  $\beta$ -ISA using the method of Greenfield *et al.*<sup>107</sup>. The white solid was dissolved in deionised water and the pH was increased to 9 with the addition of saturated calcium hydroxide solution, the solution was left to cool in the fridge for several days. After this period a very small amount of white material was visible on the surface of the flask, however, NMR analysis of the remaining solution indicated that the bulk of the  $\beta$ -ISA remained in the solution. The NMR analysis also indicated that, due to the high pH of the solution, the  $\beta$ -ISA was now present entirely in the open-chain form; however, the sample also contained large amounts of acetate.

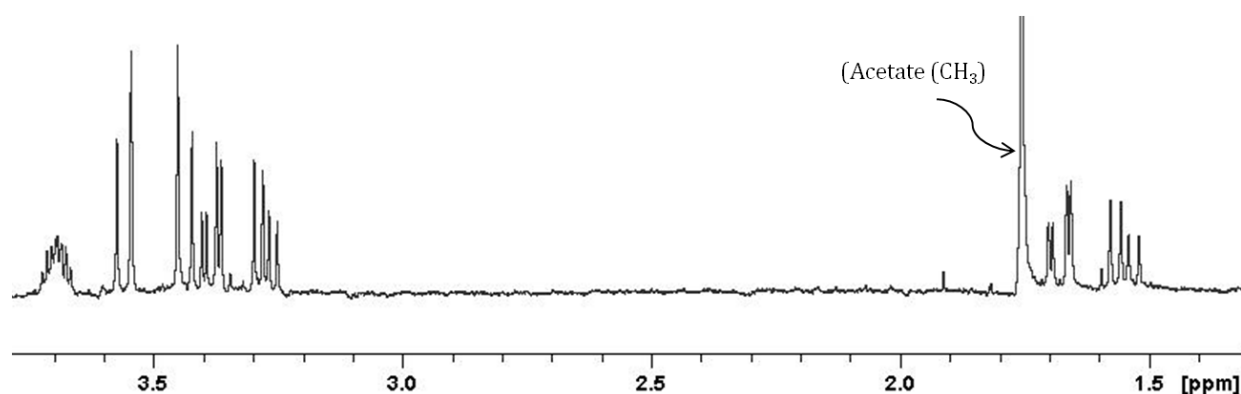


Figure 78: The open-chain form of  $\beta$ -ISA which also contains acetate

It was reported by Whistler and BeMiller<sup>148</sup> that the calcium salt of  $\beta$ -ISA was highly soluble in water, so it is understandable why the majority of the  $\beta$ -ISA remained in the solution. Some of the acetate was expected to be present as the calcium salt due to the addition of calcium hydroxide, therefore as calcium acetate is insoluble in ethanol and the calcium salt of  $\beta$ -ISA is soluble in absolute ethanol<sup>148</sup> the solution was converted into an aqueous ethanol solution (90 %, v/v) in an attempt to precipitate any calcium acetate. The solution was left to stand at  $4 \text{ }^\circ\text{C}$  for several days and following this period of time no significant precipitation occurred. A portion of the ethanol solution (10 ml) was removed and allowed to slowly evaporate, which produced a white residue; the residue was dissolved in  $\text{D}_2\text{O}$  and analysed by NMR which indicated  $\beta$ -ISA with the presence of

acetate, indicating that both  $\beta$ -ISA and the acetate were at least partially soluble in the ethanol solution. The entire 90 % ethanol solution was filtered through a sintered funnel; resulting in the removal of a small amount of pale brown solid (~ 14 mg). The brown solid was insoluble in  $D_2O$  but sparingly soluble in dimethyl sulfoxide- $d_6$  which allowed for NMR analysis. The resulting NMR chromatograph of the brown solid indicated that very minor amounts of  $\beta$ -ISA and acetate were present; but both were probably the result of residual solution sorbed to the small amount of solid impurity. To remove the remaining acetate from the bulk filtrate, the filtrate was evaporated under reduced pressure to remove ethanol, and the resulting small amount of white solid material was dissolved in deionised water and passed through the cation exchange column as previously described, and after the eluent and washings were evaporated, a light orange syrup remained which was dissolved in  $D_2O$  and analysed by NMR. The NMR indicated 163 mg of  $\beta$ -ISA<sub>L</sub> in greater than 95 % purity with no acetate or  $\alpha$ -ISA present (Figure 79).

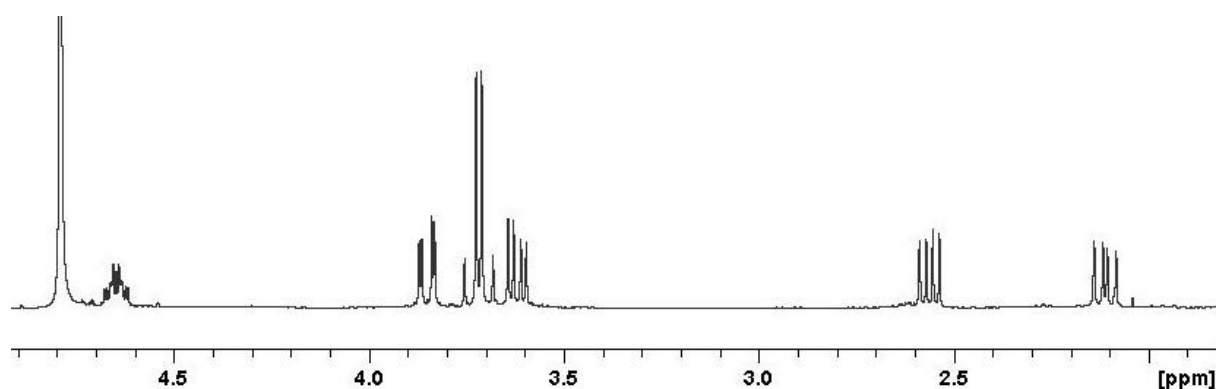


Figure 79:  $^1H$  NMR chromatogram of isolated  $\beta$ -ISA<sub>L</sub>

Several more attempts were made to increase the yield of  $\beta$ -ISA using the present method. It was found that the best results were achieved when a larger column (30 x 3 cm) was used as opposed to the 20 x 3 cm column. After experimenting with several mobile phase gradients, the best results were achieved with a gradient starting from 10 mM NaOH and increasing to 100 mM over a period of 100 minutes resulting in the collection of 100 x 2 ml fractions. As with the previous column, 5 ml aliquots of crude  $\beta$ -ISA were applied to the column. Samples were screened using HPAEC-PAD, and every fraction containing  $\geq 90$  %  $\beta$ -ISA was combined in a flask. In the previous column, on average, 3 fractions were collected per injection of 5 ml of sample, with the  $\beta$ -ISA-rich fractions eluting in approximately fraction numbers 35 – 39, i.e. between 35 – 39 minutes. With the new, larger column, the  $\beta$ -ISA-rich fractions were eluting in the fractions which were collected after 65

minutes; this slower elution in combination with the larger column resulted in  $\sim 13$  fractions being collected per injection. The column was repeated 17 times using the same conditions with a total of 232 fractions being collected. The collected fractions were lyophilised and applied to the cation exchange column as previously described, and following the evaporation of the eluent and washings, there was  $\sim 1$  g of syrup. NMR analysis indicated  $\beta$ -ISA of  $\geq 95$  % purity with no indication of the presence of acetate. Using the previous column, 163 mg of  $\beta$ -ISA was isolated after injecting approximately 3.5 g of  $\beta$ -ISA onto the column, indicating that  $\sim 5$  % of the injected  $\beta$ -ISA was isolated. Whereas, using the larger column, 1 g of  $\beta$ -ISA was isolated from a total of 2.6 g of  $\beta$ -ISA applied to the column indicating that  $\sim 39$  % of the injected  $\beta$ -ISA was isolated.

The automated system (described in section 2.6.3), was a more convenient way of isolating  $\beta$ -ISA and offered several key advantages in comparison to the manual column which was described in section 4.2. For example, in the automated system: a Rheodyne manual sample injector valve was utilised; the column was pressurised which allowed drastically increased flow rates to be used; mobile phase gradients could accurately be applied and repeated in proceeding columns to gain reproducible results; the fast flow rate used to recondition the column ( $8 \text{ ml min}^{-1}$ ) was especially useful which allowed for a fast turnover of repeat injections and the fraction collector allowed for accurate, predetermined volumes of fractionated material to be collected and when running several columns per day, the fraction collector made the operation more practicable.

Using the automated system described above, relatively large amounts of  $\beta$ -ISA were isolated in relatively short periods of time. As previously discussed, Glaus *et al.*<sup>110</sup> isolated  $\sim 220$  mg of  $\beta$ -ISA after several days and 450 injections of crude material through an analytical HPAEC system; whereas in the current method, after approximately 5 days and 17 injections, 1 g of pure  $\beta$ -ISA was isolated.

#### **4.4 Attempts to isolate $\beta$ -ISA from cellulose degradation solutions using Soxhlet extraction followed by short-path distillation**

A problem encountered in the present work and similarly in the work of Glaus *et al.*<sup>110</sup> was the soiling of anion exchange resins due to the presence of strongly bound coloured impurities. Whistler and BeMiller<sup>148</sup> reported that “syrupy  $\beta$ -ISA” ( $\beta$ -ISA<sub>L</sub>) could be isolated at a temperature range of 85 – 110 °C using vacuum distillation. So in an attempt

to avoid the use of anion exchange columns, an effort was made to isolate  $\beta$ -ISA directly from small aliquots of crude cellulose degradation mixtures using short-path (Kugelrohr) vacuum distillation (see section 2.6.1).

To produce the material to be applied to the distillation, cellulose was degraded using NaOH as above and the method described in section 2.5.1, however, the scale was increased 1 ½-fold and the duration of the reaction was 30 days as opposed to 13 days in the original method. Following the degradation period, the reaction mixture was centrifuged and filtered to remove unreacted cellulose and the pH of the filtrate was lowered to < 2 with the addition of conc. HCl. (~ 100 ml). The reason for adding the HCl was to protonate the ISA and to encourage lactone formation, which is known to occur at pHs below 4<sup>149, 150</sup>, which should increase the volatility of the ISA, making it more amenable for distillation (see section 5.2.2 about the slow rates of lactone formation). The acidified mixture was lyophilised resulting in 90 g of brown solid and to extract the organic compounds from the material, the entire freeze-dried solid was added to an extraction thimble and applied to solid-liquid continuous (Soxhlet) extraction using refluxing ethanol (500 ml) as the extractant. After approximately 24 hrs of extraction, the reaction was stopped; resulting in a white solid being present in the thimble (69 g) and the ethanol was now brown indicating that the coloured material had been extracted into the ethanol. Both HPAEC-PAD and NMR analysis of the white material indicated that no ISA or other organic compounds were present, and it was assumed that the solid was sodium chloride and unreacted cellulose. The extractant was evaporated under reduced pressure resulting in a brown syrup (16.69 g). A small portion of the syrup was dissolved in D<sub>2</sub>O and was analysed by NMR and by comparing the observed resonances with analytical samples, the resulting <sup>1</sup>H spectrum indicated that the syrup contained  $\alpha$ - and  $\beta$ -ISA<sub>L</sub> and 3,4-dihydroxybutano-1,4-lactone (DHB<sub>L</sub>) as the major compounds. There was also the presence of additional groups of resonances at 4.1 ppm and 1.2 ppm (circled), which gave relative integrations of 2 to 3 respectively and additional 2D COSY NMR analysis indicated that there was coupling between the two groups of resonances. The location of the resonances and the integration values suggest that ethyl groups were present in the crude material, suggesting that ethyl ether/ester derivatives of ISA may have been produced due to the effect of the refluxing ethanol in the Soxhlet extraction. Significant amounts of residual ethanol was also present in the un-distilled material, as indicated by the resonances present as a quartet at 3.5 ppm and as a triplet at 1.1 ppm; the location of the ethanol peaks meant that several of the

resonances of the above mentioned compounds were hidden. Also, the overlapping peaks also meant that an accurate integration of the peaks was not possible, but  $\beta$ -ISA appeared to be the major compound in the mixture (Figure 80). HPAEC-PAD analysis of the crude material indicated that the major components were  $\alpha$ -ISA (~ 25 %), DHB (~ 9 %) and  $\beta$ -ISA (66 %) (Figure 84, left).

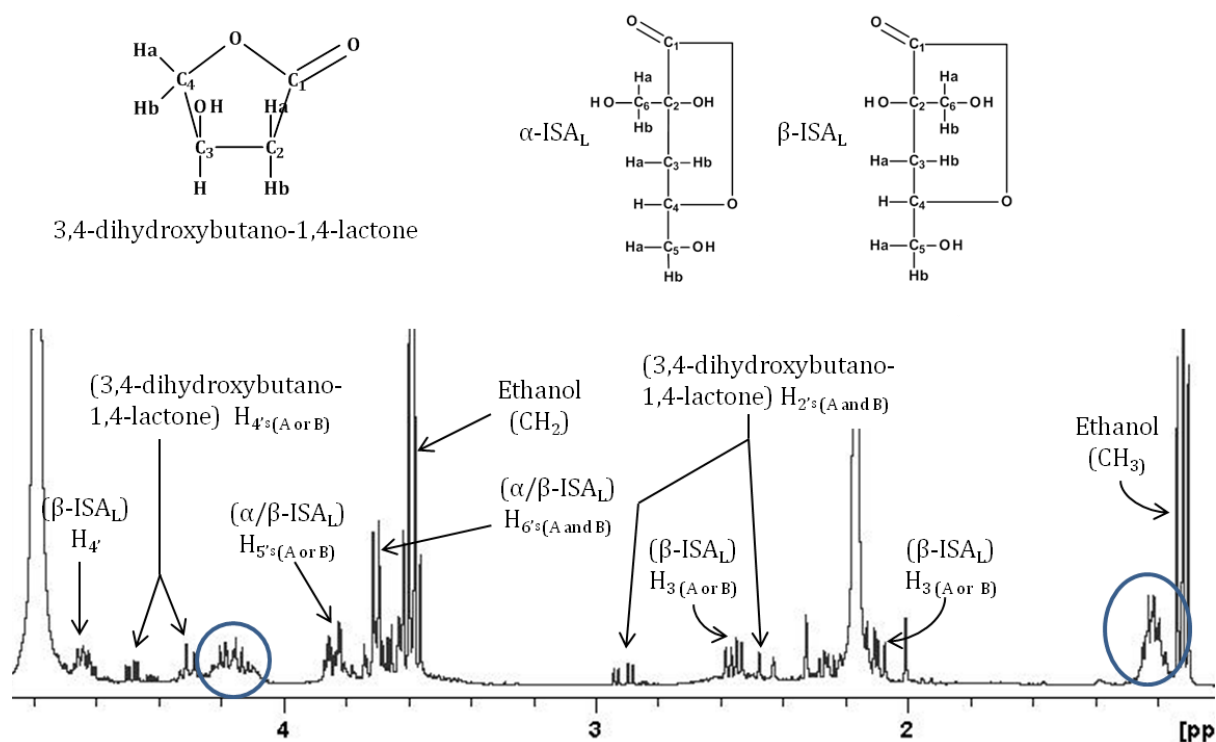


Figure 80:  $^1\text{H}$  NMR spectrum of the crude material before being applied to short-path distillation, with key resonances labelled.

The distillation was attempted 3 times, each time experimenting with different maximum temperatures; in the present work pressures of approximately 1 mm Hg were used. In each distillation attempt ~ 3 ml of sample was applied to the first bulb, which was then connected in series to two additional bulbs. In the first distillation a maximum temperature of 150 °C was used, whereas in the second and third attempts maximum temperatures of 200 °C and 250 °C were used respectively. For each distillation, the first bulb containing the sample was inserted into the cylindrical heating oven and allowed to rotate with the temperature being slowly increased to 150 °C until a small amount of the crude material condensed into the second bulb which was located outside of the heating oven. When no further distillation occurred, the second bulb, which contained the distillate was inserted into the heating oven and the distillation was allowed to proceed, the process was repeated

until there was several  $\mu\text{l}$  of material in each bulb, and the distillation was stopped after approximately 90 minutes. In the first distillation the temperature remained at  $150\text{ }^{\circ}\text{C}$  for the entire experiment, whereas for the additional distillations, the temperature was slowly increased to  $200\text{ }^{\circ}\text{C}$  and  $250\text{ }^{\circ}\text{C}$  respectively. After each of the distillation attempts, the appearance of the resulting collected fractions was very similar for all reaction temperatures: in the first bulb there was a dark brown, thick, sticky solution reminiscent of the initial crude material, which was more charred in the  $250\text{ }^{\circ}\text{C}$  experiment. In the second bulbs there was sticky brown material and in the third bulbs there was a cleaner looking orange solution/syrup. The contents of each bulb were dissolved in  $\text{D}_2\text{O}$  and analysed by NMR.

The  $^1\text{H}$  NMR spectra of the remaining un-distilled material from the 1<sup>st</sup> bulb for both the  $150\text{ }^{\circ}\text{C}$  and  $200\text{ }^{\circ}\text{C}$  distillations were very un-resolved, but by comparing the resonances with those present in the NMR spectra of analytical samples it was indicated that there was still some  $\alpha$ - and  $\beta$ -ISA<sub>L</sub> present in the first bulb (Figure 81), indicating that, until at least  $200\text{ }^{\circ}\text{C}$ , the temperature was too low to achieve a complete transfer of ISA from the first to the second bulb. In the  $150\text{ }^{\circ}\text{C}$  distillation, there was also the presence of DHB<sub>L</sub> remaining in the first bulb, but it was unclear as to whether there was any DHB<sub>L</sub> remaining in the first bulb from the  $200\text{ }^{\circ}\text{C}$  reaction due to the poor quality of the NMR spectrum. As expected, there was no presence of any residual ethanol in the initial fraction from all three distillations due to its relatively low boiling point. The  $^1\text{H}$  NMR spectrum produced from the remaining un-distilled material collected from the first bulb in the  $250\text{ }^{\circ}\text{C}$  distillation indicated that only decomposed, charred material remained and there was no indication of any ISA or other organic compounds, suggesting that at  $250\text{ }^{\circ}\text{C}$ , either all of the ISA has been distilled into the next bulb or it had decomposed, with the latter being the more likely outcome.

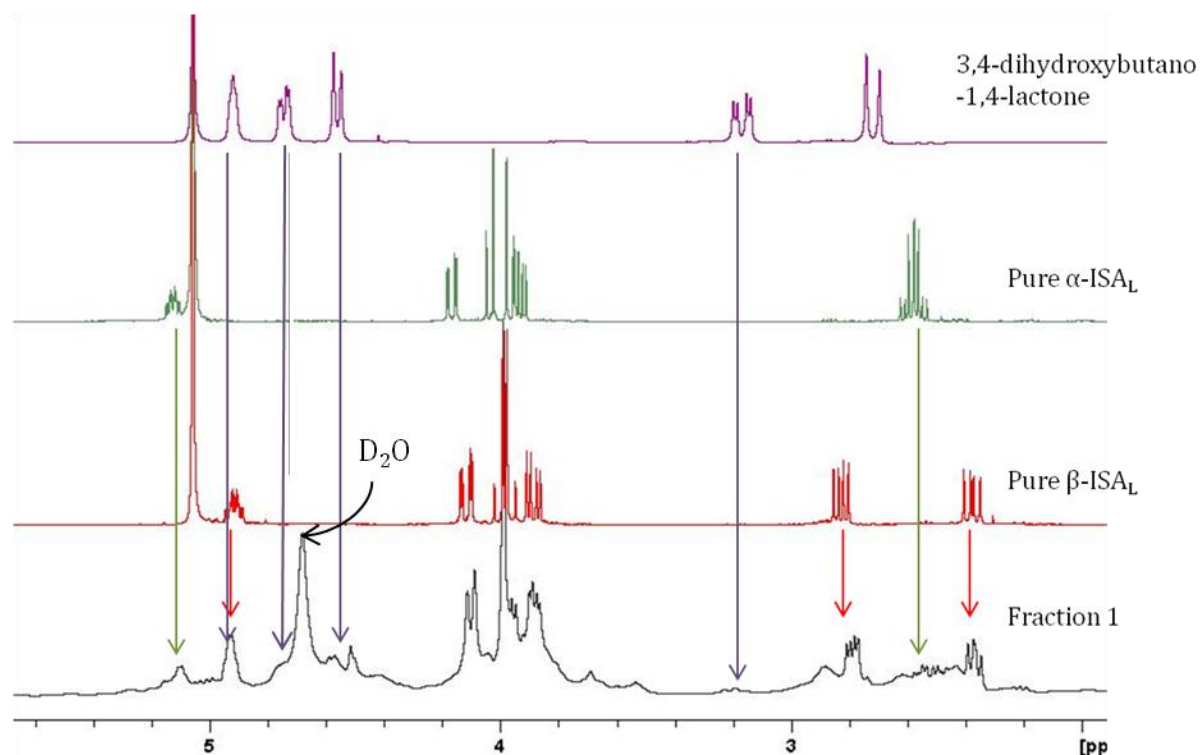


Figure 81: The  $^1\text{H}$  NMR spectrum of fraction number 1, after short-path distillation of crude  $\beta$ -ISA solution where the maximum temperature was 150 °C (bottom spectrum); which is compared with the spectra of  $\beta$ -ISA<sub>L</sub> (red),  $\alpha$ -ISA<sub>L</sub> (green) and 3,4-dihydroxybutano-1,4-lactone (purple)

NMR analysis of the collected fractions from bulb 2 from each distillation experiment indicated that, in the 150 °C distillation,  $\alpha$ - and  $\beta$ -ISA<sub>L</sub> and DHB<sub>L</sub> were all present. By integrating specific resonance peaks, it was determined that  $\beta$ -ISA<sub>L</sub> and DHB<sub>L</sub> were present in similar molar quantities (Figure 82); indicating that, due to the relatively small amount of  $\beta$ -ISA<sub>L</sub> present in relation to the amount of DHB<sub>L</sub>, at 150 °C, the majority of the  $\beta$ -ISA<sub>L</sub> had remained un-distilled in the first bulb. An accurate integration of the  $\alpha$ -ISA<sub>L</sub> peaks was not possible, due to the overlapping of the  $\alpha$ -ISA<sub>L</sub> resonances with those of other analytes, but a rough integration estimated that  $\alpha$ -ISA<sub>L</sub> was present in approximately 3-times lower quantities than  $\beta$ -ISA<sub>L</sub>, indicating that  $\alpha$ - and  $\beta$ -ISA<sub>L</sub> were co-distilling, as that is approximately the ratio of the amount of  $\beta$ - to  $\alpha$ -ISA produced when cellulose is degraded using NaOH as the base.

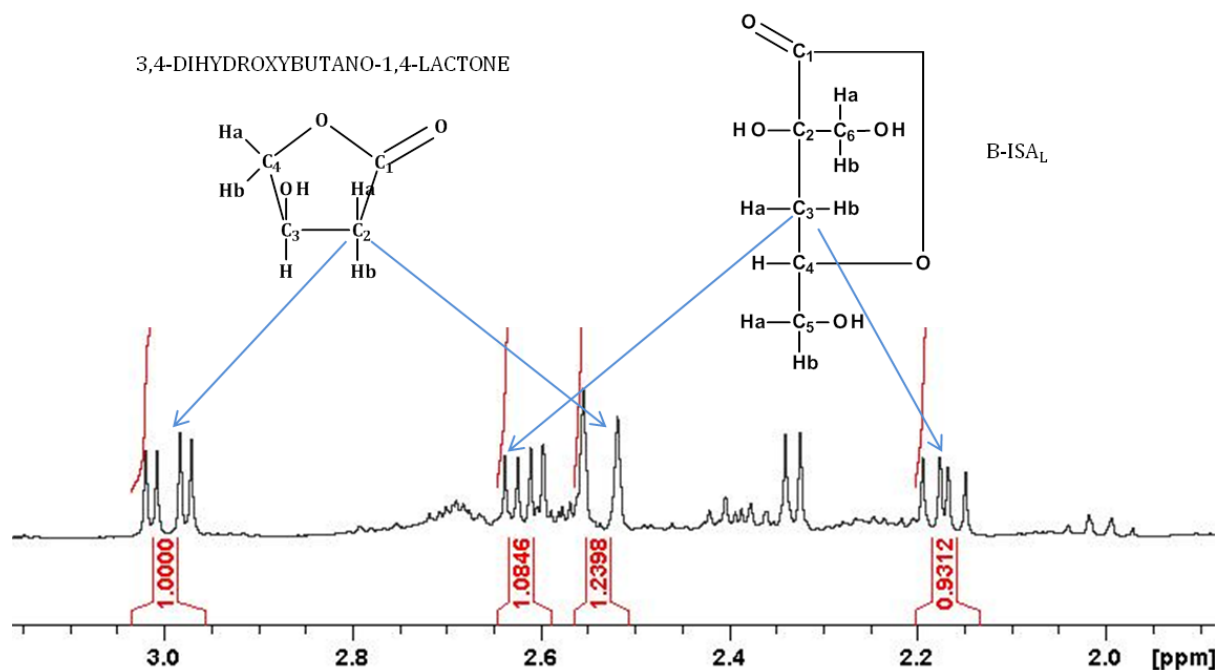
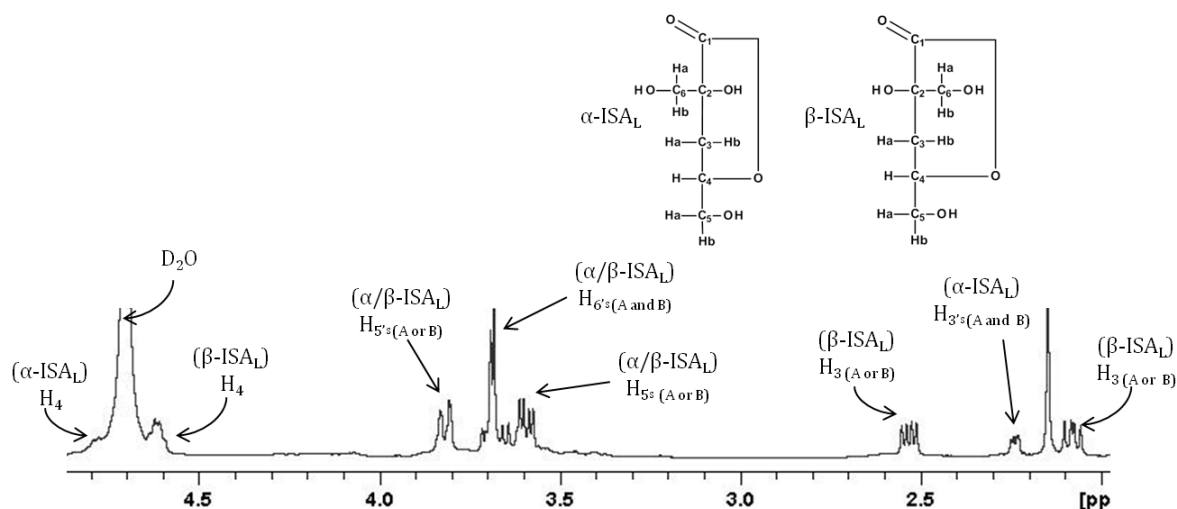
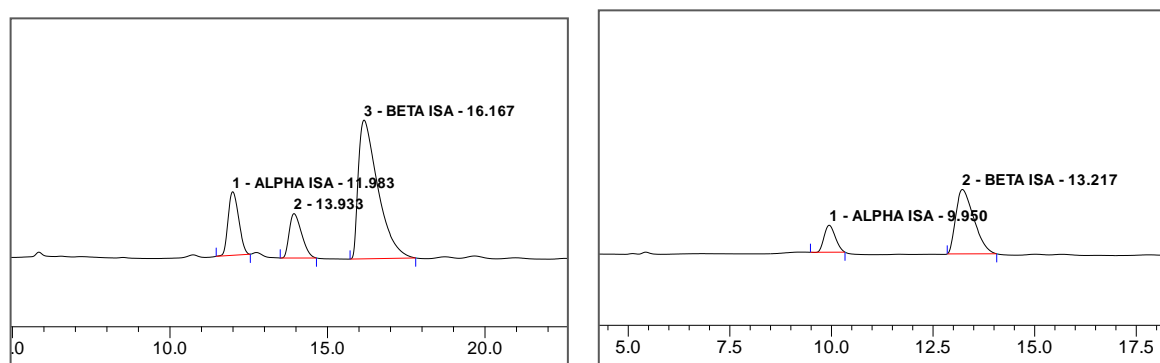


Figure 82: A section of the  $^1\text{H}$  NMR spectrum showing specific resonances which indicate that equal amounts of  $\beta$ -ISA and 3,4-dihydroxybutano-1,4-lactone were present in fraction 2, produced from the short-path distillation of crude  $\beta$ -ISA solution at 150  $^\circ\text{C}$

NMR analysis of the material in the second bulb for both the 200  $^\circ\text{C}$  and 250  $^\circ\text{C}$  distillations indicated that they both contained only  $\alpha$ - and  $\beta$ -ISA<sub>L</sub> with no indication of any DHB<sub>L</sub> or any other species being present, indicating that all the other compounds had been separated from the ISA due to the distillation (Figure 83). The integration of the C3-methylene resonances for both  $\alpha$ - and  $\beta$ -ISA<sub>L</sub> indicated that there was approximately 3 times more of the beta isomer present, which indicates that both isomers were distilling at very similar temperatures, and were not being separated under the current experimental conditions. To further confirm that all of the DHB<sub>L</sub> had been distilled away from the flask which contained the ISAs, a portion of the material which was collected in bulb 2, from the 200  $^\circ\text{C}$  distillation was analysed by HPAEC-PAD, and the results indicate that there was no presence of any DHB<sub>L</sub>, which was clearly present in the un-distilled sample (Figure 84). The results of the 150  $^\circ\text{C}$  distillation indicate that at 150  $^\circ\text{C}$  the temperature was too low, under the present conditions to separate ISA<sub>L</sub> from DHB<sub>L</sub> using distillation.



**Figure 83:**  $^1\text{H}$  NMR spectrum of fraction 2 collected from the short-path distillation of crude  $\beta$ -ISA solution which indicates a mixture of  $\alpha$ - and  $\beta$ -ISA<sub>L</sub>



**Figure 84:** HPAEC-PAD chromatogram of  $\beta$ -ISA solution before short-path distillation (left) and fraction two after short path distillation (right)

The content of the third bulbs were very similar for all distillation temperatures. The major identified product was DHB<sub>L</sub> and there was no obvious sign of any  $\alpha/\beta$ -ISA (Figure 85). However, the  $^1\text{H}$  spectrum indicates the presence of additional resonance peaks which were located in similar positions to the ISA resonances; these were probably concealed by larger ISA peaks in the crude un-distilled solution. The presence of these resonances in latter fractions indicates that the compounds they represent are more volatile than ISA, and it is likely that they represent ester derivatives of ISA due to the reflux of the crude material with ethanol, as previously discussed.

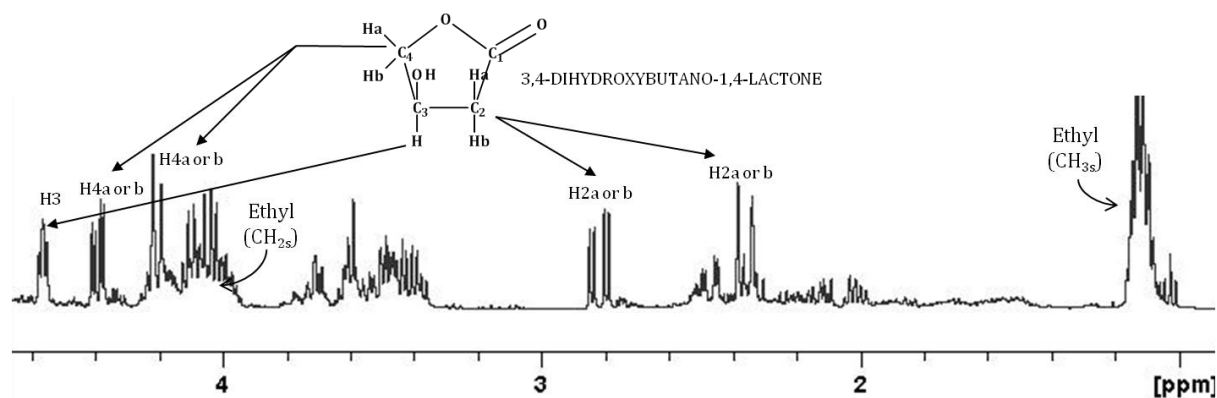


Figure 85: Fraction 3 from the 1st short-path distillation attempt indicating that large amounts of 3,4-dihydroxybutano-1,4-lactone was present in the fraction.

In summary, using short-path distillation, it was not possible to separate  $\alpha$ -ISA from  $\beta$ -ISA, likely as a result of both isomers having very similar boiling points. This became more evident when  $\alpha$ - and  $\beta$ -ISA were analysed using GC-MS (see section 4.5.2), it was determined that the retention time of the two isomers were nearly identical, confirming the similar boiling points. It was determined however that this method could be used to remove other components of crude mixtures such as  $\text{DHB}_L$  and other possibly interfering compounds, indicating that this may be a valuable clean-up method to be used before applying ISA to isolation procedures. Due to the findings of these distillation experiments, short-path distillation was utilised in section 4.5.4.3.1 to isolate small amounts of unknown compounds from solutions which contained large proportions of ISA, which then allowed for the unknown compounds to be characterised using NMR.

#### 4.5 Isolation of $\beta$ -ISA using derivatisation followed by normal phase chromatography

As previously discussed, Whistler and BeMiller<sup>148</sup> and Feast *et al.*<sup>153</sup> used normal phase chromatography to partially separate  $\beta$ -ISA from crude degradation mixtures, and it was reported by Feast *et al.*<sup>153</sup> that small amounts of  $\beta$ -ISA, present as its tribenzoate ester could be isolated using preparative thin layer chromatography. Therefore, with this in mind, in the present work, attempts were made to separate and isolate derivatives of  $\beta$ -ISA using normal phase silica chromatography. Initially, an attempt was made to isolate  $\beta$ -ISA as its triacetate ester and then a further attempt was made to isolate  $\beta$ -ISA as its tribenzoate ester; see Figure 86.

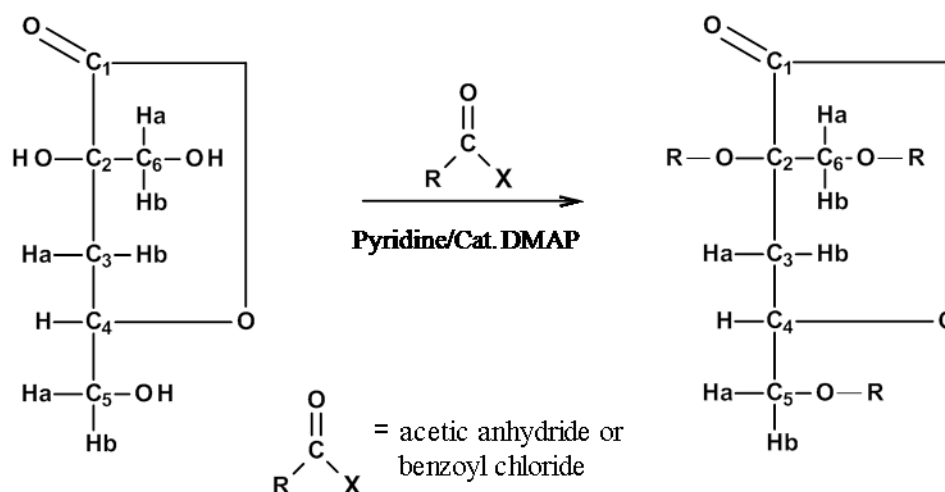


Figure 86: Derivatisation of  $\beta$ -ISA<sub>L</sub> into its tri-acetate or tri-benzoate esters

#### 4.5.1 Acetylation of crude $\beta$ -ISA solution

A portion of a  $\beta$ -ISA<sub>L</sub>-rich syrup (32 g), produced by the degradation of cellulose using the method described in section 2.5.2, was dissolved in pyridine and acetylated using acetic anhydride as the acetylating agent and 4-dimethylaminopyridine (DMAP) as a catalyst (see section 2.6.4.1 for method). A large excess of acetic anhydride was used to facilitate the acetylation, due to the unknown number of compounds present in the syrup. At the end of the reaction any remaining unreacted acetic anhydride was hydrolysed by pouring the reaction mixture onto crushed ice, converting the acetic anhydride into acetic acid. To isolate the resulting acetylated products, chloroform was added to the aqueous mixture and the acetylated products were extracted into the chloroform, which, following filtration and evaporation resulted in 36.6 g of brown syrup.

NMR analysis indicated that the syrup was rich in acetylated  $\alpha$ - and  $\beta$ -ISA<sub>L</sub> and a small amount of impurities. The successful acetylation was indicated by the presence of a large group of overlapping resonances at 2 ppm, which represent the methyls of the acetyl groups. The combined peak area of one of the H3 methylene signals of both  $\alpha$ - and  $\beta$ -ISA was approximately 9-times smaller than the peak area of the combined acetyl methyl groups, indicating that a full degree of acetylation had been achieved for both  $\alpha$ - and  $\beta$ -ISA. The spectrum was similar to that of the free lactones of  $\alpha$ - and  $\beta$ -ISA<sub>L</sub>, however, the position of several resonant peaks had moved, presumably due to the addition of the acetyl

groups (Figure 87). In general, for both  $\alpha$ - and  $\beta$ -ISA the H5 and H6 signals were present in the region of 3.5 – 3.9 ppm for the free lactones, but are shifted slightly down-field at 4.2 – 4.4 ppm for the triacetylated esters. The C4 methyne protons were not acetylated, and as a result their position remains almost unchanged. The general location of the C3 methylene protons are similar to those in the free lactones, but the most striking difference is: for the triacetylated  $\alpha$ -ISA<sub>L</sub> the chemical shifts of the two C3 methylene protons are now clearly separated by  $\sim 0.25$  ppm, whereas, for the free lactone, the chemical shifts were very similar. With the triacetylated  $\beta$ -ISA<sub>L</sub> the opposite is true, the difference between the two chemical shifts for the free lactone was  $\sim 0.4$  ppm, however, for the peracetylated form the difference is only  $\sim 0.1$  ppm.

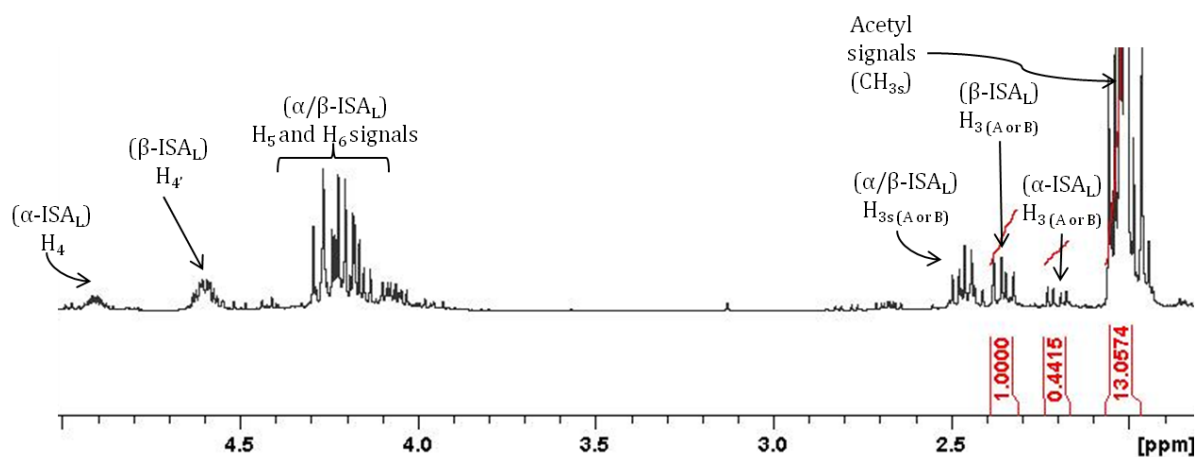


Figure 87:  $^1\text{H}$  NMR spectrum of the acetylated syrup

#### 4.5.2 Purification of 2,5,6-tri-*O*-acetyl- $\beta$ -isosaccharino-1,4-lactone using normal phase chromatography; identification of impurities

In the initial attempt to isolate the acetylated  $\beta$ -ISA and to determine the identity of impurities using normal phase silica chromatography, 16 g of the syrup, which was described in section 4.5.1 was dissolved in a minimum amount of ethyl acetate and applied to a large silica column using the method which was described in section 2.6.4.2. The NMR spectrum of the crude acetylated mixture (Figure 87) indicated that, of the total amount of triacetylated ISA, the mixture contained approximately 70 % of triacetylated  $\beta$ -ISA, 30 % of triacetylated  $\alpha$ -ISA and a small amount of other impurities. The spectrum also indicated that residual pyridine was present which was the solvent used in the acetylation reaction,

due to three resonance peaks being observed at 7.4 - 8.6 ppm (Figure 88, top spectrum). In the initial column, the products were eluted with a mobile phase consisting of 100 % ethyl acetate (1 L, collecting 50 fractions). TLC analysis of the crude syrup indicated that there was one predominant spot with a retardation factor ( $R_f$ ) value of 0.46, and two fainter, smaller spots with  $R_f$  values of 0.26 and 0.20. Fractions collected from the column were screened using TLC and eluted fractions which showed the same  $R_f$  value on the TLC plate were combined and concentrated by evaporation. From the first column, 13 x 20 ml fractions were collected and evaporated (fractions 22 - 34), to give 9 g of syrup. A portion of the syrup was dissolved in  $\text{CDCl}_3$  and analysed by NMR (see Figure 88, bottom, for the  $^1\text{H}$  spectrum).

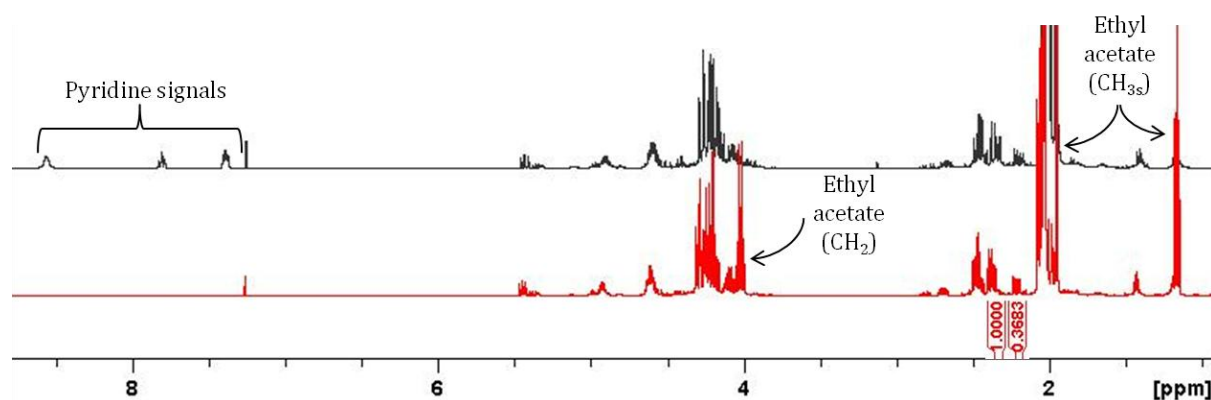


Figure 88:  $^1\text{H}$  NMR spectrum of the collected fractions from the first normal phase column (bottom) and the spectrum of the un-fractionated sample (top).

NMR analysis indicated that the column had failed to separate the triacetylated  $\beta$ -ISA from the  $\alpha$ -ISA, and the results indicated that the predominant spot which was present on the TLC plate was actually a combined spot for both of the ISA triesters. The  $^1\text{H}$  spectrum indicated that all the pyridine had been removed from the sample; however, significant amounts of ethyl acetate were now present.

The remaining syrup (16 g) was applied to another silica column to try to improve the isolation of the triacetylated  $\beta$ -ISA. Prior to the column, the crude syrup was analysed by TLC using various solvent systems, but there was no indication of any separation between the two triesters. To slow down the elution of the products through the column, a mobile phase consisting of 50 % petroleum ether and 50 % ethyl acetate was used to elute the first 80 fractions and then a further 70 fractions were eluted using 100 % ethyl acetate. The TLC of the un-fractionated syrup using the same mobile phase produced a major spot with an  $R_f$

value of 0.33, therefore any fractions eluting from the column with a similar Rf value were collected. The TLC analysis indicated that the desired products were eluting between fractions 80 to 110; those fractions were divided into 3 groups of 10 and each group was concentrated and analysed by NMR. Integration of the corresponding C3 methylene resonances for the triesters of  $\alpha$ - and  $\beta$ -ISA indicated that, as a percentage of the total triacetylated ISA,  $\beta$ -ISA accounted for 64 % in fractions 80 – 90, 72 % in fractions 91 – 100 and 76 % in fractions 101 – 110. The results indicated that the triacetylated  $\alpha$ -ISA was eluting through the column marginally before the triacetylated  $\beta$ -ISA. Also, as previously discussed, there were also several unknown impurity peaks present in the collected fractions (Figure 89).

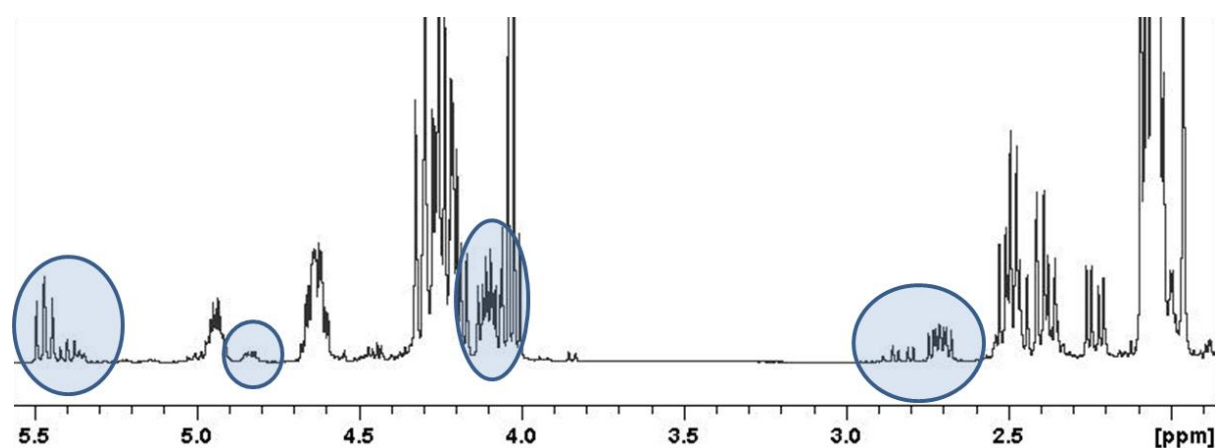
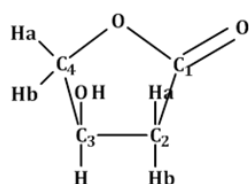
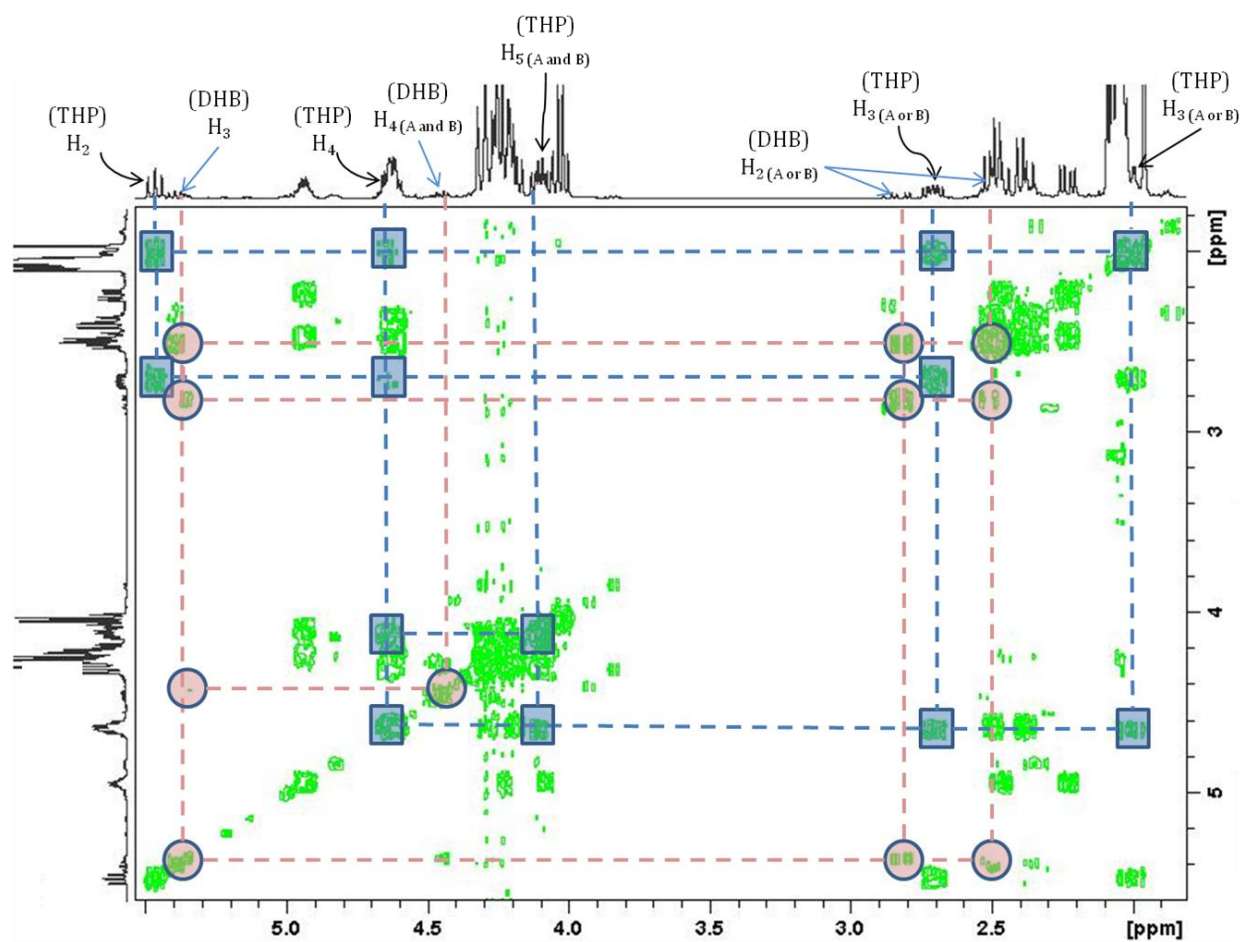


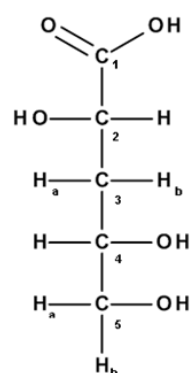
Figure 89:  $^1\text{H}$  NMR of collected fractions 80 - 89 which also indicate that several impurity products are also present (circled resonances).

The identity of the unknown compounds was investigated by analysing the combined fractions 80 – 89 using additional 1D ( $^{13}\text{C}$ , DEPT 135 and DEPT 90) and 2D (COSY, HSQC and HMBC) NMR experiments (see Figure 90 for the labelled COSY spectrum) and the results indicated that at least two additional compounds were present. As expected one of the compounds was  $\text{DHB}_L$ , which was present in minor amounts. The second compound was present in larger amounts than the  $\text{DHB}_L$ ; the integration of specific resonances representing single protons were 4 times bigger for this compound than those representing  $\text{DHB}_L$ , and the compound was identified as 2,4,5-trihydroxypentanoic acid ( $\text{THP}$ ), which was also assumed to be present in the lactone conformation ( $\text{THP}_L$ ) and like the ISA lactones, both  $\text{DHB}_L$  and  $\text{THP}_L$  will also be present as their corresponding acetate esters.  $\text{THP}_L$  has previously been identified as a degradation product in the work of Alfredsson and

Samuelson <sup>129</sup> and Shimizu *et al.* <sup>119</sup> when cellulose was degraded under similar reaction conditions to the ones used in this work.



**3,4-dihydroxybutano-1,4-lactone (DHB<sub>1</sub>)**



**2,4,5-trihydroxypentanoic acid (THP)**

Figure 90: COSY NMR spectrum of the collected fractions 80 - 89, which allowed for the identification of two unknown compounds.

Analysis of the NMR spectrum of the un-fractionated acetylated syrup allowed for an estimation of the quantity of both  $\text{DHB}_L$  and  $\text{THP}_L$  to be made, primarily by comparing the integration of specific resonances of the two additional compounds with those of the triacetylated  $\beta\text{-ISA}_L$ . The results indicated that  $\text{THP}_L$  and  $\text{DHB}_L$  were present in approximately 0.25 and 0.08 molar equivalences in respect to the amount of  $\beta\text{-ISA}_L$  present. As previously discussed, there was approximately 16 g (52 % of 32 g) of  $\beta\text{-ISA}_L$  in the syrup which was applied to the acetylation procedure, so it can be estimated that that the syrup also contained approximately 4 g of acetylated  $\text{THP}_L$  and 0.8 g of acetylated  $\text{DHB}_L$ .

TLC analysis of the fractions collected from the column described above gave no indication of the two additional compounds, probably due to their dilute concentrations in individual fractions, so their elution order was not known. Therefore, additional sets of fractions were concentrated and analysed by NMR; and the results indicated that: fractions 60 – 69 contained none of the above mentioned compounds, however, lactic acid was present indicating that a proportion of the lactic acid had been extracted into the chloroform in the acetylation procedure; fractions 70 – 79 contained  $\text{THP}_L$  as the major product, approximately equal amounts of both  $\text{DHB}_L$  and  $\alpha\text{-ISA}_L$  and smaller amounts of  $\beta\text{-ISA}_L$ ; fractions 80 – 89 contained  $\beta\text{-ISA}_L$  as the major product followed by approximately half as much  $\alpha\text{-ISA}_L$ ,  $\text{THP}_L$  was also present, but in approximately half the quantity of the  $\alpha\text{-ISA}_L$ , a minor amount of  $\text{DHB}_L$  was also present; in combined fractions 90 – 99,  $\beta\text{-ISA}_L$  was the major product, followed by approximately a third of the amount of  $\alpha\text{-ISA}_L$ , a minor amount of  $\text{THP}_L$  was also present, however, no quantifiable amounts of  $\text{DHB}_L$  was present and finally, in the combined fractions 100 – 110,  $\beta\text{-ISA}_L$  was the major product, followed by approximately a quarter of the amount of  $\alpha\text{-ISA}_L$  and there was no presence of any  $\text{THP}_L$  or  $\text{DHB}_L$  in those fractions. The results allow for an estimation of the elution order to be made: (following lactic acid)  $\text{DHB}_L$  is the first analyte to elute from the column due to it being present in relatively large quantities in fractions 70 – 79 in comparison to the amount of  $\text{DHB}_L$  present in the un-fractionated sample.  $\text{THP}_L$  appears to be the second analyte to elute from the column, also due to it being present in large quantities in fractions 70 – 79 in relation to the un-fractionated sample;  $\alpha\text{-ISA}_L$  eluted third from the column and finally  $\beta\text{-ISA}_L$  is the last analyte to elute (see Figure 91 and Table 6 for a summary of the elution order of the compounds and their approximate molar quantities respectively).

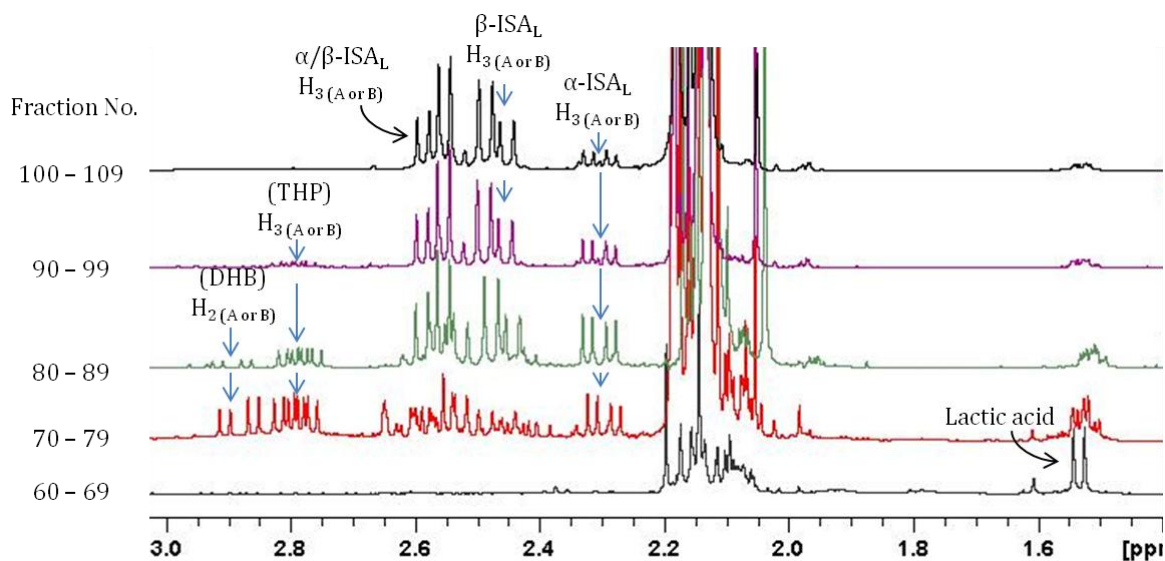


Figure 91:  $^1\text{H}$  NMR spectra showing the elution order of five acetylated compounds from the column of the acetylated crude  $\beta$ -ISA solution.

Table 6: Summary of collected fractions from the second attempt to isolate triacetylated  $\beta$ -ISA<sub>L</sub> using normal phase chromatography

Collected fractions	Approximate molar ratios of acetylated species present in collected fractions based on the integration of peak areas using $^1\text{H}$ NMR spectroscopy			
	$\beta$ -ISA <sub>L</sub>	$\alpha$ -ISA <sub>L</sub>	THP <sub>L</sub>	DHB <sub>L</sub>
70 – 79	< 0.5	0.6	1.0	0.5
80 – 89	1.0	0.6	0.3	< 0.1
90 – 99	1.0	0.4	0.1	-
100 – 110	1.0	< 0.3	-	-

The results of the first column indicated that TLC was not suitable for determining an accurate composition of the triacetylated  $\alpha$ - and  $\beta$ -ISA<sub>L</sub> in the collected fractions, due to both compounds producing the same spot on the TLC plate. To further investigate the content of the collected fractions which were described above, the combined fractions were analysed using GC-MS using the temperature programme described in section 2.6.4.2. GC-MS analysis allowed more accurate relative percentages of the triacetylated  $\alpha$ - and  $\beta$ -ISA<sub>L</sub> to be determined, due to the gas chromatography column separating each analyte and providing an individual peak area for each isomer. The GC-MS provided resolved peaks for the two triesters, however, the retention times of the two peaks were very close (21.2 min for  $\alpha$ -ISA-triacetate and 21.7 for  $\beta$ -ISA-triacetate). The results indicated that in the first set of fractions (70 - 79), the triacetylated  $\alpha$ -ISA<sub>L</sub> was present in the greater amounts, accounting for 60.8 % of the total ISA peak area; and in the subsequent sets of fractions, the

percentage of triacetylated  $\beta$ -ISA<sub>L</sub> increased, until it accounted for ~ 90 % of the total ISA by fractions 110 – 119 (see Table 7).

Table 7: GC-MS results showing the quantity of triacetylated  $\alpha$ - and  $\beta$ -ISA as a percentage of the total amount of triacetylated ISA

Fraction numbers	% of 2,5,6-tri- <i>O</i> -acetyl- $\alpha$ -isosaccharino-1,4-lactone ( $\alpha$ -ISA)	% of 2,5,6-tri- <i>O</i> -acetyl- $\beta$ -isosaccharino-1,4-lactone ( $\beta$ -ISA)
70 - 79	60.8	39.2
80 - 89	31.1	68.9
90 - 99	21.4	78.6
100 - 109	14.3	85.7
110 - 119	11.1	88.9

Fractions 90 – 119, which predominantly contained only the triacetylated  $\alpha$ - and  $\beta$ -ISA lactones were combined and applied to an additional silica column. The combined fractions were evaporated under reduced pressure resulting in 6 g of syrup. Prior to being applied to the column, the syrup was analysed by both GC-MS, which indicated that the syrup contained 84 % of the  $\beta$ -ISA triester and 16 % of the  $\alpha$ -ISA triester. The sample was also analysed by NMR, to investigate the amount of impurities present. The results indicated that there was no indication of any acetylated DHB<sub>L</sub> and only minor amounts of acetylated THP<sub>L</sub> were present (Figure 92).

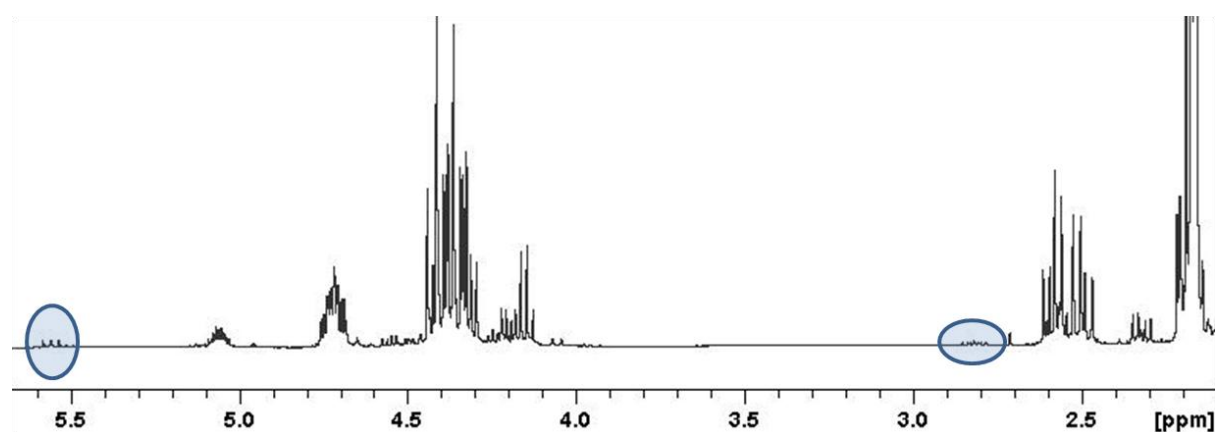


Figure 92:  $^1\text{H}$  NMR spectrum of the combined fractions (90 - 119) showing only minor amounts of THP<sub>L</sub> being present (ringed) and no indication of any DHB<sub>L</sub>.

The syrup was dissolved in ethyl acetate and applied to the column and the products were slowly eluted using a mobile phase which consisted of 50 % petroleum ether and 50 %

ethyl acetate. Altogether 350 fractions were collected and to determine when the products were beginning to elute from the column, the fractions were screened using TLC using the same mobile phase, which indicated that the desired products were eluting after the 75<sup>th</sup> collected fraction. To carefully screen the collected fractions for their triacetylated  $\beta$ -ISA<sub>L</sub> content, after the 75<sup>th</sup> fraction, every 5<sup>th</sup> fraction was directly analysed by GC-MS using the conditions described in section 2.6.4.2. The results indicated that in fractions 75 – 85 triacetylated  $\alpha$ -ISA<sub>L</sub> was the major product; and the peak area (arbitrary units) indicated that maximum concentrations were achieved in the 85<sup>th</sup> fraction, where the triacetylated  $\alpha$ -ISA<sub>L</sub> accounted for 56 % of the total peak area and after the 85<sup>th</sup> fraction, the amount of the triacetylated  $\alpha$ -ISA<sub>L</sub> began to fall. In the 90<sup>th</sup> fraction, the triacetylated  $\beta$ -ISA<sub>L</sub> constitutes 75 % of the peak area and gradually increases until it accounted for 90 % by the 100<sup>th</sup> fraction, and the percentage remained at ~ 90 % until the 150<sup>th</sup> fraction, following this the triacetylated  $\beta$ -ISA<sub>L</sub> content gradually increases to  $\geq 99$  % by the 350<sup>th</sup> fraction. Maximum concentrations of the triacetylated  $\beta$ -ISA<sub>L</sub> were observed in the 105<sup>th</sup> fraction, and following this the concentration began to fall until only trace amounts were present in the final fractions (a summary of the composition of selected fractions is presented in Table 8).

Table 8: The percentage and magnitude of triacetylated  $\alpha$ - and  $\beta$ -ISA<sub>L</sub> in collected fractions, determined using GC-MS

Fraction numbers	% of 2,5,6-tri- <i>O</i> -acetyl- $\alpha$ -isosaccharino-1,4-lactone	% of 2,5,6-tri- <i>O</i> -acetyl- $\beta$ -isosaccharino-1,4-lactone	Magnitude of the $\alpha$ -ISA peak area	Magnitude of the $\beta$ -ISA peak area
75 - 85	56	44	$4.4 \times 10^7$	$3.5 \times 10^7$
90	25	75	$2.2 \times 10^7$	$6.6 \times 10^7$
95	14	86	$1.3 \times 10^7$	$8.4 \times 10^7$
100	10	90	$1.1 \times 10^7$	$9.4 \times 10^7$
105	10	90	$1.1 \times 10^7$	$1.0 \times 10^8$
110	10	90	$8 \times 10^6$	$7.2 \times 10^7$
150	10	90	$4.9 \times 10^6$	$4.5 \times 10^7$
200	6	94	$8.0 \times 10^5$	$1.2 \times 10^7$
235	0.25	99.75	$4.7 \times 10^3$	$1.9 \times 10^6$
240 - 350	< 1	> 99	-	-

The GC-MS analysis of the fractions allowed for the fractions rich ( $\geq 90$  %) in triacetylated  $\beta$ -ISA<sub>L</sub> to be combined. Combined fractions 100 – 350 were evaporated under reduced pressure to remove the solvent resulting in 2.51 g of pale yellow syrup. NMR analysis of this syrup revealed high purity triacetylated  $\beta$ -ISA<sub>L</sub> in greater than 90 % purity with minor

amounts of triacetylated  $\alpha$ -ISA being present; there was no indication of any other impurities other than residual ethyl acetate.

Several attempts were made to precipitate pure triacetylated  $\beta$ -ISA<sub>L</sub> from the syrup by dissolving portions of the syrup in either diethyl ether or acetonitrile and adding petroleum ether or water as counter solvent respectively until the solution was saturated and each solution was left to stand for several days; however, precipitation did not occur. In an additional attempt to crystallize the sample, the syrup was dissolved in ethyl acetate and the solvent was allowed to slowly evaporate to see if crystallisation could be achieved, however, this was also unsuccessful.

The triacetylated  $\beta$ -ISA<sub>L</sub>-rich syrup (2.51 g) was recovered from the crystallization attempts and taken forward to the deacetylation procedure, using the method described in section 2.6.4.3. The acetylated lactones were ring-opened by hydroxide catalysed hydrolysis and the esters were deacetylated using Zemplén methods<sup>211</sup> which resulted in 2.09 g of white solid. NMR analysis of the solid indicated the sodium salt of  $\beta$ -ISA in greater than 90 % purity (Figure 93).

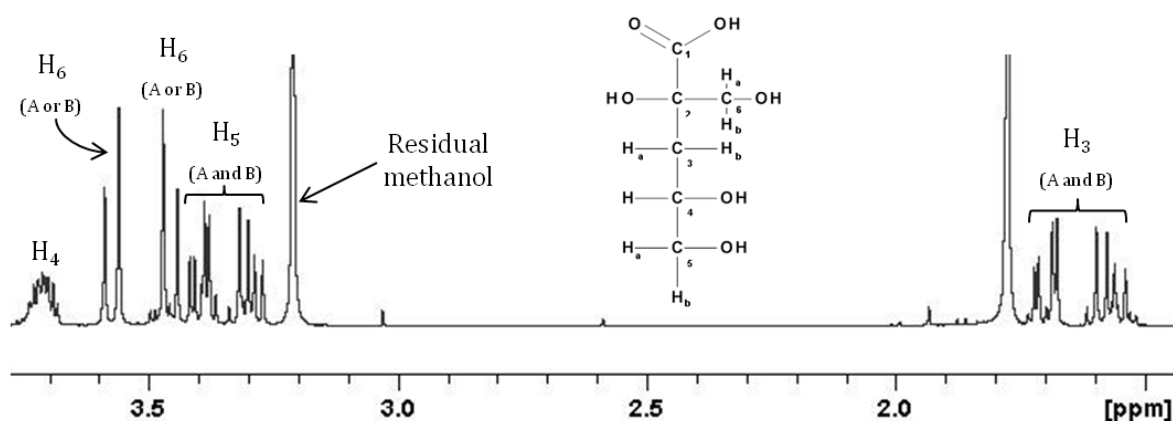


Figure 93: <sup>1</sup>H NMR spectrum of the  $\beta$ -ISA sodium salt which was isolated using normal phase chromatography.

In summary, by acetylating the components of the crude  $\beta$ -ISA solution and applying the acetylated mixture down a normal phase silica column, approximately 2 g of high purity  $\beta$ -ISA was isolated from the initial crude  $\beta$ -ISA solution which contained ~ 21 g of  $\beta$ -ISA. In the subsequent section, further attempts will be described which were made to improve the normal phase chromatography method by eluting  $\beta$ -ISA<sub>L</sub> as its tribenzoate ester. It was

hoped that by adding a larger protecting group, that crystallisation of the derivatised  $\beta$ -ISA<sub>L</sub> may be achieved.

#### 4.5.3 Benzoylation of crude $\beta$ -ISA solution

To prepare a crude mixture of tribenzoate esters of  $\alpha$ - and  $\beta$ -ISA the method of Whistler and BeMiller was followed<sup>148</sup> which was described in section 2.6.4.4. In general, a portion of the  $\beta$ -ISA<sub>L</sub>-rich syrup, which was prepared using the method described in section 2.5.2, was dissolved in pyridine and benzoyl chloride was used as the benzoylating agent, which, like the acetylation reaction, also utilised DMAP as a catalyst (Figure 86).

Prior to benzoylating the crude mixture of ISA lactones, a pure sample of  $\alpha$ -ISA<sub>L</sub> was derivatised using the same procedure so that a model NMR spectrum could be obtained and used to identify the resonances of benzoylated  $\alpha$ -ISA<sub>L</sub> when it was present in mixed solutions. The NMR spectrum of the tribenzoylated  $\alpha$ -ISA<sub>L</sub> (Figure 94) was very similar to the spectrum of the triacetylated  $\alpha$ -ISA<sub>L</sub>, with the main difference being the resonances representing the aromatic protons of the benzoyl groups, present between 7.5 and 8.5 ppm, instead of the signals for the acetyl groups, present at 2 ppm for the triacetates.

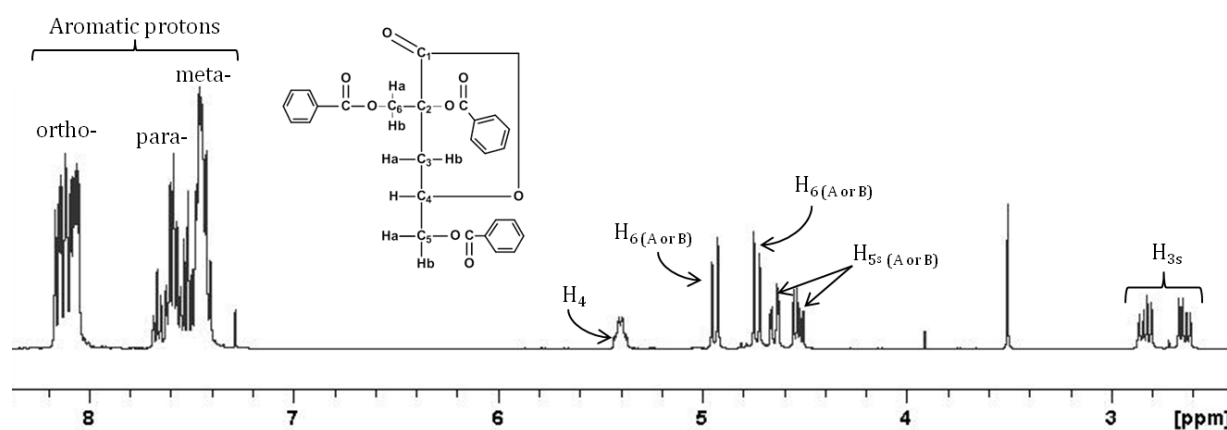


Figure 94: <sup>1</sup>H NMR spectrum of tribenzoylated alpha ISA<sub>L</sub>

A model spectrum of tribenzoylated  $\beta$ -ISA<sub>L</sub> was not available at the time of analysis, because an adequate sample of pure  $\beta$ -ISA was not available; however, during the course of the work resonances of the tribenzoylated  $\beta$ -ISA<sub>L</sub> were determined when a sample was isolated. The major difference between the <sup>1</sup>H spectra of the  $\alpha$ - and  $\beta$ -ISA<sub>L</sub> tribenzoates was: the C3 methylene signals for the tribenzoylated  $\alpha$ -ISA<sub>L</sub> were present as AMX splitting

patterns, clearly separated by  $\sim 0.2$  ppm at 2.6 and 2.8 ppm, whereas for the tribenzoylated  $\beta$ -ISA<sub>L</sub>, both protons were present as a single doublet at  $\sim 2.8$  ppm (Figure 95). This distinctive doublet, which was unlike the C3 methylene signals of all the previously witnessed forms of  $\beta$ -ISA, allowed for an easy identification of benzoylated  $\beta$ -ISA<sub>L</sub> in solutions and indicates that the two tribenzoylated isomers are conformationally quiet different (see section 4.5.4.5).

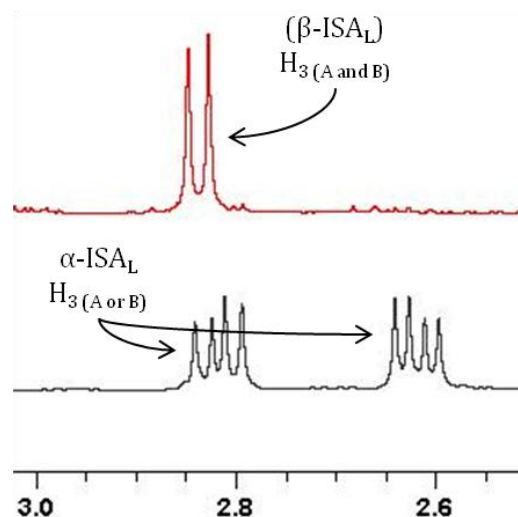


Figure 95:  $^1\text{H}$  NMR spectra showing the C3 methylene resonances of tribenzoylated  $\alpha$ - and  $\beta$ -ISA<sub>L</sub>.

In solutions of mixed tribenzoylated ISA lactones, the representative resonances of the two isomers overlap each other, so to determine the degree of benzoylation, the ratio of the combined peak areas of the C3 methylene protons to the peak area of the ortho (or meta/para) benzoyl group protons was calculated. When the mixture contains only  $\alpha$ - and  $\beta$ -ISA<sub>L</sub> tribenzoates, a ratio of 3 : 1 is expected, however, in crude mixtures, the ratio is expected to be slightly higher due to the presence of other compounds which may also contain benzoyl groups and increase the size of the ratio.

In the initial benzoylation attempt, 69 g of  $\beta$ -ISA<sub>L</sub>-rich syrup, which contained approximately 16 g of  $\beta$ -ISA and 5.4 g of  $\alpha$ -ISA, was derivatised resulting in the production of  $\sim 150$  g of a very sticky, brown syrup; a small sample of which was dissolved in  $\text{CDCl}_3$  and analysed by NMR spectroscopy. The  $^1\text{H}$  NMR spectrum of the benzoylated mixture (Figure 96) indicated that benzoylated ISA lactones were present, as indicated by the presence of the distinctive C3 methylene signal, present as a doublet for the benzoylated  $\beta$ -ISA<sub>L</sub>. However, the ratio between the C3 methylene signals and the aromatic ortho protons

was  $\sim 1 : 7$ , which was higher than expected, but can be explained by the presence of benzoic acid in the derivatised mixture. In the benzoylation reaction, an excess of benzoyl chloride was used as the benzoylating reagent, and following the completion of the reaction, the reaction mixture was poured onto crushed ice to hydrolyse any un-reacted benzoyl chloride, resulting in the production of benzoic acid. The resonances produced in the NMR chromatogram of pure benzoic acid overlap the resonances of the aromatic protons of the benzoyl groups, which results in the resonances for those protons increasing in size if benzoic acid is present (Figure 96, inset).

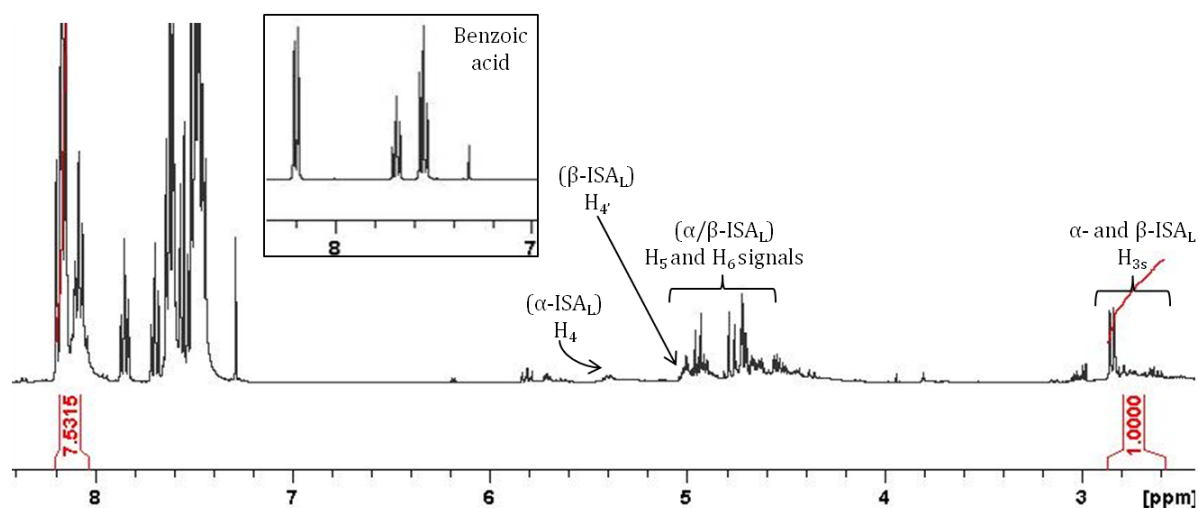


Figure 96:  $^1\text{H}$  NMR spectra of crude benzoylated ISA lactones and the  $^1\text{H}$  NMR spectra of benzoic acid, inset.

An excess of benzoyl chloride is required in the reaction because other CDPs are present in the crude syrup, which also contain alcohol groups that are amenable to react and consume some of the benzoyl chloride, producing other benzoylated compounds. The presence of residual water in the syrup will also result in the loss of some benzoyl chloride due to hydrolysis; in the presence of pyridine and water benzoyl chloride is known to produce benzoic anhydride<sup>212</sup>.

A pair of experiments was performed to investigate the effect of reducing the amount of benzoyl chloride used, to limit the production of benzoic acid. Two comparative benzoylation reactions were performed on the crude  $\beta$ -ISA solution, using the method described in section 2.6.4.4. In one of the reactions approximately 3 equivalents of benzoyl chloride was used, based on the estimated amount of ISA present in the crude syrup and in

the other reaction, a large excess of benzoyl chloride was used. In the excess reaction, 135 g of sticky black syrup was produced, and NMR analysis of the syrup indicated that successful benzoylation had taken place. However, in the equivalence reaction, the mass of the sticky black syrup was only 42.6 g and the resulting NMR analysis of the syrup indicated no evidence that benzoylation of  $\alpha/\beta$ -ISA<sub>L</sub> had taken place. The aqueous phase from the equivalence reaction was also analysed by NMR, and the resulting <sup>1</sup>H spectrum indicated that underivatized  $\alpha$ - and  $\beta$ -ISA lactones were present, whereas the NMR analysis of the aqueous phase from the excess reaction showed no indication of the presence of any ISA.

#### **4.5.4 Purification of 2,5,6-tri-*O*-benzoyl- $\beta$ -isosaccharino-1,4-lactone using normal phase chromatography**

##### **4.5.4.1 First isolation attempt**

Prior to the initial isolation attempt, it was determined that by adding hot water to the crude benzoylated syrup, small amounts of benzoic acid could be extracted into the water, and precipitated from the water upon cooling, following which, the benzoic acid slurry was decanted. This procedure was repeated 3 times, each time resulting in the removal of additional benzoic acid. The remaining insoluble syrup was dissolved in chloroform, separated from the remaining water and evaporated under reduced pressure to produce 88 g of thick, brown syrup. However, NMR analysis of the syrup revealed that large amounts of benzoic acid were still present; also the <sup>1</sup>H NMR spectrum of the crude syrup indicated the presence of DHB<sub>L</sub> and THP<sub>L</sub> benzoate esters. By integrating specific resonance peaks, it was determined that THP<sub>L</sub> and DHB<sub>L</sub> were present in approximately 0.29 and 0.19 molar equivalents in respect to the amount of  $\beta$ -ISA<sub>L</sub> present. As previously discussed, there was approximately 16 g of  $\beta$ -ISA<sub>L</sub> in the syrup which was applied to the benzoylation procedure, so it can be estimated that the syrup also contained 3.8 g of THP<sub>L</sub> and 1.9 g of DHB<sub>L</sub>.

In the initial isolation attempt, ~ 50 g of the syrup was diluted in a minimum amount of ethyl acetate and applied to a normal phase silica column (8 x 30 cm) and the syrup was eluted with a linear gradient starting with 75 % petroleum ether and 25 % ethyl acetate, rising by 25 % ethyl acetate after the addition of every 1000 ml of mobile phase, until 100 % ethyl acetate was used (6 L), collecting 300 x 20 ml fractions. TLC analysis of the crude

syrup using 50 % petroleum ether and 50 % ethyl acetate produced a major spot with an Rf value of 0.74, representing the combined ISA tribenzoates; therefore any fractions eluting from the column with a similar Rf value were collected. The TLC also indicated a second spot with an Rf value of 0.65, which gave the same Rf value as that of a pure sample of benzoic acid. The spot from the benzoic acid was distinctive due to there being an elongated tail which ran from the bottom of the spot to the base line of the TLC plate. There was also the presence of several additional minor spots on the TLC plate with smaller Rf values. TLC analysis of the eluted fractions indicated that the desired products with an Rf value of  $\sim 0.74$  were eluting very rapidly from the column, with the first spots being observed after the 15<sup>th</sup> fraction, and the same spot was present until the 200<sup>th</sup> fraction. There was also an indication that benzoic acid was eluting after the 20<sup>th</sup> fraction and two minor spots were observed after the 75<sup>th</sup> and after the 90<sup>th</sup> collected fraction respectively; fractions were divided into smaller groups and each group was concentrated and analysed by NMR.

Evaporation of fractions 5 – 15 afforded 220 mg of pale yellow syrup and NMR analysis of the syrup indicated that it contained a mixture of tribenzoylated  $\alpha$ - and  $\beta$ -ISA<sub>L</sub> in approximately equal amounts (Figure 97), and there was no indication of any benzoic acid and only minor amounts of other impurities were present.

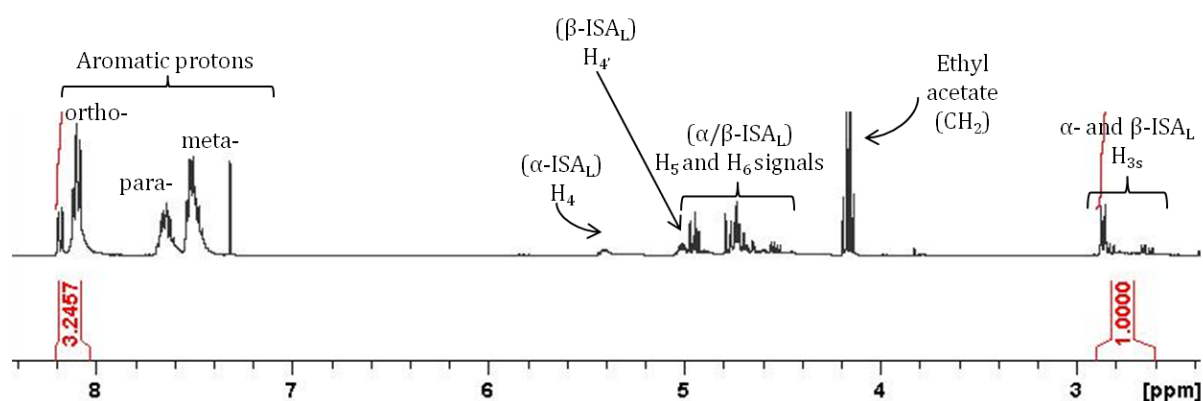


Figure 97:  $^1\text{H}$  NMR spectrum of the isolated mixture of  $\alpha$ - and  $\beta$ -ISA tribenzoate esters

In each subsequent combined set of fractions, there was a large amount of co-eluting benzoic acid. In fractions 16 – 40 tribenzoylated  $\beta$ - and  $\alpha$ -ISA<sub>L</sub> were the major (benzoylated) compounds present and THP<sub>L</sub> was also detected in the fractions, present in approximately 5-fold lower molar equivalences than  $\beta$ -ISA<sub>L</sub>. In fractions 45 – 65,  $\beta$ -ISA<sub>L</sub> was still the major detected compound, present in approximately twice the quantity of both

$\alpha$ -ISA<sub>L</sub> and THP<sub>L</sub>, and DHB<sub>L</sub> was now also present, in approximately 12-fold lower molar equivalences than the amount of  $\beta$ -ISA<sub>L</sub>. In fractions 75 – 115, the three major compounds were present in a similar ratio to the ones seen in the previous set of fractions, but DHB<sub>L</sub> was now present in larger quantities, but still approximately 4 times less than the amount of  $\beta$ -ISA<sub>L</sub> (see Table 9). The remaining fractions contained significant amounts of benzoic acid and other unknown impurities.

Table 9: Summary of collected fractions from the first attempt to isolate tribenzoylated  $\beta$ -ISA<sub>L</sub> using normal phase chromatography

Collected fractions	Molar ratio of species present in collected fractions based on the integration of peak areas using <sup>1</sup> H NMR spectroscopy				
	Appearance and mass	$\beta$ -ISA <sub>L</sub>	$\alpha$ -ISA <sub>L</sub>	THP <sub>L</sub>	DHB <sub>L</sub>
5 -15	220 mg of yellow syrup	1.0	0.8	Minor trace	Not observed
16 – 40	17.28 g of white solid	1.0	0.5	0.2	Not observed
45 - 65	4.5 g of white solid	1.0	0.5	0.4	0.1
75 - 115	10.23 g of orange syrup	1.0	0.4	0.5	0.3

The syrup which was collected in fractions 5 – 15, from the previously described column, which contained no benzoic acid and very little other impurities, was applied to a second column using a more non-polar mobile phase to slow down the elution of the products. For this isolation attempt, a smaller column was used (2 x 35 cm) and the syrup (220 mg) was dissolved in a minimum amount of ethyl acetate and eluted through the column using a linear gradient starting with 90 % petroleum ether and 10 % ethyl acetate, rising by 5 % ethyl acetate after the addition of every 500 ml of mobile phase, until 25 % ethyl acetate was used (2 L, collecting 100 fractions). TLC of the un-fractionated material using 70 % ethyl acetate and 30% petroleum ether resulted in one spot with an R<sub>f</sub> value of 0.31. Fractions 50 – 84 produced a spot with the same R<sub>f</sub> value so those fractions were collected and further divided into 3 sets of fractions, each of which afforded clear syrup upon evaporation. Fractions 50 – 60 produced 80 mg of syrup and NMR analysis indicated that the syrup was primarily a mixture of tribenzoylated  $\alpha$ -ISA<sub>L</sub> (51 %) and tribenzoylated  $\beta$ -ISA<sub>L</sub> (49 %), with little indication of any other impurities being present, other than residual ethyl acetate. Fractions 61 – 71 produced 80 mg of clear syrup and analysis using a combination of 1D (<sup>1</sup>H, <sup>13</sup>C, DEPT 135 and DEPT 90) and 2D (COSY, HSQC and HMBC) NMR spectroscopy confirmed that the syrup was rich in tribenzoylated  $\beta$ -ISA<sub>L</sub> in greater than 95 % purity (see section 2.6.4.6, for NMR data), with no indication of any tribenzoylated  $\alpha$ -ISA<sub>L</sub> being present (see Figure 98); fractions 72 – 84 produced ~ 50 mg of

syrup which contained trace amounts of tribenzoylated  $\beta$ -ISA<sub>L</sub> and other unknown impurities.

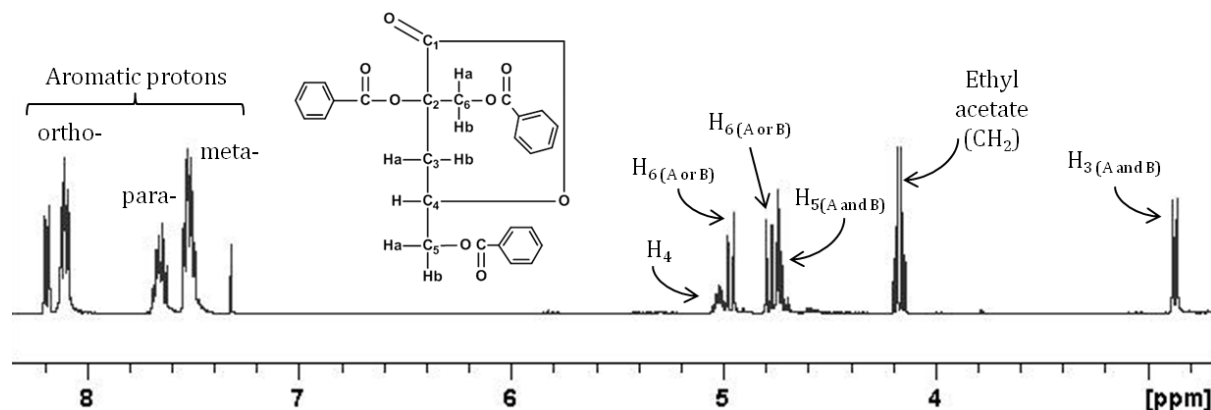


Figure 98:  $^1\text{H}$  NMR spectrum of tribenzoylated  $\beta$ -ISA<sub>L</sub>

The results of the previous two columns indicate that the key to isolating pure tribenzoylated  $\beta$ -ISA<sub>L</sub>, using normal phase silica chromatography, was to elute the crude dark-brown benzoylated syrup through an initial fast eluting “crude” column to “clean-up” the syrup; which, in the initial column, resulted in the removal of all the polar coloured impurities and finally to elute the clean syrup through an additional column using very slow elution conditions.

#### 4.5.4.2 Removal of coloured impurities

In an attempt to increase the yield of the isolated tribenzoylated  $\beta$ -ISA<sub>L</sub>, initially, the coloured impurities were removed from the remaining crude benzoylated syrup (~ 38 g) by eluting the syrup through a wide bed of silica (12 cm diameter x 5 cm depth). Using the method described in section 2.6.4.5, the brown syrup was dissolved in chloroform and the components of the syrup were directly adsorbed onto silica, producing a brown-coloured dry mixture. The dry mixture was spread evenly onto the wide bed of silica and crudely fractionated by eluting the products with 75 % petroleum ether and 25 % ethyl acetate, resulting in the collection of 8 large fractions (250 ml). The relatively non-polar mobile phase which was used, resulted in the polar coloured impurities being retained on the silica and the collection of almost clear/very pale yellow coloured fractions. TLC of the crude syrup, using the same mobile phase composition gave a strong spot with an R<sub>f</sub> value of

0.27 and TLC of the collected fractions indicated that fractions 5 to 8 contained a single spot of the same R<sub>f</sub> value, so those fractions were combined. Fractions 1 to 4 also displayed a spot with a similar R<sub>f</sub> value, but in those fractions there was also the presence of the elongated tailing which suggested that benzoic acid was present. Evaporation of fractions 1 to 4 produced 6.93 g of white solid and NMR analysis of the solid indicated the presence of approximately equal amounts of the tribenzoylated ISA lactones and minor amounts of THP<sub>L</sub> and DHB<sub>L</sub>, however, the ratio of the peaks for the combined C3 methylene protons representing the tribenzoylated  $\alpha$ - and  $\beta$ -ISA<sub>L</sub> to the aromatic ortho protons was ~ 1 : 42, indicating a large excess of benzoic acid was present. Evaporation of fractions 5 to 8 produced 5.92 g of pale yellow syrup, NMR analysis indicated that the syrup contained the tribenzoylated  $\alpha$ - and  $\beta$ -ISA<sub>L</sub> with the beta isomer accounting for approximately 70 % of the total derivatised ISA; THP<sub>L</sub> was also present in similar amounts to the amount of the tribenzoylated  $\alpha$ -ISA<sub>L</sub>; and DHB<sub>L</sub> was present in approximately half the amount of both  $\alpha$ -ISA<sub>L</sub> and THP<sub>L</sub>. The ratio of the C3 methylene protons to the aromatic ortho protons was 1 : 3.9 indicating that only minor amounts of benzoic acid were present in the sample.

#### 4.5.4.3 Second isolation attempt

The translucent syrup produced from fractions 5 – 8, described in section 4.5.4.2 (5.92 g) was dissolved in a minimal amount of ethyl acetate and applied to a large silica column (5 x 55 cm) and the products were eluted very slowly using a linear gradient starting with 95 % petroleum ether and 5 % ethyl acetate, rising by 5 % ethyl acetate after the addition of every 1000 ml of mobile phase, until 25 % ethyl acetate was used (2.5 L, collecting 300 fractions). TLC analysis of the collected fractions indicated that products were being eluted from the column after the 100<sup>th</sup> fraction; between fractions 100 to 145 there was no obvious spot but the elongated tail of benzoic acid was present, which reduced in size until it disappeared after fraction 145 and NMR analysis indicated that those fractions contained predominantly pure benzoic acid (240 mg). Upon further analysis, the NMR spectrum also indicated that at least two other compounds were present in the fraction, in minor amounts in comparison to the amount of benzoic acid. Further analysis of the fraction using a combination of 1D (<sup>1</sup>H, <sup>13</sup>C, DEPT 135 and DEPT 90) and 2D (COSY, HSQC and HMBC) NMR spectroscopy identified two additional compounds (Figure 99). One of the compounds was confidently identified as 2,5-dihydroxypentanoic acid (DHP), this compound has previously been reported as being a cellulose degradation product by both Niemela and Sjostrom<sup>117</sup> and Alfredsson and Samuelson<sup>129</sup> when cellulose was degraded

under similar reaction conditions. The second identified compound was present in approximately 4 times smaller amounts than the amount of DHP and was only tentatively identified as being 2,3-dideoxypentonic acid (DDP). This compound has also been reported as being a product of the alkaline degradation of cellulose under both anaerobic and aerobic conditions by Niemela and Sjoström<sup>117</sup> and Niemela<sup>176</sup> respectively. It is expected that both of these compounds were present as lactones, due to the low pH of the solution prior to the benzylation reaction. DHP<sub>L</sub> is expected to be present as a 1,5-linked lactone due to an hydroxyl group being present on the C5 carbon. DDP<sub>L</sub> has hydroxyl groups on both C4 and C5, but the H4 methyne proton is located significantly further down-field (~ 6 ppm) than the H5 methylene protons (~ 3 ppm), indicating that the DDP is present as a 1,4-linked lactone. If both compounds were lactones, they would both be present as singly benzyolated derivatives due to only one additional alcohol group being available. The ratio between the combined integrated peak area of the methyne protons located at C4 for DDP<sub>L</sub> and C2 for DHP<sub>L</sub> (representing 1 proton) to the peak area of the aromatic para proton of the benzoyl groups should be 1 : 1, however, in the present sample, the ratio was ~ 1 : 50, indicating that the two compounds were only present in trace amounts and the vast majority of the sample was benzoic acid.

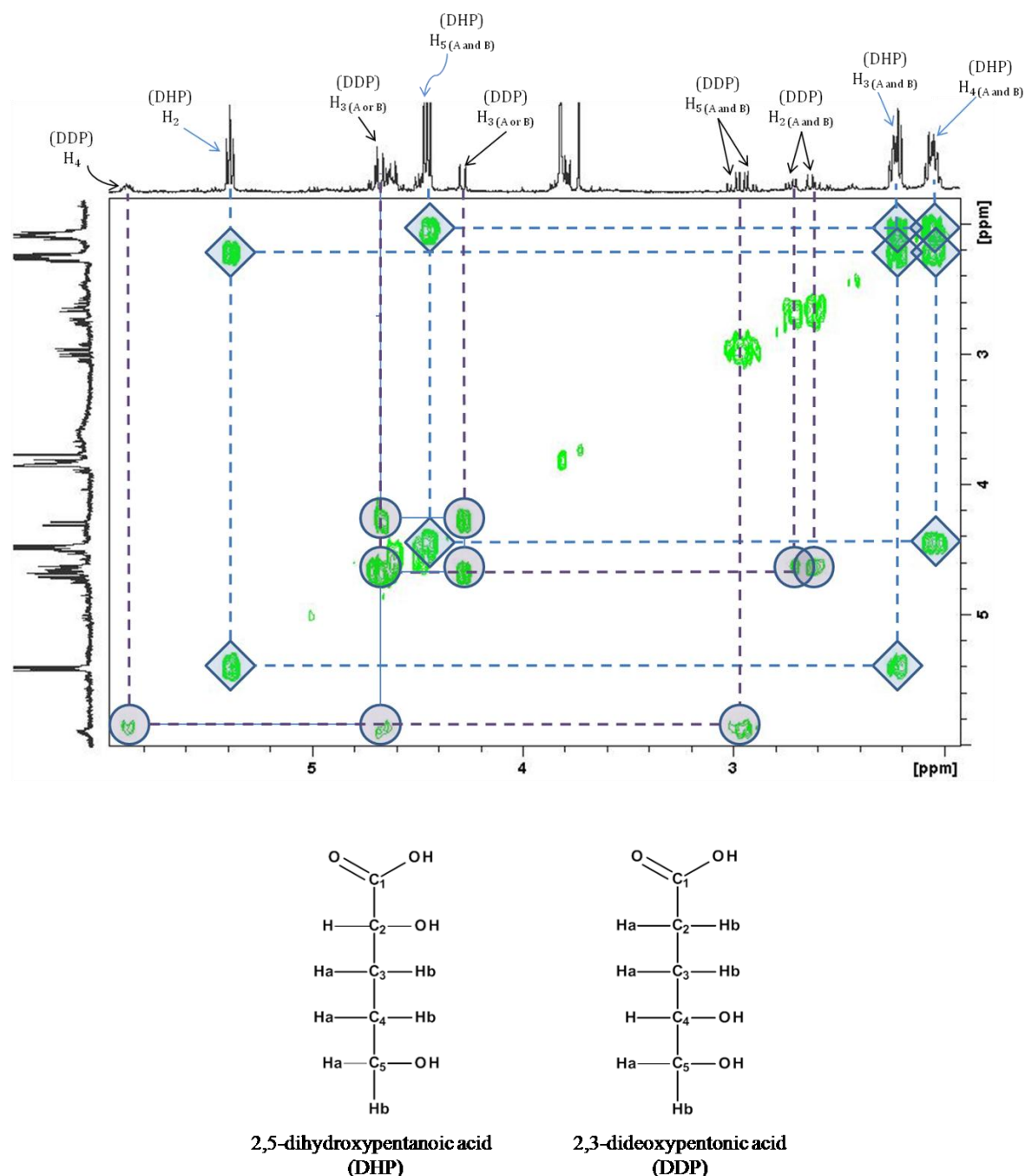


Figure 99: COSY NMR spectrum of fractions 5 - 8 indicating the presence of 2,5-dihydroxypentanoic acid and the tentative indication of 2,3-dideoxypentonic acid.

Prior to running the presently described column, TLC of the un-fractionated sample produced a large spot with an  $R_f$  value of approximately 0.6; and after the elution of the 150<sup>th</sup> fraction, a spot with a  $R_f$  value of  $\sim 0.6$  was apparent on the TLC plate. Evaporation of fractions 150 to 189, which had an average  $R_f$  value of 0.607 (3 s.f.), produced 460 mg of clear syrup, NMR analysis of the syrup indicated that it consisted of predominantly tribenzoylated  $\alpha$ -ISA<sub>L</sub>, free from any tribenzoylated  $\beta$ -ISA<sub>L</sub>; however, small amounts of

benzoic acid were also present. In this fraction there was also the indication of small amounts of  $\text{THP}_L$ , present in approximately twenty-times lower amounts than the tribenzoylated  $\alpha$ -ISA<sub>L</sub>; the presence of  $\text{THP}_L$  was unexpected because in the isolation attempt which was reported in section 4.5.4.1, the elution of  $\text{THP}_L$  proceeded the elution of the tribenzoylated  $\alpha$ -ISA<sub>L</sub>. TLC analysis of fractions 190 to 209 produced single spots which were larger than the spots produced for fractions 150 – 189 and the average R<sub>f</sub> value of those spots was 0.59 (0.592 3 s.f.) and evaporation of the combined fractions afforded 1.51 g of syrup. NMR analysis of the syrup indicated that, in agreement with the larger TLC spots, it consisted of a mixture of tribenzoylated  $\beta$ -ISA<sub>L</sub> (78 %) and tribenzoylated  $\alpha$ -ISA<sub>L</sub> (28 %), with no indication of any benzoic acid being present. Furthermore, there was no indication of the presence of any  $\text{THP}_L$  in those fractions. In fractions 210 – 219 the major spots on the TLC plate had an average R<sub>f</sub> value of 0.59 (0.587 3 s.f.), and the spots were smaller than the spots for the previous set of fractions and evaporation of the combined fractions resulted in 1.38 g of syrup, rich in tribenzoylated  $\beta$ -ISA<sub>L</sub>, free from any tribenzoylated  $\alpha$ -ISA<sub>L</sub>. The TLC results indicated that there were slight differences between the R<sub>f</sub> values of fractions containing predominantly tribenzoylated  $\alpha$ -ISA<sub>L</sub> (0.61) and fractions which predominantly contained the tribenzoylated  $\beta$ -ISA<sub>L</sub> (0.59). There was also a second smaller spot on the TLC plate with an average R<sub>f</sub> value of 0.54, and this coincided with some additional resonances which were present on the <sup>1</sup>H NMR spectrum which indicated that  $\text{THP}_L$  was also present in the collected fractions. Integration of specific resonances indicated that the  $\text{THP}_L$  was present in approximately five-times smaller amounts than the amount of the tribenzoylated  $\beta$ -ISA<sub>L</sub>. The presence of  $\text{THP}_L$  in early fractions, and then disappearance and then reappearance again indicates that, analogous to ISA, it is present as two isomeric forms; with one of the isomers having similar elution characteristics as those of the tribenzoylated  $\alpha$ -ISA<sub>L</sub> and the other eluting in similar fractions as those of tribenzoylated  $\beta$ -ISA<sub>L</sub>. Further evidence that  $\text{THP}_L$  was present as two isomers was found in the spectrum of the un-fractionated benzoylated syrup which was presented in Figure 96: expansion of the resonance peaks representing the C4 methyne proton of  $\text{THP}_L$  indicate that they were present as two overlapping AMX splitting patterns, with one set of resonances being larger than the other, indicating that one of the isomers was present in larger amounts. Slight differences in the position of the peaks indicate that the two forms of THP are not enantiomers, but more likely alpha and beta diastereoisomers at the C2 position, analogous to ISA. THP has previously been reported as being present in both alpha and beta forms in cellulose degradation solutions by Alfredsson and Samuelson

<sup>129</sup>, with the beta epimer being present in greater amounts, suggesting that the predominant form of THP produced in the present work was the beta epimer. A proposed mechanism for the formation of THP was reported by Greenfield *et al.*<sup>107</sup>.

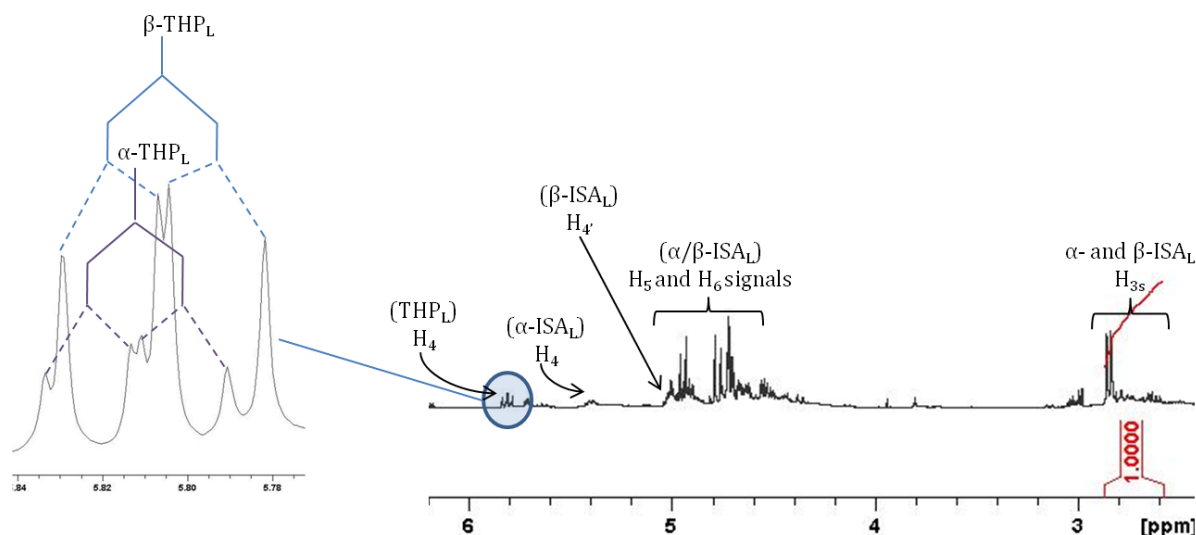
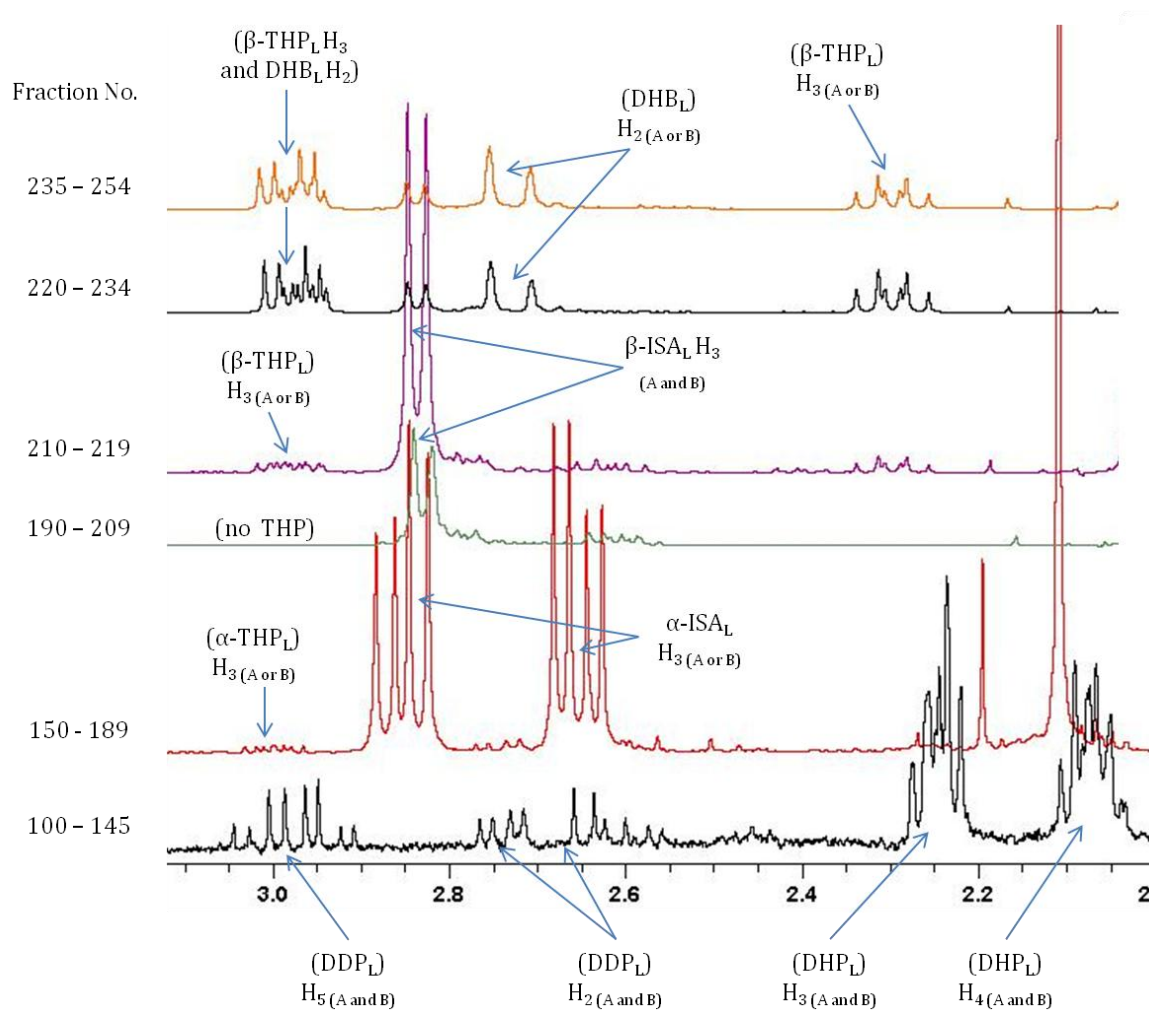


Figure 100: <sup>1</sup>H NMR spectrum of crude benzoylated syrup with the resonances representing THP<sub>L</sub> expanded which suggests that two diastereoisomers of THP are present.

In the remaining fractions, the TLC spot representing tribenzoylated  $\beta$ -ISA<sub>L</sub> was present but it was very faint, two additional spots were also visible with R<sub>f</sub> values of 0.54 and 0.46 respectively. Fractions 220 to 234 were combined and produced 770 mg of syrup upon evaporation, NMR analysis of the syrup indicated that minor amounts of tribenzoylated  $\beta$ -ISA<sub>L</sub> were present, but benzoylated THP<sub>L</sub> and DHB<sub>L</sub> were the major products, which were both present in approximately four times greater amounts than the amount of tribenzoylated  $\beta$ -ISA<sub>L</sub>. In the final set of collected fractions, there was 360 mg of syrup, and NMR analysis indicated that benzoylated DHB<sub>L</sub> was the major product, which was present in slightly greater amounts than THP<sub>L</sub>; tribenzoylated  $\beta$ -ISA<sub>L</sub> was also present, but in minor amounts (see Figure 101 and Table 10 for a summary of the elution order).



**Figure 101:**  $^1\text{H}$  NMR spectra showing the elution order of seven benzoylated compounds from the column of the benzoylated crude  $\beta$ -ISA solution after the removal of the coloured impurities.

**Table 10:** Summary of collected fractions from the second attempt to isolate tribenzoylated  $\beta$ -ISA<sub>L</sub> using normal phase chromatography

Collected fractions	Appearance and mass	Molar ratio of species present in collected fractions based on the integration of peak areas using $^1\text{H}$ NMR spectroscopy						
		$\beta$ -ISA <sub>L</sub>	$\alpha$ -ISA <sub>L</sub>	$\alpha$ -THP <sub>L</sub>	$\beta$ -THP <sub>L</sub>	DHB <sub>L</sub>	DDP <sub>L</sub>	DHP <sub>L</sub>
101 – 149	Trace	-	-	-	-	-	0.2	1.0
150 – 189	460 mg of syrup	-	1.0	0.05	-	-	-	-
190 - 209	1.51 g of syrup	1.0	0.2	-	-	-	-	-
210 – 219	1.38 g of syrup	1.0	0.02	-	0.2	-	-	-
220 – 234	770 mg of syrup	0.3	-	-	1.0	0.7	-	-
235 - 254	360 mg of syrup	0.4	-	-	0.9	1.0	-	-

#### 4.5.4.3.1 Short-path distillation of fractions 220 – 234: confirmation of the identification of DHB<sub>L</sub> and THP<sub>L</sub>

The initial identification of THP<sub>L</sub> and DHB<sub>L</sub> was made by analysing the NMR spectra of the un-fractionated, acetylated crude mixture, which was discussed in section 4.5.2. In that identification, there was significant amounts of other compounds present in the sample, which made an unequivocal identification difficult. In an attempt to definitively confirm the identity of the two major impurities, the syrup produced from fractions 220 – 234 from the previously described isolation attempt, which was rich in the two compounds, was applied to short-path distillation, using a similar method to the one described in section 2.6.1. The syrup (~ 500 mg) was applied to the first distillation bulb, which was then connected in series to an additional bulb, and the first bulb was inserted into the cylindrical heating oven, whilst the second bulb remained at ambient temperature outside the oven. The bulbs were rotated and the temperature slowly increased to 200 °C, using a vacuum of approximately 1 mmHg. After several minutes, a small amount of syrup distilled from the first to the second bulb, also some material remained in the original bulb. The distilled material was dissolved in CDCl<sub>3</sub> and analysed by NMR and the results indicated that the material which was suspected to be DHB<sub>L</sub> had distilled from the original bulb into the second bulb and NMR analysis of the material in the original bulb indicated that the suspected THP<sub>L</sub> remained in the original bulb. To confirm the identity of the DHB<sub>L</sub>, a standard sample of DHB<sub>L</sub> which was synthesised in section 0 was benzoylated using a scaled down version of the method described in section 2.6.4.4, and the NMR of the benzoylated standard was compared to the NMR spectrum of the distilled product. The results indicated that the two spectra both contained the resonances representing benzoylated DHB<sub>L</sub>, indicating that the correct assignment had been made (Figure 102); also the ratio between the integrated peak area of any of the DHB<sub>L</sub> resonances (representing 1 proton) to the peak area of the aromatic para proton of the benzoyl group was ~ 1 : 1 (not shown), confirming that the DHB<sub>L</sub> was present as a singly benzoylated species.

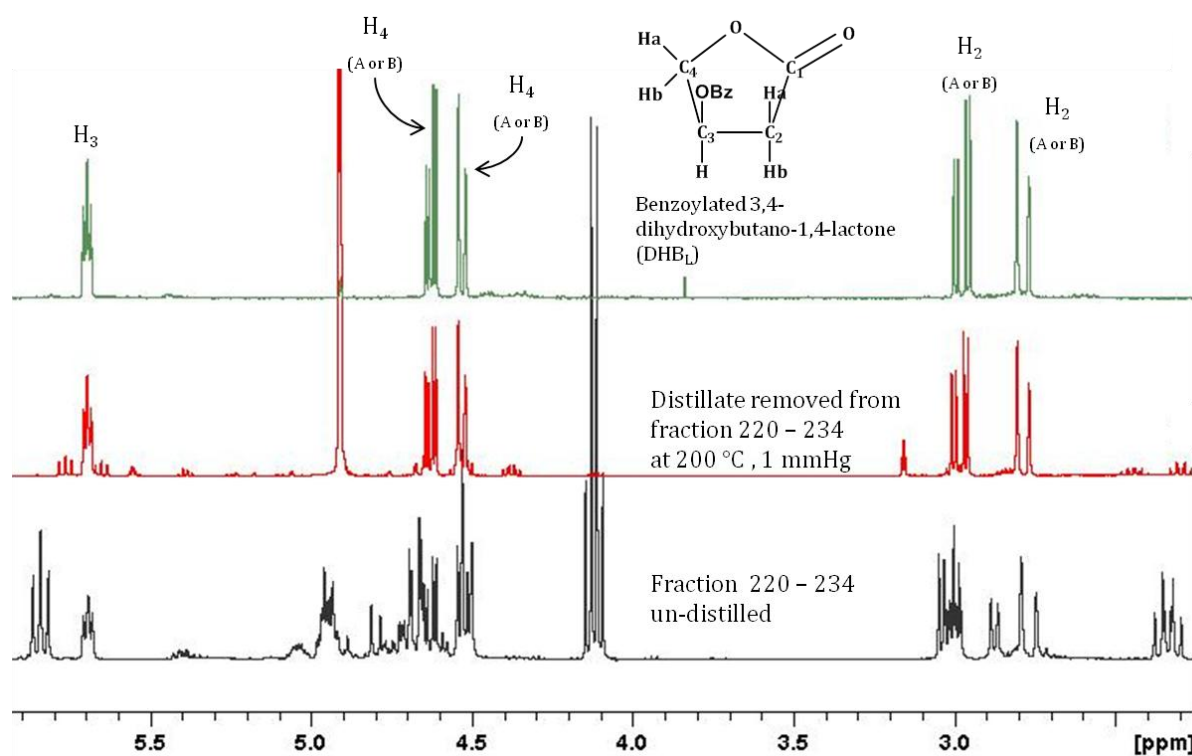
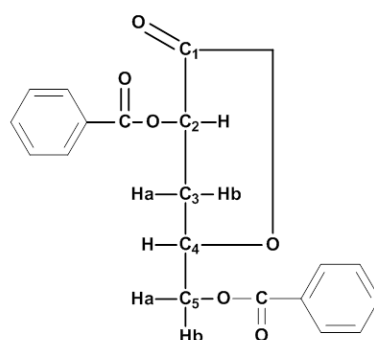
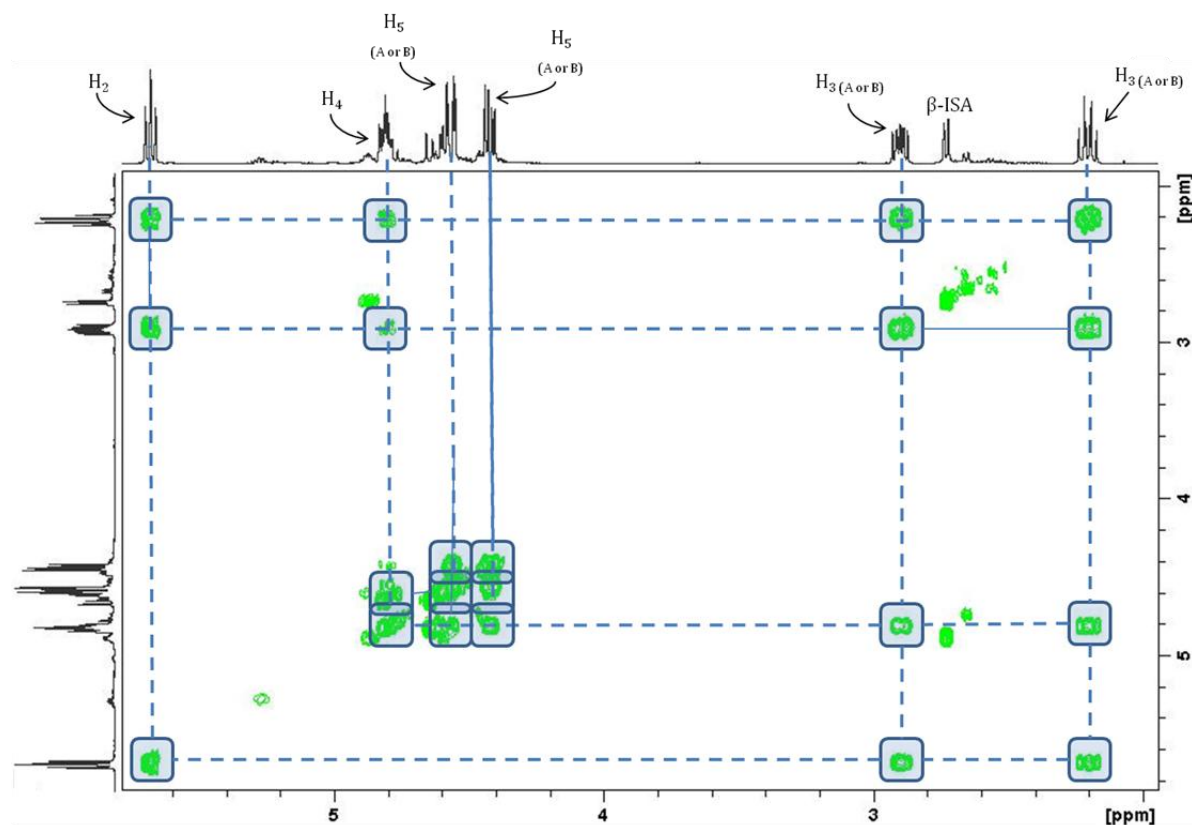


Figure 102:  $^1\text{H}$  NMR spectra of un-distilled syrup produced from fractions 220 - 234 (bottom), and the distillate (centre) and the spectrum of a standard sample of benzoylated 3,4-dihydroxybutano-1,4-lactone (top).

The remaining un-distilled material was also analysed by NMR, and the resulting  $^1\text{H}$  spectrum was now less complicated, due to the resonances of the benzoylated  $\text{DHB}_L$  now been absent. Using a combination of additional 1D ( $^{13}\text{C}$ , DEPT 135 and DEPT 90) and 2D (COSY, HSQC and HMBC) NMR experiments, the identification of the major impurity could be confirmed as being 2,4,5-trihydroxypentanoic acid ( $\text{THP}_L$ ). The ratio between the integrated peak area of any of the  $\text{THP}_L$  resonances (representing 1 proton) to the peak area of the aromatic para proton of the benzoyl groups was  $\sim 1 : 2$  (aromatic benzoyl resonances not shown), confirming that the  $\text{THP}_L$  was present as a dibenzoylated species, either as a 1,4- or a 1,5- lactone (Figure 103).



**Dibenzoylated 2,4,5-trihydroxypentano-1,4-lactone (THP<sub>L</sub>)**

Figure 103: COSY NMR spectrum and structure of the dibenzoylated THP<sub>L</sub>

#### 4.5.4.4 Extraction of collected fractions with saturated sodium carbonate solution: removal of benzoic acid

As previously discussed, combined fractions 150 to 189 and 210 to 219 from the previously described column were rich in tribenzoylated  $\alpha$ - and  $\beta$ -ISA<sub>L</sub> respectively; however, benzoic acid was also present. It was determined that by dissolving each set of fractions in ethyl acetate, the remaining sparingly soluble benzoic acid, could be extracted from the syrup

using a saturated solution of sodium carbonate, due to the benzoic acid being converted into the highly soluble sodium benzoate <sup>213</sup>. Following the extraction of the  $\alpha$ -ISA tribenzoate-rich syrup and the evaporation of the resulting organic solvent, NMR analysis indicated that there was 60 mg of highly pure tribenzoylated  $\alpha$ -ISA<sub>L</sub>, with no indication of the presence of any benzoic acid. The same treatment of the  $\beta$ -ISA tribenzoate-rich fractions afforded 980 mg of clear syrup, indicating that a small amount of benzoic acid had been removed. NMR analysis of the syrup, indicated that a small amount of impurities were still present and the tribenzoylated  $\beta$ -ISA<sub>L</sub> was present in approximately 85 % purity in the form of very thick, clear syrup. Pure, solid tribenzoylated  $\beta$ -ISA<sub>L</sub> was precipitated from the syrup by triturating the syrup with diethyl ether, resulting in 300 mg of pure solid tribenzoylated  $\beta$ -ISA<sub>L</sub>, with no indication of any impurities (Figure 104). Attempts to produce solid tribenzoylated  $\alpha$ -ISA<sub>L</sub> using the same method failed.

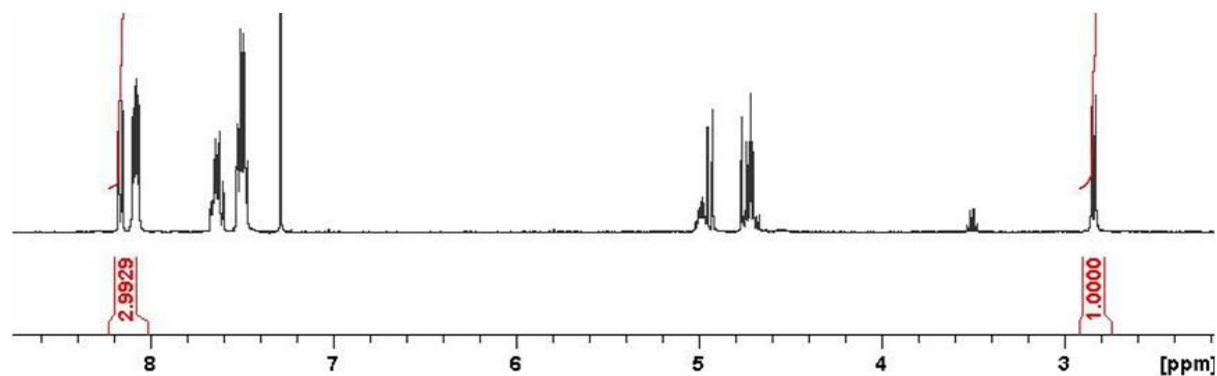


Figure 104: <sup>1</sup>H NMR spectrum of pure tribenzoylated  $\beta$ -ISA<sub>L</sub>

As described above, small amounts of benzoic acid were removed by extraction into saturated sodium carbonate solution. With this in mind it was decided that the combined fractions 1 to 4 (6.93 g), which were collected from the wide silica column, as described in section 4.5.4.2 and which contained a large excess of benzoic acid would also be extracted. NMR analysis of the combined fractions, before the extraction indicated that the ISA tribenzoates were present, but the resonances were minute in comparison to the benzoic acid resonances (the ratio of the C3 methylene protons representing the tribenzoylated  $\alpha$ - and  $\beta$ -ISA<sub>L</sub> to the aromatic ortho protons was  $\sim 1 : 42$ , Figure 105). After the extraction and the evaporation of the organic solvent there was 590 mg of syrup, NMR analysis of the syrup indicated that it consisted of approximately equal amounts of  $\alpha$ - and  $\beta$ -ISA<sub>L</sub> tribenzoates as the major products, minor amounts of dibenzoylated THP<sub>L</sub> and other impurities (Figure 105, bottom). Following the extraction, the ratio between the C3

methylene signals of the ISA tribenzoates and the aromatic ortho protons was now  $\sim 1 : 3$ , indicating that all of the benzoic acid had been removed from the syrup. Evaporation of the aqueous phase afforded  $\sim 6$  g of crystalline, white powder and NMR analysis of that powder indicated pure benzoic acid.

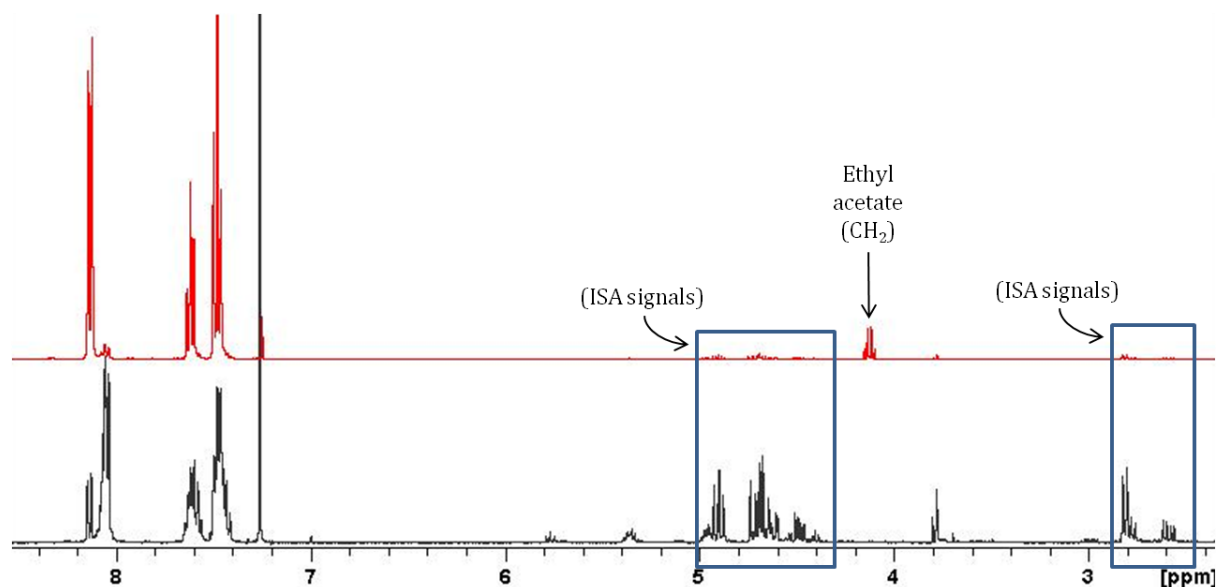


Figure 105:  $^1\text{H}$  NMR spectra of combined fractions 1 to 4 which contained large amounts of benzoic acid (top spectrum) and following the extraction of the combined fractions using saturated sodium carbonate solution (bottom spectrum).

#### 4.5.4.5 Final isolation procedure

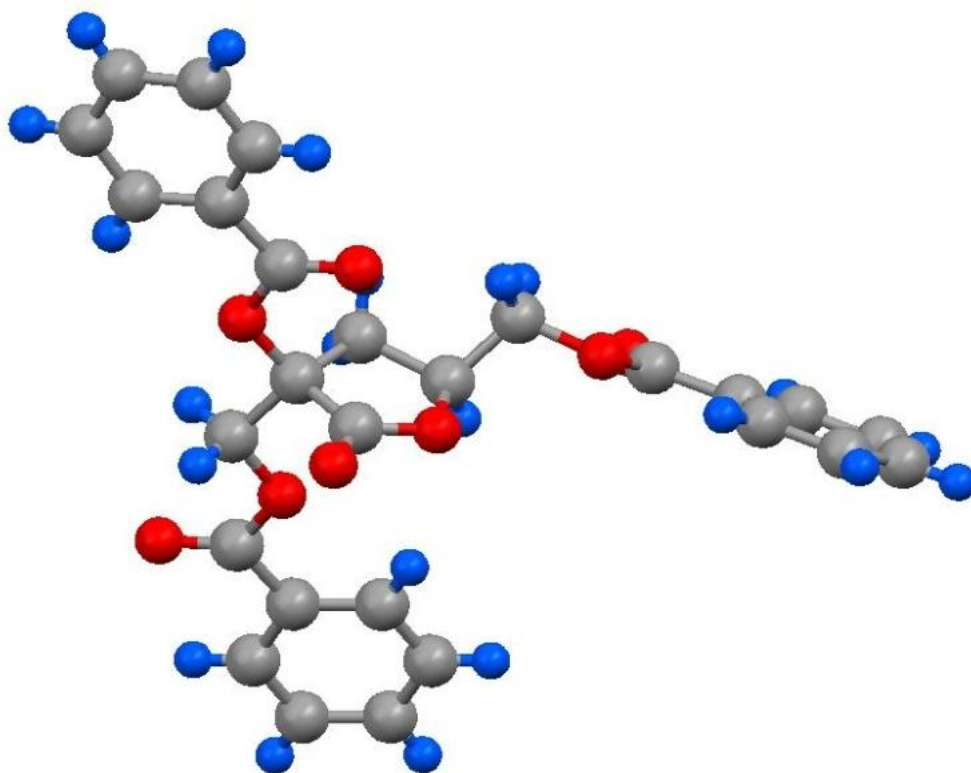
Based on the findings of the previous exploratory isolation attempts, a final method was developed to separate and isolate tribenzoylated  $\beta$ -ISA<sub>L</sub>; the final method is described in section 2.6.4.5. In a typical isolation, crude  $\beta$ -ISA<sub>L</sub>-rich syrup was prepared using the method described in section 2.5.2 resulting in 55 g of syrup. The syrup was benzoylated using the method described in section 2.6.4.4 resulting in 171 g of very thick, dark brown tar-like solid, which contained large amounts of benzoic acid. To remove the benzoic acid, the brown solid was dissolved in chloroform and the benzoic acid was extracted into saturated sodium carbonate solution which provided a brown solid upon evaporation of the organic solvent (76.08 g). NMR analysis of the solid indicated that the vast majority of the benzoic acid had been removed from the syrup. To remove the coloured impurities, the brown solid was dissolved in chloroform and converted into a dry silica mix using the method described in section 2.6.4.5 and non-polar lactones were eluted through a wide bed

of silica; the resulting eluent was evaporated under reduced pressure to produce very pale yellow syrup (24.14 g). NMR analysis of which indicated that the syrup was rich in tribenzoylated ISAs; of which,  $\beta$ -ISA accounted for ~ 66 % of the total ISA. As expected, the syrup also contained dibenzoylated  $\text{THP}_L$  which was present in approximately 4-times smaller amounts than the amount of the tribenzoylated  $\beta$ -ISA<sub>L</sub>; benzoylated  $\text{DHB}_L$  was also present in approximately 10-times smaller amounts than the amount of the tribenzoylated  $\beta$ -ISA<sub>L</sub>. The NMR analysis also indicated that there was no benzoic acid remaining in the syrup. A portion of the syrup (16 g) was dissolved in a minimum amount of ethyl acetate and applied to a large silica column (55 cm x 7 cm) and the products were eluted very slowly using the conditions described in section 2.6.4.5, for this column, large 250 ml test-tubes were used to collect the fractions. Prior to the column, TLC analysis of the crude syrup using 50 % ethyl acetate and 50 % petroleum ether provided a large spot with a R<sub>f</sub> factor of 0.61 which represented the mixed tribenzoylated  $\alpha$ - and  $\beta$ -ISA lactones. From a typical column, 30 – 35 large fractions were collected and based on the TLC analysis the products of interest were eluting after the 16<sup>th</sup> fraction.

NMR analysis indicated that in fraction 17 (29 mg) a minor amount of dibenzoylated  $\alpha$ - $\text{THP}_L$  was present, fraction 18 (88 mg) contained highly pure tribenzoylated  $\alpha$ -ISA<sub>L</sub> and minor amounts of dibenzoylated  $\alpha$ - $\text{THP}_L$ , fractions 19 – 21 (1.13 g) contained only tribenzoylated  $\alpha$ -ISA<sub>L</sub>, fractions 22 – 23 (1.82 g) contained mixed fractions of  $\alpha$ - and  $\beta$ -ISA tribenzoates with increasing amounts of tribenzoylated  $\beta$ -ISA<sub>L</sub>. Fractions 24 – 26 (6.86 g) contained tribenzoylated  $\beta$ -ISA<sub>L</sub> of greater than 95 % purity with minor amounts of dibenzoylated  $\beta$ - $\text{THP}_L$  present in the 26<sup>th</sup> fraction and fractions 27 – 30 (4.15 g) contained tribenzoylated  $\beta$ -ISA<sub>L</sub> with increasing amounts of benzoylated  $\beta$ - $\text{THP}_L$  and  $\text{DHB}_L$  and other unknown impurities. The mixed fractions (22 – 23) were combined and evaporated which resulted in very thick syrup, which, upon triturating with diethyl ether, resulted in the precipitation of mixed  $\alpha$ - and  $\beta$ -ISA tribenzoates as a white solid (~ 1 g).

It was determined that by allowing fractions which were rich in the tribenzoylated  $\beta$ -ISA<sub>L</sub> to slowly evaporate, single crystals could be produced, suitable for X-ray analysis. Several attempts were made to produce single crystals of tribenzoylated  $\alpha$ -ISA<sub>L</sub> using the same method, however they were unsuccessful. Single crystals of the alpha isomer were produced using a binary solvent system; the best results were achieved when small amounts of tribenzoylated  $\alpha$ -ISA<sub>L</sub> (~ 20 mg) were dissolved in chloroform and petroleum ether was allowed to slowly diffuse into the  $\alpha$ -ISA solution. After several days, single crystals

suitable for X-ray analysis were produced. The resulting crystal structures (Figure 106) confirmed that the 2,4-hydroxymethyl groups of the tribenzoylated  $\alpha$ - and  $\beta$ -ISA<sub>L</sub> are arranged in cis and trans geometries respectively. The trans arrangement in the beta isomer explains the characteristic doublet which is observed for the C3 methylene protons in the <sup>1</sup>H NMR spectrum of the  $\beta$ -tribenzoate, due to the C3 protons having a greater freedom of rotation due to the large 2,4-hydroxymethyl groups being on opposite planes. In the work of Glaus and Van Loon<sup>138</sup> the absolute configuration of the chiral centres at C2 and C4 for  $\beta$ -ISA<sub>L</sub> was narrowed down to being either 2S, 4R or its enantiomeric form 2R, 4S; it can be confirmed using Cahn–Ingold–Prelog priority rules, that the absolute configuration of the crystalline tribenzoylated  $\beta$ -ISA<sub>L</sub> is 2R, 4S.

Tribenzoylated  $\beta$ -ISA<sub>L</sub>

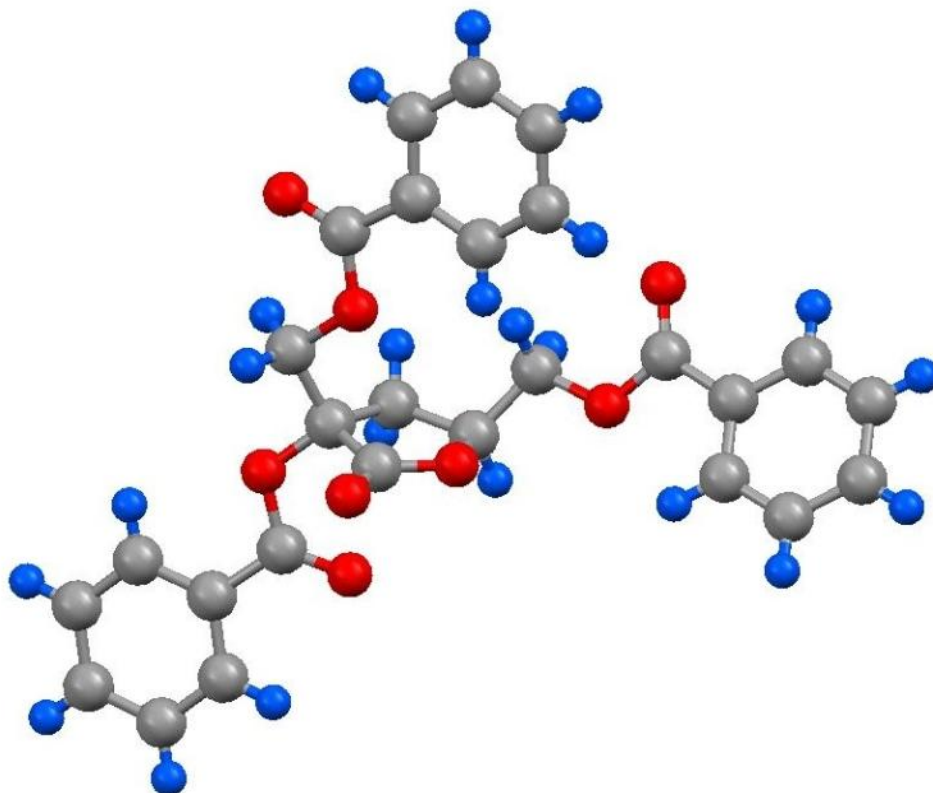
Tribenzoylated  $\alpha$ -ISA<sub>L</sub>

Figure 106: Single crystal X-ray structure of tribenzoylated  $\beta$ -ISA<sub>L</sub> (top) and tribenzoylated  $\alpha$ -ISA<sub>L</sub> (bottom)

From the column described above, 6.86 g of syrup rich in tribenzoylated  $\beta$ -ISA<sub>L</sub> was taken forward to the debenzoylation procedure, using the method described in section 2.6.4.10. The benzoylated lactones were ring-opened by hydroxide catalysis and the esters were debenzoylated using Zemplén methods<sup>211</sup> which resulted in 2.62 g of white solid. NMR analysis of the solid indicated the sodium salt of  $\beta$ -ISA in greater than 95 % purity (Figure 107 and see section 2.6.4.11 for full NMR data). The sodium salt was also analysed by high resolution mass spectrometry in the negative ion mode resulting in a determined mass of 179.0554 (calculated 179.0561) for the deprotonated form of  $\beta$ -ISA. As and when required, the sodium salt of  $\beta$ -ISA was converted into the lactone form in 95 % yield using the method described in section 2.4.2; and the lactone was converted into the calcium salt using the method described in section 2.6.4.16 in 74 % yield.

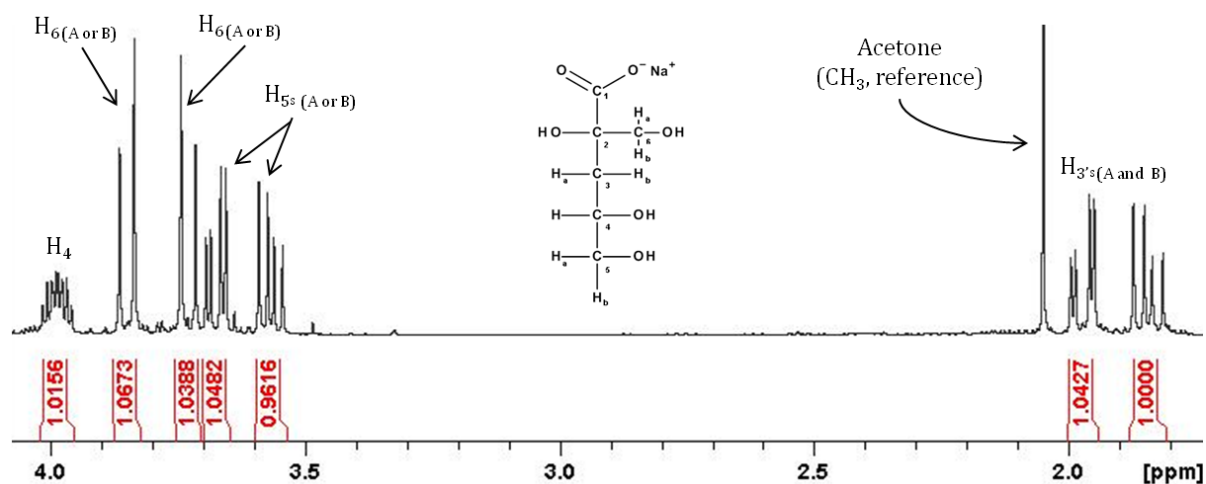


Figure 107:  $^1\text{H}$  NMR spectrum of sodium 2-C-(hydroxymethyl)-3-deoxy-D-threo-pentionate ( $\beta$ -ISA)

In summary, using the method described above,  $\sim 2.5$  g of high purity  $\beta$ -ISA was isolated from the  $\alpha$ -ISA and other cellulose degradation products in the elution of a single column. One of the key steps in the isolation procedure was the removal of the coloured impurities by eluting the benzoylated mixture through a bed of silica which eradicated the problem of column fouling. Another key step was the very slow elution of the benzoylated products through the normal phase silica column which resulted in  $\alpha$ - and  $\beta$ -ISA being fully separated, and also allowed for the identification of several additional compounds.

## 5 Physical properties of $\beta$ -ISA in aqueous solution

As discussed in section 1.3.6, the physical properties of  $\alpha$ -ISA have been extensively studied, however, until now, due to the difficulties in obtaining large quantities, very little is known about the physical properties of  $\beta$ -ISA.

### 5.1 Determination of the aqueous $pK_a$ of $\beta$ -ISA using $^{13}\text{C}$ NMR spectroscopy

#### 5.1.1 Introduction

A key area of research, in relation to the underground disposal of radioactive waste, is the ability of ISA to form complexes with radioactive nuclides, the ability of which will be effected by the acidity of the carboxylate group or the basicity of its conjugate base. However, measurement of its acidity is complicated because of its conversion to the lactone at acidic pH values, which prevents a direct  $pK_a$  measurement using acid-base titration. Rai *et al.*<sup>197</sup> determined the  $pK_a$  of  $\alpha$ -ISA by measuring the solubility of calcium isosaccharinate as a function of pH, and determined a  $pK_a$  value of 4.46, however, in a later publication<sup>214</sup> they concluded that this value was too high because they ignored the lactonisation of the carboxylic acid. Hagberg *et al.*<sup>215</sup> and Motellier and Charles<sup>216</sup> determined the  $pK_a$  for  $\alpha$ -ISA (3.87 and 4.02 respectively) using capillary zone electrophoresis (CZE) over a range of pH values; the CZE method is based on the fact that the mobility of an analyte is proportional to its degree of ionisation<sup>215</sup>. When using CZE,  $\alpha$ - and  $\beta$ -ISA co-elute, so Motellier and Charles only analysed the alpha epimer, and assumed that both  $\alpha$ - and  $\beta$ -ISA had the same  $pK_a$ ; also CZE cannot distinguish between the carboxylic acid and the lactone forms of ISA.

NMR is particularly useful for determining the  $pK_a$  of ISA because resonances for the open chain and lactone forms can be analysed independently, and also  $\alpha$ - and  $\beta$ -ISA can be differentiated. The basis of using NMR to determine  $pK_a$  is that when proton dissociation or association occurs, the electron density around the affected parts of the molecule will change resulting in a change in the chemical shift of the neighbouring carbon atoms<sup>217, 218</sup>. The  $pK_a$  can be determined if a plot of the observed shift as a function of pH results in a sigmoidal type curve<sup>218 219</sup>, which is defined by the Henderson-Hasselbach equation. The size of the shift is related to the degree of change in electron density; tracking the change in

position of the carbon (if using  $^{13}\text{C}$  NMR) which is closest to the ionisable functional group usually provides the most accurate  $\text{p}K_{\text{a}}$  determination, which, for  $\beta$ -ISA, being a carboxylic acid, is likely to be the carbonyl carbon (C1). A change in position of other resonances which are related to the ionised group, either through bonds or through space, but not necessarily ionised themselves can also produce sigmoidal changes in the position of the chemical shift<sup>217, 218 219</sup>. The pH at the point of inflection of the curve provides a direct indication of the  $\text{p}K_{\text{a}}$ ; however, accurate values of  $\text{p}K_{\text{a}}$  are normally determined by fitting the data using non-linear fitting models.

In the literature, there are examples of using both  $^1\text{H}$ <sup>218, 220-222</sup> and  $^{13}\text{C}$ <sup>150, 217, 218, 222, 223</sup> NMR spectroscopy to perform  $\text{p}K_{\text{a}}$  titrations, but for the present work,  $^{13}\text{C}$  NMR was deemed as being the most suitable method mainly due to the significant overlapping of peaks which occurs when mixtures of the open-chain and lactone forms of  $\beta$ -ISA (or  $\alpha$ -ISA) are analysed by  $^1\text{H}$  NMR. The  $^1\text{H}$  spectrum of  $\beta$ -ISA contains seven magnetically non equivalent protons, when a mixture of lactone and acid are present there are 14 resonances. However, with  $^{13}\text{C}$  NMR, there are six sharp peaks representing each carbon and when the ISA is present as a mixture of acid and lactone, the 12 peaks remain fully resolved (Figure 108).

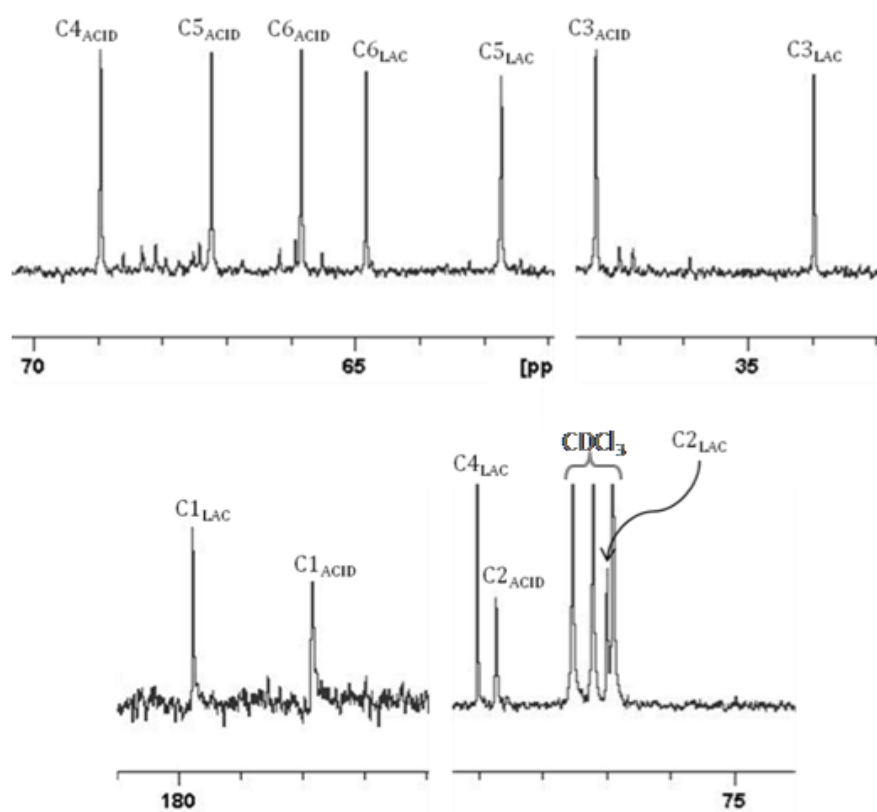


Figure 108:  $^{13}\text{C}$  NMR spectrum of a mixed sample of  $\beta$ -ISA<sub>H</sub> (acid) and  $\beta$ -ISA<sub>L</sub> (lac)

Cho *et al.*<sup>150</sup> utilised  $^{13}\text{C}$  NMR spectroscopy to determine the  $\text{p}K_{\text{a}}$  of  $\alpha$ -ISA to which an average value of 3.36 was determined. More recently Almond *et al.*<sup>224</sup> determined the  $\text{p}K_{\text{a}}$  of the analogous XISA using the same method to which a  $\text{p}K_{\text{a}}$  of 3.00 was determined; in the present work,  $^{13}\text{C}$  NMR spectroscopy was also used to determine the  $\text{p}K_{\text{a}}$  of  $\beta$ -ISA. A further advantage of using NMR spectroscopy to determine  $\text{p}K_{\text{a}}$  values is that the purity of the compound being analysed is of limited importance<sup>217, 225</sup>, so in theory, the  $\text{p}K_{\text{a}}$  of  $\beta$ -ISA, or other analytes which are present in crude solutions could be determined, however, in the present work pure  $\beta$ -ISA was used.

### 5.1.2 Results: the determination of the aqueous $\text{p}K_{\text{a}}$ of $\beta$ -ISA

To determine the aqueous  $\text{p}K_{\text{a}}$  of  $\beta$ -ISA, the variation in the chemical shifts of the carbon resonances were monitored as a function of  $\text{pD}$ , using the method described in section 2.7.1.1. In the present work, the calcium salt of  $\beta$ -ISA was used as the substrate and NMR samples were prepared at a concentration of 50 mM by dissolving ISA in  $\text{D}_2\text{O}$ , and required sample  $\text{pD}$ s were obtained with the addition of suitable amounts of deuterated nitric acid; the  $\text{pD}$  value is the recorded  $\text{pH}$  value using a  $\text{pH}$  meter + 0.4<sup>217, 226</sup>

In the work of Cho *et al.*<sup>150</sup> both  $\text{Ca}(\text{ISA})_2$  and  $\text{Na-ISA}$  were used in various concentrations ranging from 6 mM to 400 mM and they found that neither the cation present nor the concentration of the samples had any significant effect on their results. Wang<sup>223</sup> also used multiple concentrations of substrate when determining the  $\text{p}K_{\text{a}}$  of glucuronic acid using  $^{13}\text{C}$  NMR and found that concentration had little effect on the observed  $\text{p}K_{\text{a}}$ <sup>223</sup>.

In the present study, to maintain the robustness of the results, a capillary insert containing deuterated chloroform was added to the NMR sample tube as an internal standard so that accurate chemical shifts could be determined. As previously discussed, depending on the  $\text{pH}$  of the solution, the ISA will be present as either the deprotonated anion, the protonated free acid, the lactone or as mixtures of the acid and lactone; so to confidently identify and track the correct resonances, the position of the carbon resonances of standard samples of both  $\beta\text{-ISA}_\text{H}$  and  $\beta\text{-ISA}_\text{L}$  were determined by analysing pure  $\text{Ca-}\beta\text{-(ISA)}_2$  and  $\beta\text{-ISA}_\text{L}$  using a range of 1D and 2D NMR experiments (Figure 110). In comparison to the spectrum produced for the open-chain form of  $\beta$ -ISA, all of the resonances, apart from C4 are slightly up-field in the lactone spectrum; however the major difference between the two spectra was the large down-field shift of approximately 10 ppm for the C4 carbon when present as the

lactone. The down-field shift is understandable because the C4 is directly bonded to the oxygen atom which forms the new ester bond in the lactone; similar findings were reported for  $\alpha$ -ISA by Cho *et al.*<sup>150</sup> and also for the 1,4-lactonisation of the analogous XISA<sup>224</sup>.

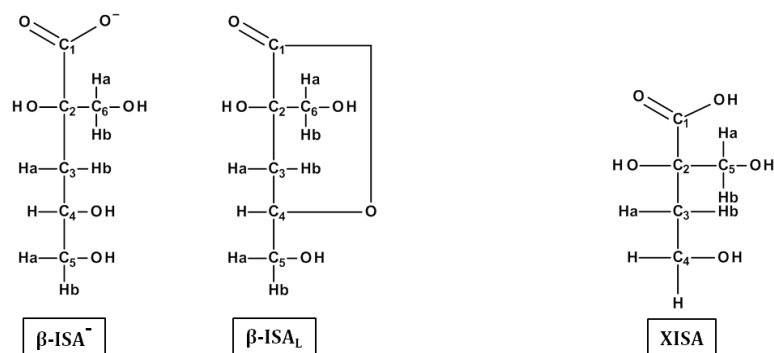


Figure 109: Structures of  $\beta$ -ISA<sup>-</sup>,  $\beta$ -ILAL and XISA

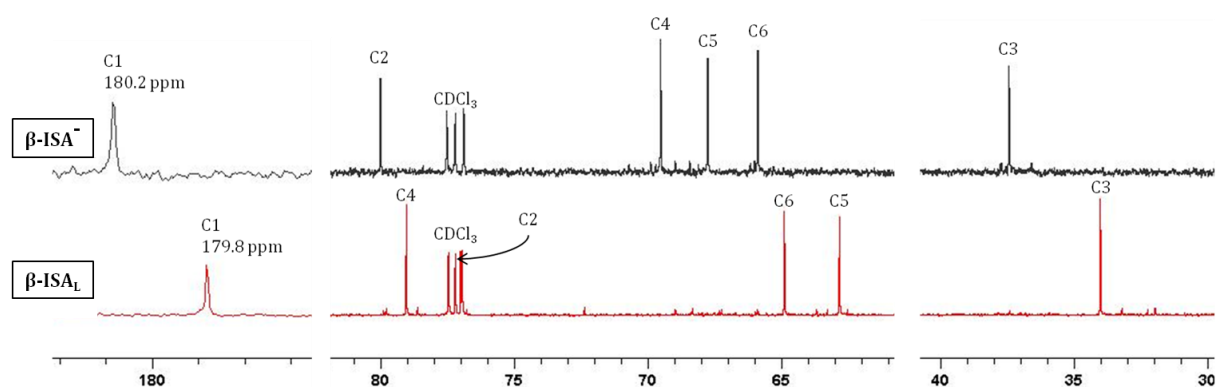


Figure 110: <sup>13</sup>C chemical shifts (ppm) of  $\beta$ -ILAL (bottom spectrum) and the deprotonated anion of  $\beta$ -ISA (top spectrum)

To determine the  $pK_a$  of the  $\beta$ -ISA, the calcium salt was analysed by NMR spectroscopy and the chemical shifts of each of the six carbon atoms (Figure 110) of the ISA were measured as a function of pD over a range of pD values between  $\sim$  pD 8 to pD 2. The initial sample was prepared by dissolving the ISA directly in D<sub>2</sub>O, for which a pD of 8.3 was observed. The resulting NMR spectrum indicated that the  $\beta$ -ISA was present as the open chain anion, due to the six corresponding resonances being present, with no evidence of the presence of any lactone. As the pD was lowered, the six additional resonances representing the lactone became visible in increasing amounts, the lactone content was: at pD 4.49 (< 1 %), pD 3.84 ( $\sim$  8 %), pD 2.83 ( $\sim$  26 %) and pD 2.16 ( $\sim$  45 %); for the duration of the experiment there was no overlapping between resonances of the lactone and the open-chain

forms of  $\beta$ -ISA which allowed the resonances of the open-chain form to be accurately tracked. The chemical shifts of the 6 individual carbon resonances of  $\beta$ -ISA as a function of pD are presented in Table 11.

Table 11:  $^{13}\text{C}$  chemical shift values (ppm) for carbons 1 - 6 for  $\beta$ -ISA as a function of pD

pD	Chemical shift, $\delta$ (ppm)					
	C1	C2	C3	C4	C5	C6
8.30	180.2019	80.01	37.43	69.51	67.74	65.87
7.32	180.2010	80.01	37.43	69.51	67.74	65.87
6.84	180.2100	80.06	37.47	69.54	67.73	65.90
6.11	180.1625	79.82	37.55	69.54	67.77	65.97
5.36	180.0632	79.97	37.43	69.50	67.73	65.87
4.87	179.8842	79.69	37.52	69.47	67.71	65.95
4.49	179.5749	79.74	37.40	69.38	67.62	65.84
3.84	178.7464	79.15	37.46	69.19	67.45	65.90
3.57	178.2179	78.98	37.33	69.03	67.29	65.79
2.83	177.8512	78.71	37.36	68.95	67.23	65.83
2.16	177.6700	78.63	37.40	68.95	67.23	65.88
<b><math>\Delta</math> in <math>\delta</math> (ppm)</b>	<b>- 2.53</b>	<b>- 1.38</b>	<b>- 0.03</b>	<b>- 0.56</b>	<b>- 0.51</b>	<b>+ 0.01</b>

The results show that as the pD drops, an up-field shift in the position of carbons C1, C2, C4 and C5 was observed whereas the position of C3 and C6 remained relatively constant for all pD values (Table 11). The largest shift was observed for the carbonyl carbon (C1,  $\Delta$  in  $\delta = 2.53$  ppm) which is very similar to the shift reported by Cho *et al.*<sup>150</sup> for  $\alpha$ -ISA (C1,  $\Delta$  in  $\delta = 2.5$  ppm), and in agreement with the shift reported by Almond *et al.*<sup>224</sup> for XISA, (C1,  $\Delta$  in  $\delta = 2.22$  ppm).

The chemical shifts of all six carbons were plotted as a function of pD, the results indicated that there was a sigmoidal dependence of the chemical shifts of carbons 1, 2, 4 and 5 (Figure 111). The variation of the chemical shifts of those 4 carbons were fitted to the following equation:  $\delta(\text{pD}) = \delta_{\text{acid}} + \delta_{\text{base}} [10^{-\text{pD}} / (K_a + 10^{-\text{pD}})]$  using least squares analysis which allowed  $\text{p}K_a$  values to be extracted; the inflection point of the curves were in agreement with the calculated  $\text{p}K_a$  values using the equation.

The large shift observed for C1 indicates that, as expected, the hydroxyl group attached to C1 is the most acid group, which is deprotonated at pH values sufficiently greater than the  $pK_a$  value, resulting in the carboxylate anion. The large up-field shift is consistent with an increase in electron density around the carbonyl carbon, resulting in a greater amount of shielding due to the protonation of the anion in acidic media, reducing the electronegativity of the carbonyl oxygen. The second largest shift ( $\Delta$  in  $\delta = 1.38$  ppm) was observed for C2, which may be expected as it is bonded directly to C1, therefore changes in electron density of C1 will directly affect the electron density of C2. Carbons C4 and C5 showed a very similar up-field shifts ( $\Delta$  in  $\delta = 0.56$  ppm and 0.51 ppm respectively). It is expected that these alcohol groups would not be deprotonated under the pD conditions of the present experiment because the  $pK_a$  of alcohol groups are traditionally much larger ( $> 12$ )<sup>227, 228</sup>; the very similar sigmoidal plots and the individual  $pK_a$  values (to be discussed) suggest that the observed shifts are more likely related to a direct interaction with the carbonyl carbon. It was hypothesised by Cho *et al.*<sup>150</sup> that a similar shift in the C4 methyne group of  $\alpha$ -ISA was as a result of hydrogen bonding between the C4 secondary alcohol and the carboxylate anion. A similar shift was reported by Almond *et al.*<sup>224</sup> for XISA for the C4 methylene carbon and was also assumed to be due to hydrogen bonding between the C4 primary alcohol group of XISA and its carboxylate anion; so it is conceivable that similar hydrogen bonding could occur in both C4 (methyne, secondary alcohol) and C5 (methylene, primary alcohol) in  $\beta$ -ISA to account for the down-field shift at basic pD values. Interestingly, however, Cho *et al.*<sup>150</sup> reported that for  $\alpha$ -ISA there was no significant change in the chemical shift for the C5 carbon as a function of pD, therefore, it is unclear as to why there would be a shift in the position of C5 for  $\beta$ -ISA; an explanation may be due to conformational differences between the two isomers which may result in hydrogen bonding between the  $-OH$  group of the primary alcohol at C5 and the oxygen of the secondary alcohol at C4. To gain a further understanding of the intra-hydrogen bonding of  $\alpha$ - and  $\beta$ -ISA computational chemistry or X-ray crystallography may prove useful.

The calculated  $pK_a$  values were very similar for all 4 resonances: 4.01 (C1), 4.00 (C2), 4.03 (C4) and 4.02 (C5) giving a mean value of  $4.01 \pm 0.07$ . It was determined by Glasoe and Long<sup>226</sup> that subtracting 0.4 would convert  $pK_a$  values determined in  $D_2O$  to a  $pK_a$  value applicable to  $H_2O$ , so the aqueous  $pK_a$  of  $\beta$ -ISA can be reported as being 3.61.

The  $pK_a$  of  $\beta$ -ISA is larger than the one reported by Cho *et al.*<sup>150</sup> for  $\alpha$ -ISA (3.36) which was determined using the same method, indicating that the beta isomer is slightly more

basic than the alpha isomer. However, as previously discussed, a wide range of  $pK_a$  values have been reported for  $\alpha$ -ISA, ranging from 3.27 – 4.46<sup>150, 151, 197, 216</sup>, therefore, further experiments, using  $^{13}\text{C}$  NMR are currently ongoing at the University of Huddersfield to determine the  $pK_a$  of both alpha and beta ISA when both isomers are present as mixtures.

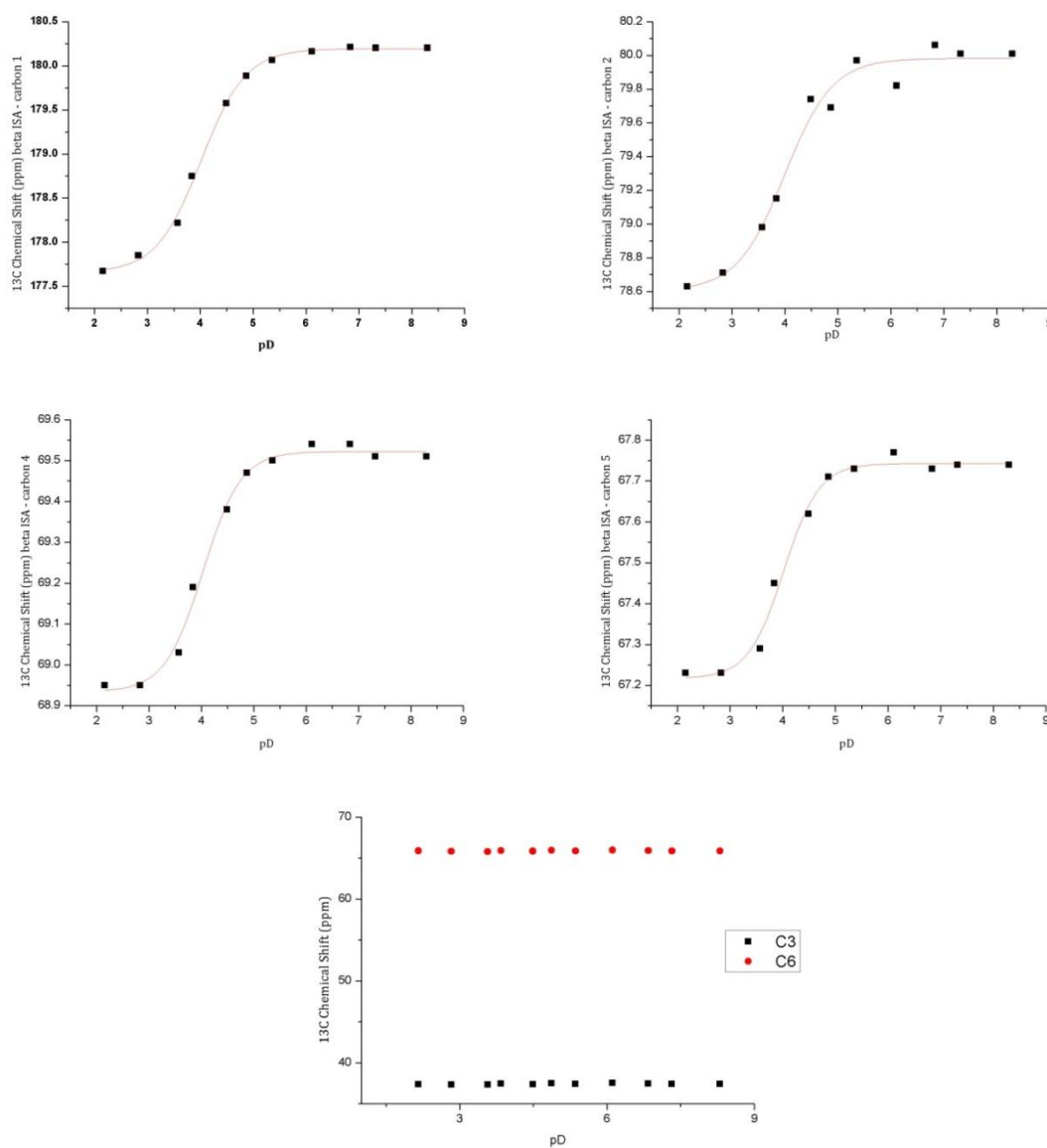


Figure 111: Variation of the  $^{13}\text{C}$  chemical shifts of beta ISA's carbon resonances (C1 – C6) as a function of pD. Solid line represents the fit to the equation:  $\delta(pD) = \delta_{\text{acid}} + \delta_{\text{base}} [10^{-pD} / (K_a + 10^{-pD})]$ .

## 5.2 Studies of the inter-conversion between $\beta$ -ISAH and $\beta$ -ISA<sub>L</sub>

As discussed in section 5.1.2, in acidic pH environments ISAH undergoes an acid catalysed conversion to the lactone conformation. In the synthetic method to produce  $\alpha$ -ISA<sub>L</sub> which was reported by Whistler and BeMiller<sup>149</sup>, this conversion was achieved by eluting salts of ISA through a cation exchange column in the H<sup>+</sup> form. Cho *et al.*<sup>150</sup> reported evidence for the formation of the lactone from the free acid at pH values of less than 4 in their NMR studies to determine the pK<sub>a</sub> of  $\alpha$ -ISA and a similar observation was seen with the results discussed in section 5.1.2 in our pK<sub>a</sub> studies. It is possible that this conversion occurs at higher pHs, but at very slow rates; in a study by Almond *et al.*<sup>224</sup> on the analogous XISA, it was estimated that at pH 3 an equilibrium concentration of XISAH and XISA<sub>L</sub> would take approximately 3 months to obtain. Getahun *et al.*<sup>229</sup> determined, using UV absorption spectroscopy, that the transformation between ISA and ISA<sub>L</sub> takes place at approximately pH 8, however, only limited studies have been undertaken to determine the kinetic rates of the inter-conversion of  $\alpha$ -ISA<sup>151</sup> and no studies have been reported for the inter-conversion of  $\beta$ -ISA.

### 5.2.1 The base catalysed conversion of ISA<sub>L</sub> to ISAH

In the present work the conversion from the lactone to the open-chain form of both  $\beta$ -ISA and  $\alpha$ -ISA was investigated. Ekberg *et al.*<sup>151</sup> attempted to determine the rate of transformation from  $\alpha$ -ISA<sub>L</sub> to the open-chain form by preparing a solution of ISA<sub>L</sub> and increasing its pH to 13 and tracking the conversion using ion chromatography; however, they stated that the transformation was faster than the resolution of the instrument. In the present work, some preliminary NMR studies were performed to gain an estimate of the time taken for the transformation from  $\alpha$ -ISA<sub>L</sub> to  $\alpha$ -ISA<sup>-</sup> at various pDs (pH + 0.4). Solutions of  $\alpha$ -ISA<sub>L</sub> were prepared in D<sub>2</sub>O (~ 25 mM) and the pD of the solution was increased to either pD 14, pD 12 or pD 11 by adding required amounts of NaOD. For all three reaction pDs, NMR analysis indicated that a rapid transformation of ISA<sub>L</sub> to ISA<sup>-</sup> was occurring, which was faster than the resolution of the instrument (< 5 min). A further, more carefully controlled NMR experiment was performed at a lower pD, (8.14) and because the ring-opening of the ISA consumes base, the analysis was performed in a pD 8.14 carbonate buffer solution, which was prepared using D<sub>2</sub>O as the solvent. To track the conversion, the sample was periodically analysed by <sup>1</sup>H NMR and the relative amounts of lactone and open-chain forms of  $\alpha$ -ISA were determined by integrating specific resonances (Figure

112). The results indicated that, as expected, the conversion was much slower at the lower pD, indicating that the reaction was pH dependent, and explains why the conversion could not be tracked at pH 13 in the work of Ekberg *et al.*<sup>151</sup>, due to the conversion being too fast at that pH.

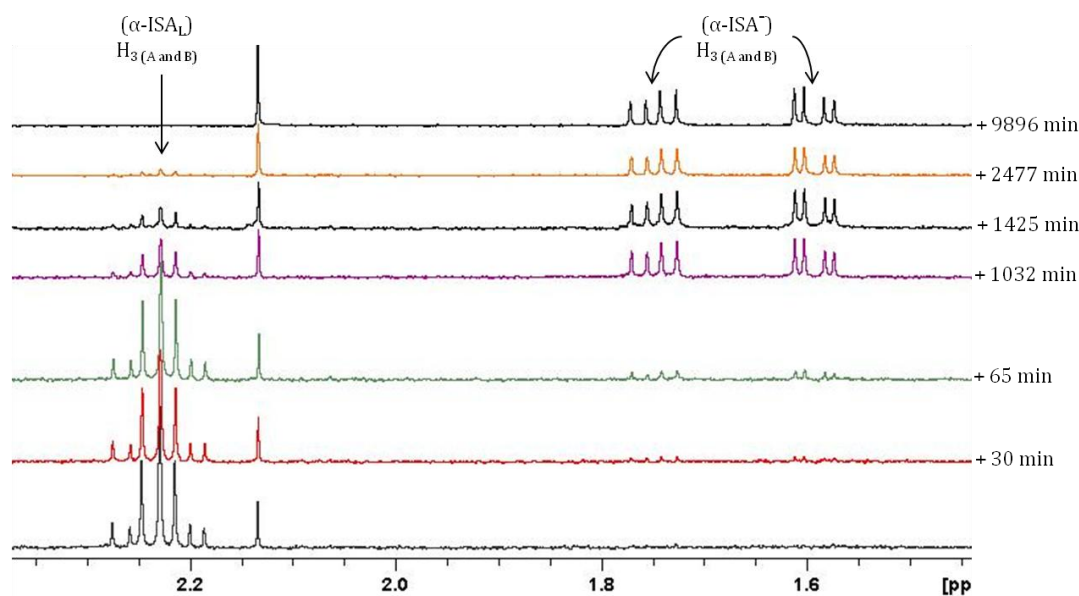


Figure 112: <sup>1</sup>H NMR spectra showing the conversion of ISA<sub>L</sub> to ISA<sup>-</sup> at pD 8.14 (H<sub>3</sub> resonances shown only).

From the NMR experiment, described above, a plot of the percentage of ISA<sub>L</sub> present in the solution versus time indicated that the base hydrolysis of α-ISA<sub>L</sub>, resulting in the production of α-ISA<sup>-</sup> was an exponential process, indicating that the reaction follows first-order kinetics (Figure 113); it can also be seen that upon completion of the reaction, 100 % of the lactone had been hydrolysed indicating that the base hydrolysis of α-ISA<sub>L</sub> was an irreversible process at the pH studied.

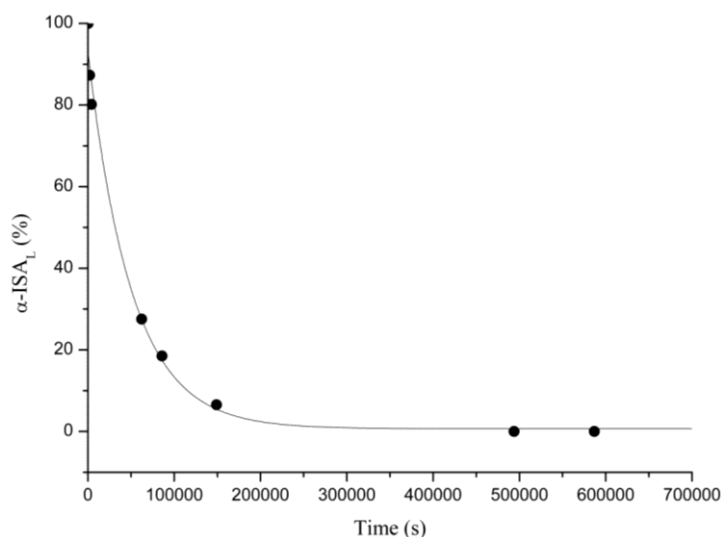


Figure 113: Graph showing the conversion of  $\alpha$ -ISA<sub>L</sub> to  $\alpha$ -ISA<sup>-</sup> at pD 8.14.

The main aim of the NMR experiments was to gain an estimate for a suitable range of pH values which could be used to measure the rates of lactone hydrolysis. The preliminary NMR study at pD 8.14 indicated that the base hydrolysis of ISA<sub>L</sub> could be monitored if the pH of the solution was fixed at intermediate values, e.g. significantly less than pH 11; however due to the possible affect of buffer catalysis, which may contribute to the overall rate of the reaction, it was decided that NMR would not be used to quantitatively determine the rate of the base catalysed hydrolysis reaction. In a further set of experiments, the kinetics of the hydrolysis reaction were monitored over a range of pH values using a pH-stat autotitrator, using the method described in section 2.7.2. The use of the autotitrator allowed for reactions to be conveniently and carefully monitored over long periods of time without the need for buffered systems. During the base hydrolysis of ISA<sub>L</sub>, hydroxide ions are not truly catalytic, as they are consumed in the reaction, which results in a drop in pH, however, with the autotitrator, the pH remains constant due to the computer controlled burette adding base to compensate for the drop in pH<sup>230</sup>. Using the autotitrator, the base hydrolysis of both  $\alpha$ -ISA<sub>L</sub> and  $\beta$ -ISA<sub>L</sub> were studied at pHs ranging from 8.5 – 10.25 so that, for the first time, pH rate profiles for the base catalysed hydrolysis of both  $\alpha$ - and  $\beta$ -ISA<sub>L</sub> could be constructed.

For each hydrolysis reaction, the volume of base added from the burette to compensate for the drop in pH (due to hydrolysis) was plotted as a function of time using Origin software (OriginLab Corporation) and each set of data was fitted to an exponential decay (Figure

114), which as previously discussed for the preliminary NMR reaction, indicated that the hydrolysis was following first-order type kinetics.

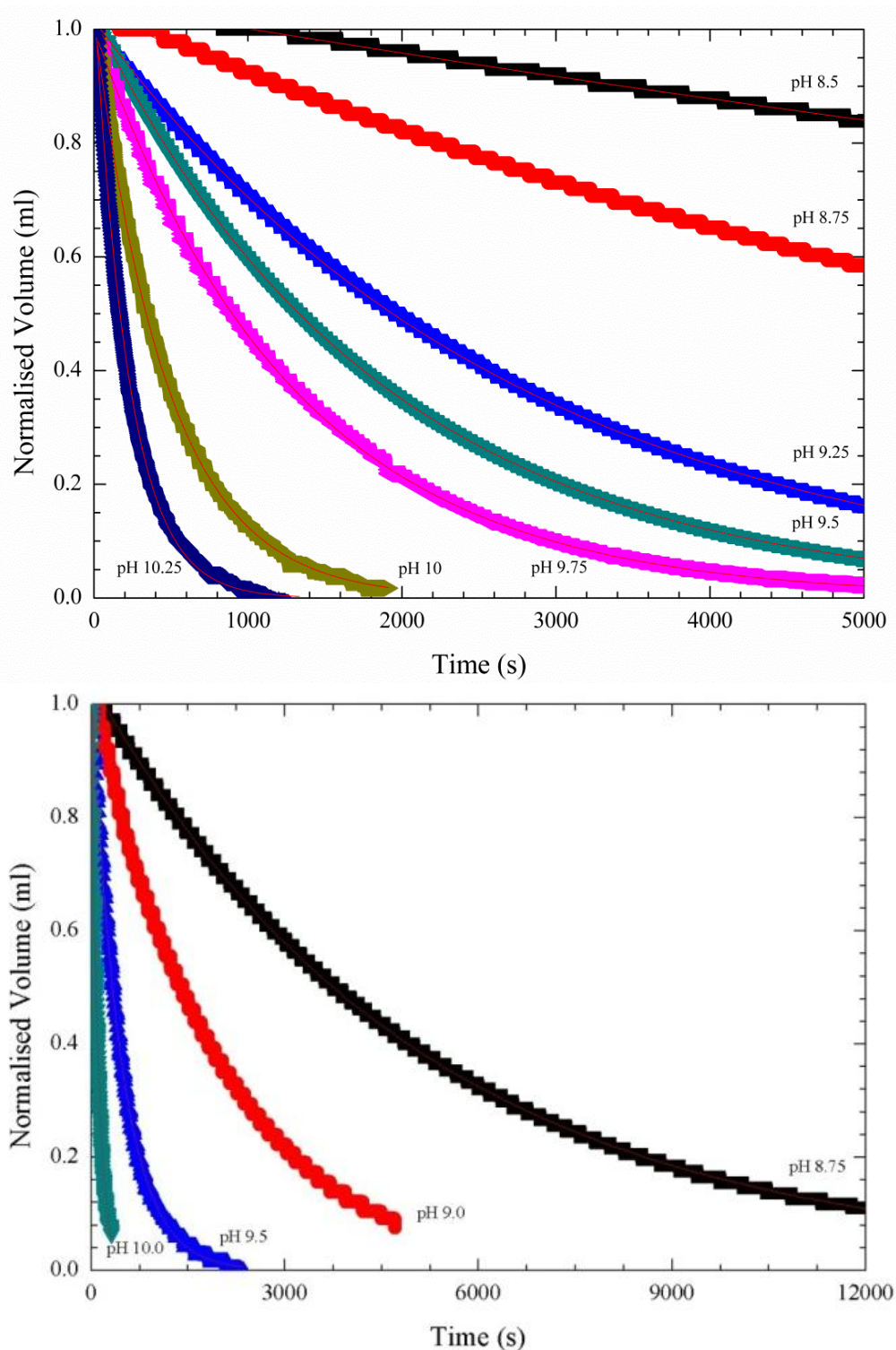
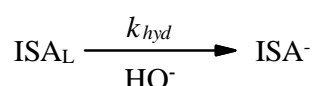


Figure 114: Normalised plots of the volume of base added (ml) over time (sec) to compensate for the fall in pH due to base hydrolysis of  $\beta$ -ISA<sub>L</sub> (top) and  $\alpha$ -ISA<sub>L</sub> (bottom).

For each reaction pH, 100 % of the lactone was hydrolysed, and the volume of base added indicated that one molar equivalent was required for a full conversion of the  $\text{ISA}_L$  to  $\text{ISA}^-$ . If the reaction was allowed to run for extended periods of time after the addition of one equivalent of base, no additional base was added confirming that above the  $\text{p}K_a$  of  $\alpha/\beta$ -ISA, the reaction was a one way process and no equilibrium between  $\text{ISA}_L$  and  $\text{ISA}^-$  exists.

A general mechanism for the base hydrolysis of  $\text{ISA}_L$  was previously presented in Figure 76 and can be described by the following scheme:



The overall reaction describing the change in  $\text{ISA}_L$  concentration is, however, a second-order process due to both  $\text{ISA}_L$  and  $\text{HO}^-$  being reactants and can therefore be described by the following differential rate law, where  $k_{hyd}$  is the overall second-order rate constant:

$$\frac{-d[\text{ISA}_L]}{dt} = k_{hyd}[\text{ISA}_L][\text{HO}^-] \quad \text{Eq. 1}$$

However, the use of the autotitrator ensured that the base concentration remained constant throughout each reaction; therefore each hydrolysis reaction can be described as being pseudo-first-order, and expressed by the following differential rate law, where  $k_{obs}$  is the pseudo-first-order rate constant:

$$\frac{-d[\text{ISA}_L]}{dt} = k_{obs}[\text{ISA}_L] \quad \text{Eq. 2}$$

Integration of equation 2 between the limits ( $t_0 = 0$ ,  $[\text{ISA}_L]_0$ ) and ( $t$ ,  $[\text{ISA}_L]_t$ ) results in the following expression:

$$\ln[\text{ISA}_L]_t = \ln[\text{ISA}_L]_0 - k_{obs}t \quad \text{Eq. 3}$$

According to equation 3, a plot of  $\ln[\text{ISA}_L]_t$  versus time will result in a straight line if the base hydrolysis of  $\text{ISA}_L$  was, as indicated in Figure 114 following first order kinetics, and the slope of the resulting plot will equal  $-k_{obs}$ . However, due to the use of the autotitrator, it is necessary to substitute  $[\text{ISA}_L]$  in equations 3, for  $(\text{Vol}_{\text{base}})$ , representing the volume of

base added from the burette to maintain a constant pH. A plot of  $\ln(\text{Vol}_{\text{base}})$  vs. time will allow  $-k_{\text{obs}}$  to be determined from the resulting slope. For each pH, for both  $\alpha$ - and  $\beta$ -ISA, linear plots were achieved and the resulting pseudo-first-order rate constants were determined (Figure 115).

Due to a straight lines being observed in Figure 115, it can be said that a definite fraction of the  $\text{ISA}_L$  will be hydrolysed at a given time, and if the fraction is  $\frac{1}{2}$ , equation 3 can be substituted which allows the half-life of the reaction to be calculated, as follows:

$$\ln[\text{ISA}_L]_{t_{\frac{1}{2}}} = \ln[\text{ISA}_L]_{0_{\frac{1}{2}}} - k_{\text{obs}}t_{1/2} \quad \text{Eq. 4}$$

and rearrangement of equation 4 provides equation 5; using this equation, half-lives ( $t_{1/2}$ ) were calculated for the base catalysed hydrolysis of  $\alpha$ - $\text{ISA}_L$  or  $\beta$ - $\text{ISA}_L$  for each reaction pH (Figure 115).

$$t_{1/2} = \frac{\ln\left(\frac{[\text{ISA}_L]_{0_{1/2}}}{[\text{ISA}_L]_{t_{1/2}}}\right)}{k_{\text{obs}}} = \frac{\ln 2}{k_{\text{obs}}} = \frac{0.693}{k_{\text{obs}}} \quad \text{Eq. 5}$$

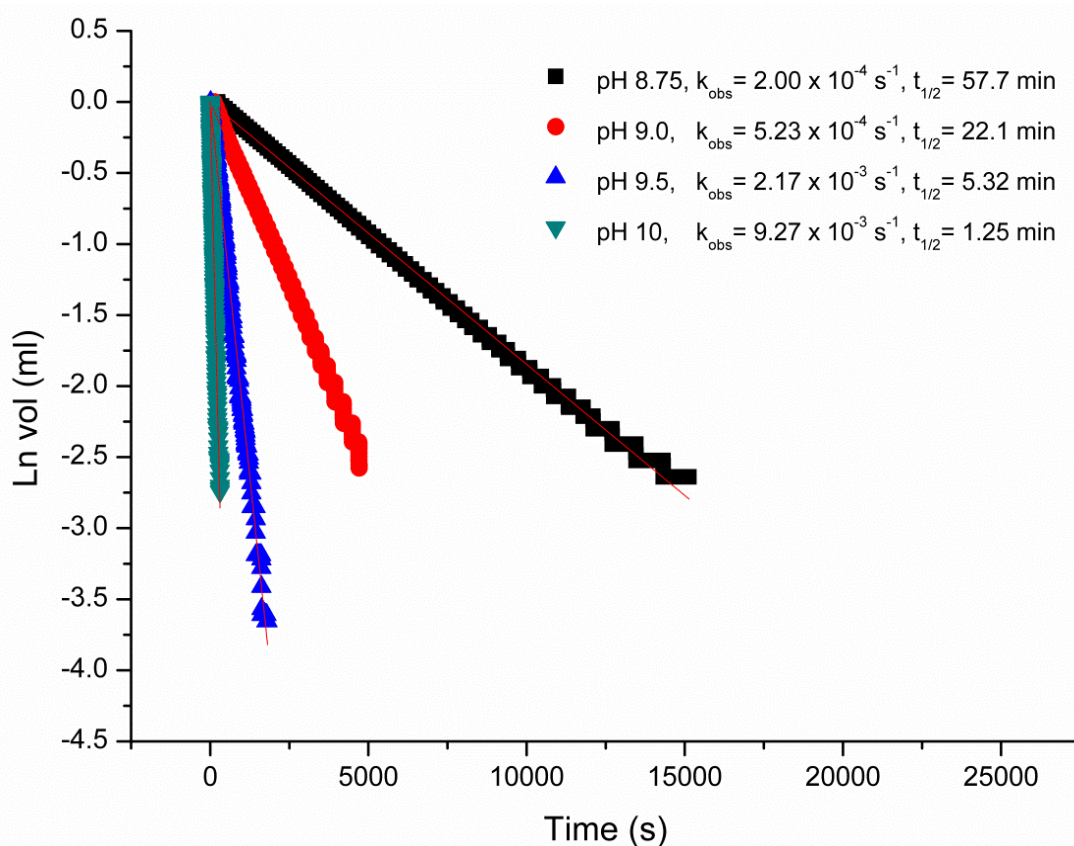
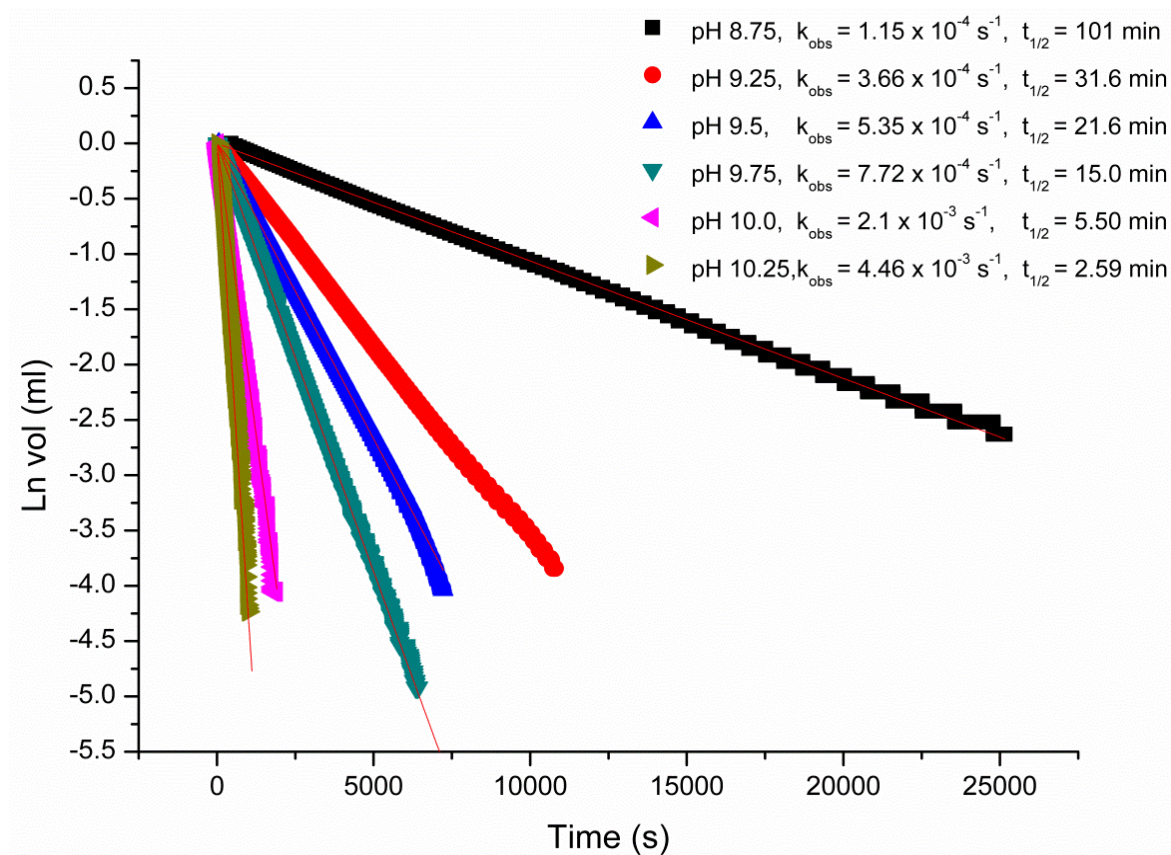


Figure 115: Plots of  $\ln[\text{Vol}_{\text{base}}]t$  versus time which provide a value of  $-k_{\text{obs}}$  as the gradient for the base catalysed hydrolysis of  $\beta$ -ISA<sub>L</sub> (left) and  $\alpha$ -ISA<sub>L</sub> (right).

Using the calculated  $k_{obs}$  values, a plot of  $\text{Log}_{10}(k_{obs})$  versus pH allowed pH rate profiles to be constructed for the base catalysed hydrolysis of both  $\alpha$ - and  $\beta$ -ISA<sub>L</sub> at 25 °C (Figure 116). Furthermore, the relative reactivity of  $\alpha$ - and  $\beta$ -ISA lactones was determined by calculating the second order rate constants ( $k_{hyd}$ ) for the hydrolysis reactions, and can be calculated as follows: given equations 1 and 2, it can be said that:

$$k_{obs} = k_{hyd}[\text{OH}^-] \quad \text{Eq. 6}$$

Rearrangement of equation 6 gives:

$$k_{hyd} = \frac{k_{obs}}{[\text{OH}^-]} \quad \text{Eq. 7}$$

The concentration of hydroxide ion  $[\text{HO}^-]$  at a given pH can be calculated from the ion product constant of water ( $K_w$ ) at 25 °C, given:

$$K_w = \frac{[\text{H}^+][\text{HO}^-]}{[\text{H}_2\text{O}]} = 1.01 \times 10^{-14} \quad \text{Eq. 8}$$

and a plot of hydroxide concentration against  $k_{obs}$  (Figure 117) for each pH provides for the average second order rate constant to be determined from the slope of the plot: 97.0  $\text{M}^{-1} \text{s}^{-1}$  for  $\alpha$ -ISA<sub>L</sub> and 25.3  $\text{M}^{-1} \text{s}^{-1}$  for  $\beta$ -ISA<sub>L</sub>.

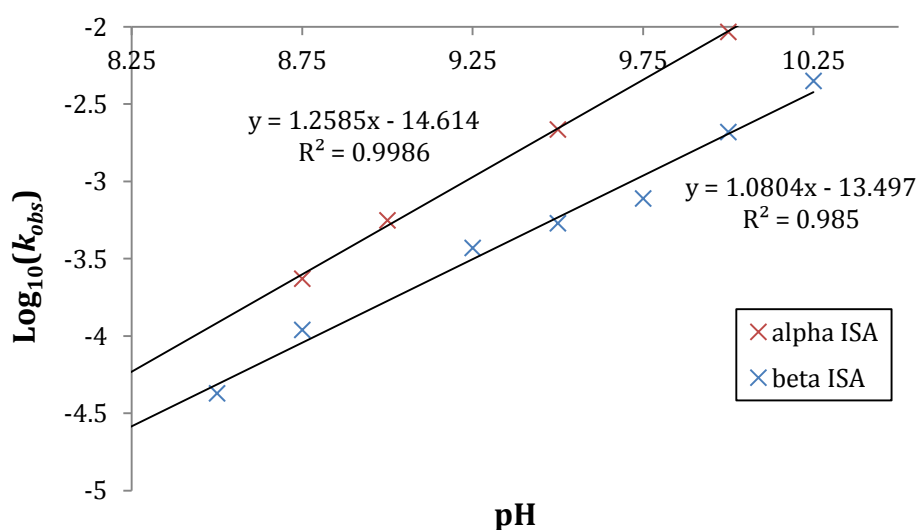


Figure 116: pH verses rate profile for the hydrolysis of  $\alpha$ -ISA<sub>L</sub> and  $\beta$ -ISA<sub>L</sub> at 25 °C

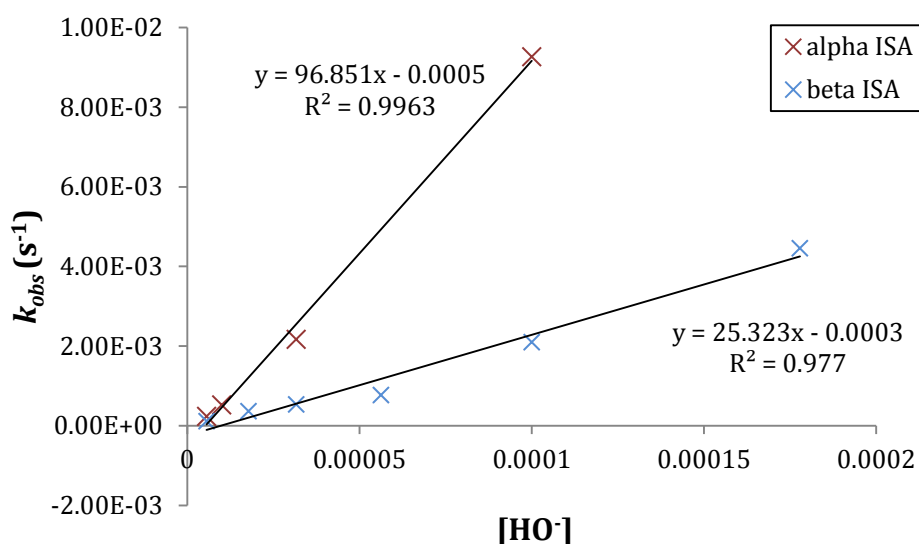


Figure 117: Plot of  $[\text{OH}^-]$  versus  $k_{obs}$  for the hydroxide catalysed hydrolysis of  $\alpha$ -ISA<sub>L</sub> and  $\beta$ -ISA<sub>L</sub>

From the pH rate profiles presented in Figure 116, it can be seen that within experimental error, both rate profiles have a slope close to one indicating that the base catalysed hydrolysis of both  $\alpha$ - and  $\beta$ -ISA<sub>L</sub> are first order processes and the profiles can be used to estimate the rate of reaction at other pH values. The profiles indicate that under the present reaction conditions, the base hydrolysis of  $\alpha$ -ISA<sub>L</sub> is a faster process than for  $\beta$ -ISA<sub>L</sub>; the half-lives of both processes are presented in Figure 115 and as expected, the rate of each reaction is pH dependent. At pH 8.75, the reaction is relatively slow, ( $t_{1/2} = 101$  min for  $\beta$ -ISA and 58 min. for  $\alpha$ -ISA), whereas, at pH 10, the reaction is much faster ( $t_{1/2} = 5.5$  min. for  $\beta$ -ISA and 1.3 min. for  $\alpha$ -ISA). The plot presented in Figure 117 indicates that  $\alpha$ -ISA<sub>L</sub> is approximately 4 times more reactive than  $\beta$ -ISA<sub>L</sub>, although, the error associated with the second order rate constant determined for  $\alpha$ -ISA was relatively large. Only four data points were collected for the hydrolysis of  $\alpha$ -ISA<sub>L</sub> compared to seven for  $\beta$ -ISA<sub>L</sub> and additional experiments would be required to improve the confidence of the  $\alpha$ -ISA<sub>L</sub> results. It can be said, however, that even with the associated errors, the reactivity of  $\alpha$ -ISA<sub>L</sub> was greater than  $\beta$ -ISA<sub>L</sub> as the reaction was consistently faster for each measured pH. It was determined by Almond *et al.*<sup>224</sup>, using isotope labelling and mass spectrometric studies, that the base hydrolysis of XISA, which is very similar in structure to ISA, occurs via a base-catalyzed, acyl-oxygen fission, bimolecular ( $B_{AC2}$ ) mechanism, therefore it is likely that the base hydrolysis of ISA<sub>L</sub> also undergoes a similar  $B_{AC2}$  mechanism. The different conformations present in the C2 carbons between the two isomers may explain the differences in reaction

rate; it is possible that the hydroxymethyl group of  $\beta$ -ISA<sub>L</sub>, when in the ring conformation hinders access of the hydroxide ion to the carbonyl group more than it does for  $\alpha$ -ISA<sub>L</sub>.

A large list of base-catalysed hydrolysis rate constants for carboxylic acid esters have been published by Hilal *et al.*<sup>232</sup>, under similar reaction conditions (water solvent and 25 °C), the constants vary from  $1.5 \times 10^{-3} \text{ M}^{-1} \text{ s}^{-1}$  for ethyl neopentate to  $12589 \text{ M}^{-1} \text{ s}^{-1}$  for phenyl dichloroacetate. Given the large range of reported values, the second order rate constants determined for  $\alpha$ - and  $\beta$ -ISA<sub>L</sub> are quiet similar; they are also similar to the second order rate constant obtained by Almond *et al.*<sup>224</sup> for XISA<sub>L</sub> ( $25 \text{ M}^{-1} \text{ s}^{-1}$ ), which was determined using the same experimental method.

The second order rate constants determined for  $\alpha$ - and  $\beta$ -ISA<sub>L</sub> (and XISA<sub>L</sub>) are slightly larger than the values estimated for valerolactone ( $15 \text{ M}^{-1} \text{ s}^{-1}$ ) and butyrolactone ( $1.0 \text{ M}^{-1} \text{ s}^{-1}$ ) which were determined by extrapolation of data reported by Blackburn and Dodds<sup>233</sup> determined at 46 °C ( $59.0 \text{ M}^{-1} \text{ s}^{-1}$ , valerolactone and  $4.03 \text{ M}^{-1} \text{ s}^{-1}$ , butyro lactone). It is possible that the increase in reactivity for ISA<sub>L</sub> and XISA<sub>L</sub>, in comparison to valerolactone and butyrolactone may be due to the additional hydroxyl and hydroxymethylene groups which are present on the ISA<sub>L</sub> and XISA<sub>L</sub> but not on valerolactone or butyrolactone (Figure 118). The crystal structure of XISA lactone<sup>234</sup> indicates that a hydrogen bond is present between the hydrogen of the hydroxyl group attached to the C5 carbon and the carbonyl oxygen atom (Figure 118). Such a bond would result in a reduction of the electron density of the carbonyl carbon due to the resulting electron withdrawing effects of the carbonyl oxygen, making nucleophilic attack by the hydroxide anion more rapid. Furthermore the electron withdrawing effect of the hydroxide group which is present on the carbon atom adjacent to the carbonyl carbon on both ISA<sub>L</sub> and XISA<sub>L</sub> (C2), which is not present on either valerolactone or butyrolactone would make ISA<sub>L</sub> and XISA<sub>L</sub> more susceptible to nucleophilic attack at the carbonyl carbon.

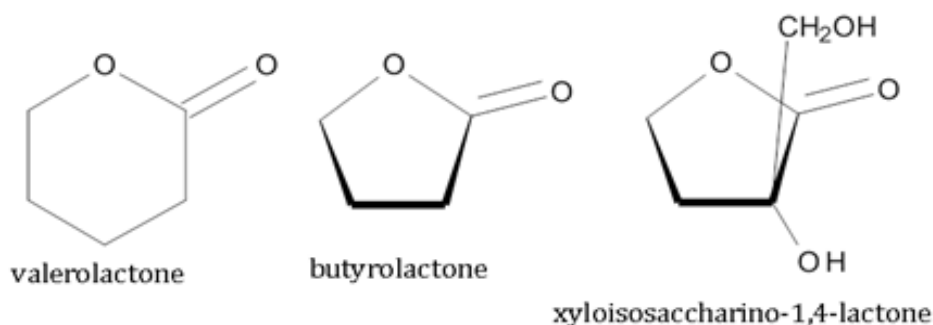


Figure 118: Structures of valerolactone, butyrolactone and XISA<sub>L</sub>

### 5.2.2 The acid catalysed conversion of ISAH to ISAL

A further set of experiments were undertaken to investigate the intramolecular transformation from the open-chain form of  $\alpha$ - and  $\beta$ -ISA to their respective lactones. Ekberg *et al.*<sup>151</sup> investigated the same conversion of  $\alpha$ -ISA using ion chromatography at a single pH. They determined that at pH 1.05, the carboxylic acid was partially transformed into the lactone, until a point of equilibrium was reached due to an opposing reverse reaction, which converts the lactone back to the carboxylic acid. Ekberg *et al.* determined an equilibrium constant ( $K_{eq}$ , 6.60) for the overall reaction, which provided a measure of the amount of carboxylic acid and lactone present in a particular sample. Pseudo-first-order rate constants for the forward ( $k_{lac} = 1.2 \times 10^{-5} \text{ s}^{-1}$ ) and reverse ( $k_{hyd} = 8.0 \times 10^{-5} \text{ s}^{-1}$ ) reactions were determined and a half-life for the conversion of the carboxylic acid to the lactone was also determined ( $t_{1/2} = 122 \text{ min}$ ).

In the present work,  $^1\text{H}$  NMR spectroscopy was used to investigate the conversion of the carboxylic acid form of  $\beta$ -ISA to the lactone conformation at various acidic pDs, using the method described in section 2.7.3, so that a rate profile similar to the one for the base hydrolysis of ISAL could be constructed. To study the conversion, solutions of the calcium salt of  $\beta$ -ISA were prepared in  $\text{D}_2\text{O}$  at five different pDs ( $\text{pD} = \text{pH} + 0.4$ ), between pDs 1 and 2.5 and their  $^1\text{H}$  NMR spectra were recorded at regular intervals at a set temperature of  $25 \text{ }^\circ\text{C}$ . In addition, a limited number of experiments were performed on the calcium salt of  $\alpha$ -ISA (pDs 1.34 and 2.25) using the same experimental conditions. To follow the progress of the reactions the ratio of the amount of  $\alpha/\beta$ -ISAH :  $\alpha/\beta$ -ISAL was determined by integrating the C3 methylene resonances for each species at a given time; the C3 methylene resonances were chosen because they were more resolved than other resonances. A plot of the percentage of ISAH present as a function of time for each of the reaction pDs indicated that the ISAH concentration decayed exponentially with time, which indicated first-order behaviour and in agreement with Ekberg *et al.*<sup>151</sup> the ISA reached a state of equilibrium between the two species (Figure 119).

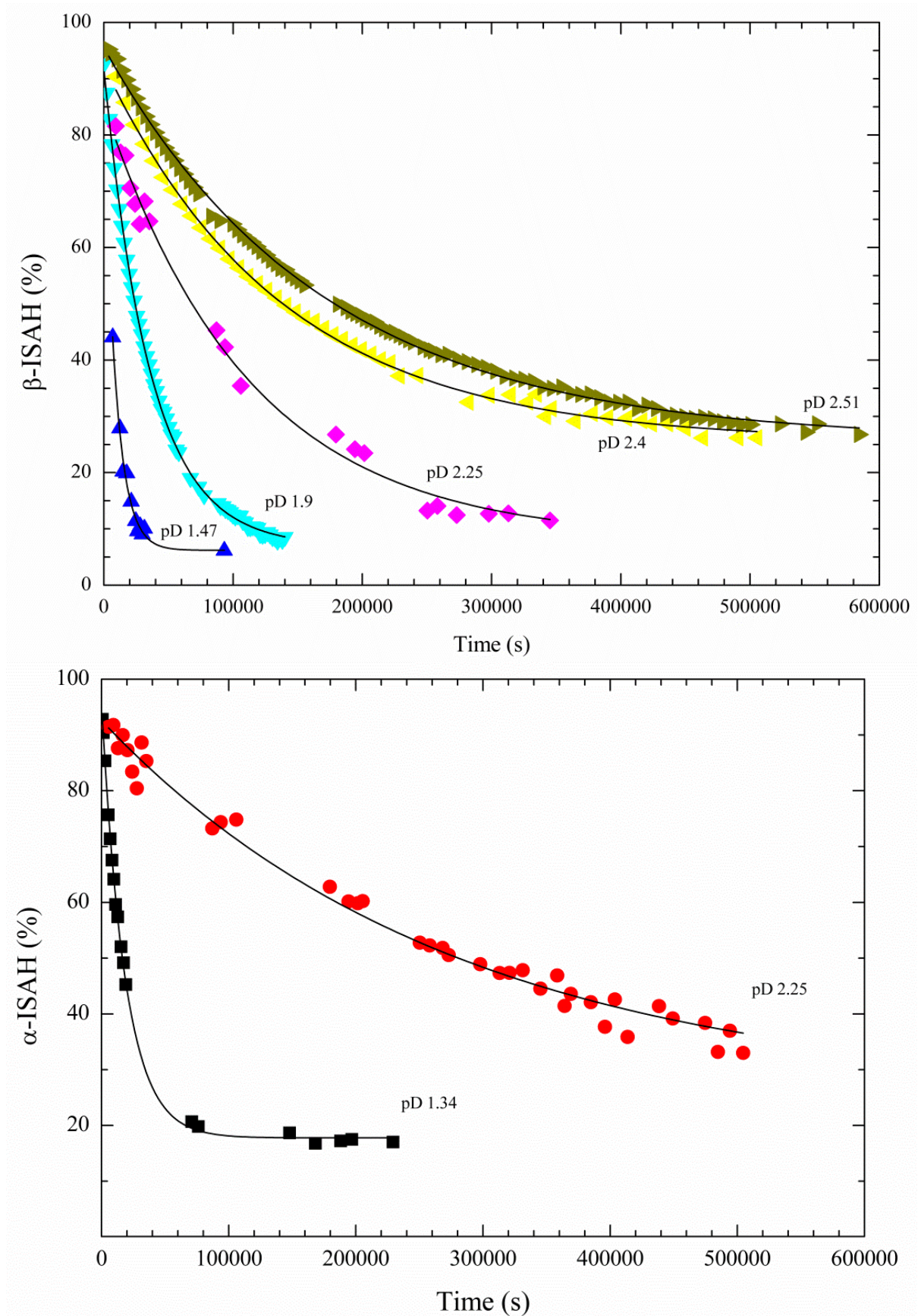
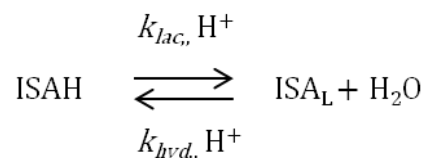


Figure 119: Plots of the percentage of  $\beta$ -ISAH (top) and  $\alpha$ -ISAH (bottom) remaining in acidic solution as a function of time.

The reversible acid catalysed inter-conversion between ISAH and  $\text{ISA}_L$  can be described by the following scheme:



and a general mechanism for the process is presented in Figure 120:

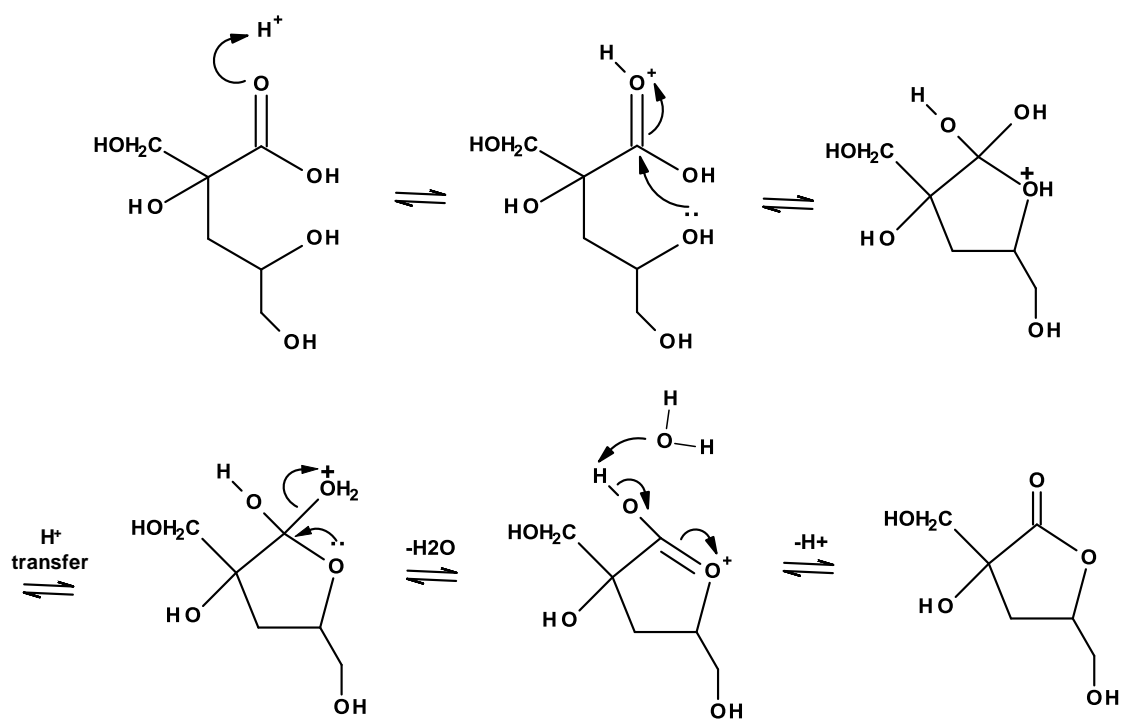


Figure 120: A general mechanism for the acid catalysed lactonization of ISAH and lactone hydrolysis

The overall second-order process, for the net disappearance of ISAH can be described by the following differential rate law, where  $k_{lac}$  and  $k_{hyd}$  are the forward and reverse second order rate constants for the lactonization and the lactone hydrolysis reactions respectively:

$$\frac{-d[\text{ISAH}]}{dt} = k_{lac}[\text{ISAH}][\text{D}^+] - k_{hyd}[\text{ISA}_L][\text{D}^+] \quad \text{Eq. 9}$$

However, due to the forward and reverse reactions being acid catalysed, the net disappearance can be described as a pseudo-first-order process, and described by the following equation, where  $k'_{lac}$  and  $k'_{hyd}$  are pseudo-first-order rate constants:

$$\frac{-d[\text{ISAH}]}{dt} = k'_{lac}[\text{ISAH}] - k'_{hyd}[\text{ISA}_L] \quad \text{Eq. 10}$$

To solve Eq. 10 it is useful to incorporate a further equation which represents the stoichiometry of the reaction <sup>235</sup>, as follows:

$$[\text{ISAH}]_0 + [\text{ISA}_L]_0 = [\text{ISAH}]_{eq} + [\text{ISA}_L]_{eq} = [\text{ISAH}]_t + [\text{ISA}_L]_t \quad \text{Eq. 11}$$

where the subscript 'o' represents the initial concentration of ISAH/L, subscript 'eq' represents the concentration of ISAH/L at equilibrium and subscript 't' represents the concentration of ISAH/L at a given time.

It is also useful to state that at equilibrium, when  $d[\text{ISAH}]/dt$  (in Eq. 10) is set to zero, the forward and reverse reactions are at an equal rate (equilibrium), which can be described by Eq. 12 <sup>235</sup> and rearrangement of Eq. 12 allows for the equilibrium constant,  $K_{eq}$ , to be introduced (Eq. 13).

$$k'_{lac}[\text{ISAH}]_{eq} = k'_{hyd}[\text{ISA}_L]_{eq} \quad \text{Eq. 12}$$

$$\frac{[\text{ISA}_L]_{eq}}{[\text{ISAH}]_{eq}} = \frac{k'_{lac}}{k'_{hyd}} = K_{eq} \quad \text{Eq. 13}$$

Using the information provided in Eqs. 11 – 13, Eq. 10 can be re-written to give an expression where  $[\text{ISAH}]$  is the only concentration variable:

$$\frac{-d[\text{ISAH}]}{dt} = (k'_{lac} + k'_{hyd})([\text{ISAH}] - [\text{ISAH}]_{eq}) \quad \text{Eq. 14}$$

Integration of Eq. 14 between the limits ( $t_0 = 0$ ,  $[\text{ISAH}]_0$ ) and ( $t$ ,  $[\text{ISAH}]_t$ ) results in the following expression:<sup>235</sup>

$$\ln \left\{ \frac{[\text{ISAH}]_t - [\text{ISAH}]_{\text{eq}}}{[\text{ISAH}]_0 - [\text{ISAH}]_{\text{eq}}} \right\} = -(k'_{\text{lac}} + k'_{\text{hyd}})t \quad \text{Eq. 15}$$

According to equation 15, a plot of  $\ln\{[\text{ISAH}]_t - [\text{ISAH}]_{\text{eq}}/[\text{ISAH}]_0 - [\text{ISAH}]_{\text{eq}}\}$  versus time will be linear if a pseudo-first-order reaction is being observed and the negative value of the resulting slope will provide the sum of the forward and reverse pseudo-first-order rate constants ( $k'_{\text{lac}}$  and  $k'_{\text{hyd}}$ ).

The sum of  $k'_{\text{lac}}$  and  $k'_{\text{hyd}}$  provides for the net rate at which equilibrium is approached and can be determined as the “natural” rate constant<sup>235</sup> or  $k_{\text{obs}}$ . Using this information and in combination with Eq. 13, individual values for  $k'_{\text{lac}}$  and  $k'_{\text{hyd}}$  can be calculated for each individual reaction pD using the following equations:

$$k_{\text{lac}} = \frac{k_{\text{obs}}}{1 + K_{\text{eq}}^{-1}} \quad \text{and} \quad k_{\text{hyd}} = \frac{k_{\text{obs}}}{1 + K_{\text{eq}}} \quad \text{Eq. 16}$$

Linear plots were achieved for each reaction pD (Figure 121), which, using the above information, allowed values to be calculated for  $k_{\text{obs}}$ ,  $k'_{\text{lac}}$ ,  $k'_{\text{hyd}}$  and  $K_{\text{eq}}$  for each reaction pD, the results of which are presented in Table 12. It is noted that there is a considerable amount of scatter, in particularly with the linear plot produced from the acid catalysed lactonization of  $\beta$ -ISAH at pD 2.25. The reason for this is because at that pD, a mixed sample of  $\alpha$ - and  $\beta$ -ISAH was used to investigate the suitability of using mixed samples to follow the progress of the lactonization. However, the presence of both analytes made it more difficult to integrate the individual resonances due to crowding of the peaks. The scatter produced from that result suggests that, for  $\alpha$ - and  $\beta$ -ISA, when using proton NMR, due to the large number of multiplet peaks, subsequent measurements should be performed on individual analytes.

Table 12: Observed constants for the lactonization of ISAH at various reaction pDs at 25 °C

substrate	pD	$k_{obs}$ ( $s^{-1}$ )	$k'_{lac}$ ( $s^{-1}$ )	$k'_{hyd}$ ( $s^{-1}$ )	$K_{eq}$
$\beta$ -ISA	1.47	$1.06 \times 10^{-4}$	$9.96 \times 10^{-5}$	$6.57 \times 10^{-6}$	15.2
$\beta$ -ISA	1.90	$2.81 \times 10^{-5}$	$2.61 \times 10^{-5}$	$1.95 \times 10^{-6}$	13.4
$\beta$ -ISA	2.25	$8.95 \times 10^{-6}$	$8.22 \times 10^{-6}$	$7.31 \times 10^{-7}$	11.2
$\beta$ -ISA	2.40	$7.26 \times 10^{-6}$	$5.41 \times 10^{-6}$	$1.86 \times 10^{-6}$	2.91
$\beta$ -ISA	2.51	$5.92 \times 10^{-6}$	$4.40 \times 10^{-6}$	$1.52 \times 10^{-6}$	2.86
$\alpha$ -ISA	1.34	$5.38 \times 10^{-5}$	$4.42 \times 10^{-5}$	$9.57 \times 10^{-6}$	4.62
$\alpha$ -ISA	2.25	$2.56 \times 10^{-6}$	$2.47 \times 10^{-6}$	$6.21 \times 10^{-7}$	3.98

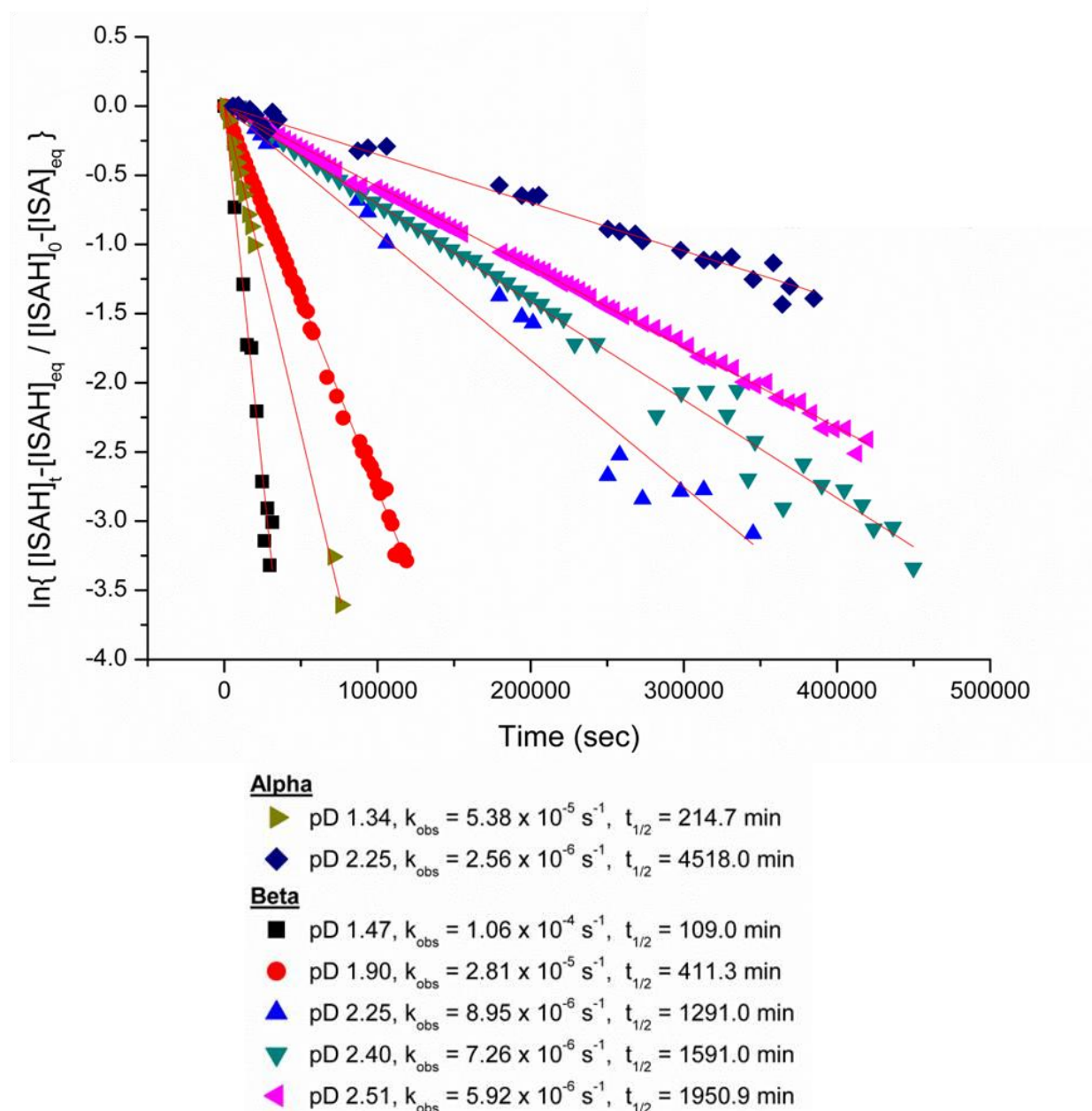


Figure 121: Plots of  $\ln\{[ISAH]_t - [ISAH]_{eq} / [ISAH]_0 - [ISAH]_{eq}\}$  versus time which provide a value of  $-k_{obs}$  ( $k'_{lac} + k'_{hyd}$ ) as the gradient for the acid catalysed hydrolysis of  $\alpha/\beta$ -ISAH.

Using the calculated  $k_{obs}$  values, a plot of  $\text{Log}_{10}(k_{obs})$  versus pD allowed rate profiles to be constructed for the acid catalysed net lactonization reaction of both  $\alpha$ - and  $\beta$ -ISA<sub>L</sub> at 25 °C (Figure 122) and the slopes close to one identify that the reactions are pseudo first order.

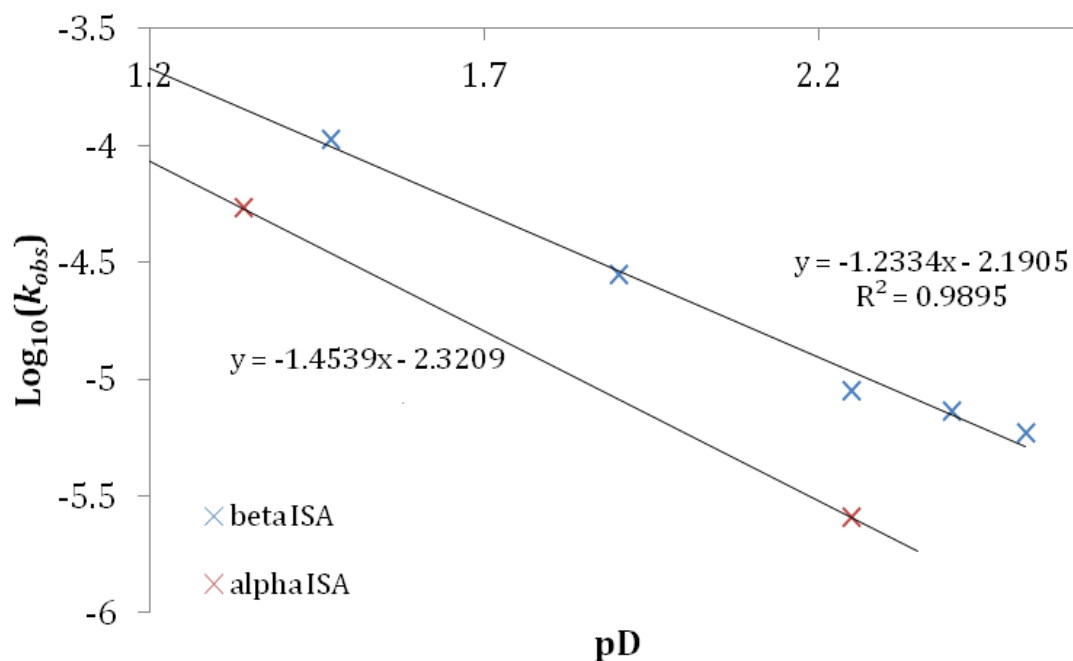


Figure 122: pD versus rate profile for the lactonization of alpha and beta ISAH at 25 °C

The second order rate constant ( $k_{lac}$ ) was also determined for the lactonization of  $\beta$ -ISAH by plotting the deuterium ion concentration against the values obtained for  $k'_{lac}$  for each reaction pD (Figure 123) and  $k_{lac}$  was determined from the slope of the resulting plot, to which a value of  $3.10 \times 10^{-3} \text{ M}^{-1} \text{ s}^{-1}$  was obtained. Furthermore, due to only two reaction pDs being investigated for the lactonization of  $\alpha$ -ISAH, the second order rate constant was determined by dividing the value obtained for  $k'_{lac}$  for both reaction pDs by the deuterium concentration and calculating the mean value, to which a value of  $7.04 \times 10^{-4} \text{ M}^{-1} \text{ s}^{-1}$  was determined.

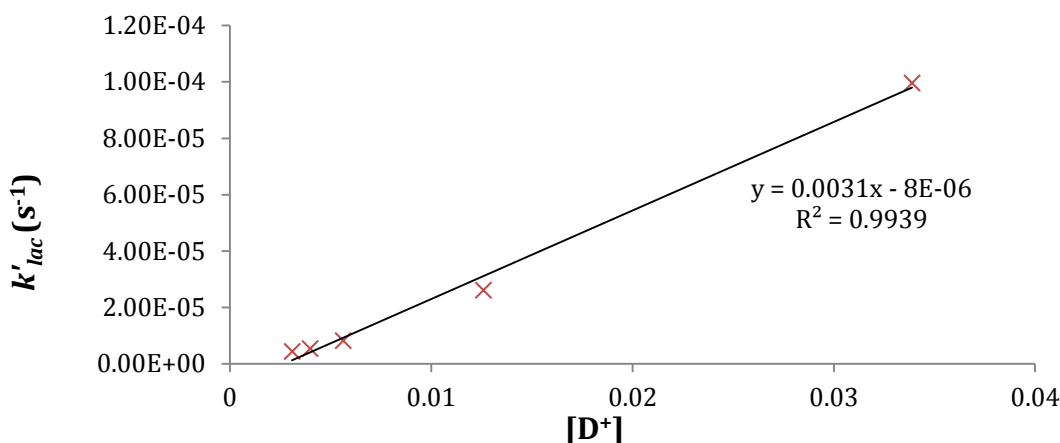


Figure 123: Plot of  $[D^+]$  versus  $k'_{lac}$  for the acid catalysed hydrolysis of alpha and beta ISA lactones.

The pseudo-first-order rate constants obtained in the present work for the acid catalysed lactonization of  $\alpha$ -ISA for the experiment performed at pD 1.34 (pH 0.94,  $k_{obs} = 5.38 \times 10^{-5}$ ,  $k'_{lac} = 4.42 \times 10^{-5}$  and  $k'_{hyd} = 9.57 \times 10^{-6}$ ) are similar to the values reported by Ekberg *et al.*<sup>151</sup> for the lactonization of alpha ISA at pH 1 ( $k_{obs} = 9.31 \times 10^{-5}$ ,  $k'_{lac} = 8.08 \times 10^{-5}$  and  $k'_{hyd} = 1.25 \times 10^{-5}$ ). However, as previously discussed, in the present study, reactions were performed in deuterated solvent, so direct comparisons should not be made due to the associated isotope effects.

Only a limited number of pD values were investigated for  $\alpha$ -ISA, however, the results indicate that in acidic media, the open-chain form of  $\beta$ -ISA was more reactive than the open-chain form of  $\alpha$ -ISA. This is indicated by the second order rate constant which was determined for the net disappearance of  $\beta$ -ISAH being approximately four-times larger than the equivalent second order rate constant for the net disappearance of  $\alpha$ -ISAH. The stability of the ring being formed is a major factor in the ease at which the ring closes<sup>236</sup>, therefore it is possible that the lactone ring of  $\alpha$ -ISA is less stable than the lactone ring of  $\beta$ -ISA, thus making  $\alpha$ -ISAH less reactive in acidic media. An indication of this are the equilibrium constants, which are presented in Table 12; when comparing the equilibrium constants for  $\alpha$ - and  $\beta$ -ISA which were both obtained at pD 2.25, the equilibrium constant for  $\beta$ -ISA was 11.2, whereas for  $\alpha$ -ISA it was only 3.98, indicating that at equilibrium, more of the beta isomer was present as the lactone. Similar findings, indicating that ring stability affects the rate of their formation were found in a study by Wilkinson *et al.*<sup>237</sup> who investigated the acid catalysed rate of formation of the cis- and trans- 5-membered lactones produced from the threo and erythro isomers of 3-methyl-4-hydroxyoctanoic acid. They determined that

the lactone of the threo isomer was produced faster than the lactone of the erythro isomer; this was attributed to the lactone produced from the erythro isomer having an unfavourable steric interaction between the methyl and butyl groups of the lactone ring when in the cis conformation. It is therefore possible that a similar unfavourable steric interaction between the two hydroxymethyl groups of  $\alpha$ -ISA<sub>L</sub>, due to being in the cis position, may result in the open-chain form of  $\alpha$ -ISA being less reactive in acidic media. It is also possible that the different conformations of the two isomers may result in the angle of approach of the attacking hydroxyl group (at C4) and the carbonyl carbon being more favourable for  $\beta$ -ISAH, allowing the reaction to occur faster for that isomer<sup>238</sup>. This is supported by the value obtained for the pseudo-first-order rate constant ( $k'_{lac}$ ) for the lactonisation of  $\beta$ -ISA ( $8.22 \times 10^{-6}$ ) being three-times larger than the value obtained for the lactonisation of  $\alpha$ -ISA at the same pD ( $2.47 \times 10^{-6}$ ), whereas, the constants for the reverse lactone hydrolysis reaction ( $k'_{hyd}$ ) for both  $\alpha$ - and  $\beta$ -ISA<sub>L</sub> were very similar (see Table 12).

In comparison to the second order rate constants which were determined for the base catalysed lactone hydrolysis of  $\alpha$ - and  $\beta$ -ISA<sub>L</sub>, the second order rate constants for the acid catalysed lactonization were several orders of magnitude smaller indicating that ISAH is relatively stable in acidic media. However, the results indicated that the rate of the lactonization reaction and the percentage of lactone formed at equilibrium were directly related to the pD of the reaction solution, however, for all reaction pDs, a complete conversion to the lactone was not achieved, even at the lowest pDs investigated. For  $\beta$ -ISA, at pD 1.47, ~ 94 % of the  $\beta$ -ISAH was lactonized and at pD 1.34, ~ 82 % of the  $\alpha$ -ISAH was lactonized. The results suggest that very strong acidic conditions are required to achieve a complete lactonization of the ISAH. This was previously indicated in the preparation of  $\alpha$ -ISA<sub>L</sub>, which was discussed in section 3.2.2. Lactonization was achieved by eluting the calcium salt of  $\alpha$ -ISA through a cation exchange column after conditioning the column with 2 M HCl and as previously discussed, it was determined that inadequate conditioning of the cation exchange resin resulted in only a partial lactonization.

According to the rate profiles, which were presented in Figure 122, good linearity was observed so estimates can be made for the time to reach equilibrium ( $5 \times t_{1/2}$ ) at a given pD; for example, at pD 1 equilibrium would occur after approximately 2½ hrs for  $\beta$ -ISA and 6 hrs for  $\alpha$ -ISA, whereas at pD 3, equilibrium would occur after approximately one month for  $\beta$ -ISA and 193 days for  $\alpha$ -ISA. In the results described in section 5.1.2, for the  $pK_a$  determination of  $\beta$ -ISA, additional lactone peaks were observed in the NMR spectra in

samples where the pD was approximately 4, however, it can be estimated that at that pD, approximately 18 months would be required for  $\beta$ -ISA and significantly longer for  $\alpha$ -ISA to reach equilibrium. In comparison to the acid catalysed lactonization results, only relatively basic conditions are required for a complete ring-opening of  $ISA_L$ . Even at pH 8.75, ring opening was complete for  $\beta$ -ISA after approximately 8 h, and above pH 10, for both  $\alpha$ - and  $\beta$ -ISA; the rate of reaction was difficult to follow due the rapid reaction rates. The results which were discussed in section 4.3 indicated that even at pH 7, a slow and complete conversion of  $ISA_L$  to  $ISAH$  was achieved.

## **6 General Summary and Conclusions**

### **6.1 Degradation of cellulose: attempts to maximise the solution concentration of $\beta$ -ISA solution**

Various properties of ISA have previously been studied due to its effect on repository safety; however, the vast majority of this work has only involved  $\alpha$ -ISA (or  $\beta$ -ISA to a very limited extent); the lack of research performed on  $\beta$ -ISA is related to the difficulty in readily obtaining adequate quantities of the compound. Therefore, the main aim of this work was to produce a robust method for the synthesis and isolation of gram scale quantities of  $\beta$ -ISA. To produce this method, an investigation was undertaken to maximize the solution concentration of  $\beta$ -ISA, whilst minimising reaction time. A comparison was made between sodium hydroxide and calcium hydroxide as the degrading alkaline species and the initial reaction parameters (type of cellulose, cellulose loading, reaction temperature, anaerobic conditions, alkaline concentration) were chosen by comprehensively reviewing the literature; a vast amount of previous research has been reported on the alkaline degradation of cellulose, particularly in relation to the pulping industry.

Monitoring the progress of degradation reactions was performed by periodically removing samples and analysing the resulting solutions using HPAEC-PAD so that the production of  $\alpha$ - and  $\beta$ -ISA as a function of time could be determined. HPAEC-PAD proved to be a suitable analytical technique for this purpose due to its ability to resolve and detect the diastereoisomers of  $\alpha$ - and  $\beta$ -ISA when present in mixtures. Quantification of both  $\alpha$ - and  $\beta$ -ISA was achieved by preparing a standard sample of  $\text{Ca}(\alpha\text{-ISA})_2$  by degrading lactose in calcium hydroxide solution using the established method of Whistler and BeMiller<sup>149</sup>, the resulting product was fully characterised using a combination of HPAEC-PAD, GC-MS and NMR. Pure samples of  $\alpha\text{-ISA}_L$  and  $\alpha\text{-HISA}$  were produced from the calcium salt and NMR spectra of all 3 forms (lactone, free acid and salt) were obtained so that their conformations, when present in reaction solutions could be determined. A linear calibration curve was produced from the highly soluble crystalline  $\alpha\text{-HISA}$  and the resulting regression equation was used to quantify the unknown concentrations of  $\alpha$ - and  $\beta$ -ISA.

Analysis of the liquors produced from the degradation of lactose (from the above synthesis of  $\text{Ca}(\alpha\text{-ISA})_2$ ) using both HPAEC-PAD and NMR indicated that the major products were

approximately equal amounts of  $\alpha$ - and  $\beta$ -ISA and  $\alpha$ - and  $\beta$ -MSA. Following the precipitation of the sparingly soluble  $\text{Ca}(\alpha\text{-ISA})_2$  an attempt was made to preferentially precipitate  $\text{Ca}(\beta\text{-ISA})_2$  from the remaining liquor using fractional precipitation and using ethanol as the precipitant. Using this method, the percentage of the total ISA present in the liquor was enriched, in comparison to the amount of MSA present; however, no pure  $\beta$ -ISA was obtained.

The major products from the degradation of cellulose using NaOH were  $\alpha$ - and  $\beta$ -ISA, present in a ratio of 1 : 3 respectively. Minor amounts of 3,4-dihydroxybutanoic acid (DHB) were also detected, the production of which was favoured when reactions were carried out at RT or when anaerobic conditions were not maintained. Under anaerobic conditions, at RT, DHB accounted for approximately 5 % of the degradation products, whereas at 90 °C, DHB accounted for less than 1 % of products. When no attempt was made to exclude oxygen from reaction systems the amount of DHB increased: at 90 °C the amount of DHB increased from 1 % to approximately 5 % of the HPAEC-PAD detectable products and at RT, when the reaction was only flushed with nitrogen for the first 24 h of a 13 day reaction, DHB made up 17 % of the detectable degradation products. The results indicate the importance of maintaining anaerobic conditions to reduce the production of fragmentation products when performing cellulose degradation reactions.

In the NaOH reactions, the production of ISA followed an initial rapid phase, the duration of which was a function of the reaction temperature. Following the rapid phase, the rate of ISA production reduced and any further production occurred at a very slow rate. In the 90 °C reaction, the initial fast stage of ISA production lasted approximately 24 h, in the 50 °C reaction it lasted approximately 7 days and in the RT reaction, a slow continuous production of ISA was observed. The amount of  $\beta$ -ISA produced was also temperature dependent with larger yields being attained in the reactions performed at the highest reaction temperature: after 30 days, maximum concentrations were 1.21 g L<sup>-1</sup> at RT, 7.2 g L<sup>-1</sup> at 50 °C and 14.1 g L<sup>-1</sup> for the 90 °C reaction. The most recently published methods for the preparation of  $\beta$ -ISA were reported by Greenfield *et al.*<sup>107</sup> and Glaus and Van Loon<sup>110</sup> and in those methods  $\beta$ -ISA was produced by degrading cellulose for long periods of time at RT. The results of the present work indicate that the maximum  $\beta$ -ISA concentration achieved at room temperature (1.21 g L<sup>-1</sup>), produced after approximately 30 days of reaction, could be achieved in less than one hour at 90 °C (2.6 g L<sup>-1</sup> after 1 h) indicating

that significantly greater yields of  $\beta$ -ISA and shorter reaction times could be achieved simply by increasing the reaction temperature.

The  $\text{Ca}(\text{OH})_2$  degradation reactions were performed under anaerobic conditions and like the NaOH reaction, the major degradation products were  $\alpha$ - and  $\beta$ -ISA which were present in a 1 : 1 ratio and only trace amounts of DHB were present for all reaction temperatures. In addition, solution concentrations of  $\alpha$ - and  $\beta$ -MSA were also detected, and as the time courses for the production of both MSA and ISA were very similar, it suggests that the MSA was primarily being produced during the peeling reaction itself and not by other mechanisms.

In the RT  $\text{Ca}(\text{OH})_2$  reaction, the production of  $\beta$ -ISA was similar to that witnessed in the equivalent NaOH reaction, this being a slow gradual increase for the duration of the reaction, resulting in a final concentration of  $1.1 \text{ g L}^{-1}$ . In the  $50 \text{ }^\circ\text{C}$  reaction the amount of  $\beta$ -ISA produced was significantly lower than the amount produced in the equivalent NaOH reaction; the initial fast stage of production lasted approximately 13 days, 6 days longer than the initial stage in the NaOH reaction, after which a  $\beta$ -ISA concentration of  $4 \text{ g L}^{-1}$  was achieved; the slower rate of ISA production was attributed to the lower pH of the  $\text{Ca}(\text{OH})_2$  reaction solution. The total concentration of ISA produced in the  $\text{Ca}(\text{OH})_2$  ( $8.6 \text{ g L}^{-1}$ ) and NaOH reactions ( $9.5 \text{ g L}^{-1}$ ) were quite similar, however due to the  $\alpha$ -ISA :  $\beta$ -ISA ratio favouring  $\beta$ -ISA in the NaOH reaction, much larger quantities of  $\beta$ -ISA were achieved in that reaction.

In the  $90 \text{ }^\circ\text{C}$   $\text{Ca}(\text{OH})_2$  reaction an initial rapid production of ISA was also observed, after 4 days maximum concentrations of both  $\alpha$ - and  $\beta$ -ISA were  $5.1 \text{ g L}^{-1}$ , however, unlike the NaOH reaction, following the initial fast stage of production, a loss of ISA from solution was observed. To investigate the loss, collected samples were analysed for their TOC content to determine if fragmentation of the ISA was occurring. However, the time courses for both the production of both ISA and the TOC content were very similar, with the loss of TOC closely mirroring the loss of ISA from solution, indicating that significant fragmentation of ISA was not occurring; the results suggested that the observed loss of ISA from solution was predominantly as a result of sorption onto the unreacted solids which were present in the reaction vessel.

The observed loss of ISA in the  $90 \text{ }^\circ\text{C}$   $\text{Ca}(\text{OH})_2$  reaction was further investigated by performing three additional degradation reactions at  $90 \text{ }^\circ\text{C}$ : the  $\text{Ca}(\text{OH})_2$  and NaOH

reactions were repeated to see if the results of those reactions were reproducible and an additional reaction containing a mixture of NaOH and Ca(OH)<sub>2</sub> was also performed, primarily to increase the pH of the Ca(OH)<sub>2</sub> reaction. The concentration of ISA and the TOC in the solutions produced from the NaOH and mixed base reactions were very similar, indicating that the presence of NaOH was dictating the composition of the CDPs being produced and the rate of their production; also no obvious loss of ISA or TOC was observed from those reactions. The repeated Ca(OH)<sub>2</sub> reaction produced results which were very similar to the previous Ca(OH)<sub>2</sub> reaction indicating that those results were reproducible.

To further investigate the loss of ISA and other CDPs from reaction solutions, the unreacted solid material, present in the collected samples was extracted with a saturated solution of sodium hydrogen carbonate and the extracts were analyzed for both their ISA and TOC contents. The results indicated that, although it was not obvious from the original HPAEC-PAD and TOC results, in all three degradation reactions, similar amounts of TOC were being lost from reaction solutions due to sorption onto unreacted solid material; however the composition of the TOC and the rate at which sorption was occurring was different for each reaction system. In the NaOH reaction, sorption of both  $\alpha$ - and  $\beta$ -ISA was rapid, the composition of the TOC of both the solution and the solid phases were very similar suggesting that the sorption was a physical process, with the CDPs being rapidly absorbed onto the hydrated, swollen cellulose fibres. The absence of solid calcium hydroxide in that reaction suggests that unreacted cellulose, and not solid Ca(OH)<sub>2</sub> was primarily the reason for the observed losses of CDPs from all three reaction systems.

In the Ca(OH)<sub>2</sub> reaction, the sorption of both ISA and other CDPs was a slow process which was occurring for the duration of the reaction and although the rate was slow, the amount of ISA sorbed eventually reached those witnessed in the NaOH reaction. Unlike the NaOH reaction, the composition of the TOC recovered from the solid phase and the composition of the TOC present in the solution phases were different, with significantly more ISA (~ 80 %) being present in the solution phase than in the solid phase (~ 60 %) suggesting that different sorption processes were occurring to those in the NaOH reaction. It is probable that in the Ca(OH)<sub>2</sub> reaction, sorption was occurring through a cation exchange mechanism between calcium salts of ISA/CDPs and the accessible carboxylate groups of the cellulose fibres. The higher percentage of small fragmentation products on the solid phase in comparison to the solution phase also suggests that solid calcium hydroxide

may have been catalysing the oxidation of some of the early produced ISA due to traces of oxygen in the reaction system, resulting in a conversion of some of the ISA into smaller fragmentation products; when the oxygen in the system was depleted, the amount of sorbed ISA would then increase. However, the presence of large amounts of insoluble calcium hydroxide in the reaction vessel, in combination with the un-swollen cellulose fibres, may have prevented a rapid sorption of either ISA, or to a lesser extent, the smaller CDPs from occurring.

The TOC analysis of the extracts produced from the unreacted solids from the mixed  $\text{Ca}(\text{OH})_2/\text{NaOH}$  reaction indicated that the amount of TOC sorbing to the solid phase was slightly more than the TOC recovered from the solids from the other two reactions. However, the percentage of ISA in the recovered TOC was much smaller in the mixed reaction (12 %) and the rate of ISA sorption was also very slow. Conversely, the TOC analysis indicated that in the mixed reaction, the small fragmentation products were being rapidly absorbed onto the unreacted solid material, faster than what was occurring in the NaOH and  $\text{Ca}(\text{OH})_2$  reactions. The results suggest that the larger quantities of solid calcium hydroxide present in the mixed reaction system may have enhanced the catalysis of the fragmentation of ISA into the smaller acids and the higher pH, due to the additional presence of the NaOH, may have facilitated a rapid loss of the small acids from the solution phase due to absorption onto the swollen and highly hydrated cellulose fibres.

Based on the above findings, to produce solutions of  $\beta$ -ISA to be used in isolation procedures, the anaerobic degradation of cellulose at 90 °C using NaOH as the base was the preferred choice and an optimised reaction time of 16 h was chosen. The preference for NaOH being: in comparison to the  $\text{Ca}(\text{OH})_2$  reaction, a greater percentage of the cellulose added to the reaction was converted into soluble organic products (35 % vs. 14 %); more of the cellulose was converted directly into  $\beta$ -ISA (15 % vs. 6.8 %), resulting in maximum concentrations of  $\beta$ -ISA being greater (15 g L<sup>-1</sup> vs. 6.8 g L<sup>-1</sup>) and the larger concentration of  $\beta$ -ISA was produced in less time (1 day vs. 4 days). Furthermore, 26 % of the  $\beta$ -ISA produced in the  $\text{Ca}(\text{OH})_2$  reaction was lost from reaction solutions due to sorption processes, whereas in the NaOH reaction, only 14 % was lost (see Table 5 for a summary of the results).

A disadvantage of using NaOH as the base was that, in comparison to the  $\text{Ca}(\text{OH})_2$  reaction, the percentage of ISA which made up the TOC was lower (52 % vs. 87 %), however the 3 :

1 ratio favouring the production of  $\beta$ -ISA in the NaOH reaction resulted in the percentage of  $\beta$ -ISA in the TOC being similar in both reaction systems (39 % vs. 43 %). The lower percentage of ISA produced from the NaOH reaction indicates that more fragmentation products were present in degradation solutions, with preliminary HPIEC analysis indicating that the major fragmentation product was formic acid; lactic acid, acetic acid and glycolic acid were also detected. The presence of small organic acids was not regarded as a significant problem: during the work-up of degradation solutions, rotary evaporation was used to remove excess water, during this procedure it was expected that the majority of the volatile organic acids would be removed. A small amount of lactic acid was identified in early eluting fractions in isolation procedures, but this was separated from the desired products without difficulty.

### **6.1.1 Future work related to the production of $\beta$ -ISA**

Several avenues of further work could be carried out to increase yields and reduce reaction times in  $\beta$ -ISA production.

Preliminary small scale experiments were described in section 3.9, with the results indicating that cellulose degradation reaction times could be drastically reduced if reactions were performed in a microwave oven. These reactions were only performed on a small scale due to the equipment which was available at the time; however, a large scale microwave reactor has recently been purchased by the University of Huddersfield, this will allow for the expansion of the use of microwave heating to produce  $\beta$ -ISA.

Future degradation reactions could also be carried out with the use of other bases as the degrading species. In previously published work, Ziderman<sup>239</sup> and Colbran and Davidson<sup>181</sup> reported that cellulose degradation is related to the size of the cation involved in the alkaline media. Colbran and Davidson<sup>181</sup> determined that barium hydroxide ( $171.34 \text{ g mol}^{-1}$ ) degraded cellulose more than strontium hydroxide ( $121.63 \text{ g mol}^{-1}$ ) and Ziderman<sup>181</sup> found that potassium hydroxide ( $56.1 \text{ g mol}^{-1}$ ) degraded cellulose more than sodium hydroxide ( $40 \text{ g mol}^{-1}$ ). In another study, Whistler and BeMiller<sup>148</sup> reported that when they degraded guar gum in trimethylbenzylammonium hydroxide, 90 % of the polysaccharide had degraded after two weeks at  $37 \text{ }^\circ\text{C}$ . Therefore, a series of cellulose degradation reactions could be performed which compare various bases to determine their effect on  $\beta$ -ISA production.

Experiments with alternative substrates could also be investigated; it is not ideal that the cellulose polymer becomes stable to alkali after only about 30 % degradation, or that degradation drastically slows down due to stopping reactions, therefore experiments involving amylose as an alternative substrate are envisioned. It has been indicated that amylose can be degraded 100 % under certain conditions, with ISA being the major product of degradation <sup>182</sup>. For example, between 0.01 and 0.1 M base concentration; a total degradation of the amylose chain was observed which had a DP of 820 with no indication of any termination reaction. Machell and Richards <sup>183</sup> also studied the alkaline degradation of amylose using sodium hydroxide solution (0.5 M) at 100 °C, it was also found that the main degradation product was ISA. It is worth noting however that isolation of pure amylose is a difficult procedure and the substrate is expensive to purchase.

When cellulose degradation reactions level-off indicating that the initial fast stage of peeling has stopped due to both the physical and chemical stopping reactions the rate limiting factor for further peeling is the alkaline hydrolysis of glycosidic linkages <sup>123</sup>. Previous work by Johansson and Samuelson <sup>131</sup> who degraded cellulose in 2 % NaOH solution at 95 °C under anaerobic conditions for times similar to the ones used in this work determined that chain cleavages were not occurring under their reaction conditions. They determined, using viscosity measurements of the remaining degradation solution that there was no further reduction in chain length and that there was no reduction in the degree of polymerisation of the remaining cellulose chains. One way to allow degradation to continue would be to increase the reaction temperature to above 170 °C for short periods of time after the onset of the physical stopping reaction, as at this temperature glycosidic bonds along the cellulose chain are likely to be cleaved <sup>106</sup> and thus allow for peeling to continue, however at these temperatures, the amount of fragmentation products may also be increased. Similarly, cellulose degradation is stopped due to the chemical stopping as a result of the formation of MSA <sup>126</sup>. It was reported by Machell and Richards <sup>101</sup> that stable MSA end groups could be removed by acid hydrolysis; alkaline degradation could then continue to the same extent if the cellulose was cycled between acidic and alkaline solution. These methods of encouraging alkaline hydrolysis and acid hydrolysis to promote further peeling after the onset of stopping reactions do not allow for rapid reaction times, but they may allow for the optimum conversion of unwanted cellulosic waste materials into valuable compounds, such as saccharinic acids.

## 6.2 Isolation of $\beta$ -ISA

In chapter 4, methods were described and discussed with the aim being to isolate large amounts of pure  $\beta$ -ISA. The identification of other cellulose degradation products, present in degradation solutions was also discussed.

Initial isolation attempts involved the manual elution of aliquots of crude cellulose degradation solutions through columns of anion exchange resin. Columns were eluted under atmospheric conditions, resulting in extremely slow flow rates and long periods of time being required to run a single column. Collected fractions were screened for their  $\beta$ -ISA content using HPAEC-PAD and initial results indicated that significant amounts of material were eluting from the column un-fractionated. An identified problem was that coloured impurities, present in degradation solutions were strongly binding to and fouling the anion exchange resin, resulting in a reduced separation performance. However, after optimising the elution conditions, small amounts of highly pure  $\beta$ -ISA (> 90 %), were isolated; enough to obtain a sample for NMR analysis. Using this method, it was impractical to obtain large amounts of  $\beta$ -ISA, however, for the first time the NMR spectrum of the open-chain form of  $\beta$ -ISA was obtained. Larger yields of  $\beta$ -ISA were obtained by utilising an automated, pressurised anion exchange system using the same resin as previously described; the system allowed significantly faster flow rates to be applied, allowing for a large throughput of material and the use of an automated fraction collector made the procedure more convenient. After optimising the conditions of the system, relatively large amounts of  $\beta$ -ISA were isolated in relatively short periods of time: after repeating the column 17 times, 1 g of pure  $\beta$ -ISA was collected, equating to 39 % of the  $\beta$ -ISA applied to the column.

The amount of  $\beta$ -ISA isolated using the automated system was an improvement on previous methods reported in the literatures (Glaus *et al.*<sup>110</sup> isolated ~ 220 mg of  $\beta$ -ISA after 450 injections of crude material through anion exchange columns), however, column fouling was still a problem, resulting in only small amounts of material being applied to each column to ensure that adequate separation was achieved. Furthermore, timely regeneration steps were required between each run and due to the column fouling; the (expensive) resin was replaced at regular intervals. This led to the conclusion that applying cellulose degradation solutions to anion exchange columns was better suited to small scale synthesis, therefore, other methods were sought to isolate  $\beta$ -ISA.

For the development of a final isolation procedure, the products of cellulose degradation reactions were derivatised and eluted through normal phase silica columns. In initial isolation attempts, mixtures of CDPs were converted into their acetyl esters using a large excess of acetic anhydride as the acetylating agent and aliquots of the derivatised syrup were applied to the column. TLC was used to monitor the elution of the products from the column, however, separating the acetylated  $\alpha$ - and  $\beta$ -ISA<sub>L</sub> using TLC proved to be difficult due to their similar retention properties. In this respect, GC-MS proved useful in monitoring the percentage of triacetylated  $\alpha$ - and  $\beta$ -ISA<sub>L</sub> in collected fractions as their respective peaks could be fully resolved. The first column produced 6 g of clear syrup which contained 84 % acetylated  $\beta$ -ISA<sub>L</sub> and the isolated syrup was eluted more slowly through a second column. TLC was used to indicate the fractions which were rich in total  $\alpha$ - and  $\beta$ -ISA and GC-MS was used to more accurately pinpoint the  $\beta$ -ISA-rich fractions. In addition, NMR analysis of collected fractions allowed for the identification of an additional CDP: 2,4,5-trihydroxypentanoic acid, which was also present as an acetylated lactone; 3,4-dihydroxybutano-1,4-lactone and lactic acid were also detected in the syrup. Using this method, 2.5 g of triacetylated  $\beta$ -ISA<sub>L</sub> of greater than 90 % purity was isolated; standard de-acetylation procedures followed resulting in approximately 2 g of Na- $\beta$ -ISA in greater than 90 % purity being produced.

Further developments to the normal phase chromatography method were attempted by converting the mixture of CDPs into benzoyl esters. In the method described above, several attempts were made to crystallize the triacetylated  $\beta$ -ISA<sub>L</sub> from concentrated fractions, however, this was unsuccessful. The aim of derivatizing with a heavier protecting group was twofold: to produce better separation when eluting material through normal phase silica columns and to encourage crystallization of the isolated products. In the initial benzoylation attempt,  $\beta$ -ISA<sub>L</sub>-rich syrup was derivatised using a large excess of benzoyl chloride as the derivatizing agent. Portions of the benzoylated syrup were applied to the column and collected fractions were monitored by TLC; fractions of interest were evaporated and the resulting syrup was analysed by NMR spectroscopy. The initial column produced a limited number of fractions rich in both tribenzoylated  $\alpha$ - and  $\beta$ -ISA<sub>L</sub>; however, due to the large excess of benzoyl chloride, collected fractions also contained large amounts of benzoic acid. However, eluting the  $\beta$ -ISA<sub>L</sub>-rich syrup through a second column using very slow elution conditions allowed small amounts of tribenzoylated  $\beta$ -ISA<sub>L</sub> to be isolated, free from benzoic acid.

An important finding was that, after passing the brown derivatised material through the first column, the collected fractions produced a very clean, clear syrup; the highly polar brown impurities were being retained at the top of the column, indicating that the initial column was a good method of “cleaning up” the solution. The key to isolating pure tribenzoylated  $\beta$ -ISA<sub>L</sub>, was to pass the dark-brown benzoylated syrup through an initial relatively fast eluting column to remove the coloured impurities and secondly to elute the clean syrup very carefully through a second column. Therefore, in future isolation attempts, derivatised mixtures were crudely eluted through a wide bed of silica, producing a very clean syrup. It was also determined that benzoic acid could be removed from collected fractions by extracting the syrup with a saturated solution of sodium hydrogen carbonate. Therefore, in all future isolation attempts, prior to the elution through the wide bed of silica, the entire benzoylated crude “tar” was dissolved in chloroform and extracted with a saturated sodium hydrogen carbonate solution.

Applying clean syrup, free of benzoic acid, to large silica columns, using very slow flow rates allowed large amounts of tribenzoylated  $\beta$ -ISA to be isolated from single columns. Furthermore, NMR analysis of collected fractions also allowed several other compounds to be identified, some of which were previously masked by the large amounts of benzoic acid. The identified products, also present as their perbenzoylated esters, and their approximate elution order from the column were as follows: lactic acid, 2,5-dihydroxypentanoic acid, 2,3-dideoxypentonic acid,  $\alpha$ -2,4,5-trihydroxypentanoic acid,  $\alpha$ -ISA,  $\beta$ -ISA,  $\beta$ -2,4,5-trihydroxypentanoic acid and 3,4-dihydroxybutanoic acid.

The identification of some of the products was initially tentative, due to some of the collected fractions being present as mixtures, making NMR interpretation more difficult. In this respect, applying collected fractions which contained more than one product to short-path distillation proved useful and resulted in the separation of 2,4,5-trihydroxypentanoic acid from 3,4-dihydroxybutanoic acid, allowing both molecules to be identified by NMR. The use of short-path distillation in this way was as a direct result of the findings which were discussed section 4.4; in that method, attempts were made to distil  $\beta$ -ISA from mixtures which also contained  $\alpha$ -ISA and other CDPs, however, due to the very similar boiling points of  $\alpha$ - and  $\beta$ -ISA they could not be separated in this way, but it was determined that 3,4-dihydroxybutanoic acid could be isolated from the ISA using that technique.

In the final isolation procedure, 16 g of clear syrup which contained approximately 70 % tribenzoylated  $\beta$ -ISA<sub>L</sub> was eluted very carefully through a silica column resulting in the isolation of approximately 7 g of highly pure tribenzoylated  $\beta$ -ISA<sub>L</sub> and 1 g of pure tribenzoylated  $\alpha$ -ISA<sub>L</sub>; the addition of the large benzoyl groups allowed single crystals of both tribenzoylated  $\alpha$ -ISA<sub>L</sub> and tribenzoylated  $\beta$ -ISA<sub>L</sub> to be obtained. From the single crystals, X-ray structures of both the tribenzoylated  $\alpha$ - and  $\beta$ -ISA<sub>L</sub> were produced for the first time which confirmed that the 2,4-hydroxymethyl groups of the tribenzoylated  $\alpha$ - and  $\beta$ -ISA<sub>L</sub> were arranged in cis and trans geometries respectively, the configuration of the crystalline tribenzoylated  $\beta$ -ISA<sub>L</sub> was also determined as being 2R,4S. The crystalline  $\alpha$ - and  $\beta$ -ISA tribenzoates were further characterised using 1D (<sup>13</sup>C, DEPT 135 and DEPT 90) and 2D (COSY, HSQC and HMBC) NMR spectroscopy and using HRMS, accurate molecular masses were determined.

Following the ring-opening of the isolated tribenzoylated  $\beta$ -ISA<sub>L</sub> and debenzoylation using established methods, the 7 g of isolated tribenzoylated  $\beta$ -ISA<sub>L</sub> resulted in 2.6 g of the sodium salt of  $\beta$ -ISA being isolated from a single column;  $\beta$ -ISA present as both the ring-opened and lactone forms was fully characterised using NMR and HRMS. The method described above required approximately 1 day to perform cellulose degradation reactions and a further day to work-up the reaction and isolate the  $\beta$ -ISA; these reaction times are significantly lower than what has previously been reported in the literature.

### **6.2.1 Future work related to the isolation of $\beta$ -ISA**

The large benzoyl protecting groups attached to the ISAs promoted crystallisation of the two isomers and allowed for a greater level of characterisation to be made due to the single crystal X-ray structures being obtained. In future work, it is hoped that that by derivatizing the ISAs with even larger protecting groups, such as the addition of naphthoyl groups, the chromatography method to isolate  $\beta$ -ISA from other cellulose degradation products can be further improved. It is possible that with larger protecting groups, the crystallisation and isolation of  $\beta$ -ISA may be achieved with very limited, or no chromatography beforehand.

The experiments which were described in 3.2.4 to fractionally precipitate  $\beta$ -ISA from mixtures of cellulose degradation products could be further explored using other solvents as the precipitant. The fractional precipitation of derivatised crude  $\beta$ -ISA may produce improved results.

### 6.3 Physical properties of $\beta$ -ISA in aqueous solution

The isolation of large amounts of  $\beta$ -ISA allowed a number of physical properties to be investigated. The first of these was the  $pK_a$ , an important parameter which will influence the complexing ability of  $\beta$ -ISA with radioactive isotopes. The  $pK_a$  was determined using  $^{13}\text{C}$  NMR spectroscopy; more traditional methods such as the use of acid-base titrations were not suitable due to ISA's ability to lactonize in acidic media. Using  $^{13}\text{C}$  NMR, the variation of the chemical shifts of carbon resonances produced from solutions of  $\text{Ca}-(\beta\text{-ISA})_2$  as a function of pD were tracked. Plots of the change in the chemical shift position of C1 (the carbonyl carbon), C2, C4 and C5 as a function of pD produced sigmoidal type curves; the pD at the point of inflection of the curves provided a direct indication of the  $pK_a$ . The largest shift was observed for the carbonyl carbon ( $\Delta$  in  $\delta = 2.53$  ppm) indicating that, as expected, the hydroxyl group attached to C1 was the most acid group. Calculated  $pK_a$  values were very similar for all 4 resonances: 4.01 (C1), 4.00 (C2), 4.03 (C4) and 4.02 (C5) giving a mean value of  $4.01 \pm 0.07$ , equating to an aqueous  $pK_a$  of  $3.61 \pm 0.07$  ( $pK_a$  in  $\text{D}_2\text{O} - 0.4$ ). Cho *et al.*<sup>150</sup> also utilised  $^{13}\text{C}$  NMR spectroscopy to determine the  $pK_a$  of  $\alpha$ -ISA to which an average value of 3.36 was determined; the results suggest that  $\beta$ -ISA is slightly more basic than  $\alpha$ -ISA. This is opposite to what was suggested in section 3.4.2: it was estimated that  $\beta$ -ISA would have a lower  $pK_a$  than  $\alpha$ -ISA because it was eluting after  $\alpha$ -ISA through HPAEC columns; however, it is possible that due to their similar  $pK_a$ 's, other separation mechanisms may be more important in determining their elution order. However, as previously discussed, a wide range of  $pK_a$  values have been reported for  $\alpha$ -ISA, ranging from 3.27 – 4.46<sup>150, 151, 197, 216</sup>, for this reason in future work it is hoped that the  $pK_a$  of mixed solutions of  $\alpha$ - and  $\beta$ -ISA will be determined simultaneously using the same method so that  $pK_a$  values under identical experimental conditions can be measured; indeed, further experiments, using  $^{13}\text{C}$  NMR are currently ongoing at the University of Huddersfield to determine the  $pK_a$  of both  $\alpha$ - and  $\beta$ -ISA when both isomers are present as mixtures.

The second physical property to be studied was the inter-conversion between  $\text{ISA}_\text{H}$  and  $\text{ISA}_\text{L}$ . In acidic environments,  $\text{ISA}_\text{H}$  undergoes an acid catalysed lactonisation, conversely in basic environments; the lactone undergoes a base catalysed ring-opening. In the present work, the rates of these inter-conversions were studied for both  $\beta$ -ISA and  $\alpha$ -ISA so their relative reactivity in acidic and basic environments could be determined – the reactivity of

ISA in basic environments is an important property of relevance to the underground disposal of radioactive waste.

In section 4.3 it was reported that even at pH 7, a slow ring-opening of  $\beta$ -ISA<sub>L</sub> occurred, and Ekberg *et al.*<sup>151</sup> reported that at pH 13 the base catalysed ring-opening of  $\alpha$ -ISA<sub>L</sub> was occurring too fast to study. To determine a suitable range of pH values to study the reaction kinetics, solutions of ISA<sub>L</sub> were analysed by NMR at various basic pHs; the results indicated that at pH 8, the complete ring-opening of  $\alpha$ -ISA<sub>L</sub> took about 1 week; whereas at pH 11 and above, the conversion was faster than the resolution of the instrument (< 5 min). Based on the NMR results, a sensible range of pH values was decided upon (8.5 - 10.5) and a further detailed study was performed using pH-stat autotitration. NMR was deemed unsuitable for detailed kinetic studies because base is consumed in the ring-opening process so stable pH values would not be maintained unless buffered systems were used, a concern was that buffers may have catalysed the hydrolysis reaction. Using pH-stat autotitration, the rate of lactone hydrolysis for both  $\alpha$ - and  $\beta$ -ISA<sub>L</sub> was determined for a range of pH values (8.5 - 10.5); a pH-stat continuously adds base to compensate for the base consumed during the reaction. In the present work, plots of the volume of base added decreased exponentially as a function of time, indicating that the base hydrolysis was following first-order type kinetics. In each reaction, 100 % of the lactone was irreversibly ring-opened upon the addition of one molar equivalent of base.

The base hydrolysis reaction is a second-order process due to the consumption of both ISA<sub>L</sub> and hydroxide ion; however, due to a constant pH being maintained, the reaction is regarded as pseudo-first-order. Converting the exponential decay plots into straight lines, allowed pseudo-first-order rate constants ( $k_{obs}$ ) to be determined for each reaction pH and a plot of  $\text{Log}_{10}(k_{obs})$  versus pH allowed pH rate profiles to be constructed for both  $\alpha$ - and  $\beta$ -ISA<sub>L</sub>; the rate profiles had a slope close to one, indicating that they can be used to estimate the rate of reaction at other pH values. The relative reactivity of the respective lactones in basic media were determined by plotting  $k_{obs}$  vs. hydroxide concentration for each reaction pH, the slope of the plots provided average second order rate constants ( $k_{hyd}$ ) for both  $\beta$ -ISA<sub>L</sub> and  $\alpha$ -ISA<sub>L</sub>, to which values of  $25.3 \text{ M}^{-1} \text{ s}^{-1}$  for  $\beta$ -ISA<sub>L</sub> and  $97.0 \text{ M}^{-1} \text{ s}^{-1}$  for  $\alpha$ -ISA<sub>L</sub> and were determined.

The results indicate that in basic environments,  $\alpha$ -ISA<sub>L</sub> is more reactive than  $\beta$ -ISA<sub>L</sub>; it is possible that the conformation of the C2 carbons may be responsible for the differences in

reactivity; the hydroxymethyl group of  $\beta$ -ISA<sub>L</sub> may hinder access of hydroxide ion to the carbonyl group more than it does for  $\alpha$ -ISA<sub>L</sub>, thus reducing the rate of nucleophilic attack. The second order rate constants produced for  $\alpha$ - and  $\beta$ -ISA<sub>L</sub> indicate that ISA<sub>L</sub> is more reactive than other similar sized lactones, such as valerolactone and butyrolactone; this may be due to the additional hydroxyl and hydroxymethylene groups which are present on the ISA<sub>L</sub> but not on valerolactone or butyrolactone.

The final physical property to be studied was the lactonisation of  $\alpha$ - and  $\beta$ -ISAH in acidic solutions. To study the kinetics of the acid catalysed reaction, Ca(ISA)<sub>2</sub> was added to acidic solutions ranging from pD 1 to pD 2.5 at a fixed temperature of 25 °C and <sup>1</sup>H NMR was used to monitor the transformation from ISAH to the lactone by determining the ratio of ISAH:ISA<sub>L</sub> at a given time. Plots of the percentage of ISAH present as a function of time indicated that the decay of ISAH was an exponential process, indicating first-order behaviour. For all reaction pDs, only a partial lactonisation of  $\alpha/\beta$ -ISAH was achieved due to an opposing acid catalysed lactone hydrolysis reaction; at each reaction pD, a state of equilibrium was reached between ISAH and ISA<sub>L</sub>.

The net loss of ISAH is a second-order process; however, due to the acid being truly catalytic, the reaction is regarded as pseudo-first-order. The exponential plots, described above were linearised and pseudo-first-order rate constants for the forward ( $k'_{lac}$ ) and reverse ( $k'_{hyd}$ ) reactions were determined; the sum of the forward and reverse rate constants, describing the net rate at which equilibrium is approached is described by the “natural” rate constant ( $k_{obs}$ ) and is provided by the slope of the linear plots and equilibrium constants ( $K_{eq}$ ), describing the relative proportion of ISAH and ISA<sub>L</sub> present at the end of each reaction, were determined by dividing  $k'_{lac}$  by  $k'_{hyd}$ . The calculated values for  $k_{obs}$ ,  $k'_{lac}$ ,  $k'_{hyd}$  and  $K_{eq}$  for each reaction pD are presented in Table 12. Rate profiles were also constructed by plotting  $\text{Log}_{10}(k_{obs})$  versus pD for the acid catalysed net lactonization reaction of both  $\alpha$ - and  $\beta$ -ISA<sub>L</sub> at 25 °C. Using the rate profiles, estimations can be made for the time taken to reach equilibrium at a given pD, and the results indicate that for both  $\alpha$ - and  $\beta$ -ISAH, above pH 3, several months would be required for a state of equilibrium to be achieved.

A plot of  $k'_{lac}$  versus deuterium ion concentrations for each reaction pD allowed the second order rate constant ( $k_{lac}$ ) to be determined for the lactonisation of  $\beta$ -ISAH ( $3.10 \times 10^{-3} \text{ M}^{-1} \text{ s}^{-1}$ ) and  $k_{lac}$  was determined from the resulting slope. The lactonisation of  $\alpha$ -ISAH was only studied at two pDs so  $k_{lac}$  was calculated by dividing the values obtained for  $k'_{lac}$  by their

respective deuterium concentrations;  $k_{lac}$  was determined by calculating the mean of the two values ( $7.04 \times 10^{-4} \text{ M}^{-1} \text{ s}^{-1}$ ).

The second-order rate constants indicate that, in acidic media,  $\beta$ -ISAH is more reactive than  $\alpha$ -ISAH which is possibly related to the  $\beta$ -ISA<sub>L</sub> ring being more stable than the  $\alpha$ -ISA<sub>L</sub> ring. Evidence for this can be found in the equivalent equilibrium constants; at pD 2.25, the equilibrium constant for  $\beta$ -ISAH was 11.2, whereas for  $\alpha$ -ISA it was only 3.98, indicating that at equilibrium, more of the beta isomer was present as the lactone. The greater stability of the  $\beta$ -ISA<sub>L</sub> ring may be due to the two hydroxymethyl groups of  $\beta$ -ISA<sub>L</sub> being in the threo conformation, making it sterically more favourable than the  $\alpha$ -ISA<sub>L</sub> ring. At pD 2.25 the rate of intra-molecular lactonisation was approximately 3 times faster for  $\beta$ -ISAH than  $\alpha$ -ISAH, a reason for this could be a more favourable angle of approach between the attacking hydroxyl group (at C4) and the carbonyl carbon in the beta isomer. The differences in reactivity were further discussed in section 5.2.2.

The very slow rates of lactonization at higher pHs indicate that in a repository for radioactive waste, where the pH is expected to be above 12.5 for a period of 100,000 years,  $\alpha$ - and  $\beta$ -ISA will be present as their open-chain anions, conditions which will favour the possible complexation of ISA with radioactive isotopes.

### **6.3.1 Future work related to further studies involving $\beta$ -ISA**

An identified area of research in the safety assessment of radioactive waste repositories was the effect that cellulose degradation products, mainly ISA, had on the migration of radionuclides through groundwater pathways. In this respect a large amount of research has been undertaken, with the vast majority of this work has been performed on  $\alpha$ -ISA, in some cases  $\alpha$ -ISA has been used as an analogy for both  $\alpha$ - and  $\beta$ -ISA. The results of both this thesis and previously published work indicate that the physical properties of  $\beta$ -ISA are significantly different to the physical properties of  $\alpha$ -ISA, including their  $pK_a$ 's, their reactivity in acidic and basic environments, their solubility when present as calcium salts and the ratios in which they are produced under certain reaction conditions; these differences will affect the ability of  $\alpha$ - or  $\beta$  ISA to complex with radioactive nuclides. Therefore, future work should include a repeat of all the research which has previously been performed on  $\alpha$ -ISA (see section 1.3) but instead using  $\beta$ -ISA. Furthermore, the sorption of ISA onto unreacted cellulose also requires further study, the results of this work indicate that a significant portion of ISA produced in a radioactive waste repository may be

removed from solution due to sorption onto un-reacted cellulose fibres; this may have an impact on the total complexing ability of ISA in a repository setting.

As previously discussed, the main aim of this work was to produce a robust method for the synthesis and isolation of gram scale quantities of  $\beta$ -ISA; it can be said that this aim was successfully achieved. It is hoped that the development of this method will make  $\beta$ -ISA readily available and allow all the suggested future work to be performed to gain a more complete understanding of the effect of both  $\alpha$ - and  $\beta$ -ISA on repository safety.

#### **6.4 Publications related to this thesis**

The method for the synthesis and isolation of  $\beta$ -isosaccharinic acid; the determination of the single crystal X-ray structures of  $\alpha$ - and  $\beta$ -ISA tribenzoate esters and the measurement of the aqueous  $pK_a$  of  $\beta$ -ISA was published in Carbohydrate Research (Shaw, Robinson *et al.*, 2012)<sup>210</sup>.

Various solution phase properties of xyloisosaccharinic acid (XISAH) including the aqueous  $pK_a$  and the rate constants for the inter-conversion between XISAH and xyloisosaccharino-1,4-lactone (XISA<sub>L</sub>), using the methods reported in this thesis for the study of ISA, was published in Carbohydrate Research (Almond, Shaw *et al.*, 2012)<sup>224</sup>.

## 7 References

1. R. H. Atalla, A. Isogai, M. Lew and L. Hung-Wen, in *Comprehensive Natural Products II*, Elsevier, Oxford, Editon edn., 2010, pp. 493-539.
2. M. Iguchi, S. Yamanaka and A. Budhiono, *Journal of Materials Science*, 2000, **35**, 261-270.
3. S. Kimura, C. Ohshima, E. Hirose, J. Nishikawa and T. Itoh, *Protoplasma*, 2001, **216**, 71-74.
4. F. Hoyle and N. C. Wickramasinghe, *Nature*, 1977, **268**, 610-612.
5. D. P. Klemm, B.; Heinze, T.; Heinze, U.; Wagenknecht, W., *Comprehensive Cellulose Chemistry Volume 1 Fundamentals and Analytical Methods*, Wiley-Vch, 1998.
6. D. Klemm, H.-P. Schmauder and T. Heinze, *Cellulose*, Wiley-VCH Verlag GmbH & Co. KGaA, 2005.
7. R. H. Atalla, V. J. Bartuska, J. C. Gast, G. E. Maciel and D. W. Sindorf, Appleton, Wisconsin : the Institute, Editon edn., 1980.
8. I. Nehls, W. Wagenknecht, B. Philipp and D. Stscherbina, *Prog. Polym. Sci.*, 1994, **19**, 29-78.
9. G. Guhados, W. Wan and J. L. Hutter, *Langmuir*, 2005, **21**, 6642-6646.
10. E. Kontturi, T. Tammelin and M. Osterberg, *Chemical Society Reviews*, 2006, **35**, 1287-1304.
11. J. C. Roberts, in *The Chemistry of Paper*, The Royal Society of Chemistry, Editon edn., 1996, pp. 52-68.
12. L. R. Van Loon, M. A. Glaus, A. Laube and S. Stallone, *Journal of Polymers and the Environment*, 1999, **7**, 41-51.
13. H. Shibazaki, S. Kuga, F. Onabe and R. M. Brown, *Polymer*, 1995, **36**, 4971-4976.
14. I. M. Saxena and R. M. Brown, *Annals of Botany*, 2005, **96**, 9-21.
15. I. Takao and S. Kimura, *Journal of plant research*, 2001, **114**, 483-489.
16. L. D. Gomez, C. G. Steele-King and S. J. McQueen-Mason, *New Phytologist*, 2008, **178**, 473-485.
17. R. M. Brown, *Journal of Macromolecular Science-Pure and Applied Chemistry*, 1996, **A33**, 1345-1373.
18. R. M. Brown and D. Montezinos, *Proceedings of the National Academy of Sciences*, 1976, **73**, 143-147.
19. P. Sarkar, E. Bosneaga and M. Auer, *J. Exp. Bot.*, 2009, **60**, 3615-3635.
20. A. N. J. Heyn, *The Journal of Cell Biology*, 1966, **29**, 181-197.
21. H. F. Jakob, P. Fratzl and S. E. Tschegg, *J Struct Biol*, 1994, **113**, 13-22.
22. Y. Nishiyama, P. Langan and H. Chanzy, *Journal of the American Chemical Society*, 2002, **124**, 9074-9082.
23. T. Virtanen, S. Liisa Maunu, T. Tamminen, B. Hortling and T. Liitiä, *Carbohydrate Polymers*, 2008, **73**, 156-163.
24. A. O'Sullivan, *Cellulose*, 1997, **4**, 173-207.
25. Y. Nishiyama, U.-J. Kim, D.-Y. Kim, K. S. Katsumata, R. P. May and P. Langan, *Biomacromolecules*, 2003, **4**, 1013-1017.
26. M. Muller, C. Czihak, H. Schober, Y. Nishiyama and G. Vogl, *Macromolecules*, 2000, **33**, 1834-1840.
27. P. T. Larsson, K. Wickholm and T. Iversen, *Carbohydrate Research*, 1997, **302**, 19-25.
28. R. F. Nickerson, *Industrial & Engineering Chemistry*, 1941, **33**, 1022-1027.
29. T. Inagaki, H. W. Siesler, K. Mitsui and S. Tsuchikawa, *Biomacromolecules*, 2010, **11**, 2300-2305.

30. A. Frey-Wyssling, *Science (New York, N.Y.)*, 1954, **119**, 80-82.
31. H. Fukuzumi, T. Saito, T. Iwata, Y. Kumamoto and A. Isogai, *Biomacromolecules*, 2008, **10**, 162-165.
32. U. Agarwal, R. Reiner and S. Ralph, *Cellulose*, 2010, **17**, 721-733.
33. S. Park, J. Baker, M. Himmel, P. Parilla and D. Johnson, *Biotechnology for Biofuels*, 2010, **3**, 10.
34. A. Thygesen, J. Oddershede, H. Lilholt, A. B. Thomsen and K. Ståhl, *Cellulose*, 2005, **12**, 563-576.
35. R. H. Newman, *J. Wood Chem. Technol.*, 1994, **14**, 451-466.
36. H. Zhao, J. H. Kwak, Z. Conrad Zhang, H. M. Brown, B. W. Arey and J. E. Holladay, *Carbohydrate Polymers*, 2007, **68**, 235-241.
37. L. Segal, *Textile research journal*, 1959, **29**, 786-794.
38. S. Andersson, R. Serimaa, T. Paakkari, P. Saranpaa and E. Pesonen, *Journal of Wood Science*, 2003, **49**, 531-537.
39. N. Wistara, X. Zhang and R. A. Young, *Cellulose*, 1999, **6**, 325-348.
40. K. Leppanen, S. Andersson, M. Torkkeli, M. Knaapila, N. Kotelnikova and R. Serimaa, *Cellulose*, 2009, **16**, 999-1015.
41. T. Liitiä, S. L. Maunu, B. Hortling, T. Tamminen, O. Pekkala and A. Varhimo, *Cellulose*, 2003, **10**, 307-316.
42. S. Maunu and B. Hortling, *Holzforschung*, 2000, **54**, 618-624.
43. T. Röder, J. Moosbauer, M. Fasching, A. Bohn, H. Fink, T. Baldinger and H. Sixta, *Lenzinger Berichte*, 2006, **86**, 85-89.
44. R. H. Atalla, in *Great Lake Bioenergy Research Center's Seminar Series Great Lakes Bioenergy*, Madison, WI Editon edn., 2011.
45. B. Doyle, *Biochemical Education*, 1992, **20**, 123-123.
46. R. D. Preston, *Discussions of the Faraday Society*, 1951, **11**, 165-170.
47. J. Blackwel and K. H. Gardner, *Biopolymers*, 1974, **13**, 1975-2001.
48. A. Sarko and R. Muggli, *Macromolecules*, 1974, **7**, 486-494.
49. K. H. Gardner and J. Blackwel, *Biochimica Et Biophysica Acta*, 1974, **343**, 232-237.
50. C. Woodcock and A. Sarko, *Macromolecules*, 1980, **13**, 1183-1187.
51. R. H. Atalla and D. L. VanderHart, *Solid State Nuclear Magnetic Resonance*, 1999, **15**, 1-19.
52. K. Hieta, S. Kuga and M. Usuda, *Biopolymers*, 1984, **23**, 1807-1810.
53. H. Chanzy and B. Henrissat, *Febs Lett*, 1985, **184**, 285-288.
54. D. L. VanderHart and R. H. Atalla, *Macromolecules*, 1984, **17**, 1465-1472.
55. D. Vanderhart, *Science (New York, N.Y.)*, 1984, **223**, 283-285.
56. F. Horii, A. Hirai and R. Kitamaru, *Macromolecules*, 1987, **20**, 2117-2120.
57. J. Sugiyama, T. Okano, H. Yamamoto and F. Horii, *Macromolecules*, 1990, **23**, 3196-3198.
58. J. Sugiyama, R. Vuong and H. Chanzy, *Macromolecules*, 1991, **24**, 4168-4175.
59. H. Yamamoto, F. Horii and H. Odani, *Macromolecules*, 1989, **22**, 4130-4132.
60. E. M. Debzi, H. Chanzy, J. Sugiyama, P. Tekely and G. Excoffier, *Macromolecules*, 1991, **24**, 6816-6822.
61. A. P. Heiner, J. Sugiyama and O. Teleman, *Carbohydrate Research*, 1995, **273**, 207-223.
62. Y. Nishiyama, J. Sugiyama, H. Chanzy and P. Langan, *Journal of the American Chemical Society*, 2003, **125**, 14300-14306.
63. V. L. Finkenstadt and R. P. Millane, *Macromolecules*, 1998, **31**, 7776-7783.
64. J. Sugiyama, J. Persson and H. Chanzy, *Macromolecules*, 1991, **24**, 2461-2466.
65. Z. Gromet-Elhanan and S. Hestrin, *J Bacteriol*, 1963, **85**, 284-292.

66. P. S. Belton, S. F. Tanner, N. Cartier and H. Chanzy, *Macromolecules*, 1989, **22**, 1615-1617.
67. H. Shibazaki, M. Saito, S. Kuga and T. Okano, *Cellulose*, 1998, **5**, 165-173.
68. W. A. Sisson, *Science (New York, N.Y.)*, 1938, **87**, 350-350.
69. F. J. Kolpak and J. Blackwell, *Macromolecules*, 1975, **8**, 563-564.
70. A. J. Stipanovic and A. Sarko, *Macromolecules*, 1976, **9**, 851-857.
71. P. Langan, Y. Nishiyama and H. Chanzy, *Journal of the American Chemical Society*, 1999, **121**, 9940-9946.
72. F. J. Kolpak and J. Blackwell, *Macromolecules*, 1976, **9**, 273-278.
73. P. Langan, Y. Nishiyama and H. Chanzy, *Biomacromolecules*, 2001, **2**, 410-416.
74. N.-H. Kim, T. Imai, M. Wada and J. Sugiyama, *Biomacromolecules*, 2005, **7**, 274-280.
75. I. Simon, L. Glasser, H. A. Scheraga and R. S. J. Manley, *Macromolecules*, 1988, **21**, 990-998.
76. E. S. Gardiner and A. Sarko, *Canadian Journal of Chemistry*, 1985, **63**, 173-180.
77. A. Sarko, J. Southwick and J. Hayashi, *Macromolecules*, 1976, **9**, 857-863.
78. J. I. Chang, C. H. Chen and G. S. Y. Liu, *Resources, Conservation and Recycling*, 2000, **30**, 333-351.
79. C. F. Cross, E. J. Bevan and C. Beadle, *Journal of the Chemical Society, Transactions*, 1893, **63**, 837-845.
80. Defra, *Municipal Waste Composition: A Review of Municipal Waste Component Analyses*, Defra Report, 2009.
81. Defra, *UK waste data (2004 - 2008)*, <http://www.defra.gov.uk/statistics/environment/waste/wrfg01-annsector/>, Accessed 9th September, 2012.
82. NDA, *The 2010 UK Radioactive Waste Inventory - Main Report*. URN 10D/985 NDA/ST/STY(11)0004 2011.
83. IAEA, *Safety Series No. III-F: The Principles of Radioactive Waste Management (Vienna, 1995)*.
84. NDA, *The 2010 UK Radioactive Waste Inventory - A Summary of Information for International Reporting*. URN 10D/987, NDA/ST/STY(11)0006., 2011.
85. *The Storage of Liquid High Level Waste at BNFL Sellafield. A Report by HM Nuclear Installations Inspectorate* <http://www.hse.gov.uk/nuclear/bnfl.pdf>, Accessed 6th April, 2012.
86. D. o. E. C. Change, *Policy for the Long Term Management of Solid Low Level Radioactive Waste in the United Kingdom*, <http://www.decc.gov.uk/assets/decc/what%20we%20do/uk%20energy%20supply/energy%20mix/nuclear/radioactivity/llw-policystatement070326.pdf>, Accessed 6th April, 2012.
87. *Radioactive Wastes in the UK: A Summary of the 2010 Inventory*, <http://www.nda.gov.uk/ukinventory/documents/Reports/upload/2010-UK-Radioactive-Waste-Inventory-Summary-of-the-2010-Inventory.pdf>, Accessed 5th April, 2011.
88. B. Flowers, *Nuclear power and the environment*, HM Stationery Office, 1976.
89. NDA, *What is the Nirex Phased Disposal Concept (2002)*, <http://www.nda.gov.uk/documents/upload/what-is-the-nirex-phased-disposal-concept-2002.pdf>, Accessed 28th August, 2012.

90. *Nirex Report: The viability of a phased geological repository concept for the long-term management of the UK's radioactive waste*, 2005.
91. C. o. R. W. Management, *Managing our Radioactive Waste Safely CoRWM's recommendations to Government*, 2006.
92. NDA, *Geological Disposal Gas status report - NDA Report no. NDA/RWMD/037*, 2010.
93. C. J. Knill and J. F. Kennedy, *Carbohydrate Polymers*, 2003, **51**, 281-300.
94. L. Van Loon and M. M. Glaus, *PSI-Bericht 98-07, Paul Scherrer Institute. Villigen, Switzerland. Also published as Nagra Technical Report Series NTB 97-04, NAGRA, Wettingen, Switzerland.*, 1998.
95. R. L. Whistler, J. N. BeMiller and L. W. Melville, in *Advances in Carbohydrate Chemistry*, Academic Press, Editon edn., 1958, vol. Volume 13, pp. 289-329.
96. X. Bourbon and P. Toulhoat, *Radiochim. Acta*, 1996, **74**, 315-319.
97. D. Rai, L. Rao, R. C. Moore, R. Bontchev and K. Holt, *Development of Biodegradable Isosaccharinate-Containing Foams for Decontamination of Actinides: Thermodynamic and Kinetic Reactions between Isosaccharinate and Actinides on Metal and Concrete Surfaces* EMSP-82715--2004; R&D Project: EMSP 82715, 2004.
98. B. F. Greenfield, G. J. Holtom, M. H. Hurdus, N. O'Kelly, N. J. Pilkington, A. Rosevear, M. W. Spindler and S. J. Williams, *Materials Research Society Symposium - Proceedings*, 1995.
99. B. F. Greenfield, M. H. Hurdus, M. W. Spindler and H. P. Thomason, *Nirex Report, NSS/R376*, 1997.
100. J. Tits, E. Wieland and M. H. Bradbury, *Applied Geochemistry*, 2005, **20**, 2082-2096.
101. G. Machell and G. N. Richards, *Journal of the Chemical Society* 1957, 4500-4506.
102. G. Machell and G. N. Richards, *Journal of the Chemical Society*, 1960, 1924-1931.
103. Isbell, *Journal of Research National Bureau of Standards* 1944, **32**, 45-59.
104. J. U. Nef, *Justus Liebig's Annalen der Chemie*, 1907, **357**, 214-312.
105. J. Kenner and G. N. Richards, *Journal of the Chemical Society* 1955, 1810-1812.
106. M. H. Johansson and O. Samuelson, *Carbohydrate Research*, 1974, **34**, 33-43.
107. B. J. Greenfield, W. N. Harrison, G. P. Robertson, P. J. Somers and M. W. Spindler, *NSS/R272, AEA-D&R-0219*, 1993.
108. M. A. Glaus and L. R. Van Loon, *Environ. Sci. Technol.*, 2008, **42**, 2906-2911.
109. M. Glaus and L. Van Loon, *Nagra Technical Report 03-08*, 2004.
110. M. A. Glaus, L. R. van Loon, S. Achatz, A. Chodura and K. Fischer, *Analytica Chimica Acta*, 1999, **398**, 111-122.
111. M. A. Glaus and L. R. Van Loon, *PSI Bericht 08-01, Nagra NTB 08-10* 2008.
112. B. Y. Yang and R. Montgomery, *Carbohydrate Research*, 1996, **280**, 27-45.
113. M. H. Hurdus and N. J. Pilkington, *United Kingdom Nirex Limited*, 2000, **1**.
114. M. A. Glaus and L. R. Van Loon, *PSI Bericht Nr 08-01*, 2009, 1-77.
115. I. Pavasars, Linköping University, 1999.
116. J. M. Krochta, S. J. Tillin and J. S. Hudson, *Journal of Applied Polymer Science*, 1987, **33**, 1413-1425.
117. K. Niemela and E. Sjostrom, *Biomass*, 1986, **11**, 215-221.
118. M. H. Hurdus and N. J. Pilkington, *United Kingdom Nirex Limited* 2000, **1**.
119. J. Shimizu, J. F. Kennedy, L. L. Lloyd and W. Hasamudin, in *The chemistry and processing of wood and plant fibrous materials*, eds. J. F. Kennedy, G. O. Phillips and P. A. Williams, Woodhead Publishing, Cambridge, Editon edn., 1996, pp. 361-368.
120. K. Niemela, *Journal of Chemical Technology and Biotechnology*, 1990, **48**, 17-28.

121. P. Warwick, N. Evans and C. Heath, in *A report prepared for the Nuclear Decommissioning Authority*, Editon edn., 2008, vol. LBORO CMNDA2.
122. M. H. Hurdus and N. J. Pilkington, *United Kingdom Nirex Limited*, 2000, **1**.
123. I. Pavasars, J. Hagberg, H. Boren and B. Allard, *Journal of Polymers and the Environment*, 2003, **11**, 39-47.
124. P. Biddle, B. F. Greenfield, N. J. Pilkington and M. W. Spindler, *AEA Technology Report, AEAT/ERRA-0154*, 2000.
125. I. Ziderman and J. Belayche, *Journal of Applied Polymer Science*, 1978, **22**, 711-718.
126. G. N. Richards and H. H. Sephton, *Journal of the Chemical Society* 1957, 4492-4499.
127. D. W. Haas, B. F. Hrutfiord and K. V. Sarkanen, *Journal of Applied Polymer Science*, 1967, **11**, 587-600.
128. L. Van Loon and M. Glaus, *Journal of Polymers and the Environment*, 1997, **5**, 97-109.
129. B. Alfredsson and O. Samuelson, *Svensk Papperstidn*, 1968, **71**, 679-686.
130. G. Machell and G. N. Richards, *Journal of the Chemical Society* 1960, 1938-1944.
131. M. H. Johansson and O. Samuelson, *Journal of Applied Polymer Science*, 1975, **19**, 3007-3013.
132. Lowendah.L and Samuelso.O, *Svensk Papperstidning-Nordisk Cellulosa*, 1974, **77**, 593-602.
133. G. Machell and G. N. Richards, *Journal of the Chemical Society* 1960, 1932-1938.
134. R. L. Whistler and J. N. BeMiller, *Journal of the American Chemical Society*, 1960, **82**, 3705-3707.
135. T. P. Nevell, in *Cellulose chemistry and its applications*, eds. T. P. Nevell and S. H. Zeronian, Ellis Horwood Limited, Chichester, Editon edn., 1985, pp. 223-242.
136. A. V. Chambers, L. J. Gould, A. W. Harris, N. J. Pilkington and S. J. Williams, 2003.
137. T. G. Heath and S. J. Williams, *A Report produced for United Kingdom Nirex Limited SA/ENV-0726* 2005.
138. M. Glaus, A. Laube and S. Stallone, *Radiochim. Acta*, 1999, **86**, 183-189.
139. D. Rai, M. Yui, D. A. Moore and L. Rao, *J. Solut. Chem.*, 2009, **38**, 1573-1587.
140. P. Warwick, N. Evans, T. Hall and S. Vines, *Radiochim. Acta*, 2004, **92**, 897-902.
141. K. Vercammen, M. A. Glaus and L. R. Van Loon, *Radiochim. Acta*, 2001, **89**, 393.
142. V. M. Gentile, L. R. Schroeder and R. H. Atalla, *Abstracts of Papers of the American Chemical Society*, 1985, **190**, 17-CEL.
143. Y. Z. Lai and K. V. Sarkanen, *Cell Chem. Technol.*, 1967, **1**, 517-527.
144. G. M. N. Baston, M. Brownsword, M. M. Cowper, M. C. Manning, N. J. Pilkington and S. J. Williams, *AEA Technology Report, AEAT/ERRA-0346*, 2002.
145. A. V. Chambers, L. J. Gould, C. P. Jackson, N. J. Pilkington, W. M. Tearle and C. J. Tweed, *AEA Technology Report, AEAT/ERRA-0377*, 2002.
146. Z. H. Hu, G. Wang and H. Q. Yu, *Biochemical Engineering Journal*, 2004, **21**, 59-62.
147. M. M. Askarieh, A. V. Chambers, F. B. D. Daniel, P. L. FitzGerald, G. J. Holtom, N. J. Pilkington and J. H. Rees, *Waste Management*, 2000, **20**, 93-106.
148. R. L. Whistler and J. N. BeMiller, *The Journal of Organic Chemistry*, 1961, **26**, 2886-2892.
149. R. L. Whistler and J. N. BeMiller, in *Methods in Carbohydrate Chemistry, vol. 2, Reactions of Carbohydrates*, eds. M. L. Wolfrom. and J. N. BeMiller., Editon edn., 1961, pp. 477-479.

150. H. Cho, D. Rai, N. J. Hess, Y. X. Xia and L. F. Rao, *J. Solut. Chem.*, 2003, **32**, 691-702.
151. S. Ekberg, C. Ekberg and Y. Albinsson, *J. Solut. Chem.*, 2004, **33**, 465-477.
152. P. L. Brown, S. Allard and C. Ekberg, *Journal of Chemical and Engineering Data*, 2010, **55**, 5207-5213.
153. A. A. J. Feast, B. Lindberg and O. Theander, *Acta Chem. Scand.*, 1965, **19**, 1127-1134.
154. R. D. Rocklin and C. A. Pohl, *Journal of Liquid Chromatography*, 1983, **6**, 1577-1590.
155. D. C. Johnson, *Nature*, 1986, **321**, 451-452.
156. T. R. I. Cataldi, C. Campa and G. E. De Benedetto, *Fresenius' Journal of Analytical Chemistry*, 2000, **368**, 739-758.
157. Dionex, *Analysis of Carbohydrates by High Performance Anion Exchange Chromatography with Pulsed Amperometric Detection (HPAE-PAD)*, 2000.
158. Dionex, *ED40 Electrochemical Detector Operator's Manual*, 1995.
159. D. C. Johnson, W. R. Lacourse and R. Ziad El, in *Journal of Chromatography Library*, Elsevier, Editon edn., 1995, vol. Volume 58, pp. 391-429.
160. M. B. Jensen and D. C. Johnson, *Anal Chem*, 1997, **69**, 1776-1781.
161. Dionex, *Optimal Settings for Pulsed Amperometric Detection of Carbohydrates Using the Dionex ED40 Electrochemical Detector*, 1998.
162. R. D. Rocklin, A. P. Clarke and M. Weitzhandler, *Anal Chem*, 1998, **70**, 1496-1501.
163. M. Weitzhandler, V. Barreto, C. Pohl, P. Jandik, J. Cheng and N. Avdalovic, *Journal of Biochemical and Biophysical Methods*, 2004, **60**, 309-317.
164. C. C. Sweeley, R. Bentley, M. Makita and W. W. Wells, *Journal of the American Chemical Society*, 1963, **85**, 2497-2507.
165. M. A. Asghar, 1990.
166. G. Petersson, *Tetrahedron*, 1970, **26**, 3413-3428.
167. G. Petersson, *Carbohydrate Research*, 1975, **43**, 1-8.
168. J. C. Sowden, M. G. Blair and D. J. Kuenne, *Journal of the American Chemical Society*, 1957, **79**, 6450-6454.
169. J. Kenner and G. N. Richards, *Journal of the Chemical Society* 1954, 278-282.
170. I. Ziderman, J. Belayche, A. Basch and M. Lewin, *Carbohydrate Research*, 1975, **43**, 255-263.
171. M. Lewin, I. Ziderman, N. Weiss, A. Basch and A. Ettinger, *Carbohydrate Research*, 1978, **62**, 393-398.
172. R. A. Gakhokidze, *Russian Chemical Reviews*, 1980, **49**, 222-236.
173. O. Samuelson and A. Wennerblom, *Svensk Papperstidn*, 1954, **57**, 827.
174. R. Atalla, *Cellulose (London)*, 1998, **5**, 309-319.
175. I. I. Ziderman and J. Perel, *Journal of macromolecular science. Physics*, 1985, **24**, 181-192.
176. K. Niemela, *Biomass*, 1988, **15**, 223-231.
177. H. Kolmodin and O. Samuelson, *Svensk Papperstidning-Nordisk Cellulosa*, 1972, **79**, 369-&.
178. E. Paart and O. Samuelson, *TAPPI*, 1974, **57**, 122-126.
179. E. Paart and O. Samuelson, *Carbohydrate Research*, 1970, **15**, 111-&.
180. V. L. Chiang and K. V. Sarkanen, *J. Wood Chem. Technol.*, 1985, **5**, 203-216.
181. R. L. Colbran and G. F. Davidson, *Journal of the Textile Institute proceedings (1923)*, 1961, **52**, 61-61.
182. Y.-Z. Lai and K. V. Sarkanen, *Journal of Polymer Science. Part C, Polymer symposia*, 1969, **28**, 15-26.
183. G. Machell and G. N. Richards, *Journal of the Chemical Society* 1958, 1199-1204.

184. G. Machell and G. N. Richards, *TAPPI* 1958, **41**, 12-16.
185. Y. Z. Lai and D. E. Ontto, *Journal of Applied Polymer Science*, 1979, **23**, 3219-3225.
186. W. D. Nicoll, Editon edn., 1954, p. 825.
187. Y. Liang, Z. Zheng, R. Hua and X. Luo, *Chemical Engineering Journal*, 2011, **174**, 175-181.
188. M. Mugdan and D. P. Young, *Journal of the Chemical Society* 1949, 2988-3000.
189. K. Niemela, R. Alén and E. Sjöström, *Holzforchung - International Journal of the Biology, Chemistry, Physics and Technology of Wood*, 1985, **39**, 167.
190. O. Franzon and O. Samuelson, *Svensk Papperstidn*, 1957, **60**, 872-877.
191. M. Albeck, *Textile research journal*, 1965, **35**, 836.
192. I. Ziderman and J. Belayche, *Journal of Applied Polymer Science*, 1978, **22**, 1151-1158.
193. J. M. MacLeod and L. R. Schroeder, *Journal of Wood and Chemical Technology*, 1982, **2** 187-205.
194. H. W. Diehl and H. G. Fletcher, Jr., *Archives of Biochemistry and Biophysics*, 1958, **78**, 386-391.
195. T. C. Yuan, J. F. Wang and Z. B. Li, *Fluid Phase Equilibr*, 2010, **297**, 129-137.
196. L. R. Van Loon, M. A. Glaus, S. Stallone and A. Laube, *Environ. Sci. Technol.*, 1997, **31**, 1243-1245.
197. D. Rai, L. Rao and Y. Xia, *J. Solut. Chem.*, 1998, **27**, 1109-1122.
198. H. Öztürk, H. Vu-Manh and T. Bechtold, *Lenzinger Berichte*, 2009, **87**, 142-150.
199. A. Dabrowski, Z. Hubicki, P. Podkościelny and E. Robens, *Chemosphere*, 2004, **56**, 91-106.
200. M. Torre, A. R. Rodriguez and F. Saura-Calixto, *J Agr Food Chem*, 1992, **40**, 1762-1766.
201. C. Fitz-Binder and T. Bechtold, *Carbohydrate Polymers*, 2012, **90**, 937-942.
202. C. Fitz-Binder and T. Bechtold, *Carbohydrate Polymers*, 2009, **76**, 123-128.
203. A. Ehrhardt, S. Groner and T. Bechtold, *Fibres & Textiles in Eastern Europe*, 2007, **15**, 46-48.
204. F. Jalilehvand, D. Spångberg, P. Lindqvist-Reis, K. Hermansson, I. Persson and M. Sandström, *Journal of the American Chemical Society*, 2000, **123**, 431-441.
205. C. J. Men and F.-M. Tao, *Journal of Theoretical and Computational Chemistry*, 2007, **06**, 595-609.
206. T. Megyes, T. Grósz, T. Radnai, I. Imre Bakó and G. Gábor Pálinkás, *The Journal of Physical Chemistry A*, 2004, **108**, 7261-7271.
207. M. Y. Kiriukhin and K. D. Collins, *Biophysical chemistry*, 2002, **99**, 155-168.
208. M. A. Moharram and O. M. Mahmoud, *Journal of Applied Polymer Science*, 2008, **107**, 30-36.
209. Sigma Aldrich Corporation,  
<http://www.sigmaaldrich.com/catalog/product/SIAL/44340?lang=en&region=GB>,  
Accessed 23rd November 2012.
210. P. B. Shaw, G. F. Robinson, C. R. Rice, P. N. Humphreys and A. P. Laws, *Carbohydrate Research*, 2012, **349**, 6-11.
211. G. Zemplén and A. Kunz, *Berichte der deutschen chemischen Gesellschaft (A and B Series)*, 1923, **56**, 1705-1710.
212. H. Adkins and Q. E. Thompson, *Journal of the American Chemical Society*, 1949, **71**, 2242-2244.
213. WHO, *Concise International Chemical Assessment Document*, 2000, **26**.
214. D. Rai, N. J. Hess, Y. Xia, L. Rao, H. M. Cho, R. C. Moore and L. R. Van Loon, *J. Solut. Chem.*, 2003, **32**, 665-689.

215. J. Hagberg, A. Duker and S. Karlsson, *Chromatographia*, 2002, **56**, 641-644.
216. S. Motellier and Y. Charles, *Anal. Chim. Acta*, 1998, **375**, 243-254.
217. K. I. Popov, N. M. Sultanova and H. Ronkkomaki, *Russian Journal of Physical Chemistry*, 2006, **80**, 1680-1682.
218. W. J. Spillane and J. B. Thomson, *Journal of the Chemical Society-Perkin Transactions 2*, 1977, 580-584.
219. D. Farrell, E. S. Miranda, H. Webb, N. Georgi, P. B. Crowley, L. P. McIntosh and J. E. Nielsen, *Proteins: Structure, Function, and Bioinformatics*, 2010, **78**, 843-857.
220. M. Liler, *Journal of the Chemical Society B: Physical Organic*, 1971, 334-338.
221. J. H. Bradbury and L. R. Brown, *European Journal of Biochemistry*, 1973, **40**, 565-576.
222. G. Gatti, B. Casu, G. K. Hamer and A. S. Perlin, *Macromolecules*, 1979, **12**, 1001-1007.
223. H. M. Wang, *Biochem J*, 1991, **278**, 689.
224. M. Almond, P. B. Shaw, P. N. Humphreys, M. J. Chadha, K. Niemelä and A. P. Laws, *Carbohydrate Research*, 2012, **363**, 51-57.
225. K. Popov, H. Ronkkomaki and L. H. J. Lajunen, *Pure and Applied Chemistry*, 2006, **78**, 663-675.
226. P. K. Glasoe and F. A. Long, *Journal Name: Journal of Physical Chemistry (U.S.); Journal Volume: Vol: 64; Other Information: Orig. Receipt Date: 31-DEC-60*, 1960, Medium: X; Size: Pages: 188-190.
227. M. J. Citra, *Chemosphere*, 1999, **38**, 191-206.
228. R. Williams, *pKa data compiled*, [http://research.chem.psu.edu/brpgroup/pKa\\_compilation.pdf](http://research.chem.psu.edu/brpgroup/pKa_compilation.pdf), Accessed 12th September 2012.
229. G. Getahun, P. Warwick, S. Zauner and N. Trautmann, *Annual Report (Institut für Kernchemie, Universität Mainz)*, 1999.
230. R. D. Cornelius and P. R. Norman, *J Chem Educ*, 1983, **60**, 98-99.
231. H. S. Harned and R. A. Robinson, *Transactions of the Faraday Society*, 1940, **36**, 973-978.
232. S. H. Hilal, S. W. Karickhoff, L. A. Carreira and B. P. Shrestha, *Qsar & Combinatorial Science*, 2004, **22**, 917-925.
233. G. M. Blackburn and H. L. H. Dodds, *Journal of the Chemical Society-Perkin Transactions 2*, 1974, 377-382.
234. R. Alen and J. Valkonen, *Acta chemica Scandinavica*, 1995, **49**, 536-539.
235. J. H. Espenson, *Chemical Kinetics and Reaction Mechanisms*, 2nd edn. pp. 46-49, McGraw-Hill, New York 1995.
236. M. A. Casadei, C. Galli and L. Mandolini, *Journal of the American Chemical Society*, 1984, **106**, 1051-1056.
237. K. L. Wilkinson, G. M. Elsey, R. H. Prager, A. P. Pollnitz and M. A. Sefton, *J Agr Food Chem*, 2004, **52**, 4213-4218.
238. D. R. Storm and D. E. Koshland, *P Natl Acad Sci USA*, 1970, **66**, 445-&.
239. I. Ziderman, *Cellulose and Chemical Technology*, 1980, **14**, 703-711.

## **8 Publications**